MARMARA UNIVERSITY
INSTITUTE FOR GRADUATE STUDIES
IN PURE AND APPLIED SCIENCES

PRODUCTION AND PROPERTIES OF ALKALI ACTIVATED BINDERS FROM INDUSTRIAL WASTE MATERIALS

GÜLDEN ÇAĞIN ULUBEYLİ

Ph.D. THESIS

Department of Metallurgical and Materials Engineering

THESIS SUPERVISOR

Prof. Dr. Recep ARTIR

ISTANBUL, 2022

MARMARA UNIVERSITY
INSTITUTE FOR GRADUATE STUDIES
IN PURE AND APPLIED SCIENCES

PRODUCTION AND PROPERTIES OF ALKALI ACTIVATED BINDERS FROM INDUSTRIAL WASTE MATERIALS

GÜLDEN ÇAĞIN ULUBEYLİ
(724711002)

Ph.D. THESIS
Department of Metallurgical and Materials Engineering

THESIS SUPERVISOR
Prof. Dr. Recep ARTIR

ISTANBUL, 2022

ACKNOWLEDGEMENTS

I would like to thank my supervisor Prof. Dr. Recep Artır without whom I would not be able to complete my thesis, for his unconditional guidance, patience, and tolerance at each step of this study.

I owe special thanks to raw materials suppliers such as top managers of Filyos Fire Brick Plant, Kardemir Iron Steel Industry, and Sançim Bilecik Cement & Concrete, as well as to kind academicians and technicians of Civil Engineering Department and Mining Engineering Department of Zonguldak Bülent Ecevit University, who provided special laboratory conditions and machines properly.

Finally, my endless darling and husband Prof. Dr. Serdar Ulubeyli, my sweet son Uygar Ulubeyli and my parents deserve the greatest thanks for their unconditional love, support, and understanding throughout my studies. They deserve special thanks because, without their patience and support, this thesis could have never been materialized as it is. I dedicate this study to them.

June, 2022 **Gülden Çağın ULUBEYLİ**

TABLE OF CONTENTS

PAGE

ACKNOWLEDGEMENTS ..... **i**
TABLE OF CONTENTS ..... **ii**
ABSTRACT ..... **vi**
ÖZET ..... **viii**
CLAIM FOR ORIGINALITY ..... **x**
SYMBOLS ..... **xi**
ABBREVIATIONS ..... **xii**
LIST OF FIGURES ..... **xiii**
LIST OF TABLES ..... **xx**
1. INTRODUCTION **1**
1.1. Hypothesis of thesis 4
1.2 Objectives of the study 4
1.3 Organization of the thesis 5
2. LITERATURE REVIEW **7**
2.1. General 7
2.2. Development of Alkali Activated Binder Systems 9
2.3. Alkali Activated Blast Furnace Slag Binders 10
2.4. Alkali Activated Industrial Waste Binder Systems 12
2.4.1. Alkali activated ceramic waste binder 12
2.4.2. Alkali activated marble waste binder 16
2.4.3. Alkali activated binary and ternary blended waste binder 18
2.5. Selection of Alkali Activators, Variable Parameters and Additives 19
2.5.1. Alkali activators 19
2.5.2. Variable parameters 20
2.5.2.1. “n” and “Ms” values 20
2.5.2.2. Water/binder and curing conditions 21
2.5.2.3. Additives 21
3. MATERIALS AND METHODS **22**
3.1. Raw Materials and Precursors 22
3.1.1. Properties of precursors and raw materials 22

3.1.2. Properties of additives (Lime) 27
3.1.3. Properties of alkali activators 28
3.2. Methods 28
3.2.1. Types and properties of used binder mixes 28
3.2.2. Stages of experimental process 29
3.2.2.1. First three stages 31
3.2.2.2. Fourth. fifth and sixth stage 34
3.2.3. Production of samples 36
3.2.4. Procedure of experiments in first, second and third stage 38
3.2.4.1. Flow table test 38
3.2.4.2. Determination of setting time 39
3.2.4.3. Flexural & compressive strength test 40
3.2.5. Procedure of experiments in fourth stage 41
3.2.5.1. Dry bulk density, apparent density and volume of voids (permeable pore space) measurement test 41
3.2.5.2. Capillary water absorbtion test 42
3.2.6. Procedure of experiments in fifth stage 42
3.2.6.1. Sulphate attack test 42
3.2.6.2. Sulphuric acid attack test 43
3.2.6.3. Drying shrinkage test 44
3.2.6.4. High temperature effect test 45
3.2.7. Procedure of experiments in sixth stage 46
3.2.7.1. SEM-EDS analysis 46
3.2.7.2. XRD analysis 46
3.2.7.3. FTIR analysis 46
4. RESULTS AND DISCUSSION 48
4.1. First Stage - Determination the Optimum Parameters of the Unary Binders 48
4.1.1. Blast furnace slag-unary binders (BFS-UB) 49
4.1.1.1. Workability properties of BFS-UB samples 49
4.1.1.2. Strength properties of BFS-UB samples 55
4.1.2. Ceramic waste-unary binders (CW-UB) 63
4.1.2.1. Workability properties of CW-UB samples 63
4.1.2.2. Strength properties of CW-UB samples 69

4.1.3. Marble waste-unary binders (MW-UB) 75
4.1.3.1. Workability properties of MW-UB samples 75
4.1.3.2. Strength properties of MW-UB samples 79
4.2. Second Stages: Determination of the Optimum Parameters of Binary Binders 85
4.2.1. Blast furnace slag/ceramic waste-binary binders (BFS/CW-BB) 85
4.2.1.1. Workability properties of BFS/CW-BB samples 85
4.2.2.2. Strength properties of BFS/CW-BB samples 94
4.2.2. Blast furnace slag/marble waste-binary binders (BFS/MW-BB) 102
4.2.2.1. Workability properties of BFS/MW-BB samples 102
4.2.2.2. Strength Properties of BFS/MW-BB Samples 109
4.2.3. Ceramic waste/marble waste-binary binders (CW/MW-BB) 116
4.2.3.1. Workability properties of CW/MW-BB samples 116
4.2.3.2. Flexural and compressive strength properties of CW/MW-BB samples 123
4.3. Third Stages: Determination The Optimum Parameters of the Ternary Binders 130
4.3.1. Blast furnace slag/ceramic waste/marble waste-ternary binders (BFS/CW/MW-TB) 130
4.3.1.1. Workability properties of BFS/CW/MW-TB samples 130
4.3.1.2. Strength properties of BFS/CW/MW-TB samples 140
4.4. Determination of the Selected Samples in The First Three Stages 145
4.5. Fourth Stage-Determination of the Mechanical Properties of the Selected (Optimum) Binders 146
4.5.1. Flexural and compressive strength of the selected binders among samples 146
4.5.2. Dry bulk density, apparent density and volume of voids (permeable pore space) measurement results 152
4.2.3. Determination of the selected samples for the rate of water absorption 156
4.6. Fifth Stage-Determination of the Durability Properties of the All Selected Binders 159
4.6.1. Drying shrinkage of the selected binders 159
4.3.2. High temperature effect on the selected binders 163
4.6.3. Selected binders against sulphate attack test 180
4.7. Sixth Stage-Microstructural and Cost Analysis and Chemical Properties of the Selected Binders 183

4.7.1. Microstructural analysis of the selected unary binders 183
4.7.1.1. Microstructural analysis of the BFS-UB samples..... 183
4.7.1.2. Microstructural analysis of the CW-UB samples..... 189
4.7.1.3. Microstructural analysis of the MW-UB samples 194
4.7.2. Microstructural analysis of the selected binary binders 199
4.7.2.1. Microstructural analysis of the BFS/CW-BB samples 199
4.7.2.2. Microstructural analysis of the BFS/MW-BB samples 204
4.7.2.3. Microstructural analysis of the CW/MW-BB samples 211
4.7.3. Microstructural analysis of the selected ternary binders 217
4.7.3.1. Microstructural analysis of the BFS/CW/MW-TB samples..... 217
4.7.4. Cost Analysis Comparison 224
5. CONCLUSIONS 226
REFERENCES 241

ABSTRACT

PRODUCTION AND PROPERTIES OF ALKALI ACTIVATED BINDERS FROM INDUSTRIAL WASTE MATERIALS

Environmental and economic losses caused by industrial wastes globally and particullarly in Turkey triggered recycling for the production of value added products. In this thesis; various types of waste/by-products (blast furnace slag, ceramic waste, and marble waste), which are produced in large quantities, after the industrial production process were activated by alkaline solutions (sodium hydroxide and sodium silicate) and the binding materials were obtained by alkali activation method. Blast furnace slag, ceramic and marble wastes were used both as unary, binary and ternary mixtures instead of reference cement raw materials. Thus, firstly the ability of these wastes to be replaced by cement, the unary binder as raw materials were investigated. Then in addition to binary and ternary mixtures strength, durability and microstructure properties of the developed binders were determined.

At the end of the experimental studies, the data obtained for the paste samples produced with new generation binders were compared with the experimental results of the control samples produced by using 100% blast furnace slag and standard cement paste samples. In this way, it was evaluated that their usability as a binding material instead of Portland cement in terms of their mechanical, physical, durability and microstructural properties of new generation binders produced by alkaline activation method.

As a result, it has been observed that the compressive strength of the binary and ternary binder samples produced by adding ceramic and marble waste are very close to the strength values of Portland cement and the wastes increase the strength values of unary component binder system produced by the blast furnace slag. Marble waste reduced considerably the drying shrinkage value of the binding systems and improve the workability properties of binary and ternary binder sample. In addition, it was determined that the binary and ternary binders produced had a much lower strength loss than the cement sample in terms of resistance to high temperature effects. Substitution of 50% of the marble waste in the blast furnace slag and 25% of the ceramic waste in the slag improved the strength values of unary binder of BFS. As a result of

microstructural analysis, although no new major phase formation was observed for binary and ternary component binder systems, secondary or minor phase formations that improved strength and durability properties were observed.

The most suitable production conditions for unary, binary and ternary component systems of all these materials determined. It was studied that these source materials could be produced as a bearing and non-bearing binder material by activating with alkali activators.

Contrary to cement production, in this study variety of binder materials were produced having cement-like strength and durability with a low energy cost production method without CO2 and other harmful gas emissions.

In the comparison of the simple cost analysis performed for the cement and the ternary component BFS/CW/MW-TB-F sample it was understood that the alkali-activated binder method is a slightly more expensive system than cement. Considering all these environmental factors, environmental restrictions such as environmental pollution and carbon footprint, this novel binder material obtained as green and sustainable materials in this study which provides lower cost values and more appropriate than cement.

It could be concluded that this work enabled the reuse of industrial waste materials and production of novel binding materials that can be used instead of cement with very low harmful gas emissions and energy, and contributed to the production of environmentally friendly and sustainable materials.

Key words: Blast furnace slag, alkali activation, ceramic waste, marble waste, mechanical and durability properties, microstructural analysis.

June, 2022 **Gülden Çağın ULUBEYLİ**

ÖZET

ENDÜSTRİYEL ATIKLARDAN ALKALİ AKTİVE EDİLMİŞ BAĞLAYICILARIN ÜRETİMİ VE ÖZELLİKLERİ

Dünyada ve özellikle Türkiye'de endüstriyel atıkların yol açtığı çevresel ve ekonomik kayıplar, katma değerli ürünlerin üretimi için, atıkların geri dönüşümünü tetiklemiştir. Bu tez kapsamında; endüstriyel üretim işlemlerinden sonra çok çeşitli ve büyük miktarlarda ortaya çıkan bazı atık/yan ürün türlerinin (yüksek fırın cürufu, seramik atığı ve mermer atığı), alkali çözeltiler (sodyum hidroksit ve sodyum silikat) ile aktive edilmesi sonucunda alkali aktivasyonu yöntemi ile bağlayıcı malzemeler elde edilmiştir. Yüksek fırın cürufu, seramik ve mermer atıkları, hammadde yerine, hem tek olarak ve hem de ikili ve üçlü karışımlar halinde kullanılmıştır. Böylece, bu atıkların tek başlarına bağlayıcı hammaddesi olabilme yetenekleri araştırılmış ve ikili ve üçlü karışımları sonucunda üretilen bağlayıcıların dayanım, dayanıklılık ve mikro yapı özellikleri belirlenmiştir.

Deneysel çalışmalar sonunda, yeni nesil bağlayıcılar ile üretilmiş pasta numuneleri için elde edilen veriler, %100 yüksek fırın cürufunun kullanılması ile üretilmiş kontrol numuneleri ve standart çimento pastası numunelerinin deneysel sonuçları ile karşılaştırılmıştır. Bu şekilde, alkali aktivasyon yöntemi ile üretilen yeni nesil bağlayıcıların; mekanik, fiziksel, dış etkilere dayanıklılık ve mikro yapı özellikleri bakımından Portland çimentosunun yerine, bağlayıcı malzeme olarak kullanılabilirlikleri değerlendirilmiştir.

Sonuç olarak, ikili ve üçlü karışım bağlayıcı numunelerinin eğilme ve basınç mukavemeti açısından Portland çimentosunun mukavemet değerlerine çok yaklaştığı ve yüksek fırın cürufunun tek bileşenli mukavemet değerlerini arttırdığı gözlemlenmiştir. Bunun yanı sıra, özellikle mermer atığın, yüksek fırın cürufunun kuruma büzülmesi değerini oldukça düşürdüğü ve işlenebilirlik özelliklerini iyileştirdiği tespit edilmiştir. Ayrıca üretilen ikili ve üçlü bağlayıcıların yüksek sıcaklık etkilerine dayanım açısından çimento numunesine göre çok daha düşük dayanım kaybına sahip olduğu belirlenmiştir. Cüruftaki mermer atığının %50'sinin ve cüruf içindeki seramik atığının %25'inin ikamesi, BFS'nin tek bileşenli bağlayıcısının mukavemet değerlerini iyileştirmiştir.

Mikroyapısal analizler sonucunda ikili ve üçlü bileşenli bağlayıcı sistemler için yeni bir majör faz oluşumu gözlemlenmemesine rağmen, dayanım ve dayanıklılık özelliklerini iyileştiren minör ve ikincil faz oluşumları gözlenmiştir.

Tüm kullanılan malzemelerin tek, iki ve üç bileşenli bağlayıcı sistemleri için en uygun üretim şartları belirlenmiştir. Bu ham maddeler ile taşıyıcı özellikte olan ve olmayan bağlayıcı malzeme üretilebileceği araştırılmıştır.

Bu çalışmada çimento üretiminin aksine, CO_2 ve diğer zararlı gaz emisyonları olmaksızın düşük enerji maliyetli üretim yöntemi ile çimento benzeri mukavemet ve dayanıklılığa sahip çeşitli bağlayıcı malzemeler üretilmiştir.

Çimento ve üçlü bileşenli BFS/CW/MW-TB-F numunesi için yapılan basit maliyet analizinin karşılaştırılmasında alkali aktivasyonlu bağlayıcı üretim yönteminin çimentoya göre biraz daha pahalı bir sistem olduğu anlaşılmıştır. Tüm çevresel faktörler, çevre kirliliği ve karbon ayak izi gibi çevresel kısıtlamalar göz önüne alındığında, bu çalışmada elde edilen yeni nesil bağlayıcı türleri, yeşil ve sürdürülebilir malzemeler olarak, çimentodan daha uygun ve düşük maliyet sağlamışlardır.

Bu çalışmanın, endüstriyel atık malzemelerin yeniden kullanılmasına ve çimento yerine kullanılabilecek çok düşük zararlı gaz emisyonları ve enerjisine sahip yeni bağlayıcı malzemelerin üretilmesine olanak sağladığı, çevre dostu ve sürdürülebilir malzemelerin üretimine katkı sağladığı söylenebilir.

Keywords: Yüksek fırın cürufu, Alkali aktivasyonu, seramik atıkları, mermer atıkları, mekanik ve dayanıklılık özellikleri, mikroyapı analizi

June, 2022 **Gülden Çağın ULUBEYLİ**

CLAIM FOR ORIGINALITY

PRODUCTION OF ALKALI ACTIVATED BINDER USING INDUSTRIAL WASTE MATERIALS AND INVESTIGATION OF ITS PROPERTIES

Leaving these industrial wastes (blast furnace slag, ceramic waste and marble waste) in an uncontrolled manner in large quantities causes environmentally irreparable damages. Storage of the wastes gives rise to an additional economic expense.

As a result of the literature review, there are studies that used blast furnace slag, ceramic and marble wastes as aggregates and/or additives in concrete and/or cement. However, a very limited number of sources have been reached for the production of binders by activating these wastes with alkaline solutions. In the limited number of studies related to these wastes, very limited experimental data on physical, mechanical, durability and microstructure properties have been obtained in order to compare the produced binder with the properties of the conventional cement binder. In addition, there is no study in which the marble waste is used in the alkaline activation method. In this context, the re-using of marble waste into a new generation structural element using the alkaline activation method contributes greatly to the original value of the thesis. And also, the strength, durability and micro structure properties of binary and ternary binder systems including these wastes have not been determined before. In this study, many experiments were carried out to determine the properties of these new generation binder according to ASTM standards that determine the cement properties.

As a result, the industrial wastes that cause great damage in the environmental and economic sense have been evaluated and their usability for the production of a sustainable material within the construction sector has been investigated. Furthermore, for the production of new generation binders from these wastes, a nature-friendly production process has been attempted with the activation of alkaline solutions, a much lower CO_2 emission than the classical cement production method and highly superior in energy consumption. This thesis, with all these aspects, will produce original data.

SYMBOLS

Al_2O_3	**:**	Aluminum Oxide
CaO	**:**	Calcium Oxide
CO_2	**:**	Carbon Dioxide
Na_2O	**:**	Sodium Oxide
Na_2SiO_3	**:**	Sodium Silicate
NaOH	**:**	Sodium Hydroxide
n	**:**	The Ratio of Na_2O in the Alkali Activator Mixture
M_s	**:**	SiO_2/Na_2O Ratio of the Alkali Activator Mixture
SiO_2	**:**	Silicon dioxide

ABBREVIATIONS

AASB	**:**	Alkali Activated Slag Binder
BFS	**:**	Blast Furnace Slag
BFS/CW/MW-TB	**:**	Blast Furnace Slag/Ceramic Waste/Marble Waste-Ternary Binder
BFS/CW-BB	**:**	Blast Furnace Slag/Ceramic Waste-Binary Binder
BFS/MW-BB	**:**	Blast Furnace Slag/Marble Waste-Binary Binder
BFS-UB	**:**	Blast Furnace Slag-Unary Binder
BSE	**:**	Back Scattered Electron
BSW	**:**	Bayburt Stone waste
CW	**:**	Ceramic Waste
CW/MW-BB	**:**	Ceramic Waste/Marble Waste-Binary Binder
CW-UB	**:**	Ceramic Waste-Unary Binder
FA	**:**	Fly Ash
FTIR	**:**	Fourier Transform Infrared Spectrophotometer
GBFS	**:**	Ground Blast Furnace Slag
MW	**:**	Marble Waste
MW-UB	**:**	Marble Waste-Unary Binder
OPC	**:**	Ordinary Portland Cement
SE	**:**	Secondary Electron
SEM-EDS	**:**	Scanning Electron Microscopy-Energy Dispersive X-ray Spectroscopy
w/b ratio	**:**	water/binder ratio
WCP	**:**	Waste Ceramic Powder
XRD	**:**	X-Ray Diffraction

LIST OF FIGURES

PAGE

Figure 1.1. Cement manufacturing (Dry Process). 1

Figure 1.2. Expected cement production by region. 2

Figure 2.1. Cement production and emissions values between 2010 and 2015 years.. 8

Figure 3.1. Photographs of raw materials and additive used in this study. 23

Figure 3.2. Particle size distribution of raw materials a) BFS b) CW c) MW. 24

Figure 3.3. XRD patterns of BFS. 25

Figure 3.4. XRD patterns of CW. 26

Figure 3.5. XRD patterns of MW. 26

Figure 3.6. SEM images of source materials a) BFS b) CW c) MW. 27

Figure 3.7. Flow chart of first, second and third experimental stages. 33

Figure 3.8. Flow chart of fourth stage. 34

Figure 3.9. Flow chart of fifth stage. 35

Figure 3.10. Flow chart of sixth stage. 36

Figure 3.11. a) 40×40×160 mm sample mold b) 25×25×285mm sample mold. 36

Figure 3.12. Manual cement mixer. 38

Figure 3.13. Flow table apparatus. 39

Figure 3.14. Full automatic vicat apparatus. 40

Figure 3.15. Flexure/compression test frame. 41

Figure 3.16. Unary, binary and ternary binders in sulphate solution. 43

Figure 3.17. Unary, binary and ternary binders in sulphric acid solution. 44

Figure 3.18. (a) Digital length mold (b) Digital length comparator. 45

Figure 3.19. Muffle furnace. 45

Figure 3.20. FTIR-ATR Spectrum100 ınstrument. 47

Figure 4.1. The flow values of BFS–UB samples according to “n” ratio (for “w/b=0.4” and for “w/b=0.45”). 51

Figure 4.2. The flow values of BFS-UB samples according to “Ms” ratio (for “w/b=0.4” and for “w/b=0.45”). 51

Figure 4.3. The setting time of BFS-UB samples according to “n” ratio a) Initial setting time b) Final setting time. 53

Figure 4.4. The setting time of BFS-UB samples according to “Ms” ratio a) Initial setting time b) Final setting time. 53

Figure 4.5. Flexural strength of BFS-UB samples for 7 days. 56
Figure 4.6. Change in flexural strength of BFS-UB according to "n" ratio a) For oven cure b) For steam cure. 58
Figure 4.7. Change in flexural strength of BFS-UB according to "M_s" ratio a) For oven cure b) For steam cure. 58
Figure 4.8. Compressive strength of BFS-UB samples for 7 days..... 59
Figure 4.9. Change in compressive strength of BFS-UB according to "n" ratio. a) For oven cure b) For steam cure. 60
Figure 4.10. Change in compressive strength of BFS-UB according to "Ms" ratio. a) For oven cure b) For steam cure. 60
Figure 4.11. Compressive and flexural strength of BFS-UB samples for 7 days. 61
Figure 4.12. The flow values of CW-UB according to "n" ratio **(**For "w/b=0.4" and For "w/b=0.45"). 65
Figure 4.13. The flow values of CW-UB according to "Ms" ratio (For "w/b=0.4" and For "w/b=0.45"). 65
Figure 4.14. The setting time of CW-UB Samples according to "n" ratio a) Initial setting time b) Final setting time. 67
Figure 4.15. The setting time of CW-UB Samples according to "Ms" ratio a) Initial setting time b) Final setting time. 67
Figure 4.16. Flexural strength of CW-UB samples for 7 days. 69
Figure 4.17. Change in flexural strength of CW-UB according to "n" ratio a) For oven cure b) For steam cure. 70
Figure 4.18. Change in flexural strength of CW-UB according to "M_s" ratio a) For oven cure b) For steam cure. 70
Figure 4.19. Compressive strength of CW-UB samples for 7 days. 71
Figure 4.20. Change in compressive strength of CW-UB according to "n" ratio a) For oven cure b) For steam cure. 72
Figure 4.21. Change in compressive strength of CW-UB according to "M_s" ratio a) For oven cure b) For steam cure. 72
Figure 4.22. Compressive and flexural strength of CW-UB samples for 7 days. 73
Figure 4.23. The flow values of MW-UB according to "n" ratio (For "w/b = 0.4" and For "w/b = 0.45"). 76
Figure 4.24. The flow values of MW-UB according to "Ms" ratio (For "w/b = 0.4" and For "w/b = 0.45"). 76
Figure 4.25. The setting time of MW-UB Samples according to "n" ratio a) Initial setting time b) Final setting time. 78
Figure 4.26. The setting time of MW-UB Samples according to "Ms" ratio a) Initial setting time b) Final setting time. 78
Figure 4.27. Flexural strength of MW-UB samples for 7 days. 80

Figure 4.28. Change in flexural strength of MW paste according to "n" ratio a) For oven cure b) For steam cure. 81

Figure 4.29. Change in flexural strength of MW paste according to "M_s" ratio a) For oven cure b) For steam cure. 81

Figure 4.30. Compressive strength of MW-UB samples for 7 days. 82

Figure 4.31. Change in compressive strength of MW-UB according to "n" ratio a) For oven cure b) For steam cure. 83

Figure 4.32. Change in compressive strength of MW-UB according to "M_s" ratio a) For oven cure b) For steam cure. 83

Figure 4.33. Compressive and flexural strength of MW-UB samples for 7 days. 84

Figure 4.34. The flow values of BFS/CW–BB samples according to "n" ratio (for "w/b=0.4" and for "w/b=0.45"). 87

Figure 4.35. The flow values of BFS/CW–BB samples according to "Ms" ratio (for "w/b=0.4" and for "w/b=0.45"). 87

Figure 4.36. The setting time of BFS/CW-BB Samples according to "n" ratio a) Initial setting time b) Final setting time. 90

Figure 4.37. The setting time of BFS/CW-BB Samples according to "Ms" ratio a) Initial setting time b) Final setting time. 92

Figure 4.38. The selected flexural and compressive strength values BFS/CW-BB systems for each mix proportion. 95

Figure 4.39. Flexural strength of 2BFS/2CW-BB samples. 95

Figure 4.40. Change in flexural strength of 2BFS/2CW-BB paste according to "n" ratio **a)** For oven cured **b)** For steam cured. 97

Figure 4.41. Change in flexural strength of 2BFS/2CW-BB paste according to "M_s" ratio **a)** For oven cured **b)** For steam cured. 97

Figure 4.42. Compressive strength of 3BFS/1CW-BB samples. 98

Figure 4.43. Change in flexural strength of 3BFS/1CW-BB according to "n" ratio a) For oven cured b) For steam cured. 99

Figure 4.44. Change in flexural strength of 3BFS/1CW-BB according to "M_s" ratio a) For oven cured b) For steam cured. 99

Figure 4.45. The flow values of BFS/MW–BB samples according to "n" ratio (for "w/b=0.4" and for "w/b=0.45"). 104

Figure 4.46. The flow values of BFS/MW–BB samples according to "Ms" ratio (for "w/b=0.4" and for "w/b=0.45"). 104

Figure 4.47. The setting time of BFS/MW-BB Samples according to "n" ratio a) Initial setting time b) Final setting time. 107

Figure 4.48. The setting time of BFS/MW-BB Samples according to "Ms" ratio a) Initial setting time b) Final setting time. 108

Figure 4.49. The selected flexural and compressive strength values in BFS/MW-BB systems for each mix proportion. 110

Figure 4.50. Flexural strength of 2BFS/2MW-BB samples. 111

Figure 4.51. Change in flexural strength of 2BFS/2MW-BB paste according to "n" ratio a) For oven cure b) For steam cure. 112

Figure 4.52. Change in flexural strength of 2BFS/2MW-BB paste according to "M_s" ratio a) For oven cure b) For steam cure. 112

Figure 4.53. Compressive strength of 2BFS/2MW-BB samples. 113

Figure 4.54. Change in flexural strength of 2BFS/2MW-BB according to "n" ratio a) For oven cure b) For steam cure. 114

Figure 4.55. Change in flexural strength of 2BFS/2MW-BB according to "M_s" ratio a) For oven cure b) For steam cure. 114

Figure 4.56. The flow values of CW/MW–BB samples according to "n" ratio (for "w/b=0.4" and for "w/b=0.45"). 118

Figure 4.57. The flow values of CW/MW–BB samples according to "Ms" ratio (for "w/b=0.4" and for "w/b=0.45"). 118

Figure 4.58. The setting time of CW/MW-BB Samples according to "n" ratio a) Initial setting time b) Final setting time. 121

Figure 4.59. The setting time of CW/MW-BB Samples according to "Ms" ratio a) Initial setting time b) Final setting time. 122

Figure 4.60. The selected flexural and compressive strength values CW/MW-BB systems for each mix proportion. 124

Figure 4.61. Flexural strength of 2CW/2MW-BB samples 125

Figure 4.62. Change in flexural strength of 2CW/2MW-BB paste according to "n" ratio a) For oven cure b) For steam cure. 126

Figure 4.63. Change in flexural strength of 2CW/2MW-BB paste according to "M_s" ratio a) For oven cure b) For steam cure. 126

Figure 4.64. Compressive strength of 2CW/2MW-BB samples. 127

Figure 4.65. Change in flexural strength of 2CW/2MW-BB according to "n" ratio a) For oven cure b) For steam cure. 128

Figure 4.66. Change in flexural strength of 2CW/2MW-BB according to "M_s" ratio a) For oven cure b) For steam cure. 128

Figure 4.67. The flow values of BFS/CW/MW-TB samples according to "n" ratio a) for "w/b=0.4" b) for "w/b=0.45" 132

Figure 4.68. The flow values of BFS/CW/MW-TB samples according to "Ms" ratio a) for "w/b=0.4" b) for "w/b=0.45" 133

Figure 4.69. The initial setting time of BFS/CW/MW-TB samples according to "n" ratio a) for "w/b=0.4" b) for "w/b=0.45". 136

Figure 4.70. The final setting time of BFS/CW/MW-TB samples according to "n" ratio a) for "w/b=0.4" b) for "w/b=0.45". 137

Figure 4.71. The initial setting time of BFS/CW/MW-TB samples according to "Ms" ratio a) for "w/b=0.4" b) for "w/b=0.45". 138

Figure 4.72. The final setting time of BFS/CW/MW-TB samples according to "Ms" ratio a) for "w/b=0.4" b) for "w/b=0.45". 139

Figure 4.73. The selected flexural and compressive strength values among samples BFS/CW/MW-TB systems for each mix proportion. 140

Figure 4.74. Flexural strength of BFS/CW/MW-TB samples..... 141

Figure 4.75. Change in flexural strength of BFS/CW/MW-TB paste according to "n" ratio a) For oven cure b) For steam cure. 142

Figure 4.76. Change in flexural strength of BFS/CW/MW-TB paste according to "M_s" ratio a) For oven cure b) For steam cure. 142

Figure 4.77. Compressive strength of 2BFS/1CW/1MW-TB samples..... 143

Figure 4.78. Change in compressive strength of 2BFS/1CW/1MW-TB according to "n" ratio a) For oven cure b) For steam cure. 144

Figure 4.79. Change in compressive strength of 2BFS/1CW/1MW-TB according to "M_s" ratio a) For oven cure b) For steam cure. 144

Figure 4.80. Codes of samples. 146

Figure 4.81. Flexural strength variation as a function of curing period. 148

Figure 4.82. Compressive strength variation as a function of curing period. 149

Figure 4.83. The effect of early and late curing on flexural and compressive strengths of the selected unary mixtures. 149

Figure 4.84. The effect of early and late curing on flexural and compressive strengths of the selected binary mixtures. 150

Figure 4.85. The effect of early and late curing on flexural and compressive strengths of the selected ternary mixtures. 152

Figure 4.86. Bulk, apparent densities and voids results of the all selected samples. 154

Figure 4.87. Apparent density and voids results of selected unary samples. 154

Figure 4.88. Apparent density and voids results of the selected binary mixtures. 155

Figure 4.89. Apparent density and voids of the selected ternary mixtures. 156

Figure 4.90. Comparison of the rate of water absorption for all the selected samples. 157

Figure 4.91. Comparison of the rate of water absorption of the selected unary samples. 158

Figure 4.92. Comparison of the rate of water absorption of the selected binary samples. 158

Figure 4.93. Comparison of the rate of water absorption of the selected ternary samples..... 159

Figure 4.94. Comparison of drying shrinkage results of the all selected binders. 160

Figure 4.95. Comparison of drying shrinkage of the selected unary binders..... 161

Figure 4.96. Comparison of drying shrinkage of the selected binary binders..... 162

Figure 4.97. Comparison of drying shrinkage of the selected ternary binders. 163

Figure 4.98. Change in a) flexural b) compressive strength and c) weight of the selected unary samples with temperature. 164

Figure 4.99. XRD analysis of the selected unary sample with temperature a) BFS-UB-(C) b) BFS-UB (F) c) CW-UB d) MW-UB..... 167

Figure 4.100. Change in a) flexural b) compressive strength and c) weight of the selected binary samples with temperature. 169

Figure 4.101. XRD analysis of the binary selected sample with temperature a) 3BFS/1CW-BB b) 2BFS/2CW-BB c) 2BFS/2MW-BB-F d) 2BFS/2MW-BB-C e)2CW/2MW-BB..... 173

Figure 4.102. XRD analysis of the BFS/MW-BB selected samples and cement sample at 800 ºC 175

Figure 4.103. Change in a) Flexural b) Compressive strength and c) Weight of the ternary selected sample with temperature..... 176

Figure 4.104. XRD analysis of the ternary selected sample with temperature a) BFS/CW/MW-TB b) 2BFS/1CW/1MW-TB..... 178

Figure 4.105. Images of the selected samples fired to a) 200^0C and b) 800^0C. 179

Figure 4.106. Images of the cement samples fired to 200^0C, 400^0C, 600^0C and 800^0C..... 180

Figure 4.107. Loss of strengths of the selected binders exposed to sulphate effect a) Flexural b) Compressive. 181

Figure 4.108. Loss of strengths of the selected binders exposed to sulphuric acid a) Flexural b) Compressive..... 182

Figure 4.109. XRD patterns of the BFS-Raw and the selected BFS-UB (for both strengths) samples. 184

Figure 4.110. FTIR results of the BFS-Raw and the selected BFS-UB samples. 185

Figure 4.111. SEM-EDS images of the BFS-Raw and the selected samples **a)** BFS-UB-F **b)** BFS-UB-C. 188

Figure 4.112. XRD pattern of the CW-Raw and selected CW-UB sample. 189

Figure 4.113. FTIR results of the CW-Raw and selected CW-UB sample. 191

Figure 4.114. SEM-EDS images of the CW-Raw and selected CW-UB sample. 193

Figure 4.115. XRD pattern of the MW-Raw and selected MW-UB sample..... 195

Figure 4.116. FTIR results of the MW-Raw and selected MW-UB sample. 196

Figure 4.117. SEM-EDS images of the CW-Raw and selected CW-UB sample. 198
Figure 4.118. XRD pattern of the selected BFS/CW-BB sample. 200
Figure 4.119. FTIR results of the selected BFS/CW-BB samples. 201
Figure 4.120. SEM-EDS images of the selected BFS/CW-BB samples a) BFS/CW-F b) BFS/CW-C 202
Figure 4.121. XRD pattern of the selected BFS/MW-BB sample. 205
Figure 4.122. FTIR results of the selected BFS/MW-BB samples. 207
Figure 4.123. SEM-EDS images of the selected BFS/MW-BB samples a) BFS/MW-F b) BFS/MW-C. 209
Figure 4.124. XRD pattern of the selected CW/MW-BB sample. 211
Figure 4.125. General EDS analysis of 2CW/2MW-BB sample. 213
Figure 4.126. FTIR results of the selected CW/MW-BB sample. 214
Figure 4.127. SEM-EDS images of the selected CW/MW-BB sample. Düzelttim 216
Figure 4.128. XRD pattern of the selected BFS/CW/MW-TB-F sample according to flexural strength. 218
Figure 4.129. XRD pattern of the selected 2BFS/1CW/1MW-TB-C sample according to compressive strength. 218
Figure 4.130. FTIR results of the selected BFS/CW/MW-TB samples. 220
Figure 4.131. SEM-EDS images of the selected BFS/CW/MW-TB samples a) BFS/CW/MW-TB-F b) BFS/CW/MW-TB-C..... 222

LIST OF TABLES

PAGE

Table 2.1. Bibliographic history of some important events about alkali-activated binders. 10

Table 3.1. Raw materials used in this study and their suppliers. 22

Table 3.2. Chemical composition of raw materials performed by XRF analysis. 25

Table 3.3. Limiting values of used alkali activators in this study. 28

Table 3.4. Types and properties of used mixes. 29

Table 3.5. Stages of experimental process. 30

Table 3.6. The standards. sample size, sample numbers and sample residence time of the experiments to be carried out in the first three stages for unary, binary and ternary pastes specimens. 33

Table 3.7. The standards, sample size, sample numbers and sample residence time of the experiments to be carried out in the fourth stages for unary, binary and ternary pastes specimens. 34

Table 3.8. The standards, sample size, sample numbers and sample residence time of the experiments to be carried out in the fifth stages for unary. binary and ternary pastes specimens. 35

Table 3.9. The mass amounts of prism sample materials for a single 40×40×160 mm and 25×25×285 mm. 37

Table 4.1. Flow values (mm) of BFS-UB samples for w/b=0.4 and w/b=0.45. 50

Table 4.2. Setting time of BFS-UB samples (w/b=0.4 and w/b=0.45). 52

Table 4.3. Experimental parameters used to obtain the selected sample of BFS-UB. 62

Table 4.4. Flow values (mm) of CW-UB samples (w/b=0.4 and w/b=0.45). 63

Table 4.5. Setting time of CW-UB samples (w/b=0.4 and w/b=0.45). 66

Table 4.6. Experimental parameters of the selected samples of CW-UB. 74

Table 4.7. Flow values (mm) of MW-UB samples (w/b=0.4 and w/b=0.45). 75

Table 4.8. Setting time of MW-UB samples (w/b=0.4 and w/b=0.45). 77

Table 4.9. Experimental parameters of the selected samples of MW-UB. 85

Table 4.10. Flow values (mm) of BFS/CW-BB samples for w/b=0.4 and w/b=0.45. 86

Table 4.11. Setting time of BFS/CW-BB samples (w/b=0.4 and w/b=0.45). 89

Table 4.12. Experimental parameters of the selected samples of BFS/CW-BB. 101

Table 4.13. Flow values of BFS/MW-BB samples for w/b=0.4 and w/b=0.45. 103

Table 4.14. Setting time of BFS/MW-BB samples (w/b=0.4 and w/b=0.45). 106
Table 4.15. Experimental parameters of the selected samples of BFS/MW-BB. 116
Table 4.16. Flow values of CW/MW-BB samples for w/b=0.4 and w/b=0.45. 117
Table 4.17. Setting time of CW/MW-BB samples (w/b=0.4 and w/b=0.45). 120
Table 4.18. Experimental parameters of the selected samples of CW/MW-BB. 129
Table 4.19. Flow diameter values (mm) of BFS/CW/MW-TB samples for w/b=0.4 and w/b=0.45. 131
Table 4.20. Setting time of BFS/CW/MW-TB samples (w/b=0.4 and w/b=0.45). 135
Table 4.21. Optimum combinations of the selected mixtures in the first three parts for mechanical properties 145
Table 4.22. Dry bulk density, apparent density and volume of voids of selected sample. 153
Table 4.22. FTIR results of BFS-Raw and both BFS-UB samples obtained in this study and their comparisons with the literature. 186
Table 4.24. FTIR results of CW-Raw and CW-UB obtained in this study and their comparisons with the literature. 191
Table 4.25. FTIR results of MW-Raw and MW-UB obtained in this study and their comparisons with the literature. 197
Table 4.26. FTIR results of BFS/CW-BB obtained in this study and their comparisons with the literature. 201
Table 4.27. FTIR results of BFS/MW-BB obtained in this study and their comparisons with the literature. 207
Table 4.28. FTIR results of CW/MW-BB obtained in this study and their comparisons with the literature. 214
Table 4.29. FTIR results of BFS/CW/MW-TB obtained in this study and their comparisons with the literature. 220
Table 4.30. Cost analysis of calculation table. 224
Table 4.31. Cost values of cement and ternary sample binder. 225

1. INTRODUCTION

Concrete is the most commonly used construction material. Its use by communities across the globe is second only to water. Customarily, concrete is produced by using Ordinary Portland Cement (OPC) as the binder; a highly energy intensive product which releases carbon dioxide (CO_2) [1]. OPC is the most widely used material for construction of built infrastructure on a global basis; and is primarily composed of mined materials which include: limestone, sand, and clay that are heated in a kiln to be processed for use [2]. Cement manufacture is a three-stage process: raw materials preparation, clinker production and clinker grinding with other components to produce cement as shown in Figure 1.

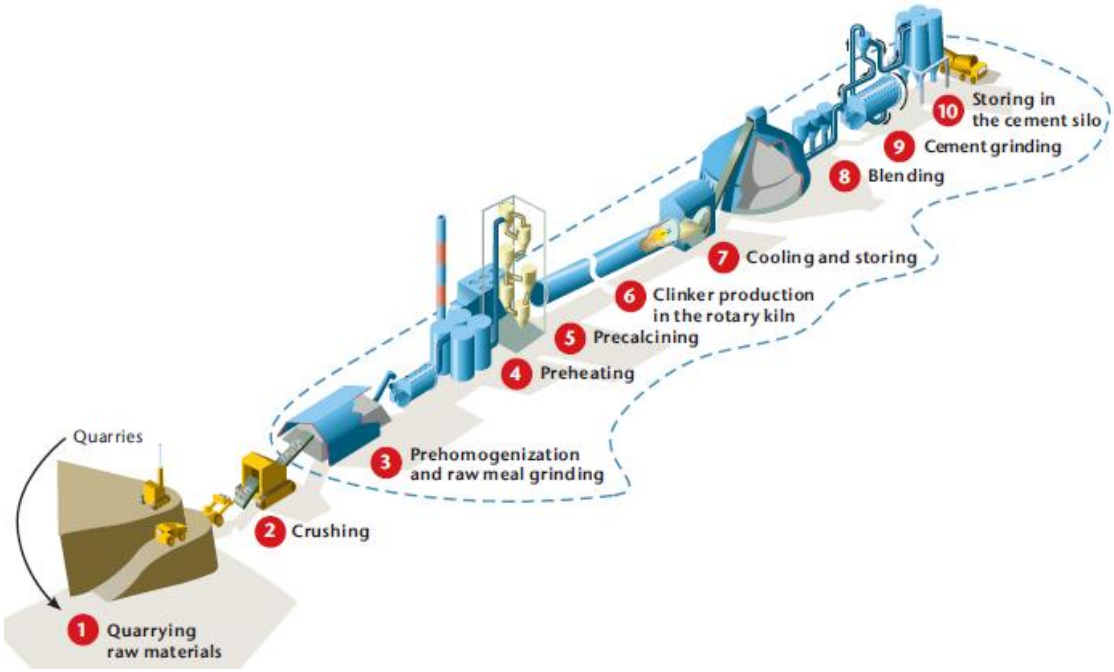


Figure 1.1. Cement manufacturing (Dry Process) [3].

There are two basic types of clinker production – "wet" or "dry" – depending on the moisture content of raw materials, and there are also different kiln designs. The wet process consumes more energy than the dry process, as the moisture needs to evaporate.

The cement sector is the third-largest industrial energy consumer and the second-largest industrial CO_2 emitter globally. Expected cement production quantity by region presented in Figure 2.

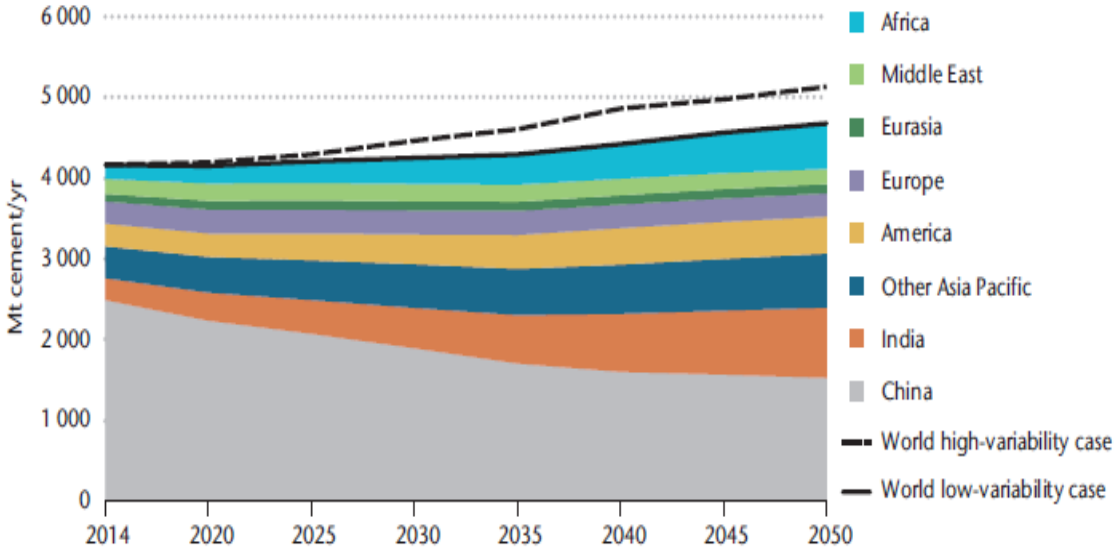


Figure 1.2. Expected cement production by region [3].

According to this figure, overall cement production in Asia Pacific remains stable over the analyzed horizon. Expected cement production growth in India (triple its current production level by 2050) and Other Asia Pacific countries (double current production levels by 2050) represents more than 90% of the envisioned decrease in cement production in China over the same period. Chinese cement production is set to lose 27% of the global cement production share in the process of adjusting national production capacity to domestic cement needs by 2050. The rest of the additional foreseen global cement production increase is in Africa (more than triple its current cement production level by 2050) and America (almost double its current cement production level by 2050), to support domestic growing demand. Rising global population and urbanization patterns, coupled with infrastructure development needs, drive up the demand for cement and concrete and increase pressure to accelerate action in reducing the carbon footprint of cement production. Under a scenario that considers announced carbon mitigation commitments and energy efficiency targets by countries, the cement sector would increase its direct CO_2 emissions just 4% globally by 2050, for an expected growth of 12% in cement production over the same period [3]. To contribute to sustainable development, the cement industry (in general) has assumed two important challenges in recent years. The first one is to reduce particle and gas emissions. The second one involves assuming the Kyoto Protocol commitments, striving to reduce greenhouse gas emissions by establishing measures in the processing stage and

implementing clean development mechanisms [4]. Therefore, the development of new binders that can be substituted for cement has an utmost importance in terms of energy saving, the conservation of natural resources, and the reduction of environmental pollution.

Alternative binder material or cement may be produced by some waste materials, which consist of vast amount of silica and is activated using alkali solutions, have been recently examined in the related academic literature. This is because these new types of binders provide considerable economic and environmental (AAB/AAC) usually have better durability properties than cement added building materials. For instance, alkali-activated cements usually consist of two components: a cementitious component and alkaline activators. Caustic alkalis or alkaline salts are normally used as alkaline activators in alkali activated cements and concretes. A variety of industrial by-products and waste as well as a number of alumina-silicate raw materials has been used as the cementitious components in alkali-activated cements and concretes. These materials include industrial wastes such as granulated blast furnace slag, granulated phosphorus slag, steel slag, coal fly ash, volcanic glass, silica fume and non-ferrous slag or as minerals like zeolite and metakaolin [4].

Using the composition of the cementitious component(s) as a criterion, alkali-activated cements can be classified into five categories [5]:

1. alkali-activated slag-based cements
2. alkali-activated pozzolan cements
3. alkali-activated lime-pozzolan/slag cements
4. alkali-activated calcium aluminate blended cements
5. alkali-activated Portland blended cements (hybrid cements)

In theory, materials that include silica and alumina can be activated by alkali solutions. In previous studies on this topic, (i) kaolinitic clay, (ii) metakaolin (MK), (iii) fly ash (FA), (iv) blast furnace slag (BFS), and (v) binary and/or ternary mixes of these materials have been employed. In many past studies about the production of binders without PC, alkali-activated industrial wastes (i.e., BFS and FA) have been produced. In the current practical applications in the industry, some wastes are used instead of PC to some extent in the production of concrete. However, because of enormous production

amounts of industrial wastes used in concrete, it seems impossible to exhaust or end these wastes by using them in concrete. It corresponds to 20-30% of these wastes only. This leads to storage problems due to other related technical and economic problems, and the environmental pollution. Besides some industrial waste materials (i.e., MK, FA, and BFS) used for the alkali activation, there are also some other industrial waste materials (that is, ceramic and marble) produced in large amounts. These latter wastes can be activated by alkalis as they have similar characteristics with former wastes in terms of their chemical contents such as silica, alkali, and CaO. In addition, it can be predicted that ceramic and marble waste can be activated by alkali activators because of their oxide contents such as silicon dioxide (SiO_2), aluminum oxide (Al_2O_3) and CaO) of these wastes similar with oxide contents of fly ash and blast furnace slag, respectively.

1.1. Hypothesis of thesis

Cement is an industrial product that releases a very high CO_2 emission to the nature and the environment during its production and has a high energy cost. Considering the harms and the hazardous effect of the environment and human health, research and production of environmentally friendly, sustainable binder types that can be used instead of cement in recent years are among the attractive research subjects. The hypothesis of this thesis is to produce alternative and environmentally friendly binders that can be used instead of cement by using solutions with high alkali content processed at relatively low temperature from some industrial waste or secondary by-products that create extra costs for storage and disposal occurs in the industrial environment and are harmful to the environment. Thus, it is anticipated that projected binder may cause reduction in CO_2 emission and energy cost and also it would be more sustainable than cement and having similar and/or superior binder types in terms of the mechanical and durability properties of the cement.

1.2 Objectives of the study

Within the scope of this thesis, it is mainly based on the idea that some industrial waste materials contain high content of SiO_2, CaO and/or Al_2O_3 in their chemical composition

which can be used as raw/constituent material after activation process by alkali activators for alternative binder production. Therefore, it is aimed to produce unary, binary and ternary binders by activating the blast furnace slag, ceramic and marble wastes with alkali activators such as sodium hydroxide (NaOH) and sodium silicate (Na_2SiO_3).

The objectives of the thesis are listed below,

- To produce alternative binders from waste/by-products (Blast Furnace Slag (BFS), Ceramic Waste (CW) and Marble Waste (MW)) remaining widely after the industrial production processes by alkaline activation method which involves activation by using alkaline mixed solutions (NaOH and Na_2SiO_3).
- To investigate of usability and comparison of the binders produced as a binding material that can be used instead of the cement in this study in terms of mechanical, physical, durability characteristics and microstructural examination.
- To determine the effects of the industrial wastes used in the scope of the thesis as raw materials of binders in unary, binary and ternary mixtures.
- To understand the effects of CW and MW on the alkali activation of BFS in binary and ternary binders.

1.3 Organization of the thesis

In this study, a six-stage program was experimentally performed.

1) Production of unary binder samples and determination of optimum experimental parameters for unary binder systems

   In the first stage, BFS, CW and MW were activated with alkaline solutions separately (NaOH and Na_2SiO_3) to produce unary binders.

2) Production of binary binder samples and determination of optimum experimental parameters for binary binder systems

   In the second stage, binary mixtures consisting of BFS-CW, BFS-MW and finally CW-MW were produced. Blend ratios were used as 25%, 50% and 75% in all binary mixtures. Thus, in addition to the other optimum experimental parameters,

the mixing ratio which reveals the most suitable composition for the binary mixtures is determined at the end of this experimental set.

3) Production of ternary binder samples and determination of optimum experimentally parameters for ternary binder systems

   In the third stage, four types of ternary binders were produced. In the first type, the percentage of BFS, CW and MW in the mixture is equal, whereas second type of ternary binder consists of 50% BFS, 25% CW and 25% MW. In the third type of ternary binder consists of 25% BFS, 50% CW and 25% MW whereas second type of ternary binder consists of 25% BFS, 25% CW and 50% MW.

4) Determination of the optimum paste samples for physical and mechanical properties in the first three stages

   In the fourth stage, the secondary experimental part that consists of compressive & flexural strength tests (for curing time of 1, 7, 14, 28, 56 and 90 days), water absorption test, determination of density and porosity test was also carried out for the determination of optimum physical and mechanical properties of selected unary, binary and ternary paste samples.

5) Determination of durability characteristics for the most suitable paste samples to be obtained in the first three stages.

   In the fifth stage, the third experimental part consisting of drying shrinkage, resistance to sulphate and sulfuric acid effect and high temperature effect tests were conducted in order to determine the durability characteristics for the most suitable paste samples to be obtained in the first three stages.

6) Determination of microstructural characterization for the most suitable paste samples to be obtained in the first three stages.

   Finally, in the sixth stage, SEM-EDS (Scanning Electron Microscopy), XRD (X-Ray Diffraction) and FTIR (Fourier Transform Infrared Spectrophotometer) analyzes were performed for the microstructural characterization of the most appropriate paste samples to be obtained in the first three stages.

2. LITERATURE REVIEW

2.1. General

Considering the 180 years of established history of Portland cement, it is clear that it is the main binder used for concrete production in the construction sector. Because of the Portland cement is both easy and abundant availability of raw materials and superior in mechanical and durability properties, it is still the most consumed binder type in the construction industry in the world. As of 2018, the total amount of cement produced worldwide is approximately 4 billion tons in each year [6]. About 60 million tons of cement is produced in Turkey [7]. In addition to this, cement production is a sector that creates 7-8% of the annual total CO_2 gas emissions and requires 12-15% of the total industrial energy need in the world [8-9]. Cement production and emissions values was depicted in Fig.1 between the year of 2010 and 2015. When all these numerical values are evaluated, it is clear that construction and cement sectors need alternative energy, fuel and raw material due to the technical, economic and environmental factors.

Because of the large energy demand and high amount of CO_2 release in Portland cement production, next generation of binder production have brought forward with recycling of other industrials wastes. At the present time, industrial wastes can be used such as fly ash, blast furnace slag, silica fume in cement and in concrete production. However, the use of these wastes in the cement has only been realized as additive material at certain ratios. For this reason, the production of binders using almost all or fully recycled waste is one of the alternative binder production methods that have recently attracted attention but have not been yet realized so far [10]. Therefore, there has been many ongoing research on them.

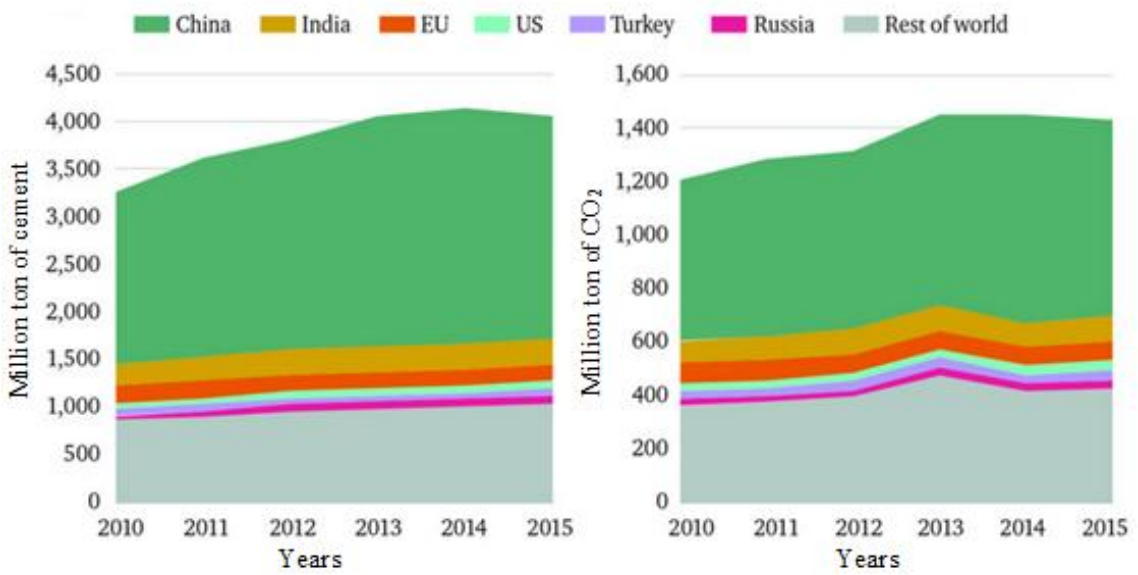


Figure 2.1. Cement production and emissions values between 2010 and 2015 years. [11].

When all these factors are evaluated, the question that this thesis will try to answer; Could it be possible to produce new generation binders in replacement of Portland cement produced by using blast furnace slag, ceramic waste and marble waste alone activated by alkaline activators (sodium silicate and sodium hydroxide). In this way, the effects of these wastes on blast furnace slag will also be observed. It is anticipated that these wastes (ceramic and marble) will have positive effects on drying shrinkage and strength properties of new mortar samples produced as a result of activation of blast furnace slag with alkaline solutions. Other expected improvements or contribution of this thesis is to obtain better new mortar performance produced by waste materials and could likely to increase the waste recycling and thus are reduced the environmental impact of wastes.

Alkali activated cements are binder materials produced by the alkali activation of certain industrial wastes or by-products (fly ash, metakaolin, blast furnace slag, kaolin clay, red mud, etc.) with alkali solutions [12-16]. Recently, in addition to these waste materials, natural pozzolans are also activated by alkali solution to produce the new binders [17]. New generation binders (alkaline activated mortar/cement) produced by alkali activation process of these alkali sources are superior to Portland cement in terms of less energy consumption and relatively less CO_2 release. In addition, it is also known that the mortar samples produced using these new generation binders have superior

mechanical and durability properties than the mortar samples produced with Portland cement [18-20].

In this study, three different raw materials and two different types of alkali activators were used. These source raw materials were blast furnace slag, ceramic waste and marble waste. The type of activator to be used in the project was a mixture of sodium hydroxide and sodium silicate solutions. As a result of literature survey of previous studies, the selected activator mixture was most preferred type of activator mixture in the literature due to ıts positive contributions in the strength and durability properties of the material in activation of blast furnace slag, metakaolin and fly ash [15, 21].

2.2. Development of Alkali Activated Binder Systems

Alkali-activated binders receive increasing attention as an alternative to Portland cement because of their high strength and durability and low environmental impact. Reported studies in the literature based on alkali-activated binders are made by mixing solid aluminosilicate powders such as fly ash, blast furnace slag, or metakaolin with an alkaline activating solution. The reaction product, or gel, can have a network structure similar to those of organic thermoset polymers, and thus the binders are sometimes called “inorganic polymers” or “geopolymers” [22].

The historical background about important events in the field of alkali-activated binders was given in Table 2.1. Purdon studied alkali activated slag with sodium hydroxide in the 1940s and he make a great contribution on production alkali-activated binders [23]. However, Glukhovsky investigated a new type of binders that called as ‘‘soil–cement’’ [23]. The ‘‘soil–cement’’ was obtained from ground aluminosilicate mixed with rich alkalis industrial wastes. He concluded that they were composed of aluminosilicate calcium hydrates similar to the ones of Portland cement and also of crystalline phases of analcites, $Na(AlSi_2O_6)$. H_2O, a natural rock that would explain the durability of those binders [23]. After 15 years, French scientist Davidovits developed and patented a binder obtained from the alkali-activation of metakaolin, having named it after the term ‘‘geopolymer’’ in 1979 [23]. According to Davidovits, geopolymers are polymers because they transform, polymerize and harden at low temperature. But they are also geopolymers, because they are inorganic, hard and stable at high temperature and also

non inflammable [23]. According to that author, the new binder is generated by an adjustment of the

Table 2.1. Bibliographic history of some important events about alkali-activated binders [24].

Author	Year	Significance
Feret	1939	Slags used for cement
Purdon	1940	Alkali-slag combinations
Glukhovsky	1959	Theoretical basis development of alkaline cements
Glukhovsky	1965	First called ‘‘alkaline cements’’
Davidovits	1979	‘‘Geopolymer’’ term
Malinowski	1979	Ancient aqueducts characterized
Forss	1983	F-cement (slag-alkali superplasticizer)
Langton and Roy	1984	Ancient building materials characterized
Davidovits and Sawyer	1985	Patent of ‘‘Pyrament’’ cement
Krivenko	1986	DSc thesis, R_2O–RO–SiO_2–H_2O
Malolepsy and Petri	1986	Activation of synthetic melilite slags
Malek. et al.	1986	Slag cement-low level radioactive wastes forms
Davidovits	1987	Ancient and modern concretes compared
Deja and Malolepsy	1989	Resistance to chlorides shown
Kaushal et al.	1989	Adiabatic cured nuclear wastes forms from alkaline mixtures
Roy and Langton	1989	Ancient concretes analogs
Majundar et al.	1989	$C_{12}A_7$ – slag activation
Talling and Brandstetr	1989	Alkali-activated slag
Wu et al.	1990	Activation of slag cement
Roy et al.	1991	Rapid setting alkali-activated cements
Roy and Silsbee	1992	Alkali-activated cements: an overview
Palomo and Glasser	1992	CBC with metakaolin
Roy and Malek	1993	Slag cement
Glukhovsky	1994	Ancient, modern and future concretes
Krivenko	1994	Alkaline cements
Wang and Scrivener	1995	Slag and alkali-activated microstructure

Process which had used by the Roman and the Egyptians. Davidovits even suggests that the pyramids were not been made with natural stone but were made of man-made binders instead. Based on chemical and mineralogical studies he stated that the pyramid blocks were made of a mixture, with limestone sand, calcium hydroxide, sodium carbonate and water [23].

2.3. Alkali Activated Blast Furnace Slag Binders

Blast furnace slags are emerged as an industrial by-product during iron production in blast furnaces. During the production of pig iron, considerable amounts of blast furnace

slag are formed. Blast furnace slag, which has an amorphous structure, exhibits pozzolanic properties due to the presence of CaO and SiO_2 in high amounts. It is also similar to Portland cement in terms of its high pH value and its CaO content. Blast furnace slags can be reacted and activated pozzolanically when used with effective and sufficient catalysts such as alkaline salts [25].

Numerous studies have been carried out so far on the activation of blast furnace slag with alkali solutions. One of the pioneering study was conducted by Purdon [23]. In his study, new generation of binder was produced by activated blast furnace slag and lime with alkaline solutions which was particularly strong in terms of mechanical strength in 1940. Some of the previous studies have included workability, mechanical and drying shrinkage properties of binders that was produced by the activation of blast furnace slag with alkali solutions [18, 26-32].

The strength properties, microstructural investigations and behavior under high temperature of these new generation binders have also been the subject of many studies [33-37]. Although there have been so many studies on the activation of blast furnace slag, there are several disadvantages of activated slag, such as activated marble sludge, micro-crack formation following rapid set-up and high drying shrinkage [38-40]. In this thesis, these aforementioned drawbacks of the activated slag will be studied and an attempt will be made to improve the properties of activated slag in the binary and ternary alkali-activated mixtures. These mixtures are going to be prepared mainly by activated blast furnace slag, ceramic waste and marble waste and by the incorporation of these wastes together.

In the scope of the thesis, the mortar samples to be produced by alkaline activation of the blast furnace slag alone will be the control sample for the mortar samples to be produced with other waste types in the study.

The main concern that will be the basis for this study are production of alternative binders that can be used in place of cement by using these wastes alone and by replacing these wastes with blast furnace slag in binary and triple alkali activated mixtures. In addition, the effects of these wastes on the strength and drying shrinkage properties of the blast furnace slag will also be determined. Limited number of studies have been published in the literature review related to these subjects. These studies in the related

literature are summarized below. First of all, the ceramic and marble waste alone was investigated to find out whether they could be activated or not with alkaline solutions.

2.4. Alkali Activated Industrial Waste Binder Systems

2.4.1. Alkali activated ceramic waste binder

In this study, porcelain and vitreous waste will be used as ceramic waste. Limited studies have been found in the literature related to alkali activation of ceramic waste alone. A total of six studies have been found in which such ceramic wastes are singly activated [41-46]. Five of these publications were carried out by the same scientists [41-45]. Reig et al. activated clay bricks and porcelain ceramic wastes by sodium hydroxide (NaOH) and sodium silicate (Na_2SiO_3) solution mixes to produce the binders [41]. They studied the effect of the type and dosage of activator on the binder prepared waste clay bricks activated with an alkaline solution mixture [42]. Furthermore, the same research group investigated the effects of calcium dosage and alkali activator concentration on plastic behavior, mechanical and microstructural properties of alkali activated porcelain ceramic waste mortar [43]. As a result of these three studies, the highest compressive strength value of 41 MPa of the mortar produced from the brick waste was obtained at a Na^+ concentration of 7 kg/mol, when the highest compressive strength value of 30 MPa produced by mixing the porcelain waste with the alkali activator solution was tested by using 9 kg/mol Na^+ concentration. It was observed that as the sodium concentration increased, the material density increased and the porcelain waste had a more compact structure than the brick waste at different sodium concentration values [41]. In addition, it was found that the highest compressive strength value was achieved for 5 mol/kg Na^+ without using sodium silicate and keeping the w/b (water/binder) ratio at 0.45. As a result of SEM, XRD and FTIR analysis, it was determined that the crystalline quartz and mullite structures detected in the raw material preserved their existence after alkali activation process. This situation showed that the main crystal phases in the raw material did not react or reacted only partially during the alkaline activation process [42, 43]. However, it was observed that the amorphous phase such as alumina silicate gel and calcium silicate hydrate gel (C-(A)-S-H)), concentration obtained after the activation increased compared to the raw material in the samples with

high sodium concentration. This also explained the increase in compressive strength in samples with high sodium concentrations [43]. In the third study [43] by the same research group found that the setting of the binder produced can only be achieved by $Ca(OH)_2$ addition at a certain level (2 wt. %). It was observed that the ratio of the most suitable alkali solution (Ms: SiO_2/Na_2O) to be used for the activation of the porcelain waste was between 1 and 2.5 and the compressive strength value was increased as the sodium concentration of the mixture increased when the calcium ratio (Ca^{+2}) was kept constant. According to mineralogical XRD analysis result throughout the microstructure revealed quartz and mullite phases which were determined as the main crystal phase before and after the activation process. In addition to, it was noted that Ca^{+2} and Na^{+} replaced each other to produce amorphous reaction product in alkali activation systems. This reaction product expressed as "C, N-(A)-S-H (C: CaO, N: Na_2O, A: Al_2O_3, S: SiO_2)". But $Ca(OH)_2$ or the presence of a newly formed crystal phase was not found in this study [43].

Reig et al studied the effect of calcium aluminate cement (CAC) additions on the alkali activation of red clay brick waste (RCBW) at room temperature and at 65°C. RCBW was partially replaced with CAC (0-50 wt. %) and blends were activated with NaOH and sodium silicate solutions. The compressive strength measurement was performed on mortars and the nature of the reaction products was analyzed by infrared spectroscopy, X-ray diffraction, thermo-gravimetric analysis, microscopic examination studies and pH measurements. The results show that the use of CAC accelerates the activation process of RCBW so that 50 MPa were obtained in the blended mortars containing 40 wt. % CAC cured for 3 days at room temperature. CAC did not undergo normal hydration and only the C_3AH_6 phase was identified in the pastes blended with more than 30 wt. % CAC and cured at 65°C, while the main reaction product was a cementitious gel containing Ca and Al from CAC [44].

In the last study of Reig et al. tile ceramic waste (TCW) was used as both a recycled tile ceramic waste aggregate (TCWA) and a tile ceramic waste precursor (TCWP) to obtain a binding matrix by the alkali-activation process. Mortars with natural siliceous (quartz) and calcareous (limestone) aggregates, and with other ceramic waste materials (red clay brick (RCB) and ceramic sanitary ware (CSW) waste), were also prepared for the purpose of comparison. The compressive strength of the mortars prepared with TCWA

progressively increased with curing time revealing 53 MPa at 65°C for 28 days. 50 wt% proportion of TCWA was observed as an optimum for the limestone/TCWA mortars which revealed ≈43 MPa, for 3 days at 65°C, whereas the compressive strength of that sample prepared with siliceous particles measured as 10 MPa. After a progressively increased TCWA content, up to 100 wt% substitutions, compressive strength of 23 MPa was obtained. Limestone particles interacted with the binding matrix, and played an interesting beneficial role at the 20°C curing temperature, with a slight reduction in compressive strength when cured long term for 28 days at 65°C. The results demonstrated promising output and a potential added value for these ceramic waste materials [45].

The last study on the activation of ceramic wastes alone, the ceramic wastes were activated by mixing of alkali solutions consisting sodium silicate, sodium hydroxide (NaOH) and potassium hydroxide (KOH) prepared at different ratios and the high temperature performance of the produced binder was investigated [46]. In this study, the highest compressive strength value was observed on the mortar sample produced by the activation of ceramic waste using with activator solution mixture consisting of KOH, NaOH and sodium silicate. This result is explained by the fact that the presence of a proper amount of soluble silicon in the alkali solution is caused improvement in the compressive strength properties of the mortar. Accordingly, it has been concluded that silicate solutions have more positive effects on mechanical properties than hydroxide solutions in production of alkali activated binder. In order to investigate the effect of high temperature on the compressive strength of mortar, samples were heated to different temperature values between 100-1000°C and their compressive strength values were determined. After a sudden decrease in compressive strength due to the evaporation of the structural/physical water in the specimen at about 100°C, a gradual increase in compressive strength was observed with increasing temperature. It has been observed that this increase in compressive strength occurs as a result of the geopolymerisation reaction and the condensation effect of the internal structure of the sintered mortar. As a result of the TG-DSC analysis, it was noted that a mass loss of about 9% occurred between 40-1100°C and 88% of this mass loss was below 250°C. In the SEM, XRD and FTIR analyzes, it was determined that the main phases formed before and after exposure to high temperature in the samples were quartz and albite. In

addition, it was reported that in the samples exposed to high temperature, geopolymerisation increases especially above 1000°C and with much more compacted structure and compressive strength is improved by the effect of viscous sintering process [46].

In the literature, there are studies about activation of ceramic waste with other precursor materials. Huseien et al. presents the experimental findings of a study on the performance of waste ceramic powder (WCP) as binder on the mechanical and microstructure properties of alkali activated mortars (AAM) containing ground blast furnace slag (GBFS) and fly ash (FA) [47] and they reported the effects of high volume waste WCP addition on the mechanical and microstructure properties of AAM exposed to elevated temperatures [48]. As a result of these studies, test results indicated that high volume WCP produced environmental friendly alkali activated mortars with compressive strength value of higher than 70 MPa for 28 days curing and they concluded that the workability and setting time of alkali activated mortars enhanced with the increase in WCP content [47]. And also, the fire resistance of the proposed AAM which subjected to elevated temperatures was enhanced with the increase WCP contents from 50 to 70%. Furthermore, the replacement of GBFS by FA in the ternary blends led to the reduction of the mortar deterioration up to 900°C. In addition, they are investigated the impacts on sustainability of waste WCP based AAM incorporating FA as a replacement of GBFS, which were exposed to various harsh environments. The findings suggested that freezing-thawing resistance increased and better durability was observed by increasing the FA content in AAM. Furthermore, AAM with high FA content led to enhance the performance in terms of sulphate and acid environments and elevated temperatures. Apart from the increased durability, replacing GBFS with FA also resulted in decreased energy consumption, AAM cost, and CO_2 emission [49].

In addition to all these studies, Abdollahnejad et al. conducted research on combination of ceramic waste and ground-granulated blast furnace slag in the preparation of one-part alkali-activated binders. Moreover, the effect of fiber type and content on hardened-state properties and shrinkage were studied under two different curing conditions. The experimental results showed that fibers improved mechanical properties, and enhancement was governed by fiber type and curing conditions [50].

When these all studies on the activation of the ceramic waste are evaluated, it is understood that these waste types can be activated with alkaline activators and mortar samples having improved properties in terms of strength and durability can be produced.

2.4.2. Alkali activated marble waste binder

During the literature survey, only one publication was found for one-component alkali activation of marble waste [51]. Cappola et al was aimed to activate the waste marble sludge using alkali activators under different curing conditions (air, moisture and water). In addition, the effect of SiO_2 from waste glass on the activation of marble waste was investigated by adding waste glass powder (2% and 5%). Sodium hydroxide and sodium silicate mixture was used as alkali activator. The w/b ratio used in the experiments was 35%. Waste marble mud had a calcite ($CaCO_3$) structure and for raw material characterization of marble sludge, XRD, XRF, Particle Size Distribution and SEM techniques were employed. Microstructural, physical (drying shrinkage, FT-IR spectroscopy, X-ray spectroscopy, DTA-TGA and mechanical (flexural and compressive strength) properties were also investigated. Air curing was the most favorable curing condition for mechanical properties development (compressive strengths ranging between 38 and 45 MPa after 28 days of curing were measured).

There were different aspects to the activation of marble waste carried out within the scope of this thesis from the work of Cappola et al [51]. For example, in this thesis, rate of activator solution for marble waste activation used in the activation by 3 different “n” and 3 different “Ms” ratios. But, Cappola et al reported that the rates (n and Ms) used for activator solution were not variable. In addition, the workability properties of fresh paste samples produced in this study were not performed. In this thesis, the workability properties of alkali activated marble sludge in fresh state were determined. The w/b ratios and curing conditions that we used in our study were also different from the study conducted by Cappola et al.

Because of limited publication in the literature regarding alkali activation of direct marble waste alone. Therefore, it was decided in this study to work on alkali activation

of limestone or calcium carbonate minerals, which have very similar structure to the waste marble chemical structure.

Only one study was reported in the literature in which limestone has been activated alone [52]. In this study, alkaline cements were studied using limestone as the only precursor activated with solutions of sodium hydroxide and water glass; the activator was used at concentrations of 7 and 10%Na_2O using modules of Ms=0, 1 and 1.5. The compressive strength was measured on pastes and mortars for up to 360 days after an initial curing at 60°C for 24 h. For the pastes activated with 7% Na_2O, the highest compressive strength at 360 days was for paste P-7-1.5 with Ms=1.5, reaching 24 ± 2.28 MPa. This paper presented that limestone was a cheap and widely available precursor, so these binders could have a positive impact and promising alternative for Portland cement.

In another study carried out by Yip et al. [53] calcite and dolomite minerals (calcium carbonate containing minerals) have been substituted at a varying proportions (0-20-40-60-80-100%) as a raw material, like metakaolin, for the investigation of Ca^{+2} ion effect in the production of metakaolin-based geopolymer. Three different Ms ratios (1,2-1,5-2,0) were used in Yip et al's study. Thus, it was tried to determine how the strength and microstructure properties of the system change with high and low alkalinity ratios. As a result, it was observed that the alkali-activated binder produced from 100% calcite had a compressive strength of 9.3 MPa (after 28 days curing) in a high alkaline environment (Ms: 1,2). The highest compressive strength value (45.4 MPa) was obtained in the activation of a mixture of 20% calcite - 80% metakaolin for 28 days curing. Consequently, it was observed that as the calcite content in the mixture increased more than 20%, the compressive strength of the samples decreased.

Suhong et al. [54] investigated the thermodynamics of reactions between carbonatite which consists of calcite or dolomite and sodium silicate solution at ordinary temperature (25°C). The results indicated that the reactions taking place between dolomite, calcite and sodium silicate solution formed cementitious products of hydrated calcium silicate or hydrated magnesium silicate at ordinary temperature. Further, it was investigated that the dissociation degree of dolomite and calcite and the activity of sodium silicate solution were the key factors to influence the alkali activated reactions.

In this thesis, as well as the alkali activation of the marble waste by using alkaline activator solution containing sodium silicate and sodium hydroxide, the combination of binary and ternary blended activation with blast furnace slag and CaO and SiO_2 containing ceramic waste samples were produced. In this context, the combinations of marble waste, minerals with limestone and calcium carbonate content with other raw materials were also investigated during the literature survey.

Tekin [55] produced two different alkali activated pastes consisting of a kind of natural pozzolan zeolite minerals-volcanic tuff and a kind of zeolite minerals-marble waste (MW) with 1 M, 5 M and 10 M NaOH as alkali-activator. Zeolite minerals called Bayburt Stone waste (BSW) because of grounded in Bayburt region in Turkey. Curing process performed at 20, 45 and 75°C temperatures for 24 hours in an oven. And after that Geopolymer Polymer Composite exposed to wet and dry condition separately. The compressive strength tests were carried out on 2nd, 3rd, 7th, 28th and 90th days of curing period. TW and MW were substituted ratio of 20, 40, 60, and 80% in BSW. In the binary mixture of marble and BSW, the highest compressive strength value was obtained at 20°C for the mixture in which the marble waste was replaced by 20% in BSW.

There were also studies in which the limestone exists in the process of binary and ternary component and alkali activation together with blast furnace slag [56-58], blast furnace slag and fly ash mixture [59-60], metakaolin [61] and clay [62].

2.4.3. Alkali activated binary and ternary blended waste binder

In recent years, the activation of two and/or three component raw material mixtures (blast furnace slag/fly ash [63-66], blast furnace slag/metakaolin [21, 67-68], blast furnace slag/silica fume [69-70], blast furnace slag/fly ash/metakaolin [71-73], blast furnace slag/fly ash/silica fume [74] have attracted much interest by researchers as alkali activation and new binder production methods. In this thesis, an attempt will be made to answer the questions of what effects of ceramic waste and calcined marble waste on blast furnace slag in the alkali activation process of binary and ternary mixtures with each other. The results of various studies related to this subject in the literature were summarized in this section. High drying shrinkage and associated crack

formation of blast furnace slag in alkali activation process were known as a significant disadvantage compared with cement [29, 33]. It was expected that the alkali activation of binary and ternary mixes containing ceramic wastes increase the mechanical properties of blast furnace slag [42] and marble waste mixture decreasing the drying shrinkage [27, 75] which will be in the scope of this thesis. No alkali activated marble waste and with the ceramic waste together was found in the literature. However, in a study, when calcined marble powder was incorporated with clay, which is the basic raw material of the ceramic waste, calcium silicate and calcium alumina silicate bonds formed without firing (at low temperature: 110-120°C) [76]. As a result of this approach, it was believed that the marble waste can act as a source of active CaO component during alkali activation of ceramic waste to produce binding material.

Very limited number of studies reached in a literature review with regard to the alkali activation of these industrial wastes, which arise as a natural result of industrial production and cause great environmental and economic threats. All of these studies were summarized as a part of literature review. In addition to these limited studies in the literature also supported the originality of the thesis.

2.5. Selection of Alkali Activators, Variable Parameters and Additives

2.5.1. Alkali activators

The current knowledge about alkaline activators shows that the most appropriate activators are made of hydroxides and soluble silica. Despite the fact that the influence of sodium hydroxide concentration and the ratio water glass/hydroxide ratio is not completely understood, because it is not expected that when different prime materials were used, the optimum alkaline concentration and the optimum silica modulus remain the same [15].

Each precursor needs the appropriate activator (or combination of activators) to be identified, specified and sourced. There is currently little systematic or predictive information available regarding methodologies or heuristic procedures by which activators can be optimally matched to precursors, so this is currently achieved largely

through parametric testing, but the need for improvements in this area has been identified [77].

As an alkali-activators, the most commonly used compounds used are MOH and $M_2O{\cdot}rSiO_2$, where M is either Na or K [78]. In the light of this information, a mixture of sodium silicate and sodium hydroxide is used as the alkaline activator in this thesis.

2.5.2. Variable parameters

In the literature review, it was understood that there were some important parameters that directly affect the properties of final product in the production of alkali activated material. The most important parameters among them were i) "Ms" (SiO_2/Na_2O) and "n" (Na_2O/activator) values that vary with the content and amount of activator used, ii) water/binder ratio and curing conditions and finally iii) additives.

2.5.2.1. "n" and "Ms" values

The "n" value represents the ratio of total oxide in the activator, while the "Ms" value represents the ratio of silicon oxide and sodium oxide in the activator. In this study, the type of activator to be used for activation of all source materials was chosen to be the same. However, for the determination of the optimum amount of activator, three different Ms ratios and three different n values were used in preparing of the activator mixture. The selected activator type and Ms ratios were determined by considering the studies in the literature. When these studies were evaluated, it was observed that the Ms ratios used for alkali activation of the ceramic waste varied between 1-2.5 [43, 46]. In addition, the Ms values used for alkali activation of limestone were taken into account in the literature for Ms values used for alkali activation of the marble waste. This is due to the fact that no paper was found in previous studies reporting the alkali activation of the marble waste. In a single work only, 100% activation of limestone was achieved [53]. When these studies related with activation of limestone both alone and in replace the different source materials were evaluated, it was found that the Ms values change between 1.2-2 [53, 59].

2.5.2.2. Water/binder and curing conditions

In the method of producing binder materials by alkali activation, other factors affecting the properties of the final product are water/binder ratio and curing conditions. According to the literature review, it was determined that the water/binder ratio was selected between 0.35-0.40 for the activation of the ceramic waste [41, 44]. However, the studies about alkali activation of limestone have been taken as a reference. Because no study had been conducted on the activation of marble or calcined marble waste for the selection of water/binder parameter during activation of calcined marble waste [53, 75]. As a result, in this study the water/binder ratio has been selected for each combination considering the properties of the source materials.

When the curing conditions are determined, the chemical structures of the source materials to be used in the thesis and the previous studies in the literature are taken into consideration. It was reported that the alkaline activation of Al_2O_3-rich source materials leads to better results in an oven curing for a few hours [64], while for alkaline activation of CaO-rich materials, a few hours of holding time under steam curing has yielded much better results in terms of mechanical properties [10]. In this study, both curing methods have been performed for all component combinations. Consequently, steam curing for 4 hours and oven curing at 65°C for 4 hours were carried out for all combinations.

2.5.2.3. Additives

During the literature review, it was found that additives such as gypsum and lime which are commonly used in the construction sector and economically cheap and commercially available in large quantities have positive contributions to the binder production processes by the alkali activation method [30, 41, 79].

In this study, it was predicted that the activated slag, ceramic waste and marble waste sample would make a positive contribution to accelerate the hydration reaction, strength and durability properties. Therefore, during the experiments, the effects of lime that is used for the replacement by 4% of the total mass of the source materials were investigated on the mixture types having the most appropriate additive as experimental parameters.

3. MATERIALS AND METHODS

3.1. Raw Materials and Precursors

3.1.1. Properties of precursors and raw materials

In this study, three different main precursors (source/raw/constituents) materials and two different types of alkali activators were used. The names of these materials and their suppliers were listed in Table 3.1 and photographs of raw materials and additives were shown in Figure 3.1. The main purpose in this study are production of alternative binders which can be used instead of cement by alkali activation of ceramic waste (CW), marble waste (MW) and blast furnace slag (BFS) both alone and binary and ternary mixtures each other's. The pastes produced by alkaline activation of blast furnace slag were used as the control sample for the pastes produced with other types of wastes during the experiments. Prior to the experimental process, some analyzes were performed on all source materials for material characterization. In first of these experiments was X-ray Fluorescence Analysis (XRF) that determined the oxide quantities in the primary source materials. Then. X-Ray Diffraction (XRD) analysis was then performed to determine the crystal and amorphous structures of the materials. In addition. Blaine and pycnometer tests were applied on the source materials to determine the fineness and specific gravity, respectively.

Table 3.1. Raw materials used in this study and their suppliers.

Precursor (Raw) Materials	**Suppliers**
Blast Furnace Slag (BFS)	Kardemir Iron Steel Industry
Ceramic Waste (CW)	Filyos Fire Brick Factory
Marble Waste (MW)	Sancim Bilecik Cement & Concrete
Additive	
Lime (L)	Kimtaş Lime Industry- Supercalco (M)
Alkali Activator	
Sodium Hydroxide (NaOH)	Merck Chemical
Liquid Sodium Silicate	Merck Chemical



Figure 3.1. Photographs of raw materials and additive used in this study.

The chemical compositions. specific surface areas and specific gravity values of the raw materials are shown in Table 3.2 were determined by X-ray florescence analysis (XRF, Model: Panalytical Epsilon 5), BET (Model: Quantachrome Autosorb IQ) and ultra-pycnometer (Model: Ultrapycnometer 1200e), respectively. The basicity coefficient (K_b) of slag was equal to 0.73. Hydraulic module of slag was also equal to 1.18.

$$K_b = (CaO + MgO)/(SiO_2 + Al_2O_3)$$

$$H_M = (CaO + MgO\ + Al_2O_3\ )/SiO_2$$

The particle size distribution of raw materials were measured by particle size analyzer (Mastersizer 2000. Malvern Instruments). As shown in Figure 3.2. both powders (BFS and MW) presented a similar particle distribution with particles ranging from 1 to 100 μm whereas in CW particles are more coarser than the others with a d_{50}=30 micron. Both ceramic and marble waste materials had almost same particle size distrubition.

But, this caused the surface areas of ceramic and marble waste to be lower than the blast furnace slag (see Table 3.2.).

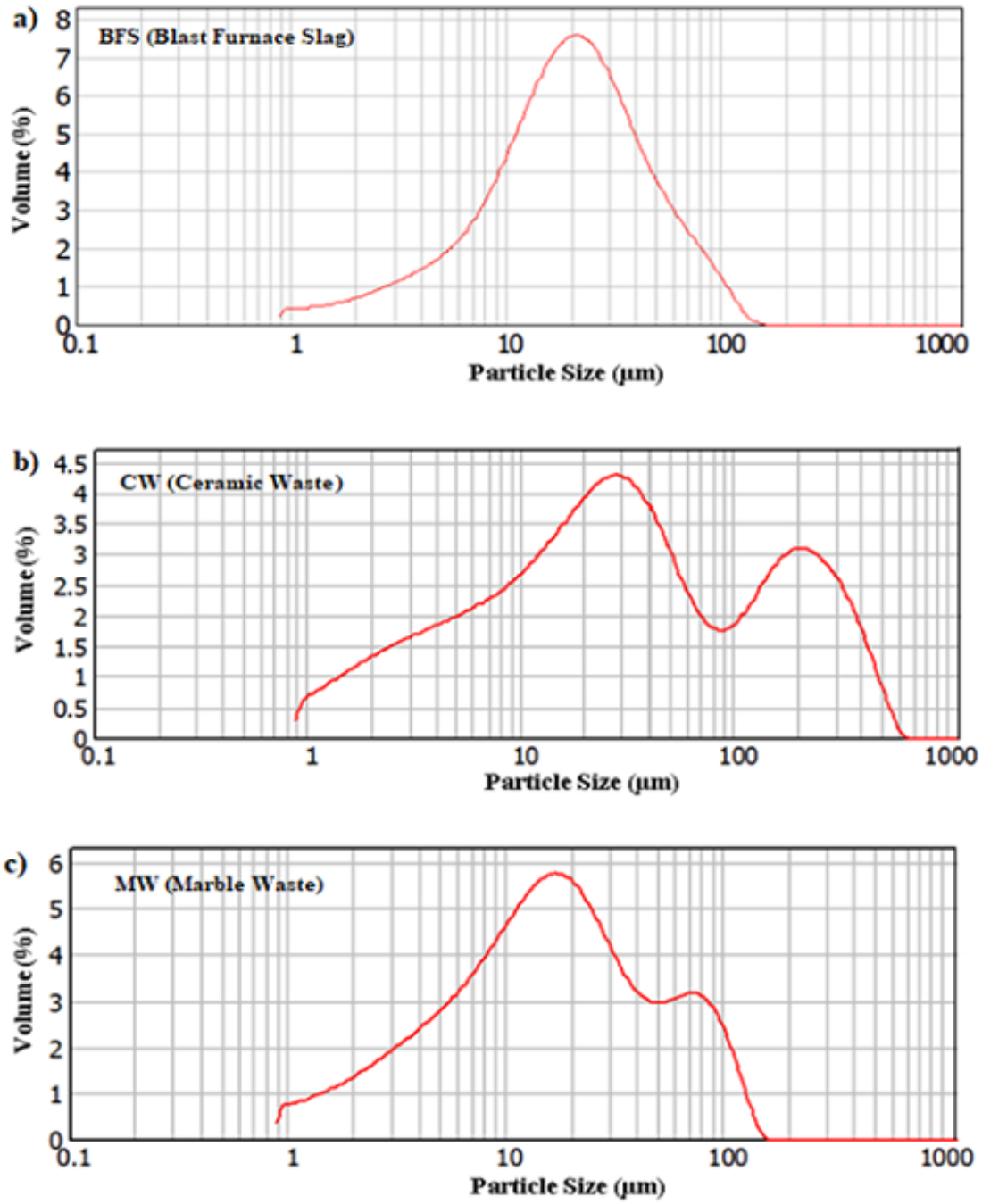


Figure 3.2. Particle size distribution of raw materials a) BFS b) CW c) MW.

Table 3.2. Chemical composition of raw materials performed by XRF analysis.

Oxides	BFS Wt.%	CW Wt.%	MW Wt.%	CEM 42.5 R (OPC) Wt.%
SiO_2	42.36	73.23	1.75	20.43
Al_2O_3	11.07	21.02	0.56	5.48
Fe_2O_3	0.79	-	0.29	3.27
CaO	31.16	2.26	-	63.8
MgO	7.82	-	-	1.69
TiO_2	2.34	1.25	0.001	-
Mn_2O_3	2.38	-	0.001	-
Na_2O	0.26	0.379	0.006	0,82
ZrO_2	-	1.07	-	-
$CaCO_3$	-	-	96.82	-
SO_3	-	-	-	2,81
Loss on Ignition	-	-	-	2.17
Specific Surface-BET (m^2/g)	0.93	4.29	10.16	0,32
Specific Gravity (g/cm^3)	2.72	2.09	2.43	3.09

The mineralogical compositions of raw materials were determined by X-ray diffraction (XRD. Panalytical Empyrean with Cu Kα radiation. 45 kV and 40 mA). The XRD analysis' patterns were shown in the Figure 3.3. Figure 3.4 and Figure 3.5 for BFS. CW and MW respectively.

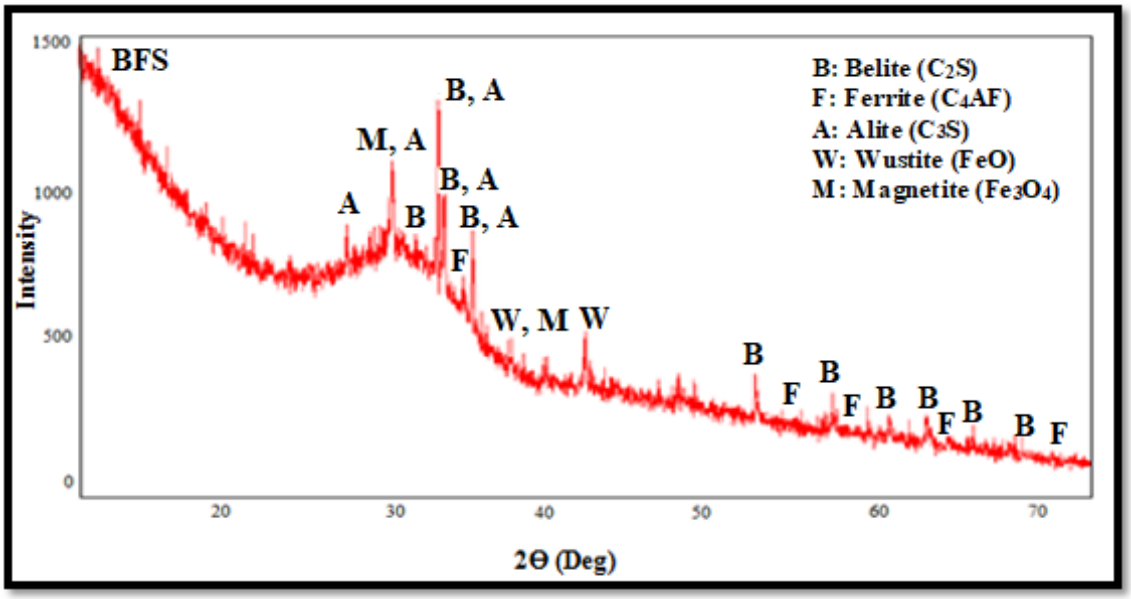


Figure 3.3. XRD patterns of BFS.

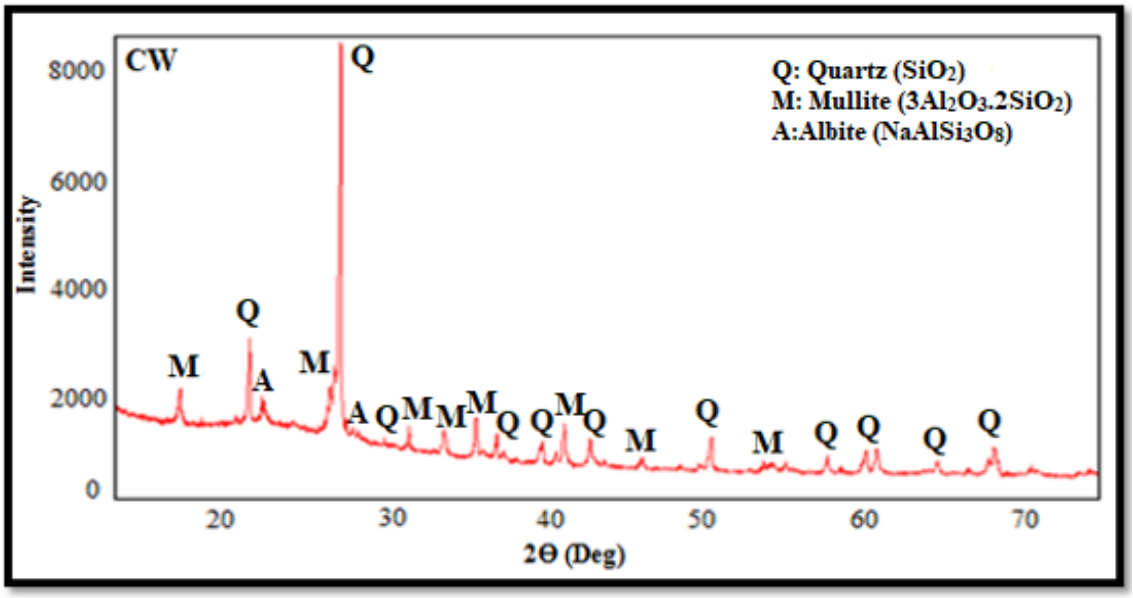


Figure 3.4. XRD patterns of CW.

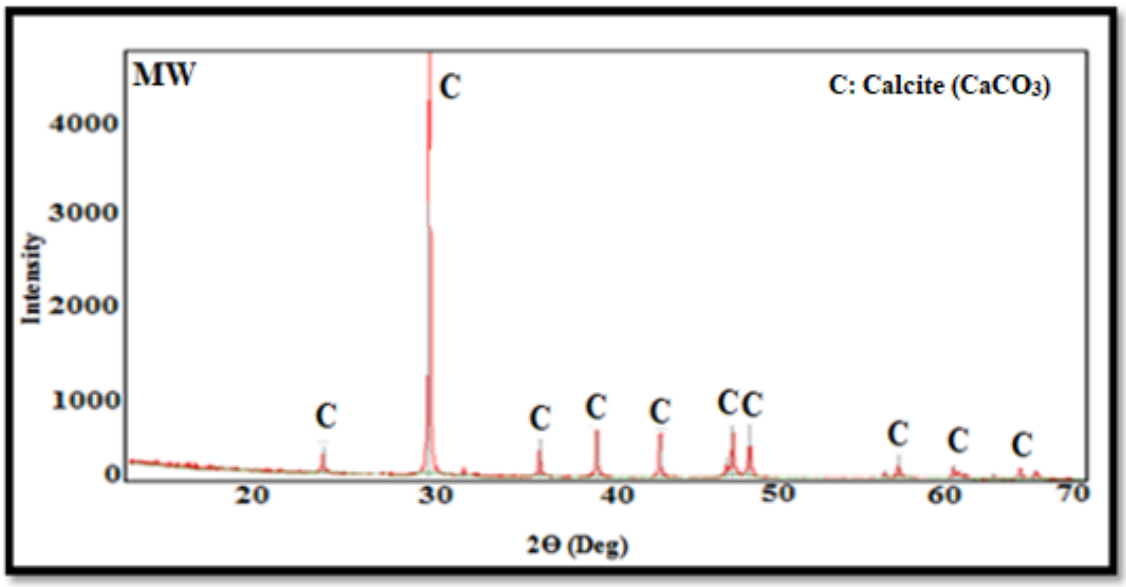


Figure 3.5. XRD patterns of MW.

The particle morphologies of raw materials were examined using scanning electron microscopy (SEM. Quanta FEG 450). While the SEM images of BFS and CW indicated mainly irregular and angular shaped particles, the SEM micrographs of MW exhibited a narrow particle size distribution as shown in Figure 3.6.

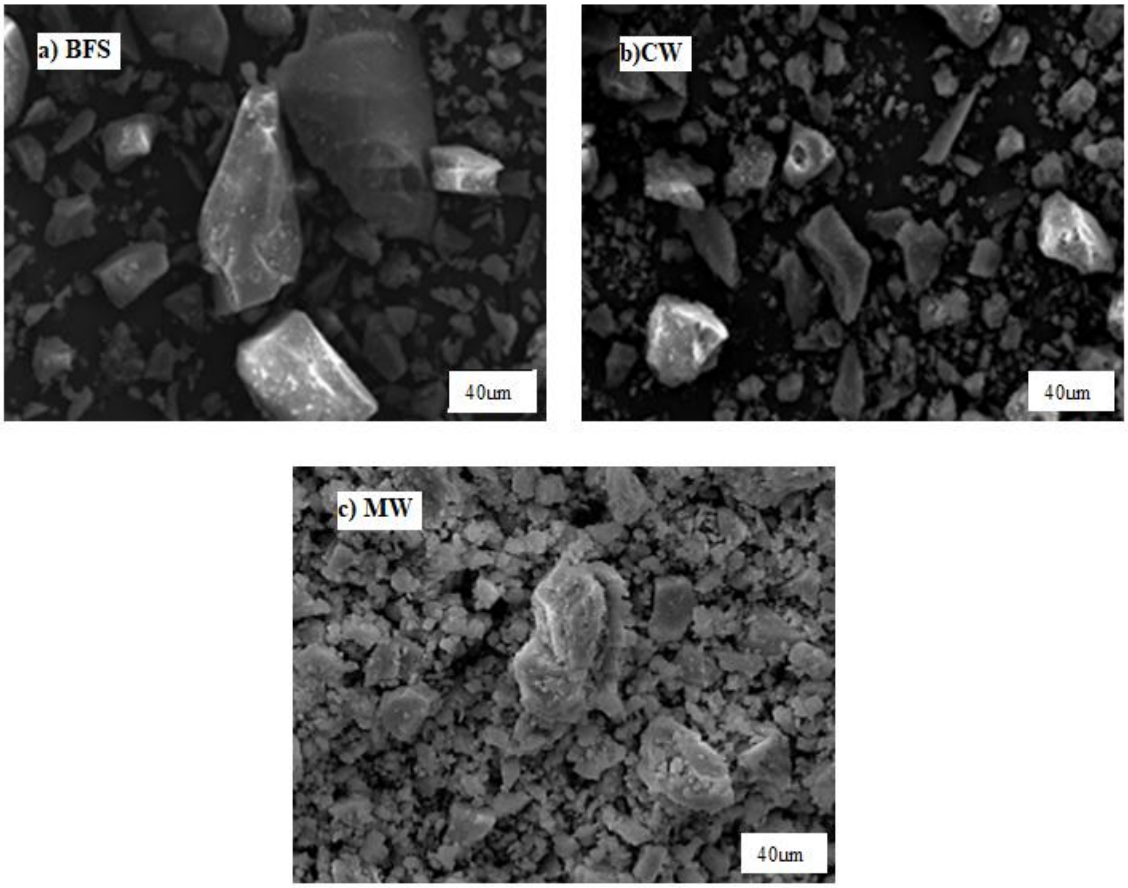


Figure 3.6. SEM images of source materials a) BFS b) CW c) MW.

3.1.2. Properties of additives (Lime)

The additive (main admixture) material used in this thesis was lime hydrate. In the construction sector, lime is the most preferred building material and produced according to certain standards (for lime: TS EN 13279-1) has been preferred. During the literature review, it has been found that additives such as lime, which is frequently used in the building material sector, is economically cheap and commercially accessible in abundance, has positive contributions to the binder production processes by the alkali activation method [27, 29]. In this study, it was decided that lime, especially alkali activated waste ceramic paste binder specimen, would contribute to accelerate the hydration reaction, so it was decided to use 4% of all mixture types in the experiments to be carried out in the first three stages.

3.1.3. Properties of alkali activators

During the experimental process, the same mixture of alkali activator solution was applied for all the sample types. This mixture was composed of sodium hydroxide and liquid sodium silicate. Liquid NaOH solution was prepared the day before mixing by dissolving the pellets in a predetermined amount of deionised water. For the two chemicals forming the alkali activator mixture, some limit values required in the experimental calculations are given in Table 3.3.

Table 3.3. Limiting values of used alkali activators in this study.

	Specification	**Limiting Values**
Sodium Silicate Solution (Extra Pure)	Na_2O (acidimetric)	7.5 - 8.5 %
	SiO_2 (acidimetric)	25.5 – 28.5 %
	Density (20^oC)	1.296 - 1.396 g/ml
Sodium Hydroxide Pellets	NaOH	≥ 98 %
	Molecular Weight	40 g/mol
	Used Molarity in this study	8 M

Pure water was used throughout the experimental part. The tap water distilled by water treatment devices used as pure water. Corresponding to the concentration of the alkaline activator added in a solution, the amount of water was varied to maintain a constant w/b ratio.

3.2. Methods

3.2.1. Types and properties of used binder mixes

When all the literature studies are evaluated, optimum "n" and "M_s" values, water/binder ratio, curing conditions and ratios of additives were determined as shown in Table 3.4 for the activation of blast furnace slag, ceramic waste and marble waste. In this study, three different "n" and "M_s"values were employed for each paste mixture. In addition to that, it was tried to determine the most suitable composition using with two different water/binder ratio and curing conditions.

Table 3.4. Types and properties of used mixes.

Type of Mix	Type of Activaor[2]	Total Na_2O/ Activator (n) (%w)[3]	SiO_2/Na_2O (M_s)	Water / Binder	Cure Conditions	Additive Material
BFS[1]	Sodium Silicate + Sodium Hydroxide	2-4-6	1.2-1.5-1.8	0.40-0.45	1^4-2^5	Lime (4%)
CW	Sodium Silicate + Sodium Hydroxide	2-4-6	1.2-1.5-1.8	0.40-0.45	1^4-2^5	Lime (4%)
MW	Sodium Silicate + Sodium Hydroxide	2-4-6	1.2-1.5-1.8	0.40-0.45	1^4-2^5	Lime (4%)
BFS/CW	Sodium Silicate + Sodium Hydroxide	2-4-6	1.2-1.5-1.8	0.40-0.45	1^4-2^5	Lime (4%)
BFS/MW	Sodium Silicate + Sodium Hydroxide	2-4-6	1.2-1.5-1.8	0.40-0.45	1^4-2^5	Lime (4%)
CW/MW	Sodium Silicate + Sodium Hydroxide	2-4-6	1.2-1.5-1.8	0.40-0.45	1^4-2^5	Lime (4%)
BFS/CW/MW	Sodium Silicate + Sodium Hydroxide	2-4-6	1.2-1.5-1.8	0.40-0.45	1^4-2^5	Lime (4%)

[1] BFS and OPC paste sample were control specimens
[2] The same mixture of alkali activator solution was applied for all the paste sample types
[3] The Na_2O ratio is a percentage of the mass of the source material (unary, binary and ternary combinations of source materials)
[4] Steam cure at 65 °C for 4 hour
[5] Oven cure at 65 °C for 4 hour

3.2.2. Stages of experimental process

During the entire experimental period, six-steps experimental program was followed. The types of paste mixtures used and the experiments carried out at these stages were given in Table 3.5.

Table 3.5. Stages of experimental process.

Binder Codes		Experiments					
		Flow Table Test	**Setting Time Test**	**Flexural Strength Test**	**Compressive Strength Test**	**Dry Bulk Density, Apparent Density and Volume of Permeable Pore Space Measurement Results**	**Capillary Water Absorbtion Test**
First Stage (Unary Pastes)	BFS	X	X	X	X	--	--
	CW	X	X	X	X	--	--
	MW	X	X	X	X	--	--
Second Stage (Binary Pastes)	BFS/CW	X	X	X	X	--	--
	BFS/MW	X	X	X	X	--	--
	CW/MW	X	X	X	X	--	--
Third Stages (Ternary Paste)	BFS/CW/MW	X	X	X	X	--	--
Fourth Stage (Selected Unary, Binary, Ternary Pastes)	BFS	--	--	X	X	X	X
	CW	--	--	X	X	X	X
	MW	--	--	X	X	X	X
	BFS/CW	--	--	X	X	X	X
	BFS/MW	--	--	X	X	X	X
	CW/MW	--	--	X	X	X	X
	BFS/CW/MW	--	--	X	X	X	X

		Experiments			
		Drying Shrinkage Test	**Effect of Sulphate Attack Test**	**Effect of Sulphric Acid Attack Test**	**High Temperature Effect Test**
Fifth Stage (Selected Unary, Binary, Ternary Pastes)	BFS	X	X	X	X
	CW	X	X	X	X
	MW	X	X	X	X
	BFS/CW	X	X	X	X
	BFS/MW	X	X	X	X
	CW/MW	X	X	X	X
	BFS/CW/MW	X	X	X	X

		Experiments		
		SEM	**XRD**	**FTIR**
Sixth Stage (Selected Unary, Binary, Ternary Pastes)	BFS	X	X	X
	CW	X	X	X
	MW	X	X	X
	BFS/CW	X	X	X
	BFS/MW	X	X	X
	CW/MW	X	X	X
	BFS/CW/MW	X	X	X

3.2.2.1. First three stages

In the first three stages, unary, binary and ternary pastes were produced as a result of activation of blast furnace slag. ceramic waste and marble waste using with alkali activator solution (mixing of sodium hydroxide and sodium silicate), respectively. The aim of this section is to compare the properties of produced unary, binary and ternary pastes with the control sample produced with 100% blast furnace slag and OPC paste sample. The flow chart of the experimental program in the first three stages was shown in Figure 3.7.

Figure 3.7 shows the flow chart for the first three stages of the first experimental part. At the end of the first three stages, there are two important experimental parameters that affect the properties of the produced paste samples. These parameters are "n" and "Ms" parameters in the alkali activator solutions. "n" parameter is that the activator dosage (sum of % Na_2O ratio in the activator mixture) of the activator solution and the "Ms" parameter is ratio of SiO_2/Na_2O in the alkali activator solutions. The primary experimental set consisting of workability test (flow table and setting time), compressive and flexural strength tests was carried out to the paste samples for both three different "n" and "M_s" ratio during selection of the experimental parameters (Table 3.6). Two different curing systems (steam and oven) and two different water/binder ratios (0.4/0.45) were applied for each unary, binary and ternary binder samples. Flow table and setting time tests were carried out to determine the workability properties of each sample. As a result of this three-stage experiment set, paste samples giving the highest flexural and compressive strength were selected for unary, binary and ternary binders and all other experiments in the other stage which were applied on these selected samples. As a result, the most appropriate parameter for samples. (n and M_s ratio), mixing ratio, curing condition and water/binder ratio and workability properties were determined for each mixture type in unary, binary and ternary experimental systems after the first three stages. Determination of physical and mechanical properties of unary, binary and ternary binder samples selected according to optimum experimental criteria.

The optimum “n” and “M_s” values, water/binder ratios and optimal curing conditions were determined according to the test results at the end of the first three stages. The successful sample criterion for each type of binders (unary, binary and ternary) was determined as the samples with the highest compressive and highest flexural strength value suitable for workability properties, separately. Therefore, the samples were evaluated separately for both compressive and flexural strength. In the second stage, the replacement ratios of CW and MW used for the two-component system (binary system) in BFS for 25% 50%, and 75% by mass. In the third phase, for three component systems (ternary system), the sum of CW and MW were substituted with BFS in 3 different ratios (25, 50 and 75% by mass). As a result, the optimum parameter conditions to be used in the production of unary, binary and ternary binders were determined at the end of the first three stages.

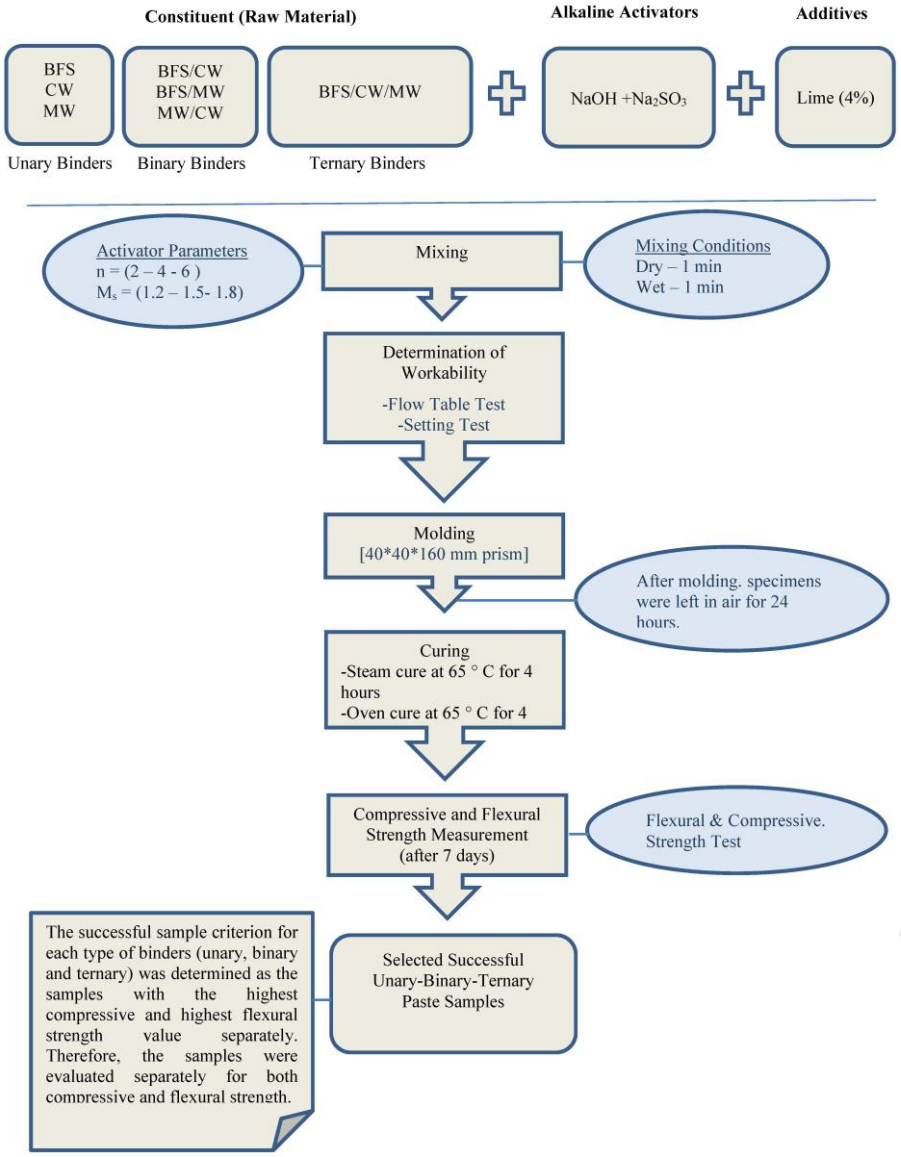


Figure 3.7. Flow chart of first, second and third experimental stages.

Table 3.6. The standards. sample size, sample numbers and sample residence time of the experiments to be carried out in the first three stages for unary, binary and ternary pastes specimens.

Experiment	Standard	Sample Size	Sample Number	Sample Residence Time (Days)
Flow Table Test	ASTM C 230M	-	-	-
Setting Time Test	ASTM C 191-13	-	-	-
Flexural Strength Test	ASTM C 348	40*40*160 mm prism	3	7
Compressive Strength Test	ASTM C 349	40*40*160 mm prism	6	7

3.2.2.2. Fourth. fifth and sixth stage

In the fourth stage, selected paste samples were produced from paste sample which had most suitable parameter ("n". "M_s", w/b ratio and cure condition) in the first three stages. During this stage, flexural and compressive strength, density and total porosity tests and water absorption test were performed to determine the mechanical and physical properties. The experiments and its standards at the fourth stage were listed in Table 3.7. The flow chart of the experimental program to be implemented in the fourth stage were shown in Figure 3.8.

Table 3.7. The standards, sample size, sample numbers and sample residence time of the experiments to be carried out in the fourth stages for unary, binary and ternary pastes specimens.

Experiment	Standard	Sample Size	Sample Number	Sample Residence Time (Days)
Flexural Strength Test	ASTM C 348	40*40*160 mm prism	3	1, 7, 14, 28, 56, 90
Compressive Strength Test	ASTM C 349	40*40*160 mm prism	6	1, 7, 14, 28, 56, 90
Density, Absorption and Pore Volume Test	ASTM C 642	40*40*160 mm prism	3	28
Capillary Water Absorbtion Test	ASTM C 1403	40*40*160 mm prism	3	28

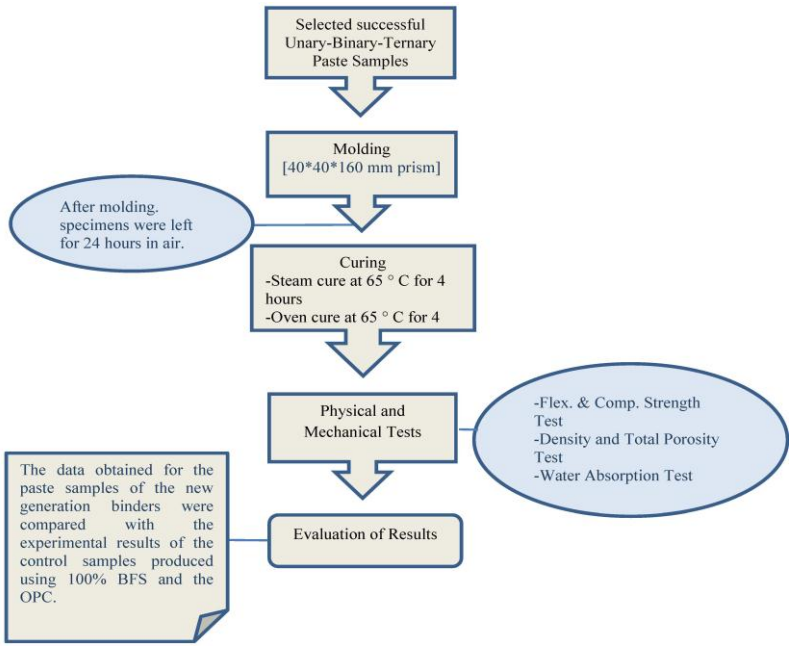


Figure 3.8. Flow chart of fourth stage.

In the fifth stage experiments, the flow chart schematized in Figure 3.9 were applied in order to determine the durability properties of pastes having optimum values. The experiments and its standards at the fifth stage were listed in Table 3.8. In the determination of the durability tests to be applied within the scope of this thesis. The durability properties most commonly studied in alkali activated systems have been taken into consideration in general.

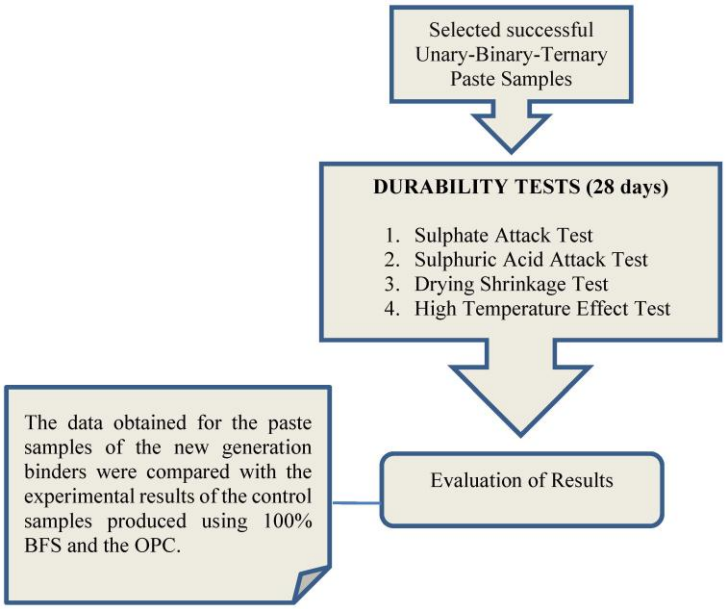


Figure 3.9. Flow chart of fifth stage.

Table 3.8. The standards, sample size, sample numbers and sample residence time of the experiments to be carried out in the fifth stages for unary. binary and ternary pastes specimens.

Experiment	Standard	sample size	Sample Number	Sample Residence Time (Days)
Sulphate Attack Test	--	40*40*160 mm prism	3	28
Sulphuric Acid Attack Test	--	40*40*160 mm prism	3	28
Drying Shrinkage Test	ASTM C 596	25*25*285 mm prism	2	28
High Temperature Effect Test	--	40*40*160 mm prism	3	28

Finally, a set of micro-structure analysis including SEM-EDS, XRD and FTIR tests were carried out in sixth stage. The flow chart shown in Figure 3.10 were applied in order to determine the microstructural properties of the pastes having optimum values.

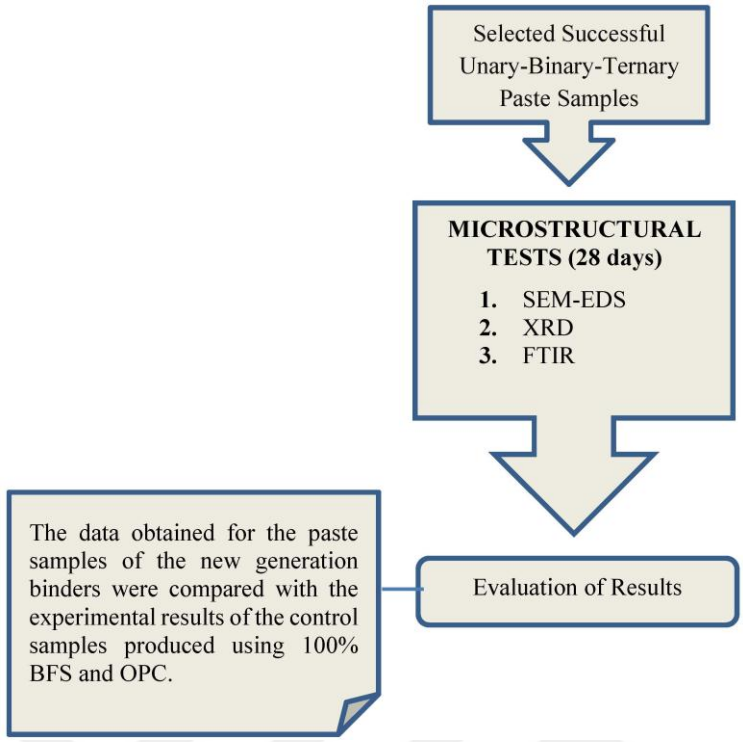


Figure 3.10. Flow chart of sixth stage.

3.2.3. Production of samples

The dimensions of the binder samples prepared within the scope of the thesis are in two different sizes as 40×40×160 mm prismatic shape (see Figure 3.11/a) and 25×25×285 mm prism (see Figure 3.11/b).

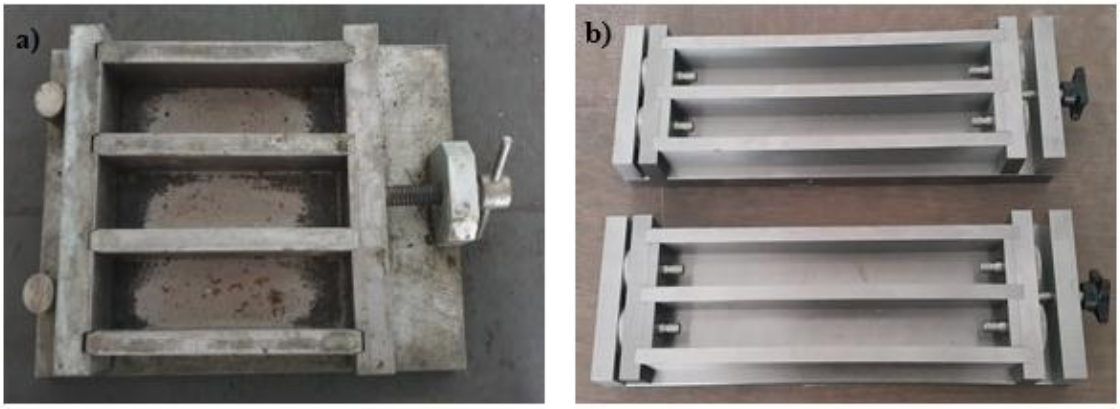


Figure 3.11. a) 40×40×160 mm sample mold b) 25×25×285mm sample mold.

The prismatic shape sample dimensions used for each test system were indicated in the previous sections (see Table 3.6, 3.7, 3.8). The mass amounts of used materials in

experiments for a single 40×40×160 mm and 25×25×285 mm prism sample produced as single, two and three components were given in Table 3.9.

Table 3.9. The mass amounts of prism sample materials for a single 40×40×160 mm and 25×25×285 mm.

	Binder Codes (n/Ms)	Source Materials* (g)	Na_2SiO_3 (ml)	NaOH (ml)	Lime (g)	Water (ml)	
						w/b 0.4	w/b 0.45
40*40*160 mm	**2/1.2**	400	25	21	16	135	157
	2/1.5	400	32	18	16	136	157
	2/1.8	400	38	15	16	136	158
	4/1.2	400	51	43	16	109	131
	4/1.5	400	63	37	16	109	132
	4/1.8	400	76	31	16	110	134
	6/1.2	400	76	64	16	82	106
	6/1.5	400	95	55	16	83	108
	6/1.8	400	114	46	16	84	109
25*25*285 mm	**2/1.2**	300	19	16	12	101	117
	2/1.5	300	24	14	12	101	118
	2/1.8	300	29	12	12	102	118
	4/1.2	300	38	32	12	81	98
	4/1.5	300	48	28	12	82	99
	4/1.8	300	57	23	12	82	100
	6/1.2	300	57	48	12	61	79
	6/1.5	300	71	41	12	62	80
	6/1.8	300	86	35	12	63	81

* For the two and three component system (binary and ternary system), the replacement ratios of CW and MW were 25%, 50% and 75% by mass in BFS.

For all samples, the raw materials used were mixed in a manual cement mixer branded Test U Test (Figure 3.12). The cement mixer has 2 different operating speeds (speed 1: Beater Speed (140 rpm) and speed 2: Beater Speed (285 rpm)). When the samples were produced, firstly the dry materials were mixed at speed 1 for 1 min, then the solutions and water were added. All materials were then first mixed at speed 1 for 1 min and then at speed 2 for 1 min. The prepared mixture was placed in the mold. The molds were kept under laboratory conditions at room temperature for 24 hours and then cured.



Figure 3.12. Manual cement mixer.

3.2.4. Procedure of experiments in first, second and third stage

3.2.4.1. Flow table test

The workability of the paste mixtures is determined by the flow table defined in ASTM C 230 "Standard Specification for Flow Table for Use in Tests of Hydraulic Cement" standard. This test procedure was carried out in accordance with ASTM C1437-15 "Standard Test Method for Flow of Hydraulic Cement Mortar" standard. According to this procedure, a layer of paste was placed about 25 mm in thickness in the mold and tamped 20 times with the tamper. Then, the mold was filled with paste three times and tamped as specified for the first layer. Paste was cut off the to a plane surface flush with the top of the mold by drawing the straightedge. Finally, the mold was lifted away from the paste 1 min after completing the mixing operation. The table was immediately droped 25 times in 15 s. The diameter of the paste was measured along the four lines scribed in the table top, recording each diameter to the nearest millimetre. The flow was recorded as average of four readings in millimetres for all specimens. The flow table aparatus used in this study was shown in Figure 3.13.



Figure 3.13. Flow table apparatus.

3.2.4.2. Determination of setting time

Full automatic Vicat apparatus branded Vicamatic-2 was used during this test process (Figure 3.14). The automatic Vicat apparatus had a needle and probe that falls freely in the sample at regular intervals. The depth of penetration was measured with the help of a sensor with a resolution of 0.1 mm. During hardening, immersion depth reduced and the initial and final setting times of the samples were automatically measured when the threshold penetration depths defined by the standards were measured and recorded. Additionallly, set-up times of samples were taken in graphical and numerical format with using internal printer. The experiments were carried out according to the ASTM 191-13 standard, which was automatically defined in the Vicat apparatus.



Figure 3.14. Full automatic vicat apparatus.

3.2.4.3. Flexural & compressive strength test

The flexural strength test was carried out on a 40x40x160 mm prismatic specimen using 120 mm effective span and load-controlled loading from single point method according to ASTM C 348 standard. The compressive strength is determined on two parts obtained after flexural strength test according to ASTM C 349 standard. The test recorded as the average of the resultant three sample while the compressive strength test was performed on the average of the six sample as it is carried out in the case of the post-flexural strength test. In preliminary studies, both tests were performed on steam cured or oven cured specimens for 4 hours and kept in laboratory conditions for 7 days. Then steam curing provided better results in mechanical properties. Therefore the rest of all experiments were conducted by using steam cured samples. Flexural/compression frame (capacity: 2000/15 kN) designed and manufactured by "SBEL" (Simulation Based Engineering Laboratory) from Arizona/USA was used for flexural and compresive strength tests (see Figure. 3.15).



Figure 3.15. Flexure/compression test frame.

3.2.5. Procedure of experiments in fourth stage

3.2.5.1. Dry bulk density, apparent density and volume of voids (permeable pore space) measurement test

This test was carried out according to ASTM C 642 "Standard Test Method for Density, Absorption. and Voids in Hardened Concrete" for the determination of void volume in relation to the amount of water absorbed and density. Firstly, the weight of all samples were determined after drying at 100ºC. At the next stage, the samples were immersed in water tank at 21ºC for 48 hours and the saturated surface was dried througly and then weight of samples were measured. Then, these samples were boiled in water for 5 hours and cooled down to room temperature for 16 hours in a controlled manner. Then the saturated surface was dried and weight of samples were determined. By using this data,

absorption after immersion, bulk dry density, apperent density and volume of permeable pore space (voids) were obtained for all samples.

3.2.5.2. Capillary water absorbtion test

The capillary water absorbtion of the mortars were examined on the samples exposed to water which were cured at 20 ºC for 90 days according to ASTM C 1403 “Standard Test Method for Rate of Absorption of Masonry Mortars”. After the mortar samples were dried at a temperature of 110 ºC for 24 hours and cooled to room temperature, the amount of water absorbed by the capillary was measured by immersing in approximately 3 mm of water from one surface. The amount of water absorption of samples were obtained using a balance with 0.001 g precision for 15 minutes, 1 hour, 4 hours and 24 hours. In order to prevent evaporation and loss of the water absorbed by the mortar samples, the samples were kept in an insulated container during the experiment.

3.2.6. Procedure of experiments in fifth stage

In this section, durability tests including “sulphate attack test”, “sulfuric acid attack test”, “drying shrinkage test” and “high temperature effect tests” have been applied on the best unary, binary and ternary component among the samples.

Durability properties are features that can be standardized in commercially common products over the years, with real-life results in the long term [80]. Therefore, there are no appropriate protocols, specifications, and standards for a uniform durability testing method yet. In this thesis, "sulphate attack test", "sulfuric acid attack test" and "high temperature effect test were carried out by considering the applications reported in the literature.

3.2.6.1. Sulphate attack test

Sulphate Attack Test was conducted on the alkaline activated samples which were kept in Na_2SO_4 (such as 5M, 10M) solution with different concentrations and different curing times (3 months to 1 years), and the loss of strength, mass loss and microstructure changes were analyzed at the end of the experiment [10, 81-83].

In this thesis, samples of unary, binary and ternary component paste binders produced were exposed to a 10% $NaSO_4$ solution (pH = 7.1) for 6 months (Figure 3.16). The change in mechanical properties and weight was determined using prismatic samples with 40x40x160 mm dimensions. The solution was renewed at the end of the 1st and 3rd months.



Figure 3.16. Unary, binary and ternary binders in sulphate solution.

3.2.6.2. Sulphuric acid attack test

Sulphate Attack Test was conducted on the alkaline activated samples which were kept in H_2SO_4 (such as 5M, 10M) solution with different concentrations, with different curing times (3 months to 1 years), and the loss of strength, mass loss and microstructure changes were analyzed at the end of the experiment [10, 84-85]. Samples of unary, binary and ternary component paste binders produced were exposed to a 5% H_2SO_4 solution for 6 months (Figure 3.17). The change in mechanical properties and weight was determined using prismatic samples with 40x40x160 mm dimensions. The solution was renewed at the end of the 1st and 3rd months.



Figure 3.17. Unary, binary and ternary binders in sulphric acid solution.

3.2.6.3. Drying shrinkage test

Drying shrinkage test was performed in accordance with ASTM C 596 "Standard Test Method for Drying Shrinkage of Mortar Containing Hydraulic Cement" on prismatic mortar specimens of 25x25x285 mm dimensions (see Figure 3.18/a). Prepared mixtures were removed from the mold after 24 hours and kept in laboratory conditions for 1 day. Then, the samples were cured at 60°C for 4 hours with steam and oven. Finally, specimens protected in laboratory conditions for 7 days were tested. The testing set consists of a length measuring frame with comprator device attached to it. The height change of the mortar bars were measured with the help of the comparator device with the precision of 0.001*12.7 mm (see Figure 3.18/b). The test results were recorded as the average of two samples.



(a) (b)

Figure 3.18. (a) Digital length mold (b) Digital length comparator.

3.2.6.4. High temperature effect test

Prismatic samples with 40x40x160 mm dimension were heated at 200, 400, 600 and 800 ºC at 10 ºC / min by muffle furnace marked Nuve (Figure 3. 19) and exposed to the relevant temperature for 3 hours. Changes in the weight and mechanical properties (compressive strength and flexural strength) of the samples were determined with the effect of high temperature. Measurements were made after the sample reached at room temperature.



Figure 3.19. Muffle furnace.

3.2.7. Procedure of experiments in sixth stage

3.2.7.1. SEM-EDS analysis

Microstructure and compositions of hydration products were examined by SEM-EDS analysis. In SEM analysis, both broken samples were examined in secondary electron (SE) mode. Samples used in SEM were obtained from fractured surface after flexural measurements. Since the samples were electrically insulating, they were analyzed under low vacuum so that they did not require any preparation before microstructural analysis. Sample was examined in SE mode by sticking with double sided adhesive carbon tape on the brass plate without being processed. Tüm örnekler SEM investigations were performed using Philips Quanta FEG 450 brand SEM instrument. SEM-EDS analysis carried out by Science and Technology Application and Research Center at Zonguldak Bülent Ecevit University.

3.2.7.2. XRD analysis

This analysis was performed to determine the crystal structure characterization of the samples produced. The mineralogical compositions of samples were determined by X-ray diffraction (XRD. Panalytical Empyrean with Cu Kα radiation. 45 kV and 40 mA). Samples were milled and sieved to 25-50μm in size and prepared as powder. XRD analysis carried out by Science and Technology Application and Research Center in Zonguldak Bülent Ecevit University (ZBEUN).

3.2.7.3. FTIR analysis

Molecular bond characterization of the samples was made by this test method and supportive analyzes were performed on the bonds in the structure of the compounds and molecules formed in the sample. Perkin Elmer's FTIR-ATR Specturum 100 was used for the analysis. The scanning frequency range of the device is 4000-450 cm^{-1}. Samples were milled and sieved to 25-50μm in size and prepared as powder. FTIR analysis carried out by Department of Chemical Science in Zonguldak Bülent Ecevit University (Figure 3.20).



Figure 3.20. FTIR-ATR Spectrum100 ınstrument.

4. RESULTS AND DISCUSSION

4.1. First Stage - Determination the Optimum Parameters of the Unary Binders

In the first stage, unary (one component) binder (UB) system produced by alkali activation process of "Blast Furnace Slag" (BFS), "Ceramic Waste" (CW) and "Marble Waste" (MW) was investigated with workability and strength experiments. In the second stage, the replacement ratios of CW and MW used for the binary (two component) binder system (BB) in BFS were 1:3, 2:2 and 3:1 by mass. In the third phase, for ternary (three component) binder systems (TB), the sum of CW and MW were substituted in BFS in three different ratios (1:3, 2:2 and 3:1 by mass). The workability and strength experiments were also applied to the BB and TB samples in the second and third stages. The optimum experimental parameters (optimum "n" and "M_s" values, water/binder) and the selected samples were determined according to test results of the UB, BB and TB paste samples in all stages.

The workability tests were consisted of two different experiments. These tests were determination of flow table and setting time of all binders (UB, BB and TB). In the test of the flow diameter, the flow radiuses of the samples were determined and their consistency was compared with each other and with the cement sample. According to the test conditions, 100 mm was the minimum spreading diameter and 300 mm was the maximum spreading diameter for samples (ASTM C 230 M). Therefore, 100 mm limit was defined as "Rapid Setting" (R.S) and 300 mm limit was defined as "Liquid Consistency" (L.C) in the graph. When the w/b ratio was equal to 0.4, the flow radius of cement paste samples was determined as 225 mm, and for the 0.45 w/b ratio, the flow radius of cement was determined as 290 mm in this test.

In the test of setting time, limit values of initial and final setting time were 202 min and 312 min respectively according to ASTM C 191-13 Standard in the experiment. These limit values described as of "Limit of OPC (Ordinary Portland Cement)" in the setting time graphs. Samples with exceeding these limit values were completed the setting time within 8-10 hours. Phrase of "no setting (after 48h)" was used for the samples which could not be completed within 48 hours and these samples were excluded from the evaluation. "Rapid Setting" was used in the graphs for samples with an initial setting

time before 90 minutes and a final setting time before 150 minutes. The setting time also indicated as “Half-Setting” because of initial setting time was within the ASTM standard but the final setting time was not within the standard for some examples. In addition, “short period difference” phrase was used for sample with a difference between the initial and final setting times less than 30 min.

The strength tests were consisted of flexural and compressive tests. During these tests, the successful sample criterion for each type of binders (UB, BB and TB) was determined as the samples with the highest compressive and highest flexural strength value separately. Therefore, the samples were evaluated separately for both compressive and flexural strength.

As a result, the optimum parameter conditions to be used in the production of UB, BB and TB were determined at the end of the first three stages.

4.1.1. Blast furnace slag-unary binders (BFS-UB)

4.1.1.1. Workability properties of BFS-UB samples

- ✓ *Flow Table Test of BFS-UB*

For all BFS-UB samples, flow diameter values were given in Table 4.1. In all BFS-UB samples, the increase in water/binder (w/b) value from 0.4 to 0.45 naturally increased the flow diameter (consistency). In general, for both w/b ratios, the flow diameter of the samples was much higher than for the cement sample having the same w/b ratio. When the “n” ratio increased (n=6), the consistency of BFS-UB samples produced by alkali activation became liquefied, but because the transition speed from liquid consistency to solid consistency was very short, the consistency property was considerably decreased compared to cement. The rate of transition from liquid consistency to solid consistency was much faster for samples with 0.4 w/b than samples with 0.45 w b. Therefore, there was a high loss of workability for both w/b ratios in samples with a high activator dosage. During the alkali activation process of BFS-UB, it was found that most of the samples had a more liquid consistency than the cement sample for both w/b ratios.

Table 4.1. Flow values (mm) of BFS-UB samples for w/b=0.4 and w/b=0.45.

BFS-UB Flow Diameter (mm)	**M_s (SiO_2/Na_2O)**					
	(w/b=0.4)			**(w/b=0.45)**		
n (Na_2O%/Activator)	**1.2**	**1.5**	**1.8**	**1.2**	**1.5**	**1.8**
2	260	250	180	290	L	230
4	290	290	250	L	L	280
6	HRS	HRS	HRS	LRS	LRS	LRS

L: Liquid HRS: High-Rate Rapid Setting LRS: Low-Rate Rapid Setting

The changes in the flow diameter according to the "n" and "Ms" ratios for both "w/b" values of BFS-UB samples were given in Figures 4.1 and 4.2.

Especially for the BFS-UB samples activated with a high amount of Na_2O (high "n" values=high activator dosage), the increase in "w/b" ratio liquefied the consistency of the samples. Increasing the "n" value in the samples increased the consistency up to a point and then decreased it. This was the point where n was equal to 4. This means that as the dosage of activator solution (total amount of mixture of sodium silicate and sodium hydroxide = "n" ratio) used for the activation of the samples increased up to 4, the consistency of the samples increased and then decreased. That was, for the n=4 ratio, the flow diameter of the samples has reached the maximum value. However, when "n" ratio was equal to 6, the transition from liquid to solid consistency was rapid.

The change in the "Ms" ratio did not result a general trend in the flow diameter values of the BFS-UB samples (see Figure 4.2). However, especially for high "n" ratios, the increase in "Ms" ratios greatly reduced the consistency of the samples. That was, as the ratio of sodium silicate in the activator solution increased, the consistency of samples decreased. Due to the increase in the "Ms" value, the decrease in consistency especially in the samples with low "n" values was much more pronounced than the samples with high "n" values. This means that; when the dosage of activator solution used for the activation of the samples was small ("n" ratio decreased), the increase in sodium silicate ratio and the decrease sodium hydroxide ratio in the solution (increase of "Ms" ratio) decreased the consistency of samples. Consequently, the dosage of solution used for activation of samples increased ("n" ratio increased), the effect of increasing "Ms" ratio on the consistency of samples decreased.

✓ *Setting Time Test of BFS-UB*

In this experiment, initial and final setting time values of BFS-UB samples for both w/b ratios were given in Table 4.2. As a result of this experiment, it was determined that as the w/b ratio of BFS-UB samples increased (from 0.4 to 0.45), initial and final setting times increased. The initial and final setting times of the BFS-BB samples with low (n=2) and high level (n=6) activators for the 0.4 w/b ratio were much shorter than the cement sample. When the w/b ratio increased to 0.45, it was observed that the setting times of the other BFS-BB samples were longer than the cement sample except the samples with low activator dosage.

The change in the initial and final setting times of the samples according to the "n" ratio for both w/b ratios was shown in Figure 4.3.

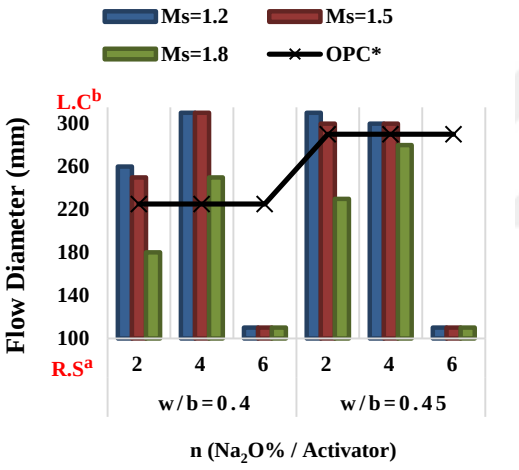


Figure 4.1. The flow values of BFS–UB samples according to "n" ratio (for "w/b=0.4" and for "w/b=0.45").

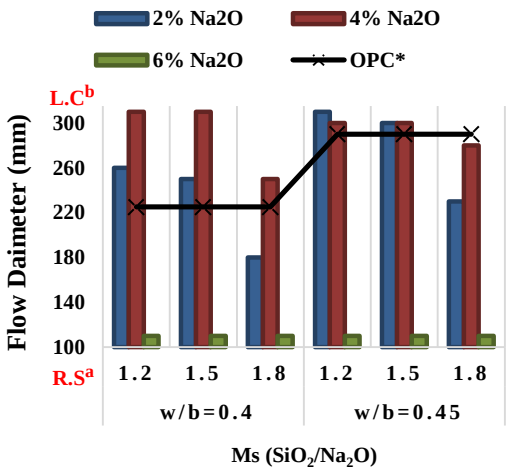


Figure 4.2. The flow values of BFS-UB samples according to "Ms" ratio (for "w/b=0.4" and for "w/b=0.45").

* The cement paste was formed only with water without using an alkaline activator.
[a] Below the flow radius of 100 mm was the "Rapid Setting" limit.
[b] Above flow radius of 300 mm was "Liquid Consistency" limit.

It was observed that the setting time of BFS-UB samples set for n=2 ratio shorter than the cement sample for both w/b ratios. For the n=4 ratio, the initial and final setting times were extended between 8-10 hours for both w/b ratios. However, when the value of "n" reached (n=6), a sudden setting event was observed. This means that increasing the Na_2O content in the samples increased the workability to some point (n=4).

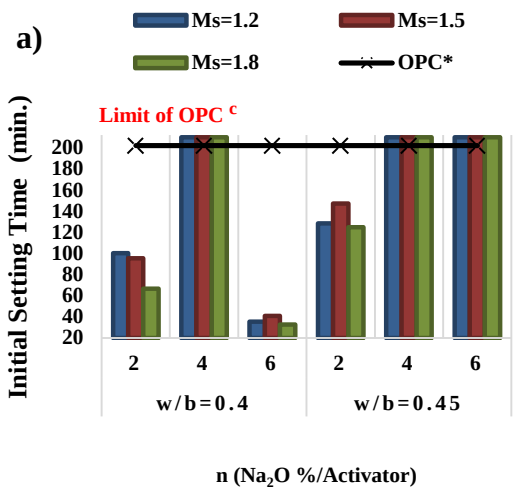
However, the increase in this ratio (n=6) significantly shortened the setting times. This had a negative effect on the workability of the samples.

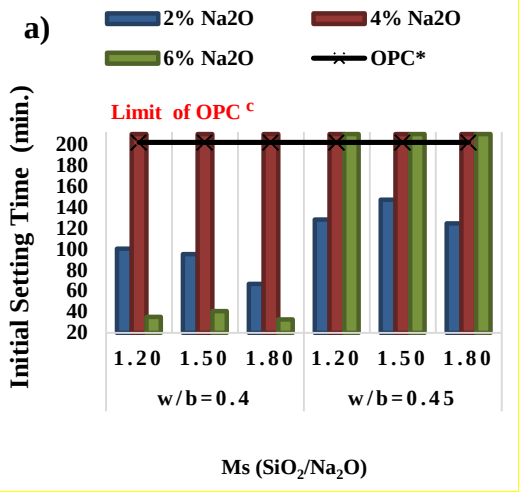
Table 4.2. Setting time of BFS-UB samples (w/b=0.4 and w/b=0.45).

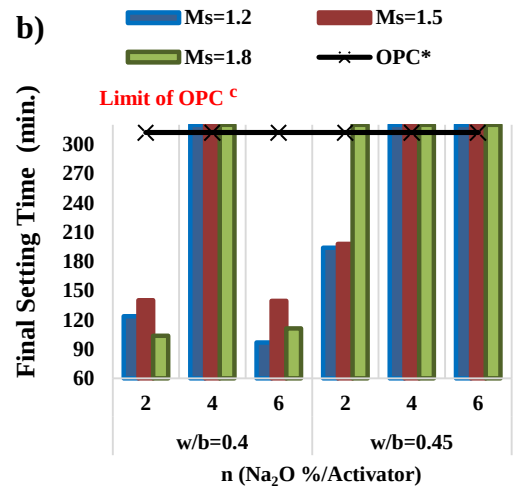
Sample Code	Initial Setting Time (min.)	Final Setting Time (min.)	Note
BFS-2/1.2/0.4	100	124	
BFS-2/1.5/0.4	95	140	
BFS-2/1.8/0.4	67	104	RS
BFS-4/1.2/0.4	>202	>312	
BFS-4/1.5/0.4	>202	>312	
BFS-4/1.8/0.4	>202	>312	
BFS-6/1.2/0.4	35	97	RS
BFS-6/1.5/0.4	41	140	RS
BFS-6/1.8/0.4	33	111	RS
BFS-2/1.2/0.45	128	194	
BFS-2/1.5/0.45	147	198	
BFS-2/1.8/0.45	125	244	
BFS-4/1.2/0.45	>202	>312	
BFS-4/1.5/0.45	>202	>312	
BFS-4/1.8/0.45	>202	>312	
BFS-6/1.2/0.45	>202	>312	
BFS-6/1.5/0.45	>202	>312	
BFS-6/1.8/0.45	>202	>312	

RS: Rapid Setting

The initial and final setting times of the samples according to the “Ms” ratio was shown in Figure 4.4. According to these graphs, it was observed that there was no general tendency to change the setting times with “Ms” ratios for both w/b ratios. It was concluded that the effect of the “Ms” ratio on the samples had no more determinative effect than the effect of the “n” ratio. However, for both the w/b ratios, especially for samples containing low and high activator dosages (n=2 and n=6), the increase in the “Ms” ratio shortened both the initial and final setting times. BFS-UB samples had a set completion time of 8-10 hours for all “Ms” values for samples with moderate activator dosage (n=4).







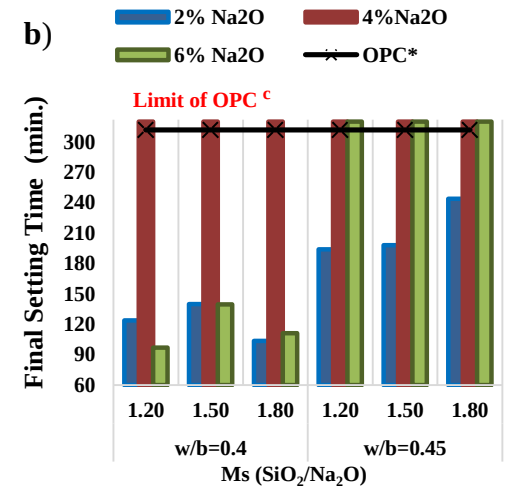


Figure 4.3. The setting time of BFS-UB samples according to "n" ratio a) Initial setting time b) Final setting time.

Figure 4.4. The setting time of BFS-UB samples according to "Ms" ratio a) Initial setting time b) Final setting time.

* The cement paste was formed only with water without using an alkaline activator.
[c] These limit values were defined in ASTM C 191-13 Standard.

✓ *Workability Properties of BFS-UB*

As a result of the workability tests carried out for BFS-UB samples, the samples containing low activator dosage were found to have lower consistency and shorter setting times than cement samples. When the activator dosage was at medium level, it became liquefaction and the setting time was between 8-10 hours. When the activator dosage increased further, rapid transition from liquid to solid state and rapid setting events were observed in the consistency of the samples. Thus, it observed that samples

with moderate activator dosage were the most suitable samples in terms of workability. The ratio of the activator dosage was the “n” ratio. Additionally, none of the samples had any negative effect on the workability properties of the hardened sample during mixing and molding.

It was observed in other studies that the workability decreases in alkali activation systems formed with BFS-UB when the “n” ratio (amount of activator solution) increases during the activation process. Aydın and Baradan [86] activated blast furnace slag with an alkali activator solution consisting of sodium hydroxide and sodium silicate mixture and examined the improvements in workability properties by changing “n” and “Ms” ratios. According to the results of the study, the consistency and setting times of the samples with high “n” (6% and 8% Na_2O) and moderate “Ms” values (0.4 and 0.8) were found to be unsuitable for normal construction works and the setting times were considerably shortened. In other study, Bakharev et al. [30] reported different alkali activated slag pastes which was produced using sodium silicate, sodium hydroxide, sodium carbonate, sodium phosphate, and combinations of these activators. According to the results of this study, fast workability loss was observed in samples with high Na^+ concentration (n) and “Ms” values. The most appropriate “n” ratio was selected as 4% in this study. In our study, similar to the results of other studies, the workability of the samples and the setting times were decreased for medium “n” values (n>4) and high “Ms” (Ms>1) rates.

It was observed that “n” ratio was more effective than the “Ms” ratio on the consistency and setting times of the samples in this study. Similar results have been found in other studies. Chang [87] investigated several factors, such as the pH value of the activator, the alkali modulus and the alkali activator dosage for a sodium silicate-based activator which influences the setting time of alkali-activated slag paste. According to Chang’s results, the activator dosage (“n” ratio), which was defined as the sum of the SiO_2 and Na_2O concentrations, shows a significant trend with the setting time. It was also found that the influence of SiO_2 on the setting time was more apparent than that of Na_2O. In general, it was found that the increase of “n” (activator dosage) and “Ms (ratio (decrease of sodium hydroxide amount while increasing the amount of sodium silicate in the activator dosage) had a negative effect on the workability of the BFS-UB samples. Zivica [88] found that increasing the sodium silicate dosage (increasing the “n” ratio) in

the activator significantly reduced the setting time and reduced the workability of the samples, similar to our results. It was also found in this study that the increasing in the amount of sodium silicate in the activator effected the reducing of setting time and workability of the samples were higher than sodium hydroxide. Zivica had shown that this was due to the fact that sodium hydroxide contains simpler cations (Na^{+}) and anions (OH^{-}) than sodium silicate. According to Zivica's study, the silicate ion was present at the time of addition to the solution and was an important finalizing component in the hardening of AAS binders. This was effective in the fast setting and loss of workability. It was stated that the fast setting of BFS paste containing sodium silicate was due to the formation of initial C-S-H. In the case of sodium hydroxide-activated samples, the setting of samples was reported to be due to the formation of poly-silicate hydrate. As a result, it was determined that high "n" and "Ms" ratios had negative effects on slag workability for BFS-UB samples. It had been found that sodium silicate used in the activator was more effective than sodium hydroxide in the process of slag activation.

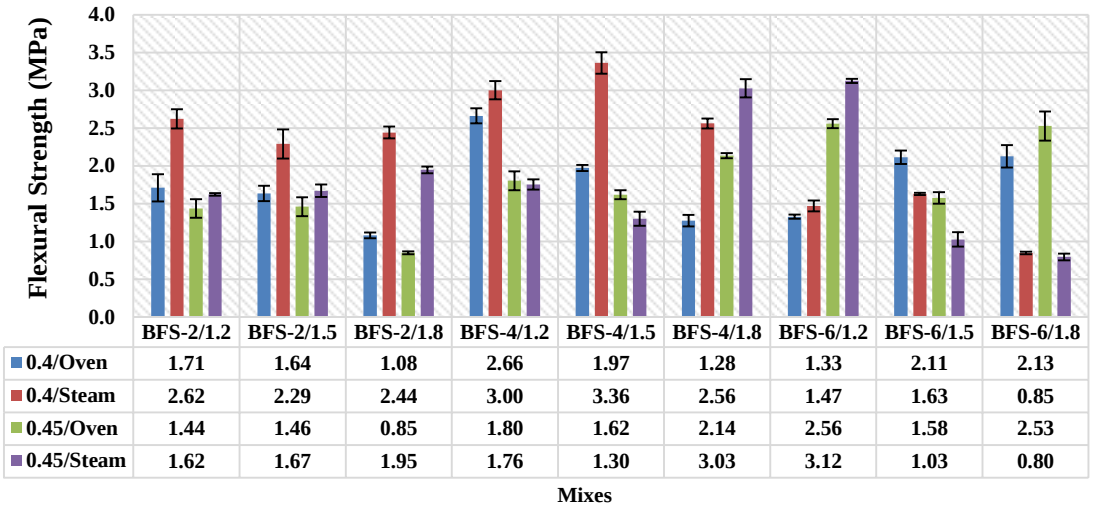
4.1.1.2. Strength properties of BFS-UB samples

✓ *Flexural Strength Test of BFS-UB*

The flexural strength values of the BFS-UB were given in Figure 4.5 for both w/b ratios (0.4 and 0.45) and for both curing conditions (oven and steam).

The highest flexural strength value for BFS-UB samples set was for the "BFS 4/1.5/0.4/Steam" sample. Thus, the highest flexural strength value was determined for w/b = 0.4 ratio and steam curing.

In this test set, the flexural strength values of samples with a value of w/b = 0.45 were lower than those value of w/b = 0.4 for both curing conditions. BFS 4/1.8/0.45/Steam or Oven, BFS 6/1.2/0.45/Steam or Oven and BFS 6/1.8/0.45/Oven were the three examples that were outside this general trend. That was, apart from these three samples, increasing w/b ratios of the samples decreased the flexural strength values of BFS-UB samples.



	BFS-2/1.2	BFS-2/1.5	BFS-2/1.8	BFS-4/1.2	BFS-4/1.5	BFS-4/1.8	BFS-6/1.2	BFS-6/1.5	BFS-6/1.8
0.4/Oven	1.71	1.64	1.08	2.66	1.97	1.28	1.33	2.11	2.13
0.4/Steam	2.62	2.29	2.44	3.00	3.36	2.56	1.47	1.63	0.85
0.45/Oven	1.44	1.46	0.85	1.80	1.62	2.14	2.56	1.58	2.53
0.45/Steam	1.62	1.67	1.95	1.76	1.30	3.03	3.12	1.03	0.80

Figure 4.5. Flexural strength of BFS-UB samples for 7 days.

The variation of flexural strength values of samples according to “n” ratio was given in Figure 4.6 for two different curing conditions. It has been found that the change of “n” value does not create a general tendency on the flexural strength of the samples. Increasing the “n” ratio for oven cured samples generally increased the flexural strength values of BFS-UB samples. However, a different result was observed for steam cured samples. When the “n” ratio of the steam cured samples increased from 2 to 4, flexural strength generally increased, but when “n” ratio increased to 6, a decrease was observed. Therefore, this results suggest that the oven cure gave better results for the samples with high level “n” ratio (n=6). However, the highest flexural strength among the samples were realized for steam curing as a result of moderate “n” ratio (n=4).

For this test set, the effect of the change of the “Ms” ratio on the flexural strength of the samples was not as significant as the “n” ratio. The changes in flexural strength values according to the “Ms” ratio were given in Figure 4.7 for two different curing conditions. Increasing the “Ms” ratio reduced the flexural strength value of BFS-UB samples for low “n” ratios for oven cure. For steam curing, the increase in the “Ms” ratio caused a decrease in flexural strength for high “n” ratios as opposed to oven curing.

These result reveal that “n” ratio was more effective than “Ms” ratio on the change of flexural strength as in the same workability properties. The highest flexural strength value in this set of samples were obtained for the “BFS/4/1.5/0.4/Steam” sample. Thus, the highest flexural strength value for the unary binder system consisting of blast

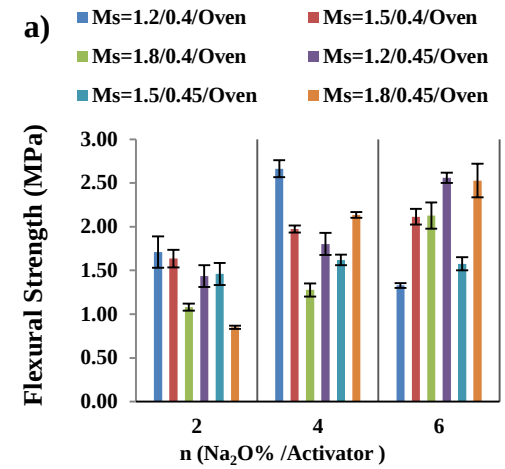
furnace slag was in the case of w/b = 0.4 and steam curing at ratios “n” = 4 and “Ms” = 1.5.

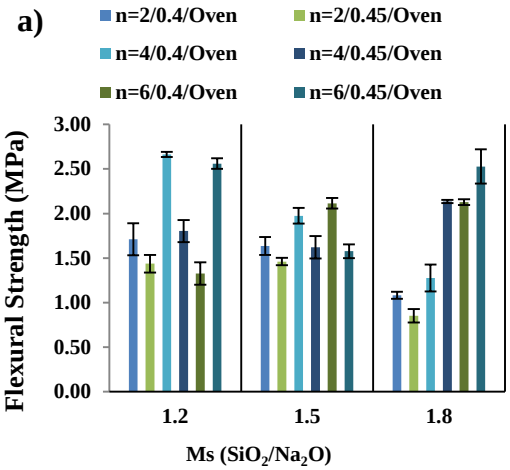
- ✓ *Compressive Strength Test of BFS-UB*

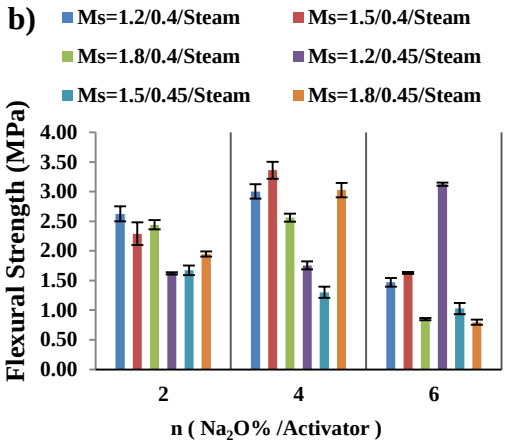
The compressive strength values of BFS-UB were given in Figure 4.8 for both w/b ratios (0.4 and 0.45) and both curing conditions (oven and steam).

The highest compressive strength value in BFS-UB sample set was for the “BFS 6/1.5/0.4/Steam” sample. Thus, the highest compressive strength value was determined for w/b = 0.4 ratio and steam curing.

In this test set, the compressive strength values of samples with a value of w/b = 0.45 were lower than those value of w/b = 0.4 for both curing conditions. BFS 6/1.2/0.45/Steam cured sample was the one example that was outside this general trend. That was, apart from this sample, generally increasing w/b ratios of the samples decreased the flexural strength values of BFS-UB samples.







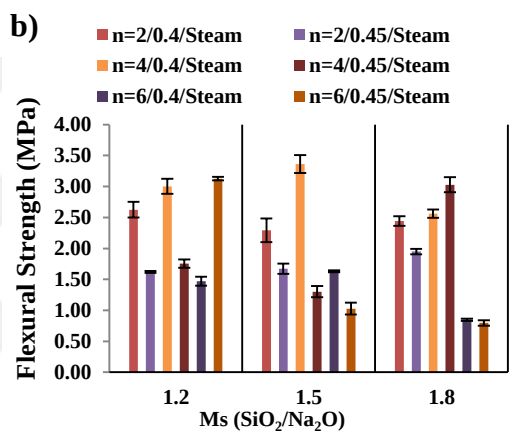
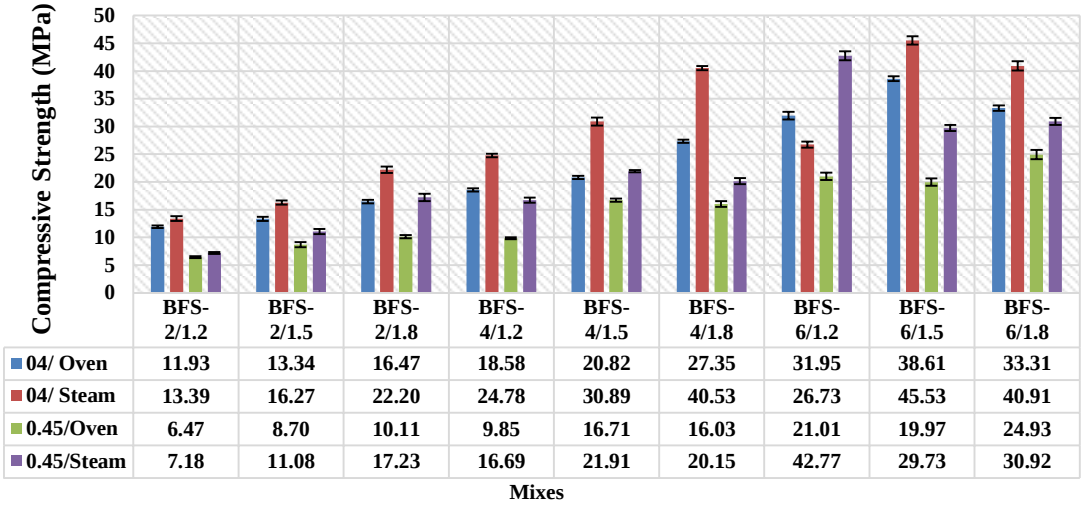


Figure 4.6. Change in flexural strength of BFS-UB according to "n" ratio a) For oven cure b) For steam cure.

Figure 4.7. Change in flexural strength of BFS-UB according to "M_s" ratio a) For oven cure b) For steam cure.

The variation of compressive strength values of samples according to "n" ratio was given in Figure 4.9 for two different curing conditions. It has been determined that when the "n" ratio increased, the compressive strength values of the samples increased. For low "n" ratios (n=2), while the compressive strength values of the samples subjected to steam and oven curing were close to each other, But as the "n" ratio increased (n=6), the increase in compressive strength values of the samples subject to steam curing was much higher than that of the oven cure. For samples with high "n" ratios, steam curing was found to be a better curing method in terms of compressive strength.



	BFS-2/1.2	BFS-2/1.5	BFS-2/1.8	BFS-4/1.2	BFS-4/1.5	BFS-4/1.8	BFS-6/1.2	BFS-6/1.5	BFS-6/1.8
04/ Oven	11.93	13.34	16.47	18.58	20.82	27.35	31.95	38.61	33.31
04/ Steam	13.39	16.27	22.20	24.78	30.89	40.53	26.73	45.53	40.91
0.45/Oven	6.47	8.70	10.11	9.85	16.71	16.03	21.01	19.97	24.93
0.45/Steam	7.18	11.08	17.23	16.69	21.91	20.15	42.77	29.73	30.92

Figure 4.8. Compressive strength of BFS-UB samples for 7 days.

For this test set, similar to the flexural strength results, the effect of the change of the "Ms" ratio on the compressive strength of the samples was not as significant as the "n" ratio. The changes in compressive strength values according to the "Ms" ratio were given in Figure 4.10 for two different curing conditions. The highest compressive strength value for oven and steam curing was determined for the ratio Ms=1.5. With increasing "Ms" ratio, it was observed that for both curing conditions, compressive strength increase in samples with low "n" ratio was less than that of samples with high "n" ratios.

These result point it out that "n" ratio was more effective than "Ms" ratio on the change of compressive strength as they have the same flexural strength and workability properties. The highest compressive strength value was obtained for the "BFS/6/1.5/0.4/Steam" sample. Thus, the highest compressive strength value was obtained for the unary binder system consisting of blast furnace slag with the following parameters of w/b = 0.4 and steam curing at ratios "n" = 6 and "Ms" = 1.5.

✓ *Strength Properties of BFS-UB*

The strength tests of BFS-UB by alkali activation method were carried out on paste samples for two different w/b ratios and cure conditions. Within the scope of these experiments, flexural and compressive tests of the samples activated with activator solution consisting of liquid sodium silicate and sodium hydroxide mixture were

performed. The selected paste samples were found to be 0.4 as w/b ratio and steam curing.

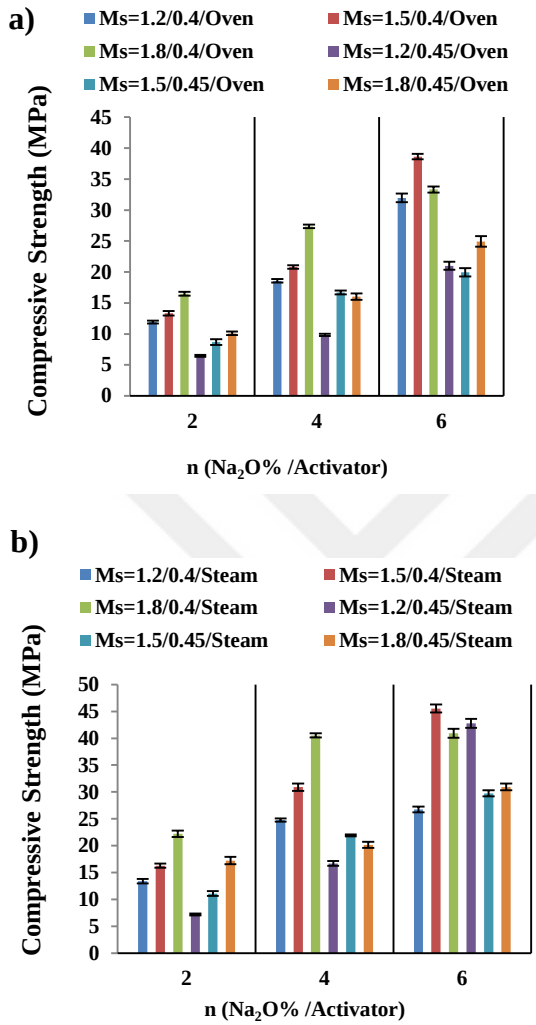


Figure 4.9. Change in compressive strength of BFS-UB according to "n" ratio. a) For oven cure b) For steam cure.

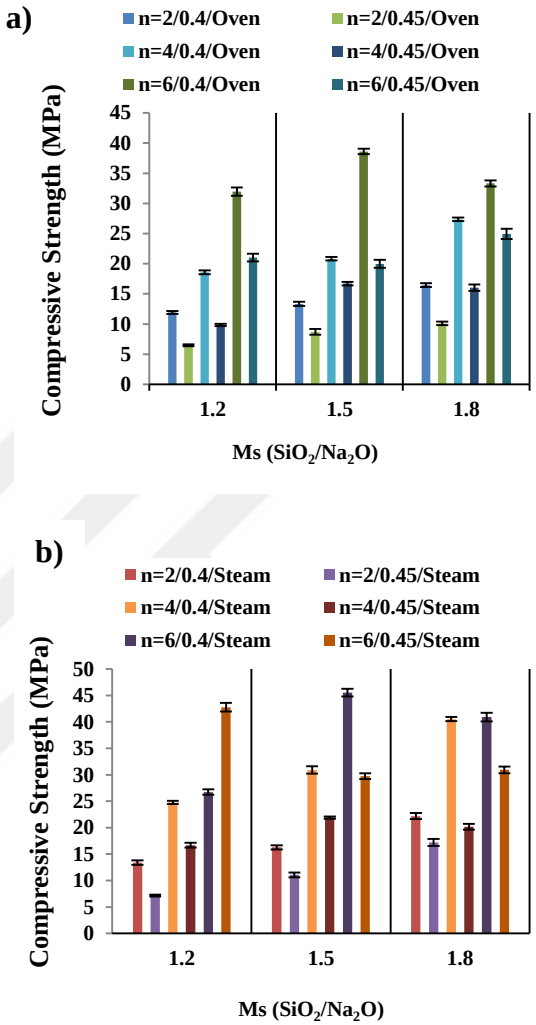


Figure 4.10. Change in compressive strength of BFS-UB according to "Ms" ratio. a) For oven cure b) For steam cure.

The results of these two experiments for steam cure and w/b=0.4 were shown in Figure 4.11.

According to these results, when the "n" ratio (activator dosage) in the sample increased from 2 to 6, the flexural strength value of the samples firstly increased and then decreased. The highest flexural strength value (3.36 MPa) was measured for the medium level "n" ratio (n = 4) and "Ms" ratio (Ms = 1.5). For compressive strength, the

highest flexural strength value (45.53 MPa) was determined for high "n" (n = 6) ratio and moderate "Ms" (Ms = 1.5) ratio. However, neither the flexural strength nor the compressive strength values of the Portland cement reference sample have been exceeded.

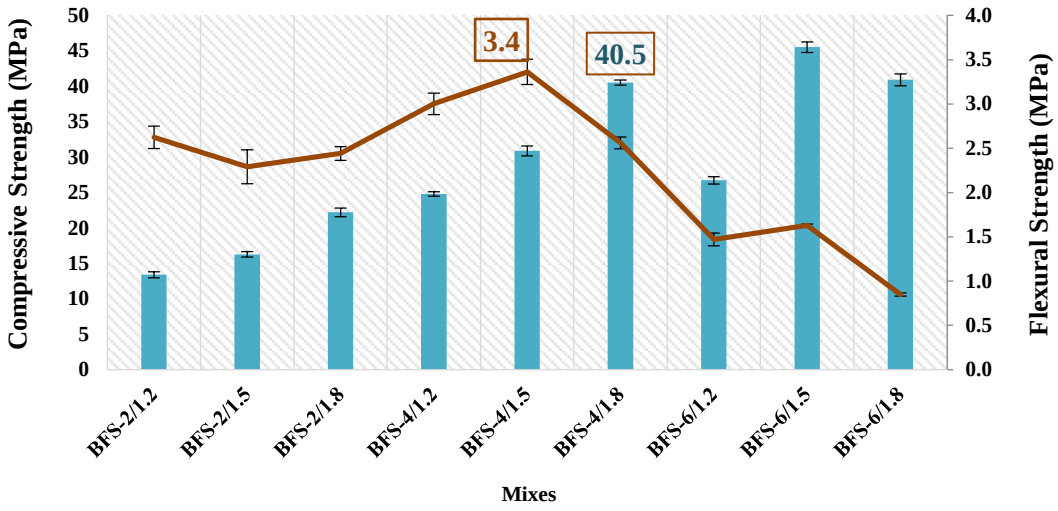


Figure 4.11. Compressive and flexural strength of BFS-UB samples for 7 days.

In the literature, several studies have been reported in which blast furnace slag was activated with a mixture of sodium silicate and sodium hydroxide activator (sodium silicate based activator solution) as a unary component paste sample. In one of these studies, Yang et al. [89] was added nano-TiO_2 into alkali activated slag paste, and its mechanical properties and shrinkage were tested to examine its effect on hardened alkali-activated slag paste. Alkali activator with a Na_2O concentration of 4.0 % (by mass of slag) and Ms. of 1.2 was used. The flexural strength and compressive strengths of reference group that was produced by alkali activation of blast furnace slag alone were 10 MPa and 33.9 MPa, for 7 days, respectively. In another study, Wang et al. [90] prepared alkali-activated blast furnace slag paste in different mixture ratios based on an orthogonal test scheme. The fluidity, setting time, mechanical strengths, and other properties were systematically evaluated to determine the optimum mixture ratio of paste. The amounts of sodium silicate and sodium hydroxide in the activator solution were planned as 3% by mass (7%, 9% and 11%) of blast furnace slag and produced 9 different types of samples in this study. The highest flexural (9.6 MPa) and compressive strength (41.8 MPa) values were obtained at 28 days for the sample containing 9%

sodium silicate and 7% sodium hydroxide. Besides these studies, Chang et al. [79] examined the effects of gypsum and phosphoric acid on the properties of sodium silicate-based alkali-activated slag paste. In this study, the effects of gypsum and/or phosphoric acid on the compressive strength development, setting time and drying shrinkage of alkali-activated slag were examined. The activator composition was not a variable and the Na_2O and Si_2O ratios were fixed (Na_2O=1.22 g/l and SiO_2=1.23 g/l). The liquid/slag (w/b) ratio was kept at 0.54. As a result, alkali-activation of blast furnace slag yielded a compressive strength value of approximately 63 MPa for 7 days. And finally, Jin et al. [91] investigated the potential of using commercial reactive MgO to reduce the drying shrinkage of alkali activated slag. The alkali-activation of blast furnace slag yielded a compressive strength value of approximately 55 MPa for 7 days. The values obtained from the literature were similar to those obtained in our study, especially in terms of compressive strength.

✓ *The Determination of the Selected Sample of BFS-UB*

At the end of the first set of experiments including workability and strength tests, two samples that selected represent this test set were determined for BFS-UB in terms of both flexural and compressive strength (BFS 4/1.5/0.4/Steam cured and BFS 6/1.5/0.4/Steam cured). The experimental parameters of the selected samples were given in Table 4.3. The criterions involved in the selection of samples were determined having the highest values in terms of flexural and compressive strengths, and with an easy processing applicability in the process of mixing, molding and setting in terms of workability.

Table 4.3. Experimental parameters used to obtain the selected sample of BFS-UB.

Experimental Parameters	**Mechanical Properties**	
	Compressive Strength (MPa)	**Flexural Strength (MPa)**
"n" Rate	6	4
"Ms" Rate	1.5	1.5
"w/b" Rate	0.4	0.4
Curing Condition	Steam	Steam

4.1.2. Ceramic waste-unary binders (CW-UB)

4.1.2.1. Workability properties of CW-UB samples

✓ *Flow Table Test of CW-UB*

For all CW-UB samples, flow diameter values were given in Table 4.4. In all CW-UB samples, the increase in water/binder (w/b) value from 0.4 to 0.45 naturally increased the flow diameter (consistency). In general, for both w/b ratios, the flow diameter of the samples was much higher than for the reference portland cement sample having the same w/b ratio. However, for CW-UB samples with a ratio of 0.45 w/b, flow radius values close to the consistency of cement sample were obtained at low "n" ratios (n=2). Accordingly, during the alkali activation process of CW-UB, it was found that most of the samples had a more liquid consistency than the reference cement sample for both w/b ratios.

Table 4.4. Flow values (mm) of CW-UB samples (w/b=0.4 and w/b=0.45).

CW-UB Flow Diameter (mm)	**M_s (SiO_2/Na_2O)**					
	(w/b=0.4)			**(w/b=0.45)**		
n (Na_2O%/Activator)	**1.2**	**1.5**	**1.8**	**1.2**	**1.5**	**1.8**
2	230	240	250	250	280	290
4	260	270	L	L	L	L
6	R.S	R.S	R.S	L	L	L

L: Liquid R.S: Rapid Setting

The changes in the flow diameter according to the "n" and "Ms" ratios for both "w/b" values of CW-UB samples were given in Figures 4.12 and 4.13.

For samples with a ratio of 0.4 w/b, when the value of "n" ratio was equal to 2 and 4, the flow radius values of the samples were higher than for the cement samples with the same w/b value. However, it was found that CW-UB samples had much lower flow radius and consistency properties compared to BFS-UB samples at the same w/b ratio. When the "n" ratio increased (n=6), the consistency of CW-UB samples produced by alkali activation became liquefied, because the transition speed from liquid consistency to solid consistency was very short (5-10 minutes), therefore the workability property was considerably decreased compared to cement. For w/b=0.45 ratio, it was determined

that the flow diameter of all samples were higher than the reference cement sample and other CW-UB with ratio of w/b=0.4. However, for CW-UB samples with a ratio of 0.45 w/b, flow radius values close to the consistency of cement sample which were obtained at low “n” ratios (n=2).

For low and medium “Ms” ratio (Ms=1.2 and Ms=1.5) increasing the “n” ratio in the samples rised the consistency up to a ratio of n=4 giving the maxiumum flow diameter os sample and then decreased. This suggest that as the amount of activator solution used for the activation of the samples increased up to n=4 (mixture of sodium silicate and sodium hydroxide), the consistency of the samples increased and then decreased. However, when the n value was raised to n=6, the transition from liquid to solid consistency was rapidly occured. This rapid setting event was similar to the activation of BFS-UB. For the w/b=0.4 ratio, the closest consistency value to the reference cement was at n=2, while at w/b=0.45, the flow diameter determined at n=4 were closer to the flow diameter of cement. According to Figure 4.13, the increase in “Ms” ratio at low “n” rates (n=2) increased the consistency. However, when the ratio “n” increased slightly, consistency increased to a certain “Ms” ratio (Ms=1.5), but after a point it decreased. For high “n” ratios (n=6), very fast setting was observed for all “Ms” ratios.

As a result, it was observed that the consistency of samples with high “n” ratios (high activator dosage) during activation of CW-UB decreased considerably. For CW-UB samples, the values closest to the flow diameter of cement were determined for n=4 for both w/b ratios. This means that the use of a moderate level of activator dosage gives the values closest to the reference cement sample in terms of the consistency of the CW-UB samples. It was also found that the high “Ms” ratio (Ms=1.8) adversely affected the consistency of CW-UB samples in terms of decreasing the flow diameter. Thus, while the sodium silicate content in the activator dosage increased, the decrease in sodium hydroxide ratio significantly reduced the flow diameter of the samples.

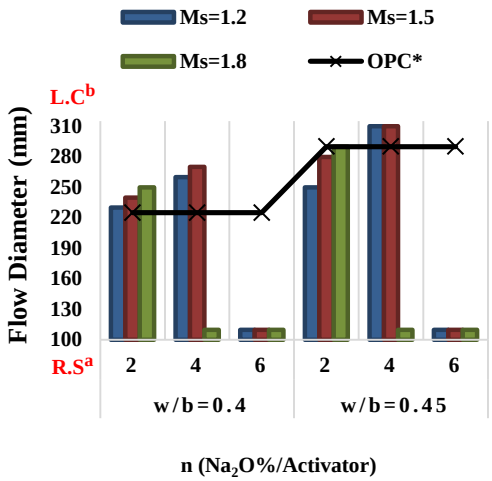


Figure 4.12. The flow values of CW-UB according to "n" ratio **(**For "w/b=0.4" and For "w/b=0.45").

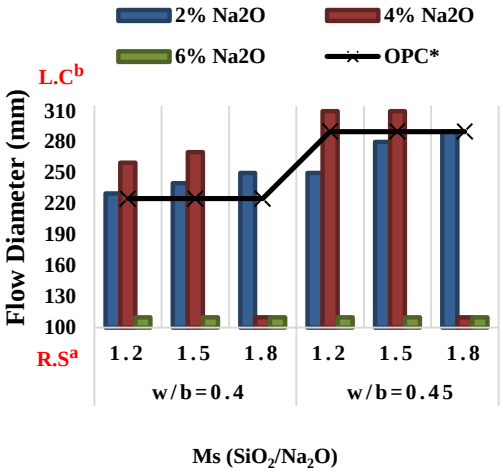


Figure 4.13. The flow values of CW-UB according to "Ms" ratio (For "w/b=0.4" and For "w/b=0.45").

* The cement paste was formed only with water without using an alkaline activator.
[a] Below the flow radius of 100mm was the "Rapid Setting" limit.
[b] Above flow radius of 300mm was "Liquid Consistency" limit.

✓ *Setting Time Test of CW-UB*

In this experiment, initial and final setting time values of CW-UB samples for both w/b ratios were given in Table 4.5. In the experiment, it was determined that as the w/b ratio of CW-UB samples increased, initial and final setting times increased.

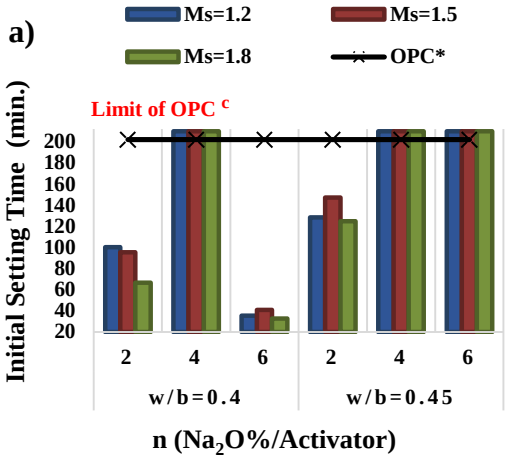
The change in the initial and final setting times of the samples according to the "n" ratio for both w/b ratios were shown in Figure 4.14. It was observed that the initial and final setting time of CW-UB samples set for n=2 ratio and ratio of w/b=0.4 faster than the reference cement sample. For both w/b ratios, the initial and final setting times were extended between 8-10 hours when "n" ratio was 4. However, when the value of "n" reached (n=6), initial setting time suddenly reduced for ratio of w/b=0.4 but final setting time of samples were extended. This means that increasing the Na_2O content (increasing activator dosage) in the samples increased the workability to some point (n=4). However, the increase in this ratio (n=6) significantly shortened the initial setting times especially for w/b=0.4. This had a negative effect on the workability of the samples.

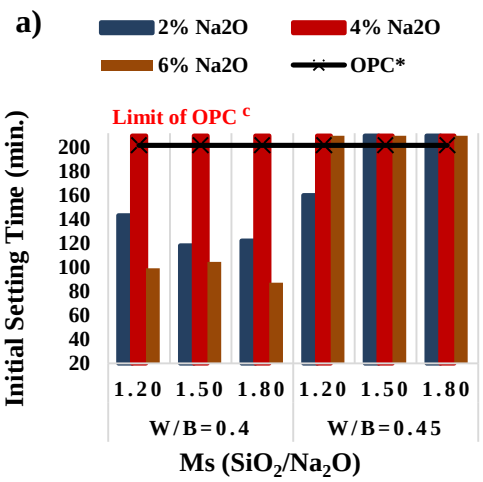
Table 4.5. Setting time of CW-UB samples (w/b=0.4 and w/b=0.45).

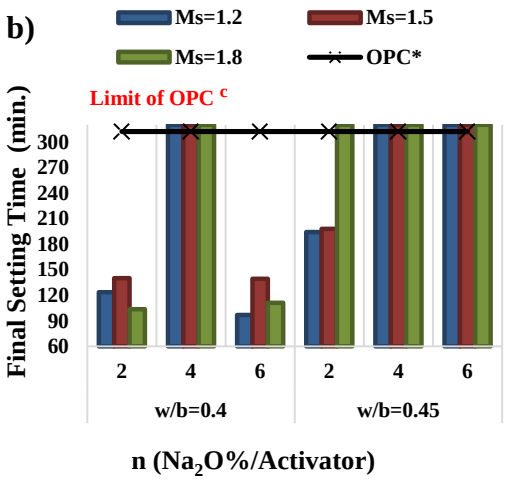
Code	Initial Setting Time (min.)	Final Setting Time (min.)	Note
CW-2/1.2/0.4	143	153	SPD
CW -2/1.5/0.4	118	121	SPD
CW -2/1.8/0.4	122	123	SPD
CW -4/1.2/0.4	>202	>312	
CW -4/1.5/0.4	>202	>312	
CW -4/1.8/0.4	>202	>312	
CW -6/1.2/0.4	99	>312	HS
CW -6/1.5/0.4	105	>312	HS
CW -6/1.8/0.4	87	>312	HS
CW -2/1.2/0.45	160	170	SPD
CW -2/1.5/0.45	>202	>312	
CW -2/1.8/0.45	>202	>312	
CW -4/1.2/0.45	>202	>312	
CW -4/1.5/0.45	>202	>312	
CW -4/1.8/0.45	>202	>312	
CW -6/1.2/0.45	>202	>312	
CW -6/1.5/0.45	>202	>312	
CW -6/1.8/0.45	>202	>312	

SPD: Short Period Difference HS: Half-Setting

The initial and final setting times of the samples according to the “Ms” ratio was shown in Figure 4.15. According to these graphs, it was observed that there was no general tendency to change the setting times with “Ms” ratios for both w/b ratios. It was concluded that the effect of the “Ms” ratio on the samples had no more determinative effect than the effect of the “n” ratio.







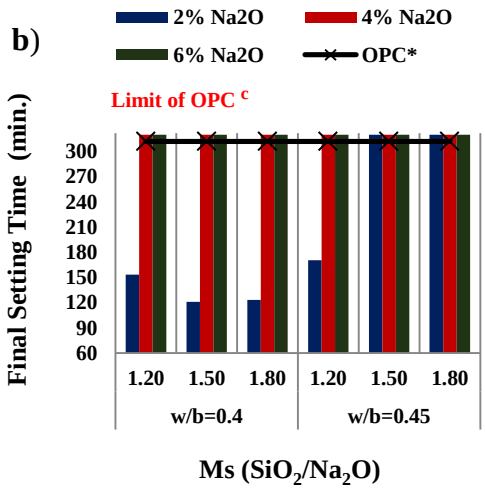


Figure 4.14. The setting time of CW-UB Samples according to "n" ratio a) Initial setting time b) Final setting time.

Figure 4.15. The setting time of CW-UB Samples according to "Ms" ratio a) Initial setting time b) Final setting time.

* The cement paste is formed only with water without using an alkaline activator.
[c] These limit values were defined in ASTM C 191-13 Standard.

✓ *Workability Properties of CW-UB*

In this study, increasing the "w/b" ratio from 0.4 to 0.45 during the alkaline activation process of CW-UB increased both the flow diameter value and setting times of the samples in general. In addition, samples with "w/b" ratio of 0.4 showed workability closer to cement, especially in terms of consistency. In samples with "w/b" ratio of 0.4 and high alkali activator dosage (n=6), rapid transition from liquid consistency to solid

state, early setting and rapid workability loss were observed. Consequently, as the activator dosage of the samples increased (that was, Na_2O and SiO_2 concentrations increased), the setting time was considerably shortened.

There are very few studies published in the literature on the production of binder with alkaline activation of CW-UB. Only two of these studies focused on the processability properties of the alkaline activation process of ceramic waste alone (CW-UB) [43, 92]. In one of these studies, similar to our study, a wide set of setting time ranging from a few minutes to 10 hours depending on the changing "n" and "Ms" ratios was obtained. They also mentioned in their study that because of the low Ca^{+2} content of the ceramic waste, it was not possible to make the setting of the samples and therefore it was necessary to add $Ca(OH)_2$ to the samples with a certain percentage [43]. In our study, $Ca(OH)_2$ was added to all samples at the rate of 2% of the total source material mass. All the CW-UB samples completed their setting within 8-10 hours at the latest.

In addition, in the same study [43], similarly to our study, it was determined that very high Na^+ concentration depending on the SiO_2 content of the activator caused a rapid setting of the samples. Therefore, it was determined that very high and very low Na^+ concentrations negatively affect the processability properties of the samples. However, contrary to our study, it was determined that there was no relationship between Na_2O concentration and setting time in samples with low SiO_2 ratio, but the increment of Na_2O ratio extended the setting time as the SiO_2 ratio increased. In our study results, no correlation was found between SiO_2/Na_2O (Ms) and Na_2O (n) ratios and setting time. However, when Na_2O % concentration was equal to n=4, setting time was prolonged and when sodium concentration increases even more (n=6), it was determined that the transition rates from solid consistency to liquid consistency increase even if the consistency of the samples becomes liquefied. However, in our study, it was observed that the setting time for the same Na_2O ratio increased as the SiO_2 ratio increased.

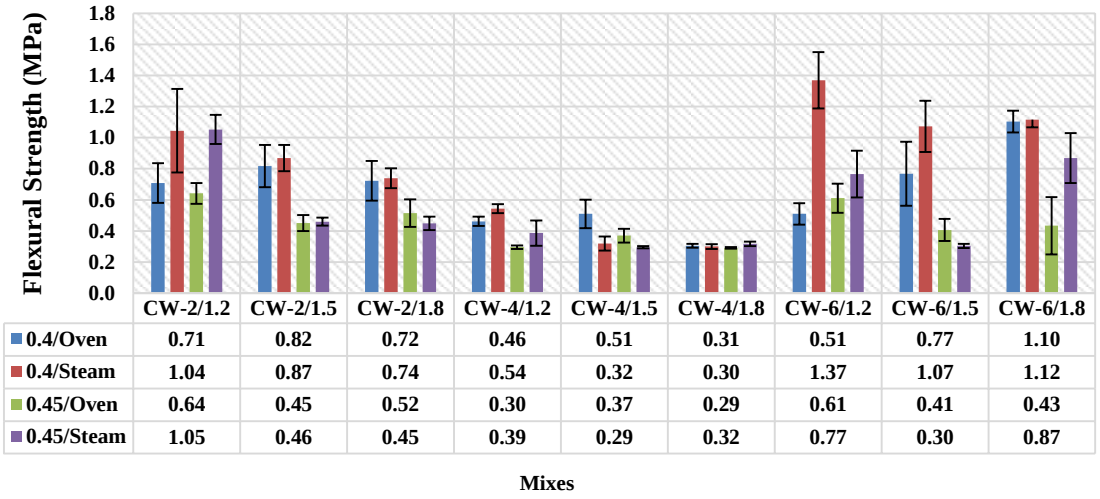
In the second study [92], 100 % ceramic and brick waste were activated with a mixture of sodium hydroxide and sodium silicate, which was the same activator employed in our study. In this work, both examples were reference samples. It was determined that ceramic waste pastes had better processability properties than brick waste pastes. The reason for this was that brick waste had a more porous and irregular particle structure.

4.1.2.2. Strength properties of CW-UB samples

✓ *Flexural Strength Test of CW-UB*

The flexural strength values of the CW-UB samples were given in Figure 4.16 for both w/b ratios (0.4 and 0.45) and for both curing conditions (oven and steam).

The highest flexural strength value for CW-UB sample set was for the "CW 6/1.2/0.4/Steam" sample. Thus, the highest flexural strength value was determined for w/b = 0.4 ratio and steam curing.



	CW-2/1.2	CW-2/1.5	CW-2/1.8	CW-4/1.2	CW-4/1.5	CW-4/1.8	CW-6/1.2	CW-6/1.5	CW-6/1.8
0.4/Oven	0.71	0.82	0.72	0.46	0.51	0.31	0.51	0.77	1.10
0.4/Steam	1.04	0.87	0.74	0.54	0.32	0.30	1.37	1.07	1.12
0.45/Oven	0.64	0.45	0.52	0.30	0.37	0.29	0.61	0.41	0.43
0.45/Steam	1.05	0.46	0.45	0.39	0.29	0.32	0.77	0.30	0.87

Figure 4.16. Flexural strength of CW-UB samples for 7 days.

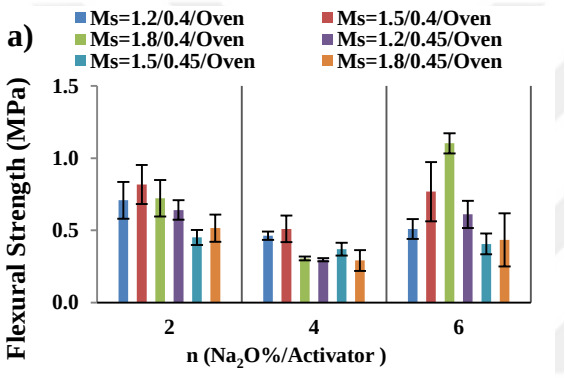
In this test set, when the w/b ratio increased from 0.40 to 0.45, the flexural strength values of the samples decreased for both curing conditions. This means that as the w/b ratio increased, the flexural strength values of CW-UB samples decreased.

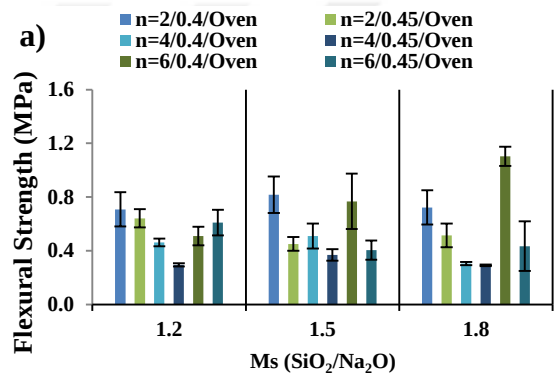
The variation of flexural strength values of samples according to "n" ratio was given in Figure 4.17 for two different curing conditions. There was no general trend between the variation of the "n" ratio and the change in flexural strength values of the samples. The highest slope strength value was n = 6 for w/b=0.4. When the n ratio increased from 2 to 4, the flexural strength values decreased for both w/b ratios. For both curing conditions, the flexural strength values for n=6 ratio generally increased.

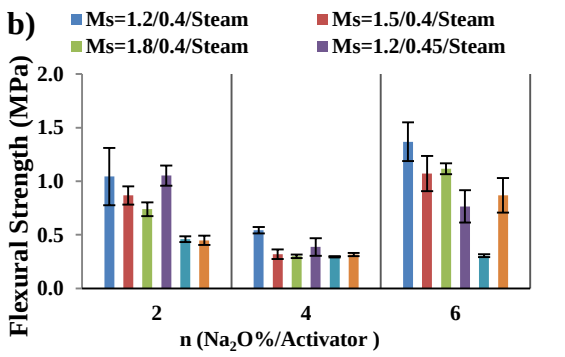
The changes in flexural strength values according to the "Ms" ratio were given in Figure 4.18 for two different curing conditions. For this test set, the effect of the change of the

"Ms" ratio on the flexural strength of the samples was not as significant as the "n" ratio for both cure conditions. Increasing the "Ms" ratio (SiO_2/Na_2O) reduced the flexural strength value for low and medium "n" ratios (n=2 and n=4) for steam cure.

These results suggest that "n" ratio was more effective than "Ms" ratio on the change of flexural strength of CW-UB system as in the same workability properties. The highest flexural strength value among CW-UB samples was obtained for the "CW/6/1.2/0.4/Steam" sample. Thus, the highest flexural strength value for the unary binder system consisting of ceramic waste was in the case of w/b = 0.4 and steam curing at ratios "n" = 6 and "Ms" = 1.2.







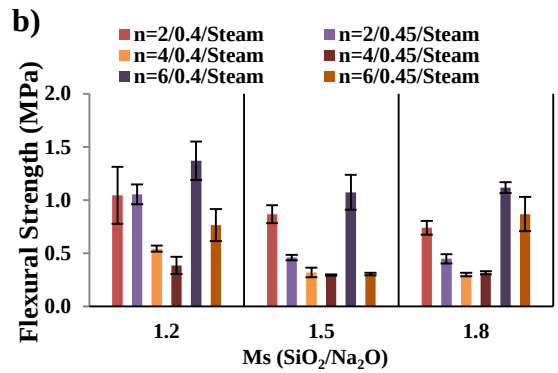


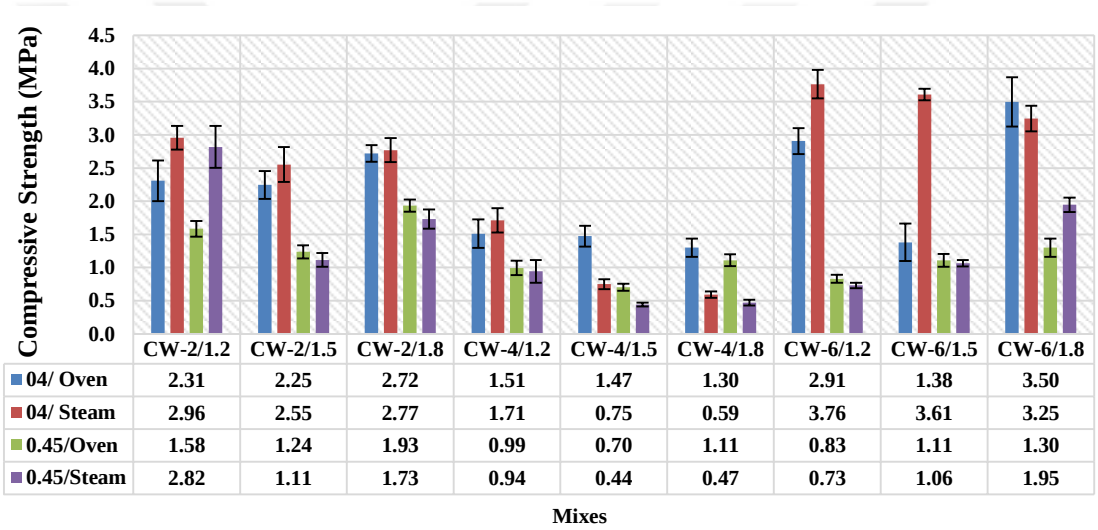
Figure 4.17. Change in flexural strength of CW-UB according to "n" ratio a) For oven cure b) For steam cure.

Figure 4.18. Change in flexural strength of CW-UB according to "M_S" ratio a) For oven cure b) For steam cure.

✓ *Compressive Strength Test of CW-UB*

The compressive strength values of CW-UB samples were given in Figure 4.19 for both w/b ratios (0.4 and 0.45) and both curing conditions (oven and steam).

The highest compressive strength value for CW-UB sample set was for the "CW 6/1.2/0.4/Steam" sample. Thus, the highest flexural strength value was determined for w/b = 0.4 ratio and steam curing. When the w/b ratio increased from 0.40 to 0.45, the compressive strength values of the samples decreased for both curing conditions as in the experimental set of flexural strength. It was determined that the steam cured samples reached higher compressive strength values than the oven cured for w/b = 0.4.



	CW-2/1.2	CW-2/1.5	CW-2/1.8	CW-4/1.2	CW-4/1.5	CW-4/1.8	CW-6/1.2	CW-6/1.5	CW-6/1.8
04/ Oven	2.31	2.25	2.72	1.51	1.47	1.30	2.91	1.38	3.50
04/ Steam	2.96	2.55	2.77	1.71	0.75	0.59	3.76	3.61	3.25
0.45/Oven	1.58	1.24	1.93	0.99	0.70	1.11	0.83	1.11	1.30
0.45/Steam	2.82	1.11	1.73	0.94	0.44	0.47	0.73	1.06	1.95

Figure 4.19. Compressive strength of CW-UB samples for 7 days.

The variation of compressive strength values of samples according to "n" ratio was given in Figure 4.20 for two different curing conditions. The increase in the "n" ratio did not create a general tendency to change the compressive strength of each samples. The increase in "n" from 2 to 4 caused a decrease in the compressive strength, while the value of n increased further to 6, the highest compressive strength values for steam cured samples were recorded for samples with w/b ratio of 0.4.

The variation of compressive strength values of samples according to "Ms" ratio was given in Figure 4.21 for two different curing conditions. The increase in the "Ms" ratio did not create a general tendency to change the compressive strength of each samples.

Thus, “n” ratio was found to be more effective than “Ms” ratio on the strength changes of the samples during the activation of CW-UB.

✓ *Strength Properties of CW-UB*

The strength tests were carried out on CW-UB paste sample produced by alkali activation method for two w/b ratios and curing conditions. Within the scope of these experiments, flexural and compressive tests of the samples activation were performed with activator solution consisting of liquid sodium silicate and sodium hydroxide mixture.

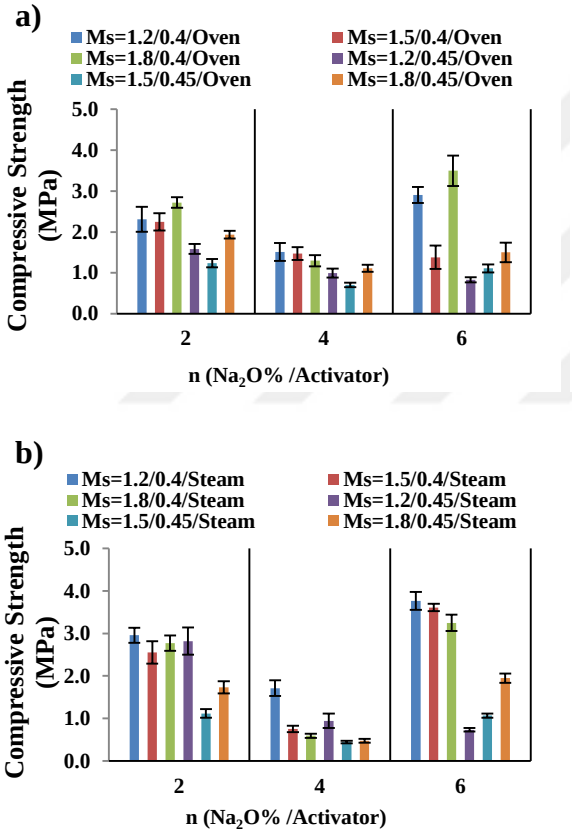


Figure 4.20. Change in compressive strength of CW-UB according to “n” ratio a) For oven cure b) For steam cure.

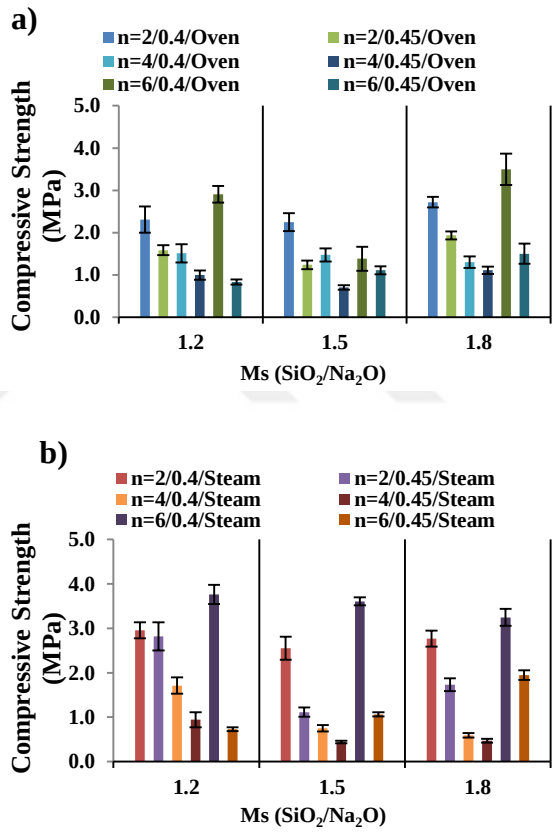


Figure 4.21. Change in compressive strength of CW-UB according to “M_s” ratio a) For oven cure b) For steam cure.

The selected paste samples among CW-UB were found to be 0.4 w/b ratio and steam curing. The results of these two experiments for steam cure and w/b=0.4 which were shown in Figure 4.22.

According to these results, when the ratio of "n" increased from 2 to 4, both flexural and compressive strength values decreased. However, when the ratio of n increased from 4 to 6, the highest flexural and compressive strength values were obtained for CW-UB.

The increase in the "Ms" ratio for each "n" ratio has resulted in reducing effect on the strength values. The strength values obtained for this set of experiments were determined below the flexural (8.1 MPa) and compressive strength (58.7 MPa) values obtained for the reference cement paste.

According to the literature, it was known that the bonding structures and products of alumina-silicate based materials such as ceramic waste and based materials such as slag in alkaline activation processes were different from each other. The former model had similarities with the zeolite formation process and final product was characterized by a polymeric model. In second model, main reaction product of alkali activated (Ca + Si) based material was C-S-H which was the main bonding structure of cement [23,93-95].

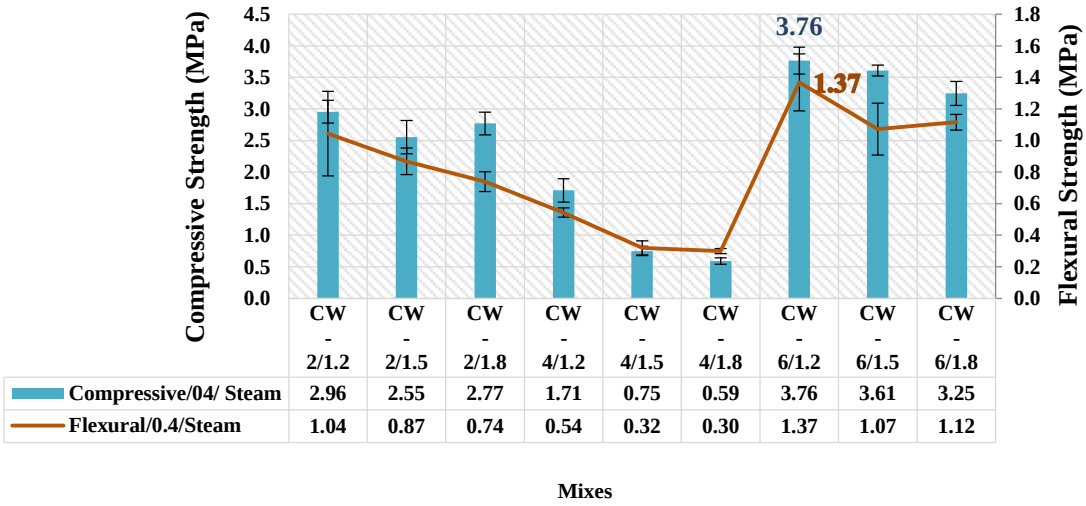


Figure 4.22. Compressive and flexural strength of CW-UB samples for 7 days.

Finally, the expected binding model in the CW-UB binder structure was similar to that of alkali-activated alumina-silicate based materials. The bond structure formed as a result of the CW-UB was determined in "Sixth Stage" by various microstructure analyzes.

In the literature, experimental processes carried out on mortar samples [43] or paste samples [46, 92] published in a limited number of studies dealing with the alkali

activation system of CW-UB. In our study, since all experimental process was carried out to produce a new type of binder, experimental studies were carried out on the paste samples. In one of the studies in the literature, the strength values could not be measured because of the paste samples containing 100% ceramic waste that could not complete the setting process [46]. In another study, compressive strength values between 30-70 MPa were reported for 100 % ceramic waste containing pastes using different alkali activators [92]. Compressive strength values between 2-16 MPa were obtained for different Na_2O ratios for the paste samples produced by red clay brick waste, which have a chemical similar content to the ceramic waste content (65% SiO_2 and 20% Al_2O_3) used in our study [96]. In our study, a compressive strength value close to 4 MPa was reached at the end of the 7-day alkali activation process of the CW-UB. Although this value does not seem sufficient for a structural material, it was thought that it can be positioned as a binding material in the construction industry as a non-structural material.

✓ *The Determination of the Selected Sample of CW-UB*

At the end of the first set of experiments including workability and strength tests, one samples that selected represent this test set were determined for CW-UB in terms of both flexural and compressive strength (CW 6/1.2/0.4/Steam). The experimental parameters of the selected samples were given in Table 4.6. The selection criterion applied during the sample selection was applied to determine the samples having the highest values in terms of flexural and compressive strengths and which were not problematic in the process of mixing, molding and setting in terms of workability.

Table 4.6. Experimental parameters of the selected samples of CW-UB.

CW-UB	**The Selected Sample**	
	Compressive Strength (MPa)	**Flexural Strength (MPa)**
"n" Rate	6	6
"Ms" Rate	1.2	1.2
"w/b" Rate	0.4	0.4
Cure Cond.	Steam	Steam

4.1.3. Marble waste-unary binders (MW-UB)

4.1.3.1. Workability properties of MW-UB samples

✓ *Flow Table Test of MW-UB*

For all MW-UB samples, flow values were given in Table 4.7 as both flow diameter (mm) and percentage of flow.

Table 4.7. Flow values (mm) of MW-UB samples (w/b=0.4 and w/b=0.45).

MW	**M_s (SiO_2/Na_2O)**					
	(w/b=0.4)			**(w/b=0.45)**		
n (Na_2O%/Activator)	**1.2**	**1.5**	**1.8**	**1.2**	**1.5**	**1.8**
2	230	210	220	270	250	270
4	280	250	230	L	270	L
6	L	L	L	L	L	L

L: Liquid

In the activation process of MW-UB, it was determined that when the w/b ratio increased from 0.4 to 0.45, the flow diameters of all samples increased. It was found that the increase of "Ms" ratio in this experimental system did not constitute a general trend for all samples. For both w/b ratios, a liquid consistency was observed in all Ms values for n=6 ratio. The consistency values of samples closest to the consistency of the cement were determined for w/b = 0.4 ratio, and for n=2 and n=4, Ms=1.8.

The changes in the flow values according to the "n" ratio for both "w/b" values of MW-UB samples were given in Figures 4.23. For both w/b ratios, the increase in the "n" ratio increased the flow diameter value of the samples. This increase was much more pronounced for the w/b = 0.4 ratio. Thus, it has been found that increasing the amount of activator dosage used for the activation of the samples (increasing the ratio of n) increases the flow diameter of the samples.

The change in flow rate and "Ms" ratio was given in Figure 4.24. According to this graph, it was found that almost all "Ms" values flow diameter values of samples with low n values (n = 2) were very close to the spread diameter value of cement sample. As a result, it was determined that the viscosity of the samples was highly liquefied and the

setting times were prolonged by increasing the dosage of activator used for the activation of the samples.

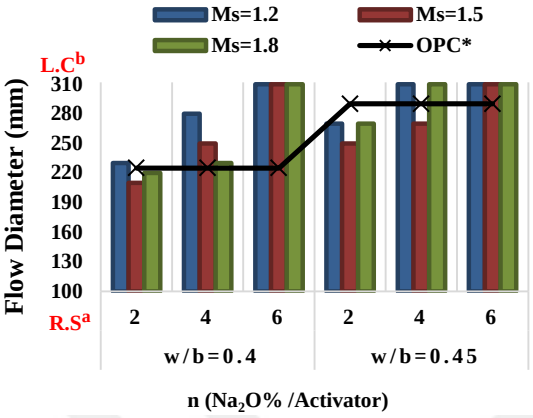


Figure 4.23. The flow values of MW-UB according to "n" ratio (For "w/b = 0.4" and For "w/b = 0.45").

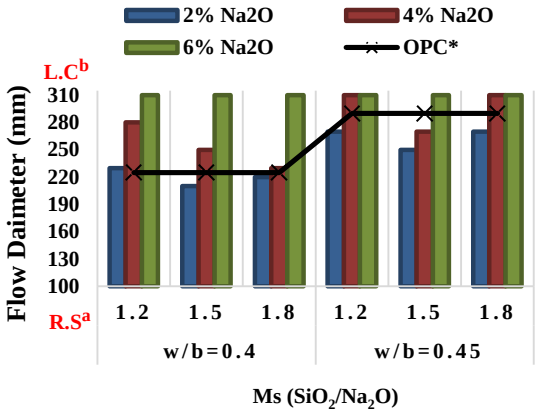


Figure 4.24. The flow values of MW-UB according to "Ms" ratio (For "w/b = 0.4" and For "w/b = 0.45").

* The cement paste was formed only with water without using an alkaline activator.
[a] Below the flow radius of 100 mm was the "Rapid Setting" limit.
[b] Above flow radius of 300 mm was "Liquid Consistency" limit.

✓ *Setting Time Test of MW-UB*

In this experiment, initial and final setting time values of MW-UB samples for both w/b ratios were given in Table 4.8. Limit values of initial and final setting time were 202 min and 312 min respectively according to ASTM C 191-13 Standard in the experiment. Samples with exceeding these limit values were completed the setting time within 8-10 hours. Phrase of "no setting (after 48h)" was used for the samples which could not be completed within 48 hours and these samples were excluded from the evaluation. "Rapid Setting" was used in the graphs for samples with an initial setting time before 90 minutes and a final setting time before 150 minutes. The setting time also indicated as "Half-Setting" because of initial setting time was within the ASTM standard but the final setting time was not within the standard for some examples. In addition, "short period difference" phrase was used for sample with a difference between the initial and final setting times less than 15 min.

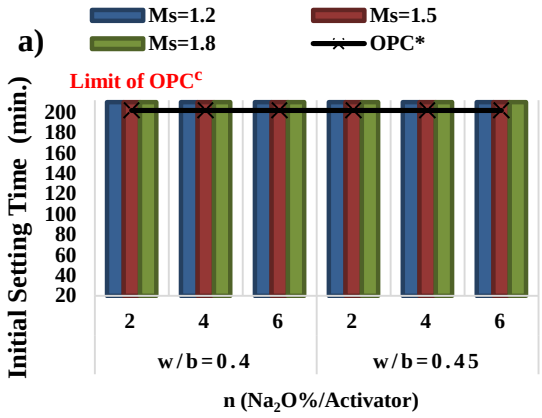
As a result of the unary component activation process of MW-UB, the setting time for all samples (for both w/b ratios) was determined between 8-10 hours. Initial and final

setting times of samples were outside the ASTM standards. Therefore, the initial setting time of all samples in this test system was found to be over 200 minutes while the final setting time was over 300 minutes.

Table 4.8. Setting time of MW-UB samples (w/b=0.4 and w/b=0.45).

Code	Initial Setting Time (min.)	Final Setting Time (min.)	Note
MW-2/1.2/0.4	>202	>312	
MW-2/1.5/0.4	>202	>312	
MW-2/1.8/0.4	>202	>312	
MW-4/1.2/0.4	>202	>312	
MW-4/1.5/0.4	>202	>312	
MW-4/1.8/0.4	>202	>312	
MW-6/1.2/0.4	>202	>312	
MW-6/1.5/0.4	>202	>312	
MW-6/1.8/0.4	>202	>312	
MW-2/1.2/0.45	>202	>312	
MW-2/1.5/0.45	>202	>312	
MW-2/1.8/0.45	>202	>312	
MW-4/1.2/0.45	>202	>312	
MW-4/1.5/0.45	>202	>312	
MW-4/1.8/0.45	>202	>312	
MW-6/1.2/0.45	>202	>312	
MW-6/1.5/0.45	>202	>312	No setting (after 48 h)
MW-6/1.8/0.45	>202	>312	No setting (after 48 h)

The change in the initial and final setting times of the samples according to the "n" and "Ms" ratios for both w/b ratios were shown in Figure 4.25 and Figure 4.26. No flash setting was observed in any sample, as observed in the activation of BFS-UB and CW-UB systems. In fact, for samples with "n" value of 6 and "Ms" value equal to 1.8, the setting for both w/b ratios could not be completed even within 48 hours. Since these samples did not complete the set time within 24 hours, they were excluded from the evaluation during this process in which optimum experimental parameters were selected without being subjected to strength tests. Therefore, it has been observed that increasing "n" and "Ms" ratios prolong setting time for unary binder activation of marble waste and even prevent occurrence of setting event. As a result, it has been found that increasing the dosage of activator used for unary binder activation of marble waste (increasing the ratio of "n") and decreasing the amount of sodium hydroxide while increasing the ratio of sodium silicate (increasing the ratio of "Ms") in the activator prolongs the setting time of the samples.



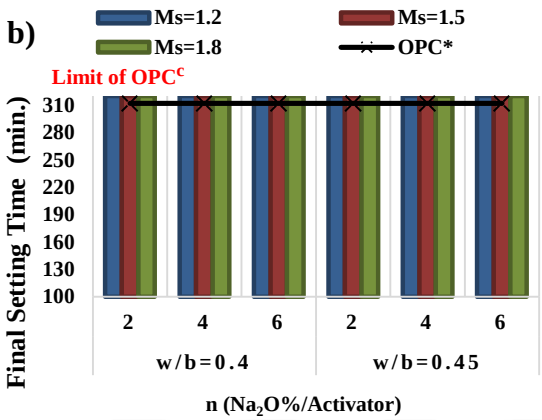
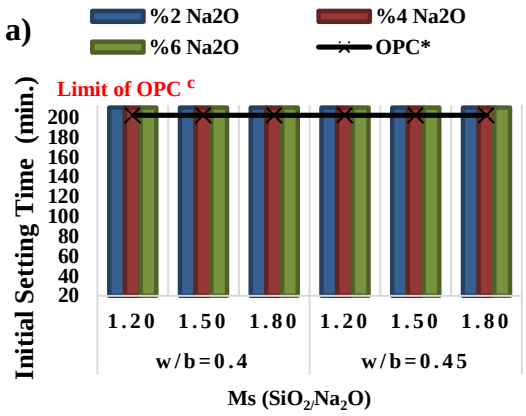


Figure 4.25. The setting time of MW-UB Samples according to "n" ratio a) Initial setting time b) Final setting time.



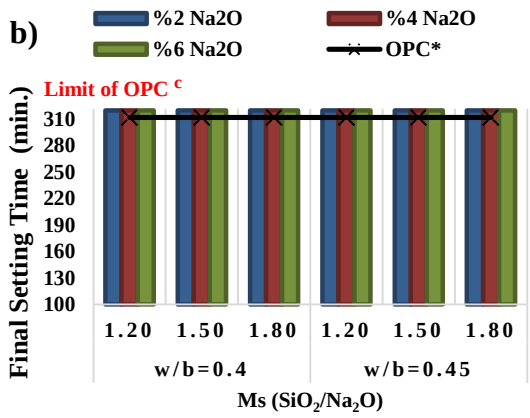


Figure 4.26. The setting time of MW-UB Samples according to "Ms" ratio a) Initial setting time b) Final setting time.

* The cement paste was formed only with water without using an alkaline activator.
[c] These limit values were defined in ASTM C 191-13 Standard.

✓ *Workability Properties of MW-UB*

In the alkaline activation of MW-UB, the consistency of the samples with low and medium "n" values for 0.4 w/b ratio was determined very close to the cement sample. But when the "n" ratio increased to 6, the samples liquefied. For the 0.45 w/b ratio, it was observed that the consistency of all samples was liquefied except for the samples having only n ratio 2. In alkali activation of MW-UB, the setting times of all samples were determined to be much longer than the cement sample according to the reference ASTM standard. Samples with a ratio of 0.45 w/b and "n' equal to 6 did not complete their setting. All samples except these samples had a setting time of 8-10 hours. As a result, when compared with the alkali activation process of BFS-UB and CW-UB, it

was found that the binder structure formed with marble waste had greater values of flow diameter and setting times.

A limited number of publications on the activation of marble waste and limestone alone were reported in the literature. Therefore, no publication had been found on the workability characteristics of the marble waste during the unary component alkali activation process. However, it was known that the presence of CO_3^{-2} ion in alkali activation systems delays the setting time, especially in systems containing Ca^{+2} [97]. As in this study, the reason for the long setting times and low strength values in the activation of MW-UB can be explained as follows.

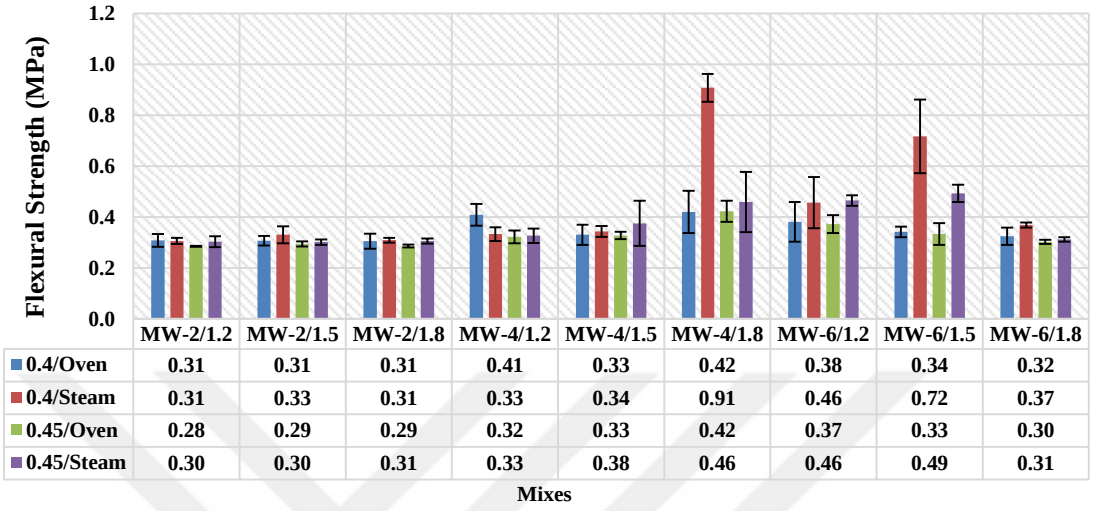
In the activation of marble, especially in high pH systems (containing high amounts of Na_2O/ high "n" values), dissolved Ca^{+2} would not participate only in the formation of C–S–H. Instead, the Ca^{+2} was more prone to react with the excessive OH^- in the pore solution, forming precipitates as calcium hydroxide [98]. In addition, CO_3^{-2} tends to react with Na^{+2} ion and these two ions have combined Na_2CO_3 as precipitated at the grain boundary. Alkali carbonates have a larger volume than that initially occupied by water and when dry, these generate internal stresses and deterioration of the alkali pastes [52]. In this case, the formation of C-S-H or N-C/(A)-S-H bond structure in the system decreases and slows down. Therefore, the setting time for these alkali activation systems was delayed or does not occur. Finally, it was clear that an excessive amount of Na_2O, could lead to processes of deterioration and collapse of the mechanical properties [99]. Within the scope of this thesis, it was determined that the setting time of the samples was not completed even after 48 hours, especially in the samples with high "n" ratio (high Na_2O content). The consistency levels of the marble waste samples were found to be much higher than the consistency of blast furnace slag and ceramic waste samples, although they had the same w/b ratio. This was thought to be due to the alkali carbonates effect as described above.

4.1.3.2. Strength properties of MW-UB samples

✓ *Flexural Strength Test of MW-UB*

The flexural strength values of the MW-UB samples were given in Figure 4.27 for both w/b ratios (0.4 and 0.45) and for both curing conditions (oven and steam).

The highest flexural strength value for MW-UB sample set was for the "MW 4/1.8/0.4/Steam" sample. Thus, the highest flexural strength value was determined for w/b = 0.4 ratio and steam curing.



	MW-2/1.2	MW-2/1.5	MW-2/1.8	MW-4/1.2	MW-4/1.5	MW-4/1.8	MW-6/1.2	MW-6/1.5	MW-6/1.8
0.4/Oven	0.31	0.31	0.31	0.41	0.33	0.42	0.38	0.34	0.32
0.4/Steam	0.31	0.33	0.31	0.33	0.34	0.91	0.46	0.72	0.37
0.45/Oven	0.28	0.29	0.29	0.32	0.33	0.42	0.37	0.33	0.30
0.45/Steam	0.30	0.30	0.31	0.33	0.38	0.46	0.46	0.49	0.31

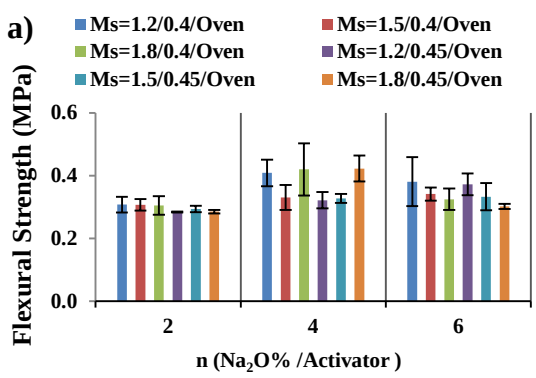
Figure 4.27. Flexural strength of MW-UB samples for 7 days.

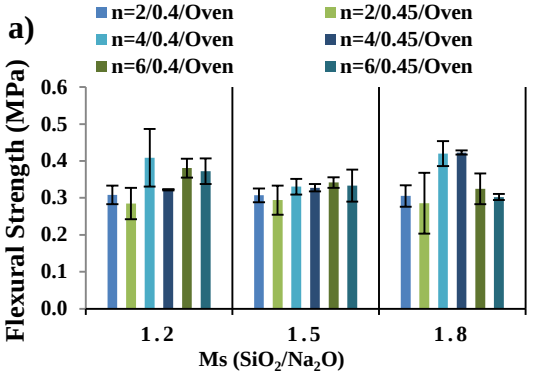
In this test set, when the w/b ratio increased from 0.40 to 0.45, the flexural strength values of the samples were almost the same for both curing conditions. This means that variation of the w/b ratio did not affect the flexural strength value very much. For the steam-cured "MW/4/1.8 and MW/6/1.5" samples, a decrease in flexural strength values was observed when the w/b ratio increased.

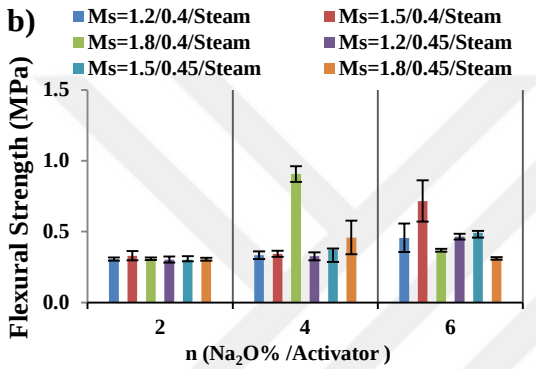
The variation of flexural strength values of MW-UB samples according to "n" ratio was given in Figure 4.28 for two different curing conditions. There was no general trend between the variation of the "n" ratio and the change in flexural strength values of the samples. The highest slope strength value was n = 4 for both curing conditions.

The changes in flexural strength values of MW-UB samples according to the "Ms" ratio were given in Figure 4.29 for two different curing conditions. For this test set also, there was no general trend between the variation of the "n" ratio and the change in flexural strength values of the samples. Increasing the "Ms" ratio (SiO_2/Na_2O) increased the flexural strength value when n ratio was equal to 4 for steam curing.

As a result, the variation of experimental parameters such as "n", "Ms" and "w/b" ratio had no significant effect on the flexural strength of MW-UB samples, especially for samples with low and medium levels of "n" and "Ms" ratio.







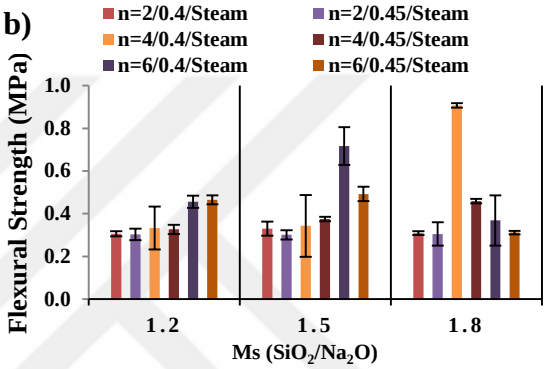


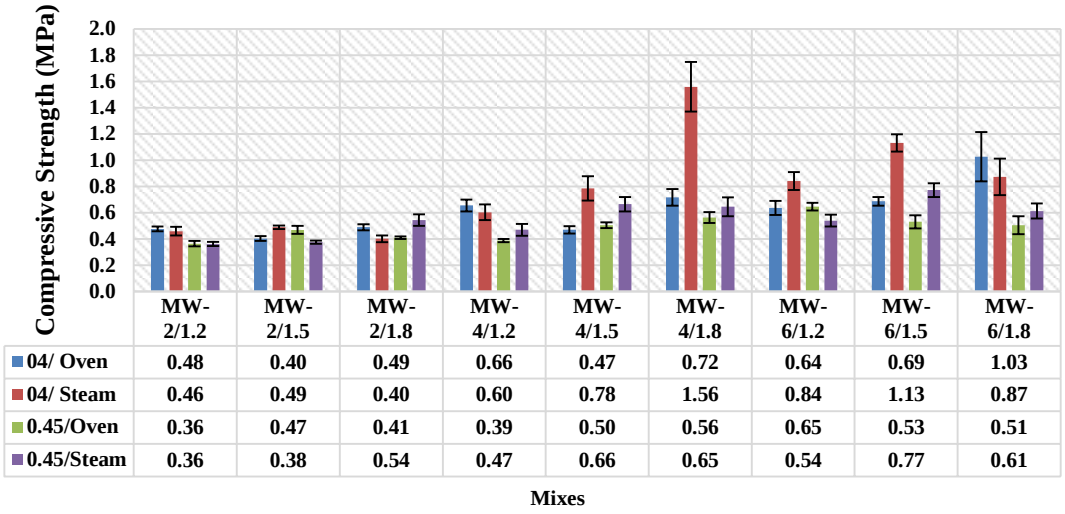
Figure 4.28. Change in flexural strength of MW paste according to "n" ratio a) For oven cure b) For steam cure.

Figure 4.29. Change in flexural strength of MW paste according to "M_s" ratio a) For oven cure b) For steam cure.

✓ *Compressive Strength Test of MW-UB*

The compressive strength values of MW-UB samples were given in Figure 4.30 for both w/b ratios (0.4 and 0.45) and both curing conditions (oven and steam).

The highest compressive strength value for MW-UB sample set was for the "MW 4/1.8/0.4/Steam" sample. Thus, the highest compressive strength value was determined for w/b = 0.4 ratio and steam curing. When the w/b ratio increased from 0.40 to 0.45, the compressive strength values of the samples generally decreased for both curing conditions. It was determined that the steam cured samples reached higher compressive strength values than the oven cured for w/b = 0.4.

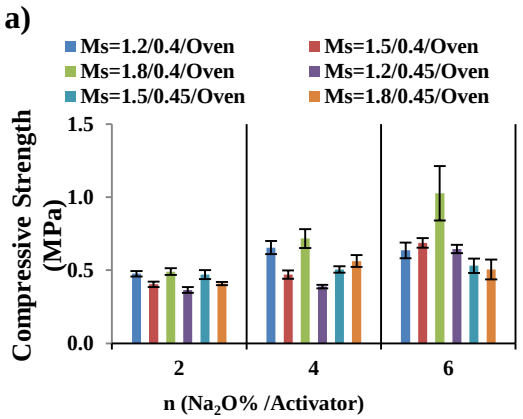


	MW-2/1.2	MW-2/1.5	MW-2/1.8	MW-4/1.2	MW-4/1.5	MW-4/1.8	MW-6/1.2	MW-6/1.5	MW-6/1.8
04/ Oven	0.48	0.40	0.49	0.66	0.47	0.72	0.64	0.69	1.03
04/ Steam	0.46	0.49	0.40	0.60	0.78	1.56	0.84	1.13	0.87
0.45/Oven	0.36	0.47	0.41	0.39	0.50	0.56	0.65	0.53	0.51
0.45/Steam	0.36	0.38	0.54	0.47	0.66	0.65	0.54	0.77	0.61

Figure 4.30. Compressive strength of MW-UB samples for 7 days.

The variation of compressive strength values of MW-UB samples according to "n" ratio was given in Figure 4.31 for two different curing conditions. The increase in the "n" ratio did not create a general tendency to change the compressive strength of each samples. While the highest compressive strength value of the oven curing was for n=6, the highest compressive strength value for steam curing was n=4 and higher than the selected value among the samples obtained for oven curing. In particular, the increase of "n" value for oven curing had a positive effect on strength of samples. However, the same tendency to increase strength did not occur for steam curing.

The variation of compressive strength values of MW-UB samples according to "Ms" ratio was given in Figure 4.32 for two different curing conditions. The increase in the "Ms" ratio did not create a general tendency to change the compressive strength of each samples. For the activation of MW-UB, the highest compressive strength values were obtained in both curing conditions for high "Ms" ratio (Ms = 1.8). However, the increase in the "Ms" ratio did not create a general tendency to change the compressive strength of each samples.



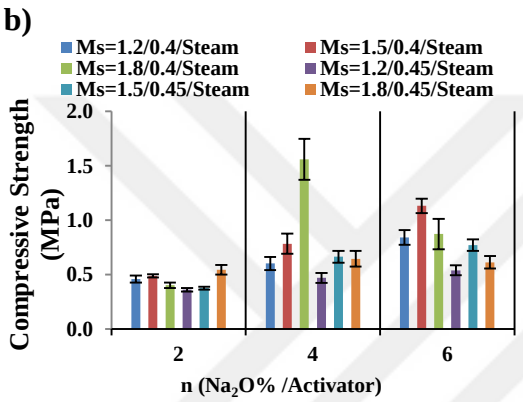
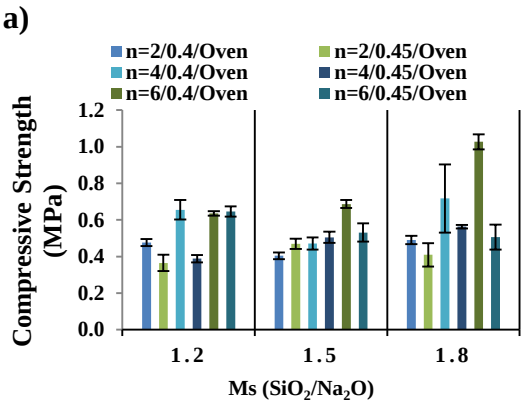


Figure 4.31. Change in compressive strength of MW-UB according to "n" ratio a) For oven cure b) For steam cure.



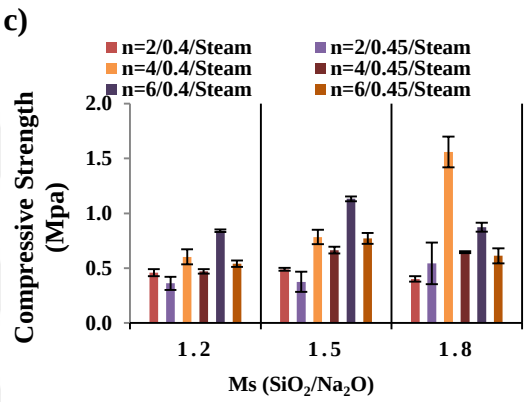


Figure 4.32. Change in compressive strength of MW-UB according to "M_s" ratio a) For oven cure b) For steam cure.

✓ *Strength Properties of MW-UB*

The strength tests of MW-UB by alkali activation method were carried out on paste samples for two w/b ratios and cure conditions. Within the scope of these experiments, flexural and compressive tests of the samples activated with activator solution consisting of liquid sodium silicate and sodium hydroxide mixture were performed. The selected paste samples were found to be 0.4 w/b ratio and steam curing. The results of these two experiments for steam curing and w/b=0.4 were shown in Figure 4.33.

According to these results, when the ratio of "n" increased from 2 to 4, both flexural and compressive strength values increased. The highest flexural and compressive strength values measured among the samples when n was equal to 4. However, when the ratio of n increased from 4 to 6, the flexural and compressive strength values decreased. For the 3 different n values (n=2, n=4 and n=6), the highest strength values were obtained when

Ms ratio was equal to 1.5. The strength values obtained for this set of experiments were determined below the flexural (8.1 MPa) and compressive strength (58.7 MPa) values obtained for the reference cement paste.

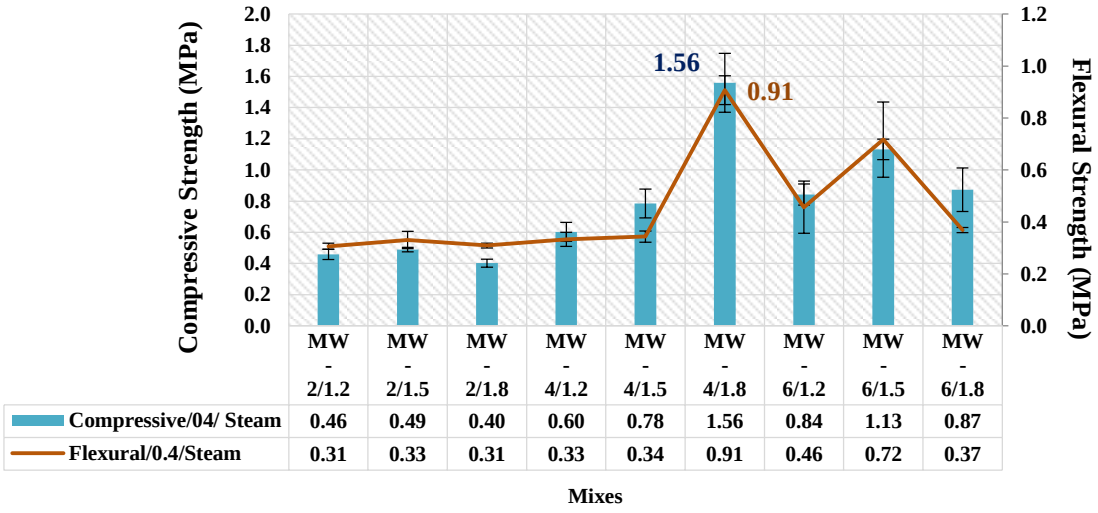


Figure 4.33. Compressive and flexural strength of MW-UB samples for 7 days.

As a result of the alkali activation of MW-UB, very low values were obtained in terms of both flexural and compressive strength. In this study, all samples were subjected to steam or oven curing at 60^0C.

In one of the limited studies in the literature, marble waste activated by an alkali activator, which was a mixture of sodium silicate and sodium hydroxide, then subjected to three different curing conditions: air, humidity and water. The selected results were achieved for air cured samples at room temperature. However, 14-day flexural and compressive strength values for humidity cured samples were determined between 2-4 MPa and 10-15 MPa, respectively [51]. In another study, Compressive strength experiment was carried out for two different "n" ratios and two different "Ms" ratios during the activation of limestone, which has a composition very close to marble waste as a chemical content. In this study, 7-day compressive strength values for all n and Ms values were recorded below 5 MPa, similar to the values in our study [52].

✓ *Determination of the Selected MW-UB Sample*

At the end of the first set of experiments including workability and strength tests, one samples that selected represent this test set were determined for MW-UB in terms of

both flexural and compressive strength (MW 4/1.8/0.4/Steam). The experimental parameters of the selected samples were given in Table 4.9. The selection criterion applied during the sample selection was applied to determine the samples having the highest values in terms of flexural and compressive strengths and which were not problematic in the process of mixing, molding and setting in terms of workability.

Table 4.9. Experimental parameters of the selected samples of MW-UB.

MW-UB Parameters	The Selected Sample	
	Compressive Strength	Flexural Strength
"n" Rate	4	4
"Ms" Rate	1.8	1.8
"w/b" Rate	0.4	0.4
Cure Cond.	Steam	Steam

4.2. Second Stages: Determination of the Optimum Parameters of Binary Binders

4.2.1. Blast furnace slag/ceramic waste-binary binders (BFS/CW-BB)

4.2.1.1. Workability properties of BFS/CW-BB samples

In the two-component (binary) alkaline activation process, CW was substituted in 3 different rates BFS. The ratio of BFS/CW samples to mass is 3:1, 2:2 and 1:3, respectively. For example, for the "3BFS-1CW" sample, the BFS and CW samples have a mass ratio of 3:1.

✓ *Flow Table Test of BFS/CW-BB*

For all BFS/CW-BB samples, flow diameter (mm) values are given in Table 4.10. In BFS/CW-BB samples, the increase in water/binder (w/b) value from 0.4 to 0.45 naturally increased the flow diameter (consistency). For the cement paste sample, while the w/b ratio was 0.4, the flow radius value was 225 mm, and the w/b ratio was 0.45, the flow radius value was 290 mm. In general, it was observed that as the amount of CW substituted in the samples increased, the flow diameter values decreased for both w/b ratios, especially for low "n" ratios. For the ratio w/b=0.4, the flow diameter values of the samples with the ratio "n=2 were found close to the flow diameter value of the

cement (225 mm). Especially for the BFS/CW-BB samples activated with a high amount of Na_2O (high "n" values / high activator dosage), the increase in "w/b" ratio liquefied the consistency of the samples for all CW substituted specimens.

When the "n" ratio increased (n=6), the consistency of BFS/CW-BB samples produced by alkali activation became liquefied, but because the transition speed from liquid consistency to solid consistency was very short (5-10 minutes), the consistency property was considerably decreased compared to cement. For w/b=0.45 ratio, the closest flow values to cement (290 mm) are generally provided for n=2 ratio. As the "n" ratio increased, the samples first liquefied and then solidified within a few minutes, similar to samples with a w/b of 0.4.

Table 4.10. Flow values (mm) of BFS/CW-BB samples for w/b=0.4 and w/b=0.45.

3BFS-1CW	**M_s**					
Na_2O (%)	**(w/b=0.4)**			**(w/b=0.45)**		
	1.2	**1.5**	**1.8**	**1.2**	**1.5**	**1.8**
2	250	250	190	280	L	270
4	290	280	230	L	L	L
6	R.S	R.S	R.S	L	L	L
2BFS-2CW	**M_s**					
Na_2O (%)	**(w/b=0.4)**			**(w/b=0.45)**		
	1.2	**1.5**	**1.8**	**1.2**	**1.5**	**1.8**
2	240	225	220	L	L	270
4	270	285	L	L	L	L
6	R.S	R.S	R.S	L	L	L
1BFS-3CW	**M_s**					
Na_2O (%)	**(w/b=0.4)**			**(w/b=0.45)**		
	1.2	**1.5**	**1.8**	**1.2**	**1.5**	**1.8**
2	230	240	220	280	290	L
4	290	280	L	L	L	L
6	R.S	R.S	R.S	L	L	L

L: Liquid R.S: Rapid Setting

The changes in the flow diameter according to the "n" and "Ms" ratios for both "w/b" values of BFS/CW-BB samples are given in Figures 4.34 and 4.35.

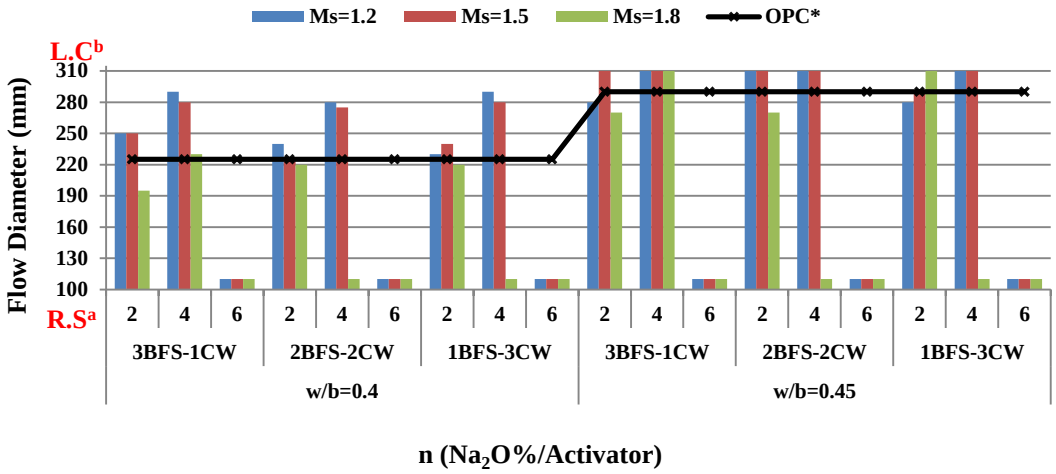


Figure 4.34. The flow values of BFS/CW–BB samples according to "n" ratio (for "w/b=0.4" and for "w/b=0.45").

* The cement paste was formed only with water without using an alkaline activator.
[a] Below the flow radius of 100 mm is the "Rapid Setting" limit.
[b] Above flow radius of 300 mm is "Liquid Consistency" limit.

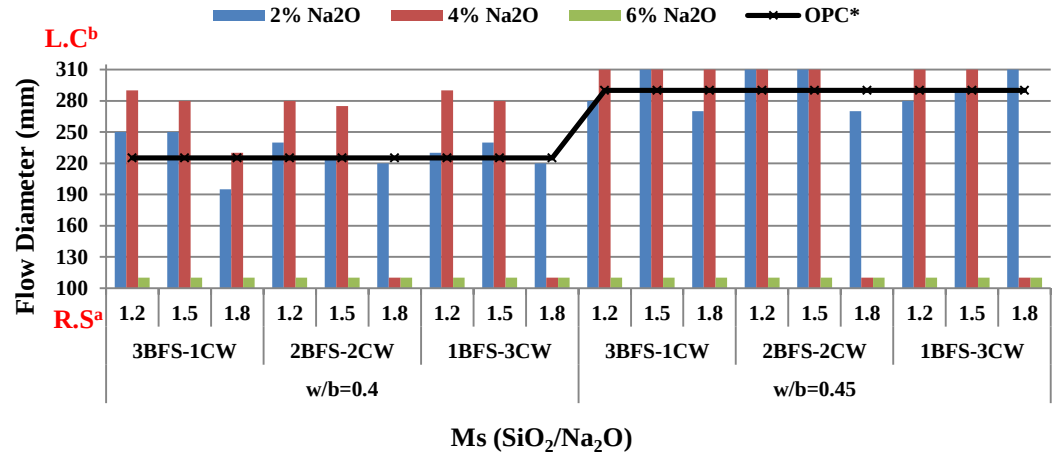


Figure 4.35. The flow values of BFS/CW–BB samples according to "Ms" ratio (for "w/b=0.4" and for "w/b=0.45").

* The cement paste was formed only with water without using an alkaline activator.
[a] Below the flow radius of 100 mm is the "Rapid Setting" limit.
[b] Above flow radius of 300 mm is "Liquid Consistency" limit.

When the w/b ratio increased from 0.4 to 0.45, the flow diameter of the samples increased and their consistency became liquefied. For these binary mixture samples, the flow diameter of the samples having a value of 0.4 w/b generally remained within the

experimental lower and upper limits. In terms of workability, the 0.4 w/b ratio was determined as a more significant ratio for this mixture. Therefore, the effects of "n" and "Ms" ratios on the flow diameter were interpreted only for samples with a value a w/b of 0.4.

According to the test conditions in the Figure 4.34, increasing the "n" value in the samples increased the consistency up to a point and then decreased it. This point is the ratio of n=4. This means that as the dosage of activator solution (total amount of mixture of sodium silicate and sodium hydroxide / "n" ratio) used for the activation of the samples increased up to n=4, the consistency of the samples increased and then decreased. That is, for the ratio n=4, the flow diameter of the samples has reached the maximum value. However, when the n=6, the transition from liquid to solid consistency was rapidly occurred.

In Figure 4.35, the increase in "Ms" ratio generally reduced the flow diameter values of the samples for all substitution rates of CW in the BFS. This means that the amount of sodium silicate in the activator solution increased while the decreased in the amount of sodium hydroxide reduced the workability of the samples. However, it can be said that "n" ratio was more effective than "Ms" ratio on the workability of all samples in this mixture.

✓ *Setting Time Test of BFS/CW-BB*

In this experiment, initial and final setting time values of BFS/CW-BB samples for both w/b ratios were given in Table 4.11.

Table 4.11. Setting time of BFS/CW-BB samples (w/b=0.4 and w/b=0.45).

Code	Initial Setting Time (min.)	Final Setting Time (min.)	Note	Code	Initial Setting Time (min.)	Final Setting Time (min.)	Note
3BFS/1CW-2/1.2/0.4	155.0	168.0	SPD	**3BFS/1CW-2/1.2/0.45**	168.0	192.7	SPD
3BFS/1CW-2/1.5/0.4	194.0	199.3	SPD	**3BFS/1CW-2/1.5/0.45**	190.7	232.0	
3BFS/1CW-2/1.8/0.4	>202	>312		**3BFS/1CW-2/1.8/0.45**	>202	>312	
3BFS/1CW-4/1.2/0.4	>202	>312		**3BFS/1CW-4/1.2/0.45**	>202	>312	
3BFS/1CW-4/1.5/0.4	>202	>312		**3BFS/1CW-4/1.5/0.45**	>202	>312	
3BFS/1CW-4/1.8/0.4	>202	>312		**3BFS/1CW-4/1.8/0.45**	>202	>312	
3BFS/1CW-6/1.2/0.4	39.7	96.3	RS	**3BFS/1CW-6/1.2/0.45**	>202	>312	
3BFS/1CW-6/1.5/04	52.3	152.7	RS	**3BFS/1CW-6/1.5/0.45**	>202	>312	
3BFS/1CW-6/1.8/0.4	38.0	125.0	RS	**3BFS/1CW-6/1.8/0.45**	>202	>312	
2BFS/2CW-2/1.2/0.4	138.3	150.0	SPD	**2BFS/2CW-2/1.2/0.45**	172.0	197.0	SPD
2BFS/2CW-2/1.5/0.4	138.0	148.3	SPD	**2BFS/2CW-2/1.5/0.45**	>202	>312	
2BFS/2CW-2/1.8/0.4	164.7	177.7	SPD	**2BFS/2CW-2/1.8/0.45**	>202	>312	
2BFS/2CW-4/1.2/0.4	>202	>312		**2BFS/2CW-4/1.2/0.45**	>202	>312	
2BFS/2CW-4/1.5/0.4	>202	>312		**2BFS/2CW-4/1.5/0.45**	>202	>312	
2BFS/2CW-4/1.8/0.4	>202	>312		**2BFS/2CW-4/1.8/0.45**	>202	>312	
2BFS/2CW-6/1.2/0.4	38.0	136.0	RS	**2BFS/2CW-6/1.2/0.45**	>202	>312	
2BFS/2CW-6/1.5/0.4	39.7	154.7	RS	**2BFS/2CW-6/1.5/0.45**	>202	>312	
2BFS/2CW-6/1.8/0.4	23.0	195.7	RS	**2BFS/2CW-6/1.8/0.45**	>202	>312	
1BFS/3CW-2/1.2/0.4	128.7	135.7	SPD	**1BFS/3CW-2/1.2/0.45**	187.7	210.3	SPD
1BFS/3CW-2/1.5/0.4	120.3	134.7	SPD	**1BFS/3CW-2/1.5/0.45**	>202	>312	
1BFS/3CW-2/1.8/0.4	>202	>312		**1BFS/3CW-2/1.8/0.45**	>202	>312	
1BFS/3CW-4/1.2/0.4	>202	>312		**1BFS/3CW-4/1.2/0.45**	>202	>312	
1BFS/3CW-4/1.5/0.4	>202	>312		**1BFS/3CW-4/1.5/0.45**	>202	>312	
1BFS/3CW-4/1.8/0.4	>202	>312		**1BFS/3CW-4/1.8/0.45**	>202	>312	
1BFS/3CW-6/1.2/0.4	>202	>312		**1BFS/3CW-6/1.2/0.45**	>202	>312	
1BFS/3CW-6/1.5/0.4	34.3	157.7	RS	**1BFS/3CW-6/1.5/0.45**	>202	>312	
1BFS/3CW-6/1.8/0.4	26.0	203.0	RS	**1BFS/3CW-6/1.8/0.45**	>202	>312	

RS: Rapid Setting SPD: Short Period Difference

As a result of this experiment, it was determined that as the w/b ratio of BFS/CW-BB samples increased, initial and final setting times increased. For these binary mixture samples, the flow diameter of the samples having a value of 0.4 w/b generally remained within the intervals of experimental lower and upper limits. In terms of workability, the 0.4 w/b ratio was determined as more significant ratio for this mixture. Therefore, the effects of "n" and "Ms" ratios on the flow diameter were interpreted only for samples with a value a w/b of 0.4. As the CW substitution in the samples increased, the initial and final setting times were shortened especially in the samples having low and high

activator dosage. The change in the initial and final setting times of the samples according to the "n" ratio for both w/b ratios was shown in Figure 4.36.

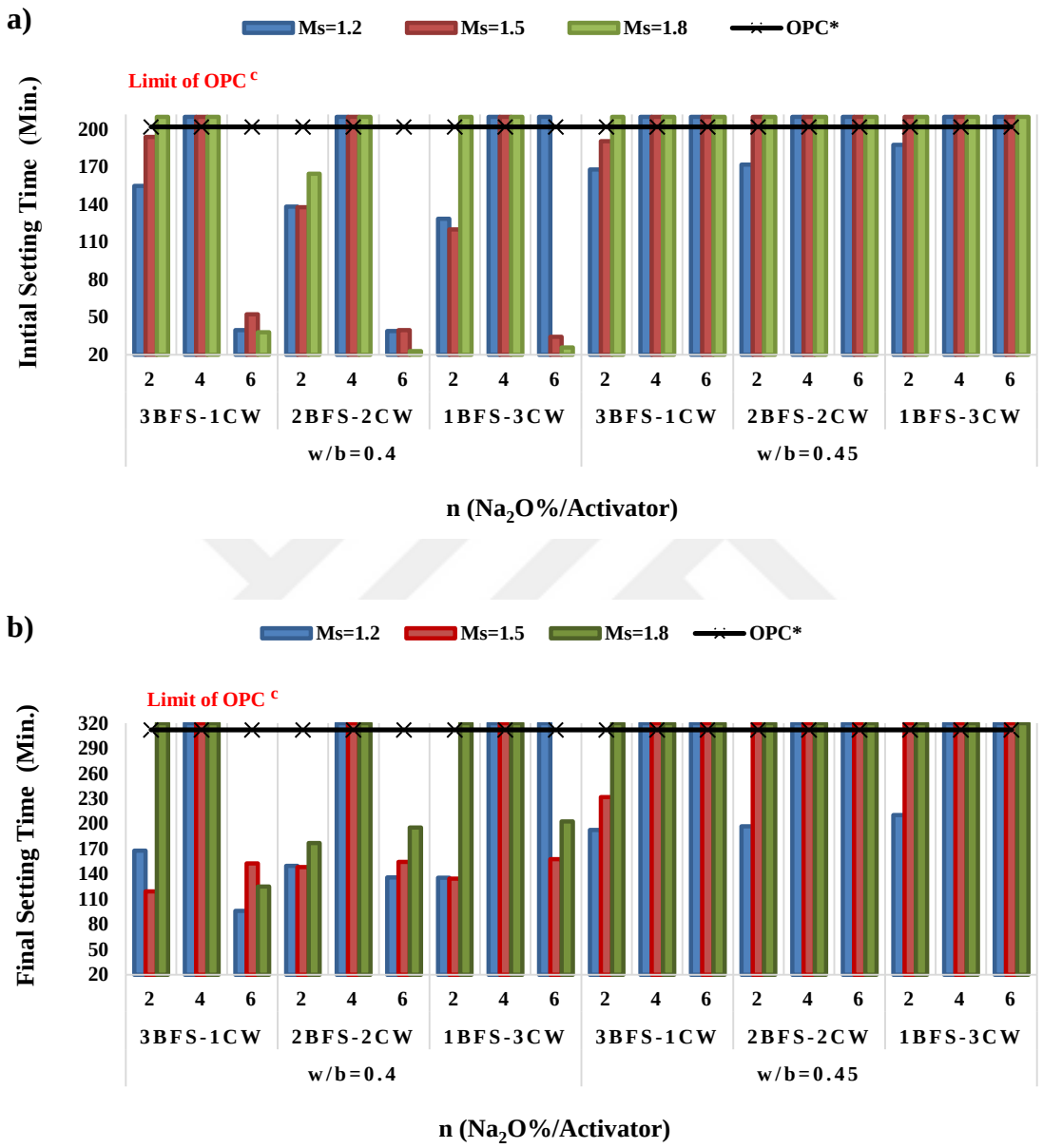


Figure 4.36. The setting time of BFS/CW-BB Samples according to "n" ratio a) Initial setting time b) Final setting time.

* The cement paste is formed only with water without using an alkaline activator.
[c] These limit values are defined in ASTM C 191-13 Standard.

In this BFS/CW binary mixture set, the initial and final setting times of the samples with the lowest activator dosage (n = 2) were very close to each other. The consistency of the samples with moderate level of activator dosage (n=4) increased. BFS/CW binary binder samples with a high activator dosage (n=6) rapidly transformed from liquid consistency to solid consistency, as in BFS and CW unary binder samples.

The initial and final setting times of the samples according to the "Ms" ratio is shown in Figure 4.37. The change in "Ms" ratio for the BFS/CW-BB samples did not cause any increase or decrease tendency on the initial and final setting times of the samples. At all substitution rates in BFS of CW, initial setting times were prolonged as the Ms ratio increased in samples containing low activator dosage (n=2). In general, it was found that both initial and final setting times of samples with high "n" and high "Ms" ratios were decreased. It was observed that the initial and final setting times of the samples containing moderate activator dosage (n=4) were not affected by the change in the ratio of "Ms" and the consistency of these samples was liquefy.

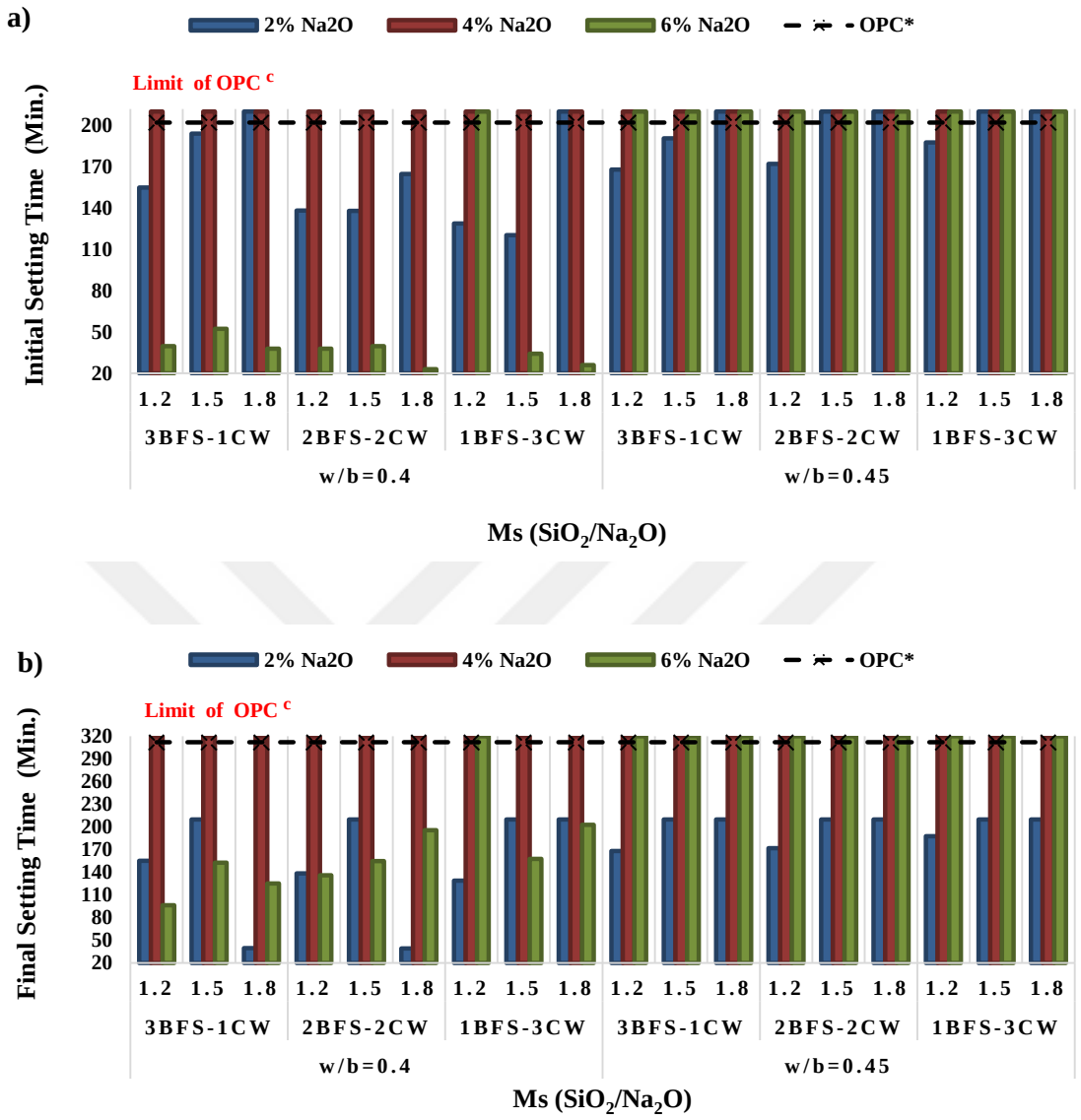


Figure 4.37. The setting time of BFS/CW-BB Samples according to "Ms" ratio a) Initial setting time b) Final setting time.

* The cement paste is formed only with water without using an alkaline activator.
[c] These limit values are defined in ASTM C 191-13 Standard.

✓ *Workability Properties of BFS/CW-BB*

When the substitution rate of CW in BFS is 50%, the lowest values in consistency and initial setting times were obtained. CW substitution in BFS has reduced BFS-UB's workability values. However, it was determined that the values closest to the flow radius values of cement for all substitution ratios of CW in BFS were realized for low activator dosage (n = 2). Especially at low and high activator dosages, there was a much

faster setting than cement. When the n ratio is equal to 4, it was determined that all the workability properties of the samples increase and the final setting time was extended (8-10 hours). In both BFS-UB and CW-UB alkaline activated samples, it was stated in the previous sections that the increment in the alkaline activator dosage (n ratio) in the samples negatively affects the workability of the samples. Same behavior was observed for BFS/CW-BB binary alkaline activated samples. In these samples, the increase in the ratio of n caused the samples to suddenly change from initial liquid consistencies to rapid consistency. This decrease in flow consistency also shortened the setting times of the samples. For samples with an n ratio equal to 6, regardless of the substitution of CW in BFS, rapid setting and workability loss were observed.

When the relevant literature is examined in detail, it had been determined that for the BFS/CW-UB samples, as the amount of CW in the samples increased, the flow radius and setting times increased compared to the control sample (BFS-UB) [47, 100]. These data were contrary to our findings of study. However, in one of these studies, activator dosages and concentrations (S.S/S.H = 0.75 and NaOH = 4M [50]) were considerably smaller than the activator dosages and concentrations used in our study. However, the increase in the activator dosage and concentration used has been emphasized in previous studies, where the sample's reaction rate of activation was increased, workability reduced and the setting time shortened [101, 88].

In the other study, where different waste glass and liquid/solid (L/S) ratios were substituted in BFS, the workability of BFS increased as the rate of waste glass increased in the system [100]. However, all "L/S" rates selected in the study were 0.45 and above. In addition, plastic consistency was not formed for the 0.45 L/S ratio and the flow radius and setting time could not be calculated. Considering that the L/S ratios selected in our study were 0.4 and 0.45, the decrease in workability of the samples might be compatible with this study.

In another study in the literature, slump values of the samples containing slag particles with nano-silica addition were found lower than reference slag samples without these addition [102]. This was in good agreement with our study results. This result suggests that since the addition of nano-size silica particles grain size was much lower than the slag's particle size which resulted in a decrease in the slump levels of the samples. This

is because of the fact that; more water was required to wet the increased surface areas of the nanoparticles. Similarly, when the grain size of the samples was examined in our study, it was seen that (see Figure 3.2) the particle size of ceramic waste below 10μm that was larger than the slag's particle size (30 μm). This has led to an increase in the surface areas of the samples added into the batch as a ceramic waste and their need for mixing water, and hence, their reduced workability.

Finally, in a study conducted by Rashad and Essa, it was observed that as the amount of CW substituted into BFS increased (from 0% to 50%), the workability decreased as in our study [103]. According to the study, the reduction in the workability with increasing CW content could be related to its higher Blaine surface area compared with slag.

4.2.2.2. Strength properties of BFS/CW-BB samples

In this binary activation system consisting of a mixture of CW and BFS, CW has been replaced in BFS in 3 different masses. The selected flexural and compressive strength values BFS/CW-BB systems for each mix proportion was shown in Figure 4.38. Accordingly, the selected flexural strength value achieved for the 2BFS/2CW composition, in which CW was substituted in the BFS in a 2:2 ratios. The highest compressive strength value was also obtained for the 3BFS/1CW composition in which CW was substituted in the BFS in a 3:1 ratio. Therefore, flexural and compressive strengths in binary component systems evaluated over the combinations that gave the selected values among the studied samples.

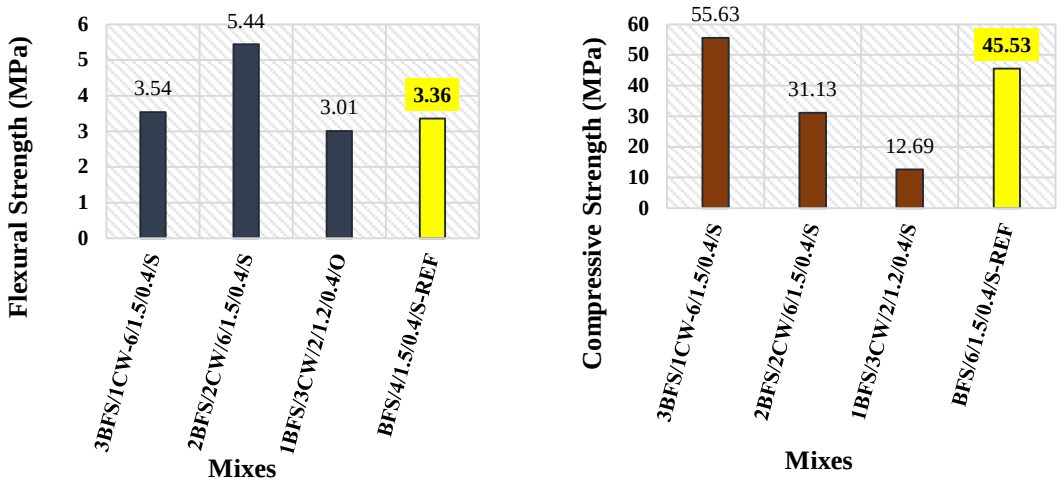
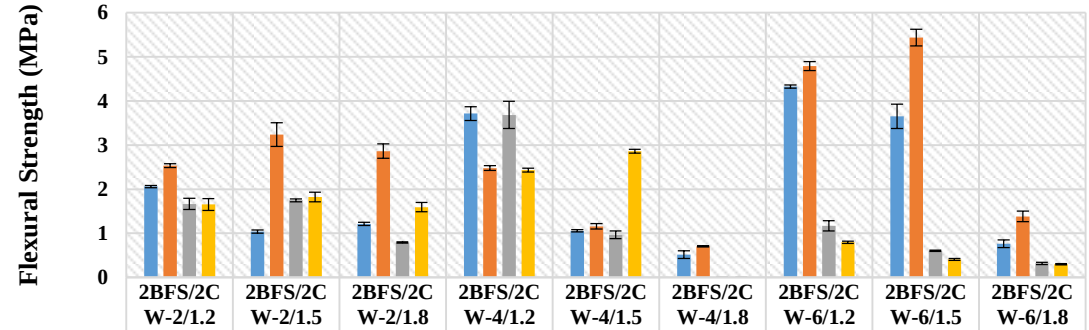


Figure 4.38. The selected flexural and compressive strength values BFS/CW-BB systems for each mix proportion.

✓ *Flexural Strength Test of BFS/CW-BB*

The flexural strength values of the 2BFS/2CW-BB samples were given in Figure 4.39 for both w/b ratios (0.4 and 0.45) and for both curing conditions (oven and steam).

The highest flexural strength value for BFS/CW-BB sample set was for the "2BFS/2CW/6/1.5/0.4/Steam" sample. Thus, the highest flexural strength value was determined for w/b = 0.4 ratio and steam curing.



	2BFS/2CW-2/1.2	2BFS/2CW-2/1.5	2BFS/2CW-2/1.8	2BFS/2CW-4/1.2	2BFS/2CW-4/1.5	2BFS/2CW-4/1.8	2BFS/2CW-6/1.2	2BFS/2CW-6/1.5	2BFS/2CW-6/1.8
0.4/Oven	2.06	1.04	1.21	3.71	1.05	0.52	4.33	3.65	0.76
0.4/Steam	2.53	3.24	2.86	2.48	1.16	0.70	4.79	5.44	1.38
0.45/Oven	1.67	1.75	0.79	3.68	0.96	0.00	1.17	0.60	0.32
0.45/Steam	1.65	1.82	1.59	2.43	2.86	0.00	0.80	0.41	0.30

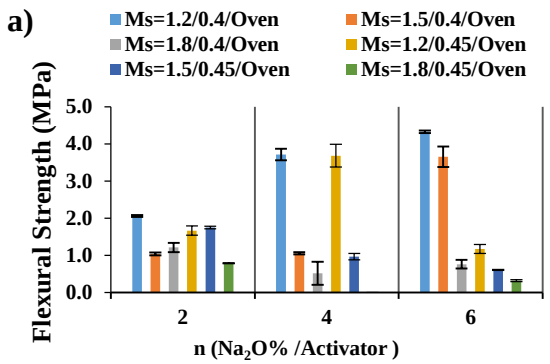
Figure 4.39. Flexural strength of 2BFS/2CW-BB samples.

In this test set, when the w/b ratio increased from 0.40 to 0.45, there was no tendency for the flexural strength value to increase or decrease for all samples in general. Some examples increased and others decreased. However, it was found that substitution of CW in BFS improved the flexural strength values obtained for alkaline activation of both BFS-UB and CW-UB. In fact, in the BFS and CW samples mixed in equal proportions by mass, the highest flexural strength value of this BFS/CW binary mixture series was obtained. In the BFS/CW activation system, there was a great difference between 0.4 w/b ratio and 0.45 w/b ratio in terms of flexural strength for the selected sample. When the w/b ratio increased from 0.4 to 0.45, the flexural strength decreased dramatically.

The variation of flexural strength values of 2BFS/2CW-BB samples according to "n" ratio is given in Figure 4.40 for two different curing conditions. For samples with low (n=2) and high activator dosage (n=6), it was determined that the steam cured samples have much higher flexural strength values than the samples that contain moderate activator dosage (n=4) and exposed to steam curing. However, when both the ratio of "n" and the ratio of "Ms" reached the highest values (n=6 and Ms=1.8), there was a rapid decrease in the flexural strength values of all samples.

The changes in flexural strength values of 3BFS/1CW-BB samples according to the "Ms" ratio were given in Figure 4.41 for two different curing conditions. The selected flexural strength value for this curing condition was formed for 1.5 "Ms". Especially, increasing the ratio of Ms for the oven cured samples, decreased the flexural strength value. For the steam cured samples, the lowest flexural strength values were obtained for the highest Ms value (Ms=1.8).

As a result, it was found that the selected flexural strength for this system has been achieved for the sample with the highest activator dosage (n=6), "Ms" value of 1.5 and steam cured for 2BFS/2CW-BB samples.



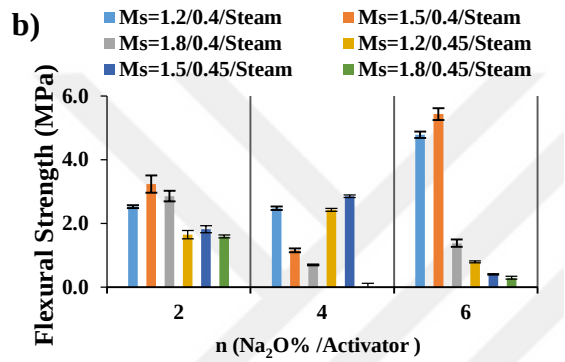
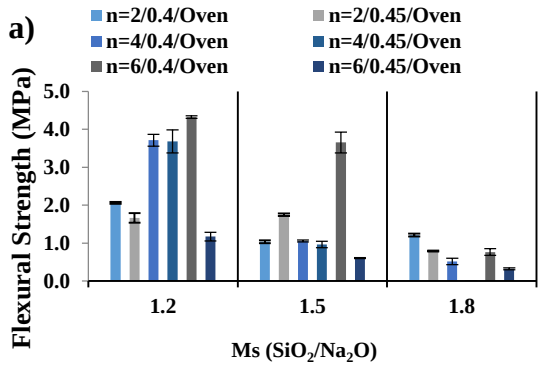


Figure 4.40. Change in flexural strength of 2BFS/2CW-BB paste according to "n" ratio **a)** For oven cured **b)** For steam cured.



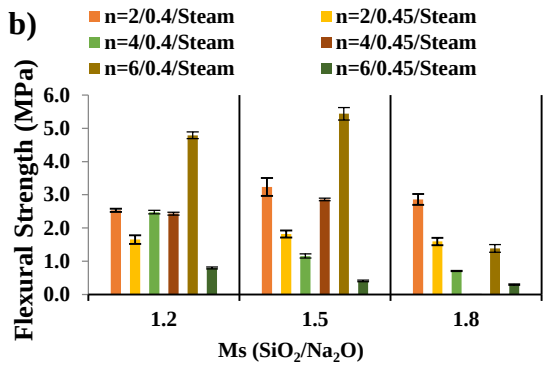


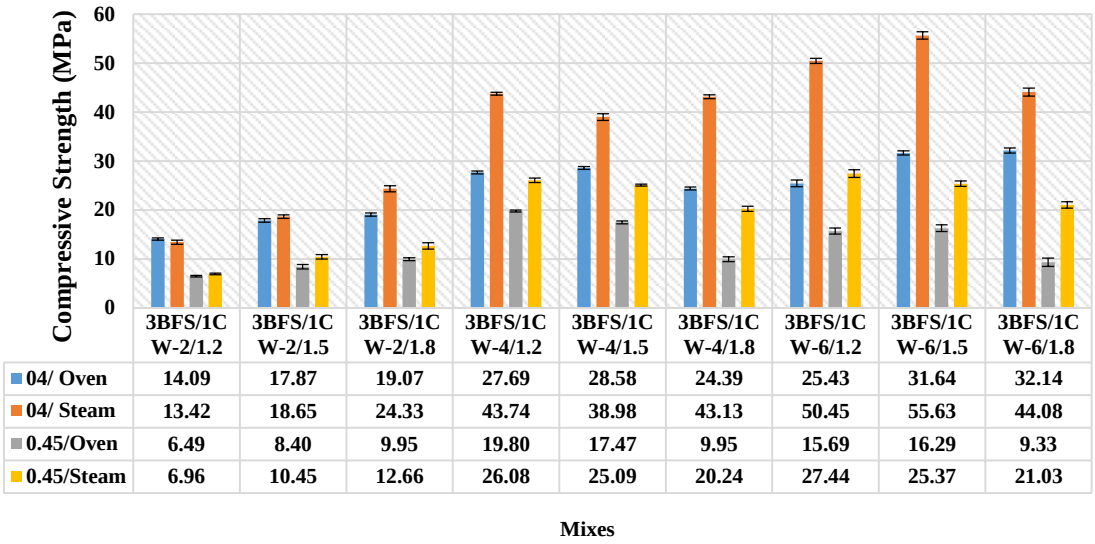
Figure 4.41. Change in flexural strength of 2BFS/2CW-BB paste according to "M_s" ratio **a)** For oven cured **b)** For steam cured.

✓ *Compressive Strength Test of BFS/CW-BB*

The compressive strength values of 3BFS/1CW-BB samples were given in Figure 4.42 for both w/b ratios (0.4 and 0.45) and both curing conditions (oven and steam).

The highest compressive strength value for BFS/CW-BB sample set was for the "3BFS/1CW-BB/6/1.5/0.4/Steam" sample. Thus, the highest compressive strength value was determined for w/b = 0.4 ratio and steam curing. When the w/b ratio increased from 0.40 to 0.45, the compressive strength values of the samples generally decreased for both curing conditions. It was determined that the steam cured samples reached higher compressive strength values than the oven cured for both w/b ratios. It was found that substitution of CW in BFS improved the compressive strength values obtained for alkaline activation of both BFS-UB and CW-UB. Results revealed that the compressive

strength value increased as the activator dosage increased for steam cured samples of 0.4 w/b ratio.

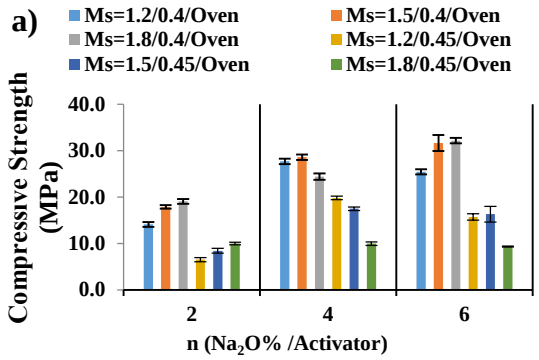


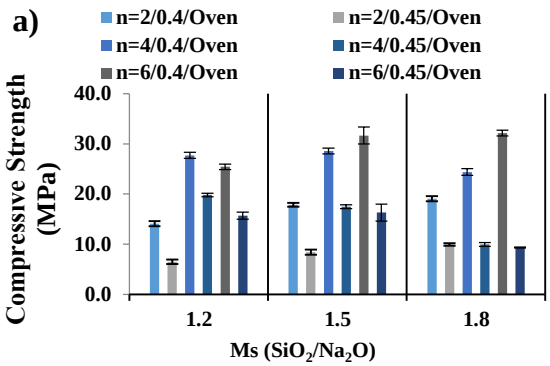
	3BFS/1CW-2/1.2	3BFS/1CW-2/1.5	3BFS/1CW-2/1.8	3BFS/1CW-4/1.2	3BFS/1CW-4/1.5	3BFS/1CW-4/1.8	3BFS/1CW-6/1.2	3BFS/1CW-6/1.5	3BFS/1CW-6/1.8
04/ Oven	14.09	17.87	19.07	27.69	28.58	24.39	25.43	31.64	32.14
04/ Steam	13.42	18.65	24.33	43.74	38.98	43.13	50.45	55.63	44.08
0.45/Oven	6.49	8.40	9.95	19.80	17.47	9.95	15.69	16.29	9.33
0.45/Steam	6.96	10.45	12.66	26.08	25.09	20.24	27.44	25.37	21.03

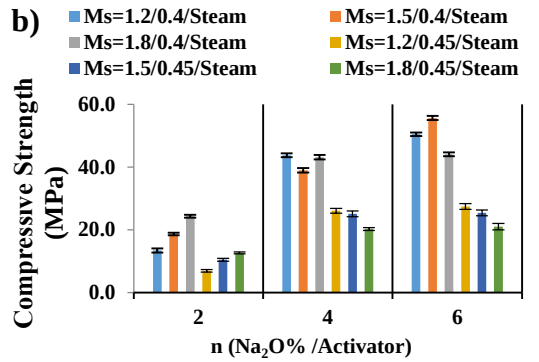
Figure 4.42. Compressive strength of 3BFS/1CW-BB samples.

The variation of compressive strength values of 3BFS/1CW-BB samples according to "n" ratio was given in Figure 4.43 for two different curing conditions. For both cure conditions, increasing the "n" ratio, that is, increasing the activator dosage, rised the compressive strength value. The highest compressive strength value was realized for the highest "n" ratio.

The variation of compressive strength values of 3BFS/1CW-BB samples according to "Ms" ratio was given in Figure 4.44 for two different curing conditions. The increase in the "Ms" ratio did not create a pronounced tendency to change the compressive strength of each samples. For both curing conditions, the highest compressive strength value was realized for the ratio where the value of "Ms" was 1.5.







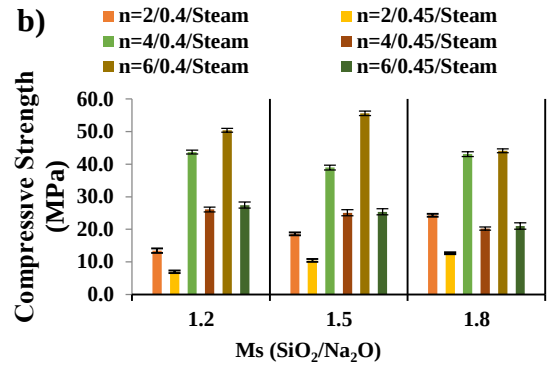


Figure 4.43. Change in flexural strength of 3BFS/1CW-BB according to "n" ratio a) For oven cured b) For steam cured.

Figure 4.44. Change in flexural strength of 3BFS/1CW-BB according to "M_s" ratio a) For oven cured b) For steam cured.

✓ *Strength Properties of BFS/CW-BB*

In this binary system, both the flexural and compressive strength values of BFS/CW-BB samples were higher than BFS-UB samples. In this system, the highest flexural strength value among the samples was realized for the "2BFS/2CW/6/1.5/0.4/Steam" sample with 50% CW substitution, while the highest compressive strength value was "3BFS/1CW/6/1.5/0.4/Steam" with a 25% CW substitution. While the selected improvement value in flexural strength was 62%, this value for compressive strength was 22% increase. In other words, the strength improvement for flexural strength was approximately 3 times higher than the improvement for compressive strength. Both flexural and compressive strength values decreased for the highest CW substitution rate (75%) within the binary system. However, this decrease was 12% compared to the flexural strength of the BFS-UB reference sample for flexural strength of BFS/CW-BB, while the decrease in compressive strength was 72%. Therefore, in the BFS/CW-BB

binary system, it has been determined that the CW substitution increased the flexural strength value more than the compressive strength and as a result of the CW increase in the system, the flexural strength value decreased less than the compressive strength value.

For the samples that given the selected results in terms of flexural and compressive strength (7 days) in the BFS/CW-BB system, the Ms ratios were the same (Ms = 1.5), while the "n" ratios were different. In the example that given better results in terms of flexural strength, the rate of "n" was equal to 4, while for the example that given the selected result in terms of compressive strength, the rate of "n" was 6. This showed that increasing activator dosage improved compressive strength value. However, the increase in the rate of "n" caused the workability values to be negatively affected. For this reason, the ratio of "n" in all experimental sets was determined as 6 at most.

When the literature was analyzed, it was found that the slag and ceramic waste components activated by the same type of activator solution (a mixture of sodium silicate and sodium hydroxide) were close to the compressive strength value determined in our study, between 55-62 MPa (28 days) [45]. In another study, it was found that slag samples which were replaced with up to 50% ceramic waste and activated with sodium silicate, reached a compressive strength of 20-35 MPa (7 days) [103]. In another study conducted by Huseien et al., The compressive strength value (7 days) of slag and ceramic waste mixture (50% BFS +50% CW) activated with a mixture of sodium silicate and sodium hydroxide was between 60-65 MPa, similar to our study [47]. However, unlike our study, the use of 50% ceramic waste showed lower strength compared to the control sample produced using a 100% slag sample in the study. In the study conducted by Abdollahnejad et al., samples were produced as a result of activation of ceramic waste and slag with sodium silicate. In the studies in which the samples used different fiber types to examine the hardened-state properties and shrinkage properties, it was observed that the flexural strength of the reference samples produced with no fiber addition was around 2 MPa and the compressive strength was around 40 MPa [50].

As a result, it was determined that the replacement of CW up to 50% in the BFS improved the mechanical properties and increased the flexural strength values above

60% compared to the mechanical properties obtained by activation of BFS-UB. There were studies in the literature where ceramic waste reduced the mechanical properties of BFS subjected to alkali activation [47, 104]. In our study, a rapid decrease in the flexural and compressive strengths of slag samples, where ceramic waste substitution of 75% and above was performed, was detected. However, similar to our study results, there was also a study which has been found to add up to 50% CW to increase the mechanical properties of alkali activated BFS [103]. It was stated that the mechanical improvement occurring in this study was caused by the ceramic particles that were smaller than the slag particles, creating a "packing effect" and filling the gaps between the slag particles, thus resulting in a more compact and void-free structure. This situation was considered to be valid for our study.

✓ *Determination of the Selected BFS/CW-BB Sample.*

At the end of the second set of experiments including workability and strength tests, one samples that selected represent this test set were determined for BFS/CW-BB in terms of both flexural and compressive strength. The experimental parameters of the selected samples were given in Table 12. The selection criterion applied during the sample selection was applied to determine the samples having the highest values in terms of flexural and compressive strengths and which were not problematic in the process of mixing, molding and setting in terms of workability.

Table 4.12. Experimental parameters of the selected samples of BFS/CW-BB.

BFS/CW-BB Parameters	**The Selected Sample**	
	Compressive Strength	**Flexural Strength**
Mixture Ratio (%)	50-50	75-25
"n" Rate	6	6
"Ms" Rate	1.5	1.5
"w/b" Rate	0.4	0.4
Cure Cond.	Steam	Steam

4.2.2. Blast furnace slag/marble waste-binary binders (BFS/MW-BB)

4.2.2.1. Workability properties of BFS/MW-BB samples

In the two-component (binary) alkaline activation process, MW was substituted in 3 different rates of BFS. The ratio of BFS/MW samples to mass is 3:1, 2:2 and 1:3, respectively. For example, for the "3BFS-1MW" sample, the BFS and MW samples have a mass ratio of 3:1.

✓ *Flow Table Test of BFS/MW-BB*

For all BFS/MW-BB samples, flow diameter (mm) values were given in Table 4.13. In BFS/MW-BB samples, the increase in water/binder (w/b) value from 0.4 to 0.45 naturally increased the flow diameter (consistency). In general, it was observed that as the amount of MW substituted in the BFS/MW-BB samples increased, unlike BFS/CW-BB samples, the flow diameter values increased for both w/b ratios. For the cement paste sample, while the w/b ratio was 0.4, the flow radius value was 225 mm, and the w/b ratio was 0.45, the flow radius value was 290 mm. For the ratio w/b=0.4 and w/b=0.45, the flow diameter values of the samples with the ratio "n"=2 were found close to the flow diameter value of the cement (225 and 290 mm). Especially for the BFS/MW-BB samples activated with a high amount of Na_2O (high "n" values / high activator dosage), the increase in "w/b" ratio liquefied the consistency of the samples. However, for the BFS/MW-BB binder samples, as the MW substitution within the samples increased, the transition time from liquid consistency to solid consistency of the samples containing high activator dosage (n=6) was considerably longer. It was observed that the samples containing high amount of marble waste (1BFS/3MW) maintained their plastic consistency even at high "n" rates for a long time (about 1-2 h).

Table 4.13. Flow values of BFS/MW-BB samples for w/b=0.4 and w/b=0.45.

3BFS-1MW	**M_s**					
Na_2O (%)	**(w/b=0.4)**			**(w/b=0.45)**		
	1.2	**1.5**	**1.8**	**1.2**	**1.5**	**1.8**
2	250	240	190	280	290	250
4	L	280	235	L	L	L
6	L	R.S	R.S	L	L	L
2BFS-2MW	**M_s**					
Na_2O (%)	**(w/b=0.4)**			**(w/b=0.45)**		
	1.2	**1.5**	**1.8**	**1.2**	**1.5**	**1.8**
2	250	240	200	280	290	260
4	L	270	240	L	L	290
6	L	L	L	L	L	L
1BFS-3MW	**M_s**					
Na_2O (%)	**(w/b=0.4)**			**(w/b=0.45)**		
	1.2	**1.5**	**1.8**	**1.2**	**1.5**	**1.8**
2	240	220	200	270	270	260
4	290	280	240	L	L	L
6	280	R.S	R.S	L	L	L

L: Liquid R.S: Rapid Setting

For w/b=0.45 ratio, the closest flow values to cement (290 mm) were generally obtained for “n”=2 ratio. As the “n” ratio increased, the samples first liquefied therefore flow diameter was measured. Workability characteristic of BFS/MW-BB revealed much longer flow diameter than those of BFS/CW-BB. The changes in the flow diameter according to the “n” and “Ms” ratios for both “w/b” values of BFS/MW-BB samples were given in Figures 4.45 and Figures 4.46.

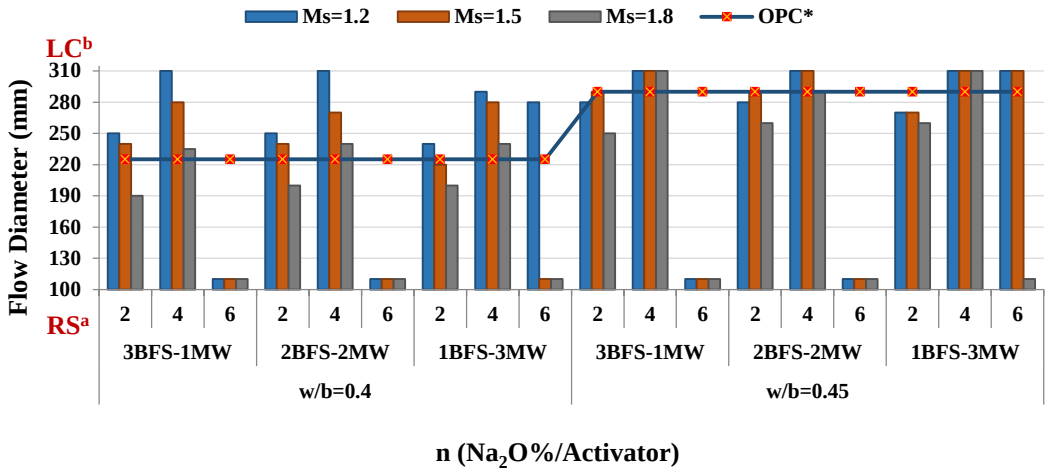


Figure 4.45. The flow values of BFS/MW–BB samples according to "n" ratio (for "w/b=0.4" and for "w/b=0.45").

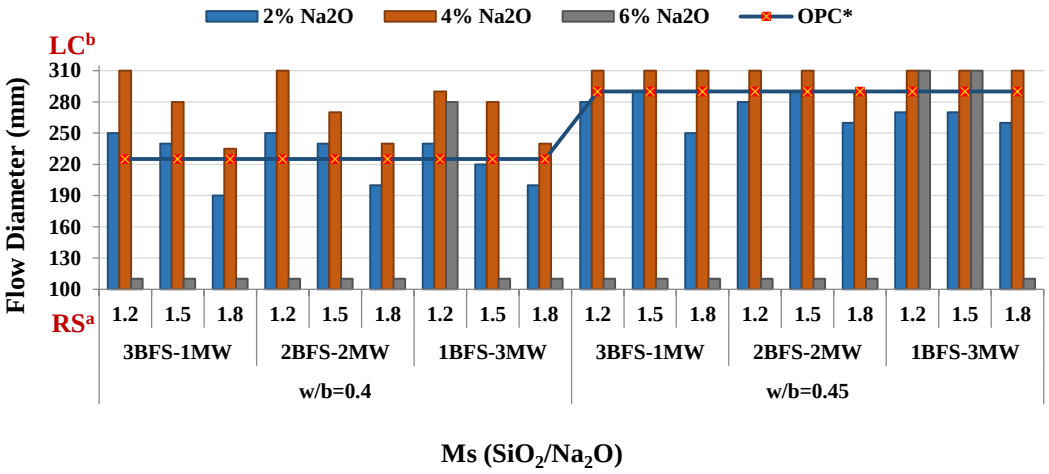


Figure 4.46. The flow values of BFS/MW–BB samples according to "Ms" ratio (for "w/b=0.4" and for "w/b=0.45").

* The cement paste was formed only with water without using an alkaline activator.
[a] Below the flow radius of 100 mm is the "Rapid Setting (RS)" limit.
[b] Above flow radius of 300mm is "Liquid Consistency (LC)" limit.

When the w/b ratio increased from 0.4 to 0.45, the flow diameter of the samples increased and their liquefaction behavior became consistent. For these binary mixture samples, the flow diameter of the samples having a value of 0.4 w/b generally remained within the experimental lower and upper limits. In terms of workability, the 0.4 w/b ratio was determined as a more significant ratio for this mixture. Therefore, the effects

of “n” and “Ms” ratios on the flow diameter were interpreted only for samples with a value a w/b of 0.4.

According to the test conditions in Figure 4.45, increasing the “n” value in the samples increased the consistency up to a point where the ratio of n=4 and then decreased. This means that as the dosage of activator solution (total amount of mixture of sodium silicate and sodium hydroxide / “n” ratio) used for the activation of the samples increased up to n=4, the consistency of the samples increased and then decreased. That is, for the ratio n=4, the flow diameter of the samples has reached the maximum value. However, when the n=6, the transition from liquid to solid consistency was rapid. However, the time of transition from liquid to solid in this mixture was much longer than that of BFS/CW-BB samples.

In Figure 4.46, the increase in “Ms” ratio generally reduced the flow diameter values of the samples for all substitution rates of MW in the BFS. This means that when the amount of sodium silicate in the activator solution increased which leads to a decline in the amount of sodium hydroxide and a reduction in the workability of the samples. However, it can be said that “n” ratio was more effective than “Ms” ratio on the workability of all samples in this mixture.

- ✓ *Setting Time Test of BFS/MW-BB*

In this experiment, initial and final setting time values of BFS/MW-BB samples for both w/b ratios were given in Table 4.14.

Table 4.14. Setting time of BFS/MW-BB samples (w/b=0.4 and w/b=0.45).

Code	Initial Setting Time (min.)	Final Setting Time (min.)	Note	Code	Initial Setting Time (min.)	Final Setting Time (min.)	Note
3BFS/1MW-2/1.2/0.4	75,0	100,3	SPD	**3BFS/1MW-2/1.2/0.45**	79,0	99,3	SPD
3BFS/1MW-2/1.5/0.4	70,0	88,0	SPD	**3BFS/1MW-2/1.5/0.45**	>202	>312	
3BFS/1MW-2/1.8/0.4	80,0	124,3		**3BFS/1MW-2/1.8/0.45**	>202	>312	
3BFS/1MW-4/1.2/0.4	>202	>312		**3BFS/1MW-4/1.2/0.45**	>202	>312	
3BFS/1MW-4/1.5/0.4	>202	>312		**3BFS/1MW-4/1.5/0.45**	>202	>312	
3BFS/1MW-4/1.8/0.4	>202	>312	NS	**3BFS/1MW-4/1.8/0.45**	>202	>312	NS
3BFS/1MW-6/1.2/0.4	>202	>312		**3BFS/1MW-6/1.2/0.45**	>202	>312	
3BFS/1MW-6/1.5/0.4	80,3	188,3		**3BFS/1MW-6/1.5/0.45**	>202	>312	
3BFS/1MW-6/1.8/0.4	66,7	130,7		**3BFS/1MW-6/1.8/0.45**	>202	>312	
2BFS/2MW-2/1.2/0.4	70,0	96,3	SPD	**2BFS/2MW-2/1.2/0.45**	72,0	93,0	SPD
2BFS/2MW-2/1.5/0.4	92,0	98	SPD	**2BFS/2MW-2/1.5/0.45**	138,3	197,7	
2BFS/2MW-2/1.8/0.4	92,0	143,3		**2BFS/2MW-2/1.8/0.45**	>202	>312	
2BFS/2MW-4/1.2/0.4	>202	>312		**2BFS/2MW-4/1.2/0.45**	>202	>312	
2BFS/2MW-4/1.5/0.4	>202	>312		**2BFS/2MW-4/1.5/0.45**	>202	>312	
2BFS/2MW-4/1.8/0.4	>202	>312	NS	**2BFS/2MW-4/1.8/0.45**	>202	>312	NS
2BFS/2MW-6/1.2/0.4	>202	>312		**2BFS/2MW-6/1.2/0.45**	>202	>312	
2BFS/2MW-6/1.5/0.4	>202	>312		**2BFS/2MW-6/1.5/0.45**	>202	>312	
2BFS/2MW-6/1.8/0.4	>202	>312		**2BFS/2MW-6/1.8/0.45**	>202	>312	
1BFS/3MW-2/1.2/0.4	36,0	52,0	SPD	**1BFS/3MW-2/1.2/0.45**	64,0	91,3	SPD
1BFS/3MW-2/1.5/0.4	71,7	100,0	SPD	**1BFS/3MW-2/1.5/0.45**	108,3	153,0	
1BFS/3MW-2/1.8/0.4	124,0	162,7		**1BFS/3MW-2/1.8/0.45**	>202	>312	
1BFS/3MW-4/1.2/0.4	>202	>312		**1BFS/3MW-4/1.2/0.45**	>202	>312	
1BFS/3MW-4/1.5/0.4	>202	>312		**1BFS/3MW-4/1.5/0.45**	>202	>312	
1BFS/3MW-4/1.8/0.4	>202	>312	NS	**1BFS/3MW-4/1.8/0.45**	>202	>312	NS
1BFS/3MW-6/1.2/0.4	>202	>312		**1BFS/3MW-6/1.2/0.45**	>202	>312	
1BFS/3MW-6/1.5/0.4	>202	>312	NS	**1BFS/3MW-6/1.5/0.45**	>202	>312	NS
1BFS/3MW-6/1.8/0.4	>202	>312	NS	**1BFS/3MW-6/1.8/0.45**	>202	>312	NS

RS: Rapid Setting SPD: Short Period Difference NS: No setting (after 48 h)

As a result of this experiment, it was determined that as the w/b ratio of BFS/MW-BB samples increased, initial and final setting times increased. As the MW substitution in the samples increased, the initial and final setting times were prolonged. For all substitution rates of the marble waste in the slag, no setting was formed in the samples when “n” was 4 and “Ms” was equal to 1.8. In the 1BFS/3MW mixture where the marble waste was substituted at the highest level in the slag, when the ratio “n” was 6 and the “Ms” was 1.5 and 1.8, the samples did not set even after 48 hours. The change in the initial and final setting times of the samples according to the “n” ratio for both w/b ratios was shown in Figure 4.47.

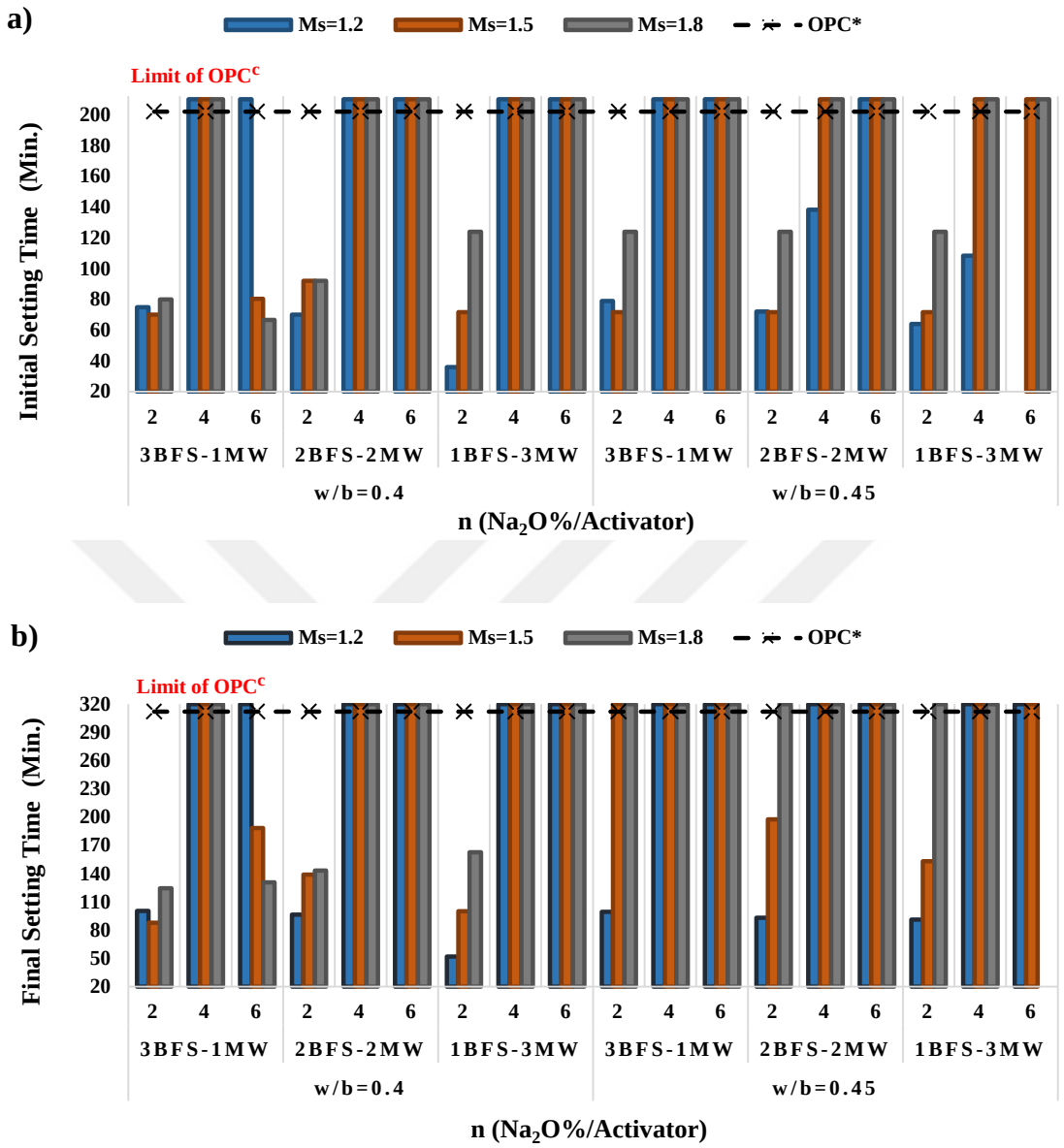


Figure 4.47. The setting time of BFS/MW-BB Samples according to "n" ratio a) Initial setting time b) Final setting time.

* The cement paste is formed only with water without using an alkaline activator.
[c] These limit values are defined in ASTM C 191-13 Standard.

In this BFS/MW binary mixture set, the initial and final setting times of the samples with the lowest activator dosage (n=2) were very close to each other. The consistency of the samples with moderate and high level of activator dosage (n=4 and n=6) increased. Even samples with high n and Ms ratios could not complete their setting.

The initial and final setting times of the samples according to the "Ms" ratio was shown

in Figure 4.48. For samples with low and medium levels of "n" in all mixtures (n=2 and n=4), the increase in "Ms" ratio prolonged both the initial and end final setting times. This changed at the highest activator dosage (n=6) for the 3BFS/1MW mixture only. The increase in the ratio of "Ms" in this binary mixture prolonged both the initial and end final setting times.

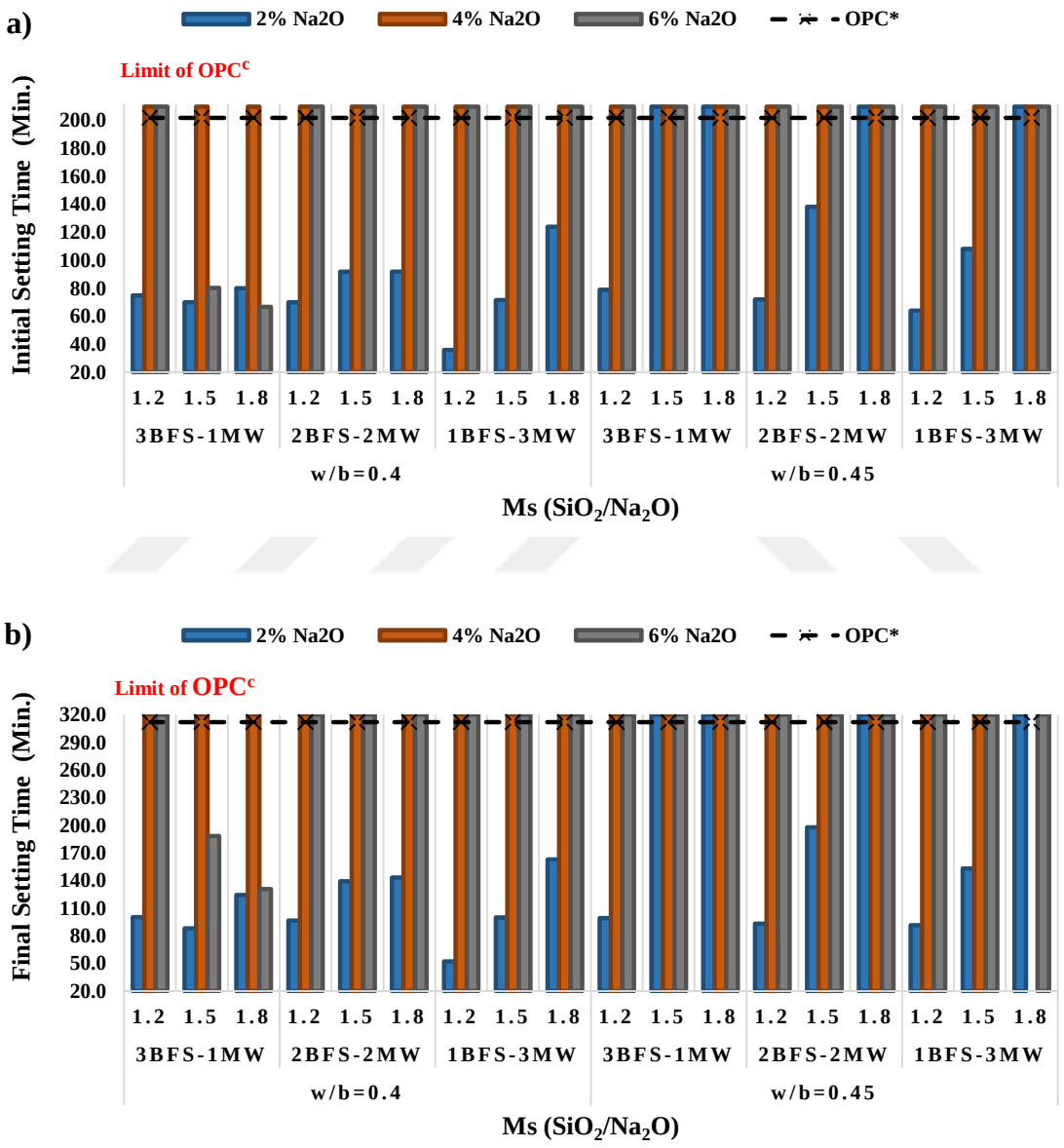


Figure 4.48. The setting time of BFS/MW-BB Samples according to "Ms" ratio a) Initial setting time b) Final setting time.

* The cement paste is formed only with water without using an alkaline activator.
[c] These limit values are defined in ASTM C 191-13 Standard.

✓ *Workability Properties of BFS/MW-BB*

When evaluated in general, it was determined that adding MW in BFS improves workability characteristics of alkali activated BFS-UB. In the previous chapters, it was stated that the setting time of the BFS-UB from plastic consistency to solid consistency was very short, especially for the high “n” ratios (as the amount of alkaline solution in the samples increased) (see Table 4.2). The addition of MW extended the setting time by approximately 2 times for high “n” ratios and preserved the plastic consistency for a longer time than the BFS-UB during mixing and molding of the samples. In BFS/MW-BB binary system, as the MW substitution in the samples increased, the workability values improved. In this system, however, the status of "Short Period Difference-SPD" (very close to the initial and final setting times) for low "n" ratios (n=2) attracted attention. At the same time, unlike medium and high "n" ratios, the increase in MW substitution in the samples shortened the setting time for low "n" ratios.

Previous studies in the literature reported that MW and BFS were subjected to an alkaline activation process together. According to related studies, it was found that the substitution of limestone, which had similar properties with the chemical composition of marble waste, in the BFS improved its workability properties [57, 59]. In these studies, it was stated that the improvement in workability was due to filling the micro-cracks of limestone which requires less water and better particle packaging. Therefore, the availability of more water can provide to lubricate the particles resulting in a higher slump flow [57, 59]. In another study, it was determined that the limestone addition up to 20% to the slag/fly ash mixture reduced the plastic viscosity of the samples [60]. Consequently, the results of all these studies reported in the literature were in good harmony with our study results, improving the processability properties of the samples in BFS/MW-BB.

4.2.2.2. Strength Properties of BFS/MW-BB Samples

In this binary activation system consisting of a mixture of MW and BFS, MW has been replaced in BFS in 3 different masses. The selected flexural and compressive strength values BFS/MW-BB systems for each mix proportion was shown in Figure 4.49. Accordingly, the selected flexural strength value achieved for the 2BFS/2MW

composition, in which MW was substituted in the BFS in a 2:2 ratios. The highest compressive strength value was also obtained for the 2BFS/2MW composition in which MW was substituted in the BFS in a 2:2 ratios. Therefore, flexural and compressive strengths in binary component systems evaluated over these combinations that gave the selected values.

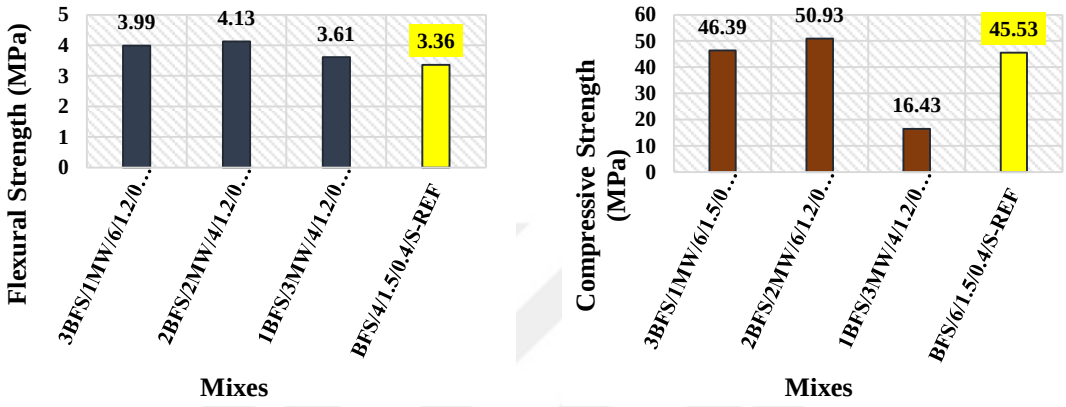
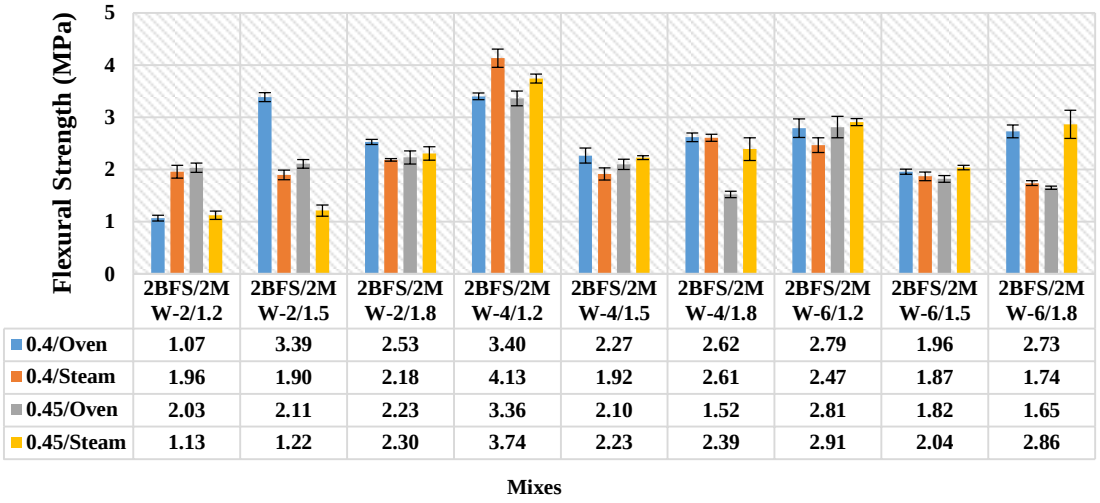


Figure 4.49. The selected flexural and compressive strength values in BFS/MW-BB systems for each mix proportion.

✓ *Flexural Strength Test of BFS/MW-BB*

The flexural strength values of the 2BFS/2MW-BB samples were given in Figure 4.50 for both w/b ratios (0.4 and 0.45) and for both curing conditions (oven and steam curing).

The highest flexural strength value for BFS/MW-BB sample set was for the "2BFS/2MW/4/1.2/0.4/Steam" sample. Thus, the highest flexural strength value among the related sample set was determined for w/b = 0.4 ratio and steam curing.



	2BFS/2MW-2/1.2	2BFS/2MW-2/1.5	2BFS/2MW-2/1.8	2BFS/2MW-4/1.2	2BFS/2MW-4/1.5	2BFS/2MW-4/1.8	2BFS/2MW-6/1.2	2BFS/2MW-6/1.5	2BFS/2MW-6/1.8
0.4/Oven	1.07	3.39	2.53	3.40	2.27	2.62	2.79	1.96	2.73
0.4/Steam	1.96	1.90	2.18	4.13	1.92	2.61	2.47	1.87	1.74
0.45/Oven	2.03	2.11	2.23	3.36	2.10	1.52	2.81	1.82	1.65
0.45/Steam	1.13	1.22	2.30	3.74	2.23	2.39	2.91	2.04	2.86

Figure 4.50. Flexural strength of 2BFS/2MW-BB samples.

In this test set, when the w/b ratio increased from 0.40 to 0.45, there was no clear tendency for the flexural strength value to increase or decrease for all samples in general. Some examples increased and others decreased. However, it was found that substitution of MW in BFS improved the flexural strength values obtained for alkaline activation of both BFS-UB and MW-UB. In fact, in the BFS and MW samples mixed in equal proportions by mass, the highest flexural strength value of this BFS/CW binary mixture series was obtained. In the BFS/MW activation system, the flexural strength values of both w/b ratios were quite close to each other for the sample which had the selected flexural strength value. In other words, the increase of w/b ratio from 0.4 to 0.45 did not affect flexural strength values much.

The variation of flexural strength values of 2BFS/2MW-BB samples according to "n" ratio was given in Figure 4.51 for two different curing conditions. For this binary activation system, changing the "n" ratio under both curing conditions did not cause a significant change in terms of flexural strength, while it was determined that the highest flexural strength value for both curing conditions was realized for the moderate level "n" ratio (n=4).

The changes in flexural strength values of 2BFS/2MW-BB samples according to the "Ms" ratio were given in Figure 4.52 for two different curing conditions. The selected flexural strength value among the samples for this curing condition was formed for 1.2 "Ms". As the "Ms" value increased in this system, it was observed that the flexural

strength values of the samples subject to the oven curing were higher than those of the steam curing samples. It was observed that there were no big differences in flexural strength values between the steam and oven-cured samples in the BFS/MW system, unlike the BFS/CW system,

As a result, it was found that the selected flexural strength for this system has been achieved for the sample with the highest activator dosage (n=4), "Ms" value of 1.2 and steam cured for 2BFS/2MW-BB samples.

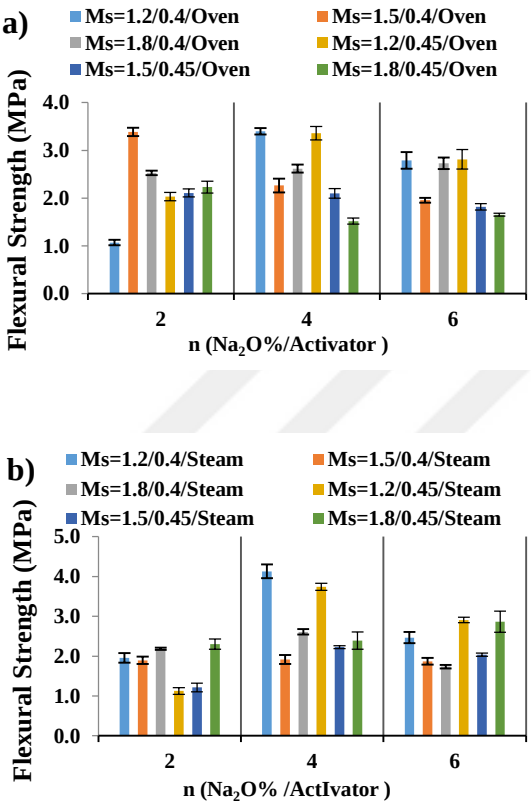


Figure 4.51. Change in flexural strength of 2BFS/2MW-BB paste according to "n" ratio a) For oven cure b) For steam cure.

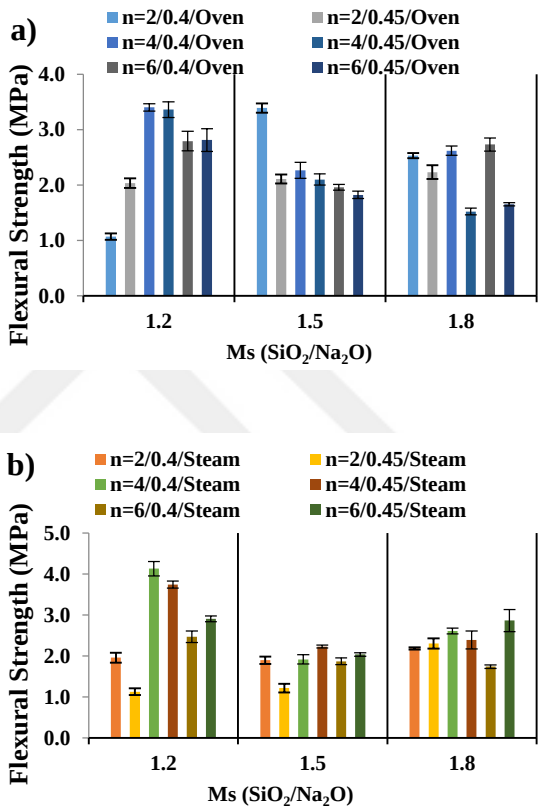
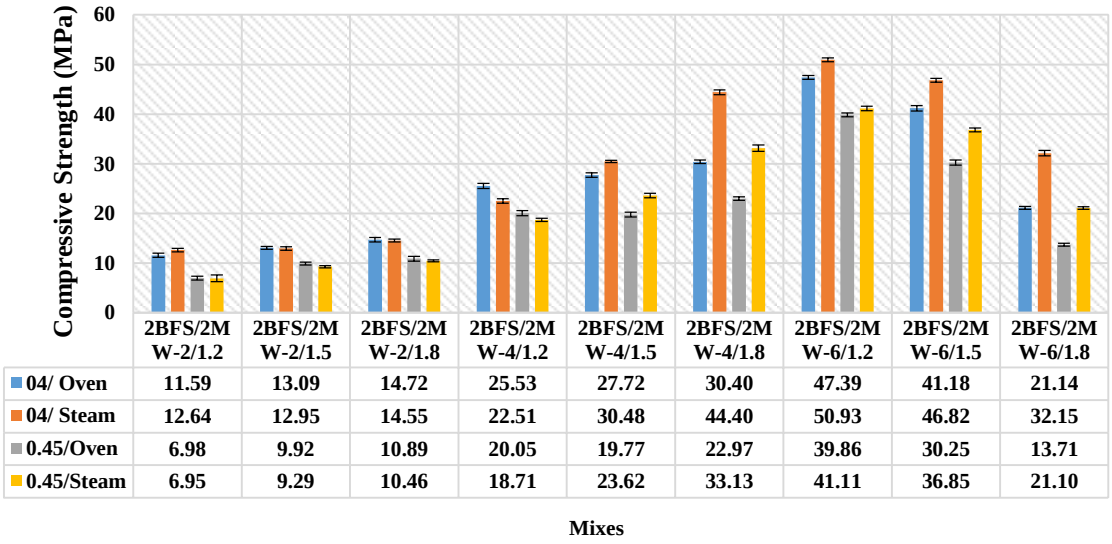


Figure 4.52. Change in flexural strength of 2BFS/2MW-BB paste according to "M_s" ratio a) For oven cure b) For steam cure.

✓ *Compressive Strength Test of BFS/MW-BB*

The compressive strength values of 2BFS/2MW-BB samples were given in Figure 4.53 for both w/b ratios (0.4 and 0.45) and both curing conditions (oven and steam curing).

The highest compressive strength value for BFS/MW-BB sample set was for the "2BFS/2MW-BB/6/1.2/0.4/Steam" sample. Thus, the highest compressive strength value was determined for w/b = 0.4 ratio and steam curing. When the w/b ratio increased from 0.40 to 0.45, the compressive strength values of the samples generally decreased for both curing conditions. It was determined that there were no considerable differences in compressive strength values between the steam and oven-cured samples in the BFS/MW system. It was found that substitution of MW in BFS improved the compressive strength values obtained for alkaline activation of both BFS-UB and MW-UB samples. These results suggest that the compressive strength value increased as the activator dosage ratio increased for a steam and as well as oven cured samples for both w/b.



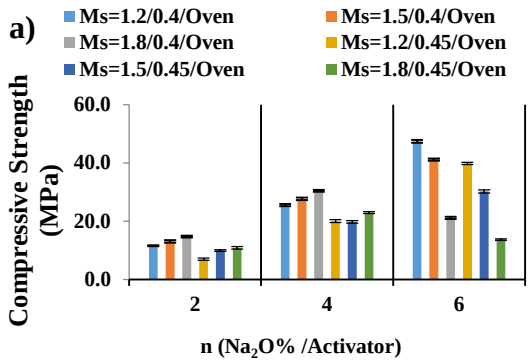
	2BFS/2MW-2/1.2	2BFS/2MW-2/1.5	2BFS/2MW-2/1.8	2BFS/2MW-4/1.2	2BFS/2MW-4/1.5	2BFS/2MW-4/1.8	2BFS/2MW-6/1.2	2BFS/2MW-6/1.5	2BFS/2MW-6/1.8
04/ Oven	11.59	13.09	14.72	25.53	27.72	30.40	47.39	41.18	21.14
04/ Steam	12.64	12.95	14.55	22.51	30.48	44.40	50.93	46.82	32.15
0.45/Oven	6.98	9.92	10.89	20.05	19.77	22.97	39.86	30.25	13.71
0.45/Steam	6.95	9.29	10.46	18.71	23.62	33.13	41.11	36.85	21.10

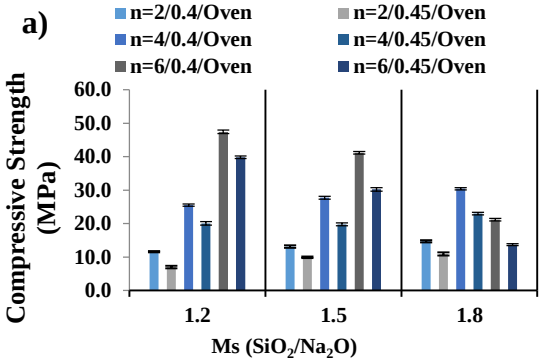
Figure 4.53. Compressive strength of 2BFS/2MW-BB samples.

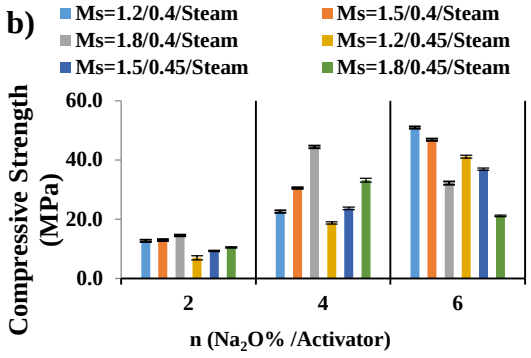
The variation of compressive strength values of 2BFS/2MW-BB samples according to "n" ratio was given in Figure 4.54 for two different curing conditions. For both cure conditions, increasing the "n" ratio leads to an increase in the activator dosage and as well as increase in the compressive strength value. The highest compressive strength value among the samples was obtained for the highest "n" ratio

The variation of compressive strength values of 2BFS/2MW-BB samples according to "Ms" ratio was given in Figure 4.55 for two different curing conditions. The increase in the "Ms" ratio did not create a general tendency to change the compressive strength of

each samples. For both curing conditions, the highest compressive strength value was realized for the "Ms" ratio value of 1.2.







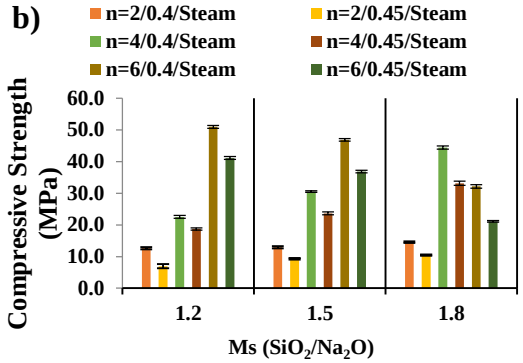


Figure 4.54. Change in flexural strength of 2BFS/2MW-BB according to "n" ratio a) For oven cure b) For steam cure.

Figure 4.55. Change in flexural strength of 2BFS/2MW-BB according to "M_s" ratio a) For oven cure b) For steam cure.

✓ *Strength Properties of BFS/MW-BB*

In this binary system, both the flexural and compressive strength values of BFS/MW-BB samples were higher than BFS-UB samples. In this system, the highest flexural strength value was realized for the "2BFS/2MW/4/1.2/0.4/Steam" sample with 50% MW substitution, while the highest compressive strength value was "2BFS/2MW/6/1.2/0.4/Steam" with a 50% CW substitution. While the selected improvement value in flexural strength was 23%, this value for compressive strength was 12 % increase. In other words, the strength improvement for flexural strength was approximately 2 times higher than the improvement for compressive strength. Although 75% MW substitution in BFS increased the flexural strength value, a decrease in the

compressive strength value of about 64% was observed compared to the reference sample (BFS-UB). In this case, it was found that high rates of MW substitution improved the flexural strength value of the BFS-UB but decreased the compressive strength value. As a result of the microstructure analyzes carried out in the following sections (see 4.7.2.2), it proven by different microstructure analyzes that a new phase did not form in the BFS/MW-BB binary binder system that contributed to the strength-enhancing C-S-H bond structure, but that the MW additive in the BFS contributed to the strength properties by creating a "packing effect". In this case, it can be thought that the increase in MW substituted in BFS increased the strength of the material especially against the flexure effect more than its strength to the compressive effect.

For the samples that given the selected results in terms of flexural and compressive strength (7 days) in the BFS/MW-BB system, the Ms ratios were the same (Ms = 1.2), while the "n" ratios were different. In the sample that gives better results in terms of flexural strength, the rate of "n" was equal to 4, while for the sample that gives the selected result in terms of compressive strength, the rate of "n" was 6. This result revealed that increasing activator dosage improved compressive strength value. However, the increase in the rate of "n" caused the workability values to be negatively affected. For this reason, the ratio of "n" in all experimental sets was determined as 6 at most.

In the literature review, the effects of limestone, which has chemically similar properties with marble, on the alkaline activation of the BFS were investigated, since there was no study in which BFS and MW were activated together. As a conclusion of the paper written by Rakhimova et al., it was determined that limestone improved the strength properties of alkali activated BFS. Rakhimova et al. [57] According their experimental findings, the addition of limestone up to 60 % depending on its fineness and chemical content did not create strength loss compared to the reference sample and even improved the compressive strength at around 50 % compared to the reference sample. In other studies, it was reported that limestone, which was replaced by 20% [60] and 30% [59] ratios in the slag/fly ash mixture, improved the strength properties. In all of these studies, the presence of limestone powder did not lead to the formation of new phases, but slightly increased both the physically and chemically bound water content [59]. In additionally, limestone improved the physical structure and compressive strength

providing higher packing density of mixed sample without increasing the water demand in these studies [57].

✓ *Determination of the Selected BFS/MW-BB Sample*

At the end of the second set of experiments including workability and strength tests, one samples that selected represent this test set were determined for BFS/MW-BB in terms of both flexural and compressive strength. The experimental parameters of the selected samples were given in Table 4.15. The selection criterion applied during the sample selection was applied to determine the samples having the highest values in terms of flexural and compressive strengths and which were not problematic in the process of mixing, molding and setting in terms of workability.

Table 4.15. Experimental parameters of the selected samples of BFS/MW-BB.

BFS/MW-BB Parameters	**The Selected Sample**	
	Compressive Strength	**Flexural Strength**
Mixture Ratio (%)	50-50	50-50
"n" Rate	6	4
"Ms" Rate	1.2	1.2
"w/b" Rate	0.4	0.4
Cure Cond.	Steam	Steam

4.2.3. Ceramic waste/marble waste-binary binders (CW/MW-BB)

4.2.3.1. Workability properties of CW/MW-BB samples

In the two-component (binary) alkaline activation process, MW was substituted in 3 different rates CW. The ratio of CW/MW samples to mass is 3:1, 2:2 and 1:3, respectively. For example, for the “3CW-1MW” sample, the CW and MW samples have a mass ratio of 3:1.

✓ *Flow Table Test of CW/MW-BB*

For all CW/MW-BB samples, flow diameter (mm) values were given in Table 4.16. CW/MW-BB samples, the increase in water/binder (w/b) value from 0.4 to 0.45 naturally increased the flow diameter (consistency). In general, it was observed that as the amount of MW substituted in the CW/MW-BB samples increased flow radius did

not show a certain increase or decrease tendency. For the cement paste sample, while the w/b ratio was 0.4, the flow radius value was 225 mm, and the w/b ratio was 0.45, the flow radius value was 290 mm. For the ratio w/b=0.4, the flow diameter values of the samples with the ratio "n=2" and "n=4" were found close to the flow diameter value of the cement (225 and 290 mm. For w/b=0.45 ratio, the closest flow values to cement (290 mm) are generally provided for n=2 ratio. As the "n" ratio increased, the samples first liquefied. Although the transition from liquid consistency to solid consistency was rapid during mixing, especially in samples with high "n" ratios for both w/b ratios, the setting could not be realized even after 48 hours. Therefore, these samples were excluded from the evaluation for strength tests. While the marble waste substitution increased the flow diameter of the samples in the BFS/MW-BB samples, it did not cause much change in the flow diameter for the CW/MW-BB samples. However, the flow diameter values of CW/MW-BB samples were found much smaller than BFS/MW-BB samples.

Table 4.16. Flow values of CW/MW-BB samples for w/b=0.4 and w/b=0.45.

3CW-1MW	**M_s**					
Na_2O (%)	**(w/b=0.4)**			**(w/b=0.45)**		
	1.2	**1.5**	**1.8**	**1.2**	**1.5**	**1.8**
2	240	230	200	280	L	250
4	L	240	240	L	L	260
6	29	RS	RS	L	RS	RS
2CW-2MW	**M_s**					
Na_2O (%)	**(w/b=0.4)**			**(w/b=0.45)**		
	1.2	**1.5**	**1.8**	**1.2**	**1.5**	**1.8**
2	230	230	210	260	270	260
4	L	230	240	L	L	L
6	RS	RS	RS	L	L	L
1CW-3MW	**M_s**					
Na_2O (%)	**(w/b=0.4)**			**(w/b=0.45)**		
	1.2	**1.5**	**1.8**	**1.2**	**1.5**	**1.8**
2	230	220	220	270	260	260
4	L	230	230	L	L	L
6	RS	RS	RS	L	L	L

L: Liquid R.S: Rapid Setting

The changes in the flow diameter according to the "n" and "Ms" ratios for both "w/b" values of CW/MW-BB samples were given in Figures 4.56 and 4.57.

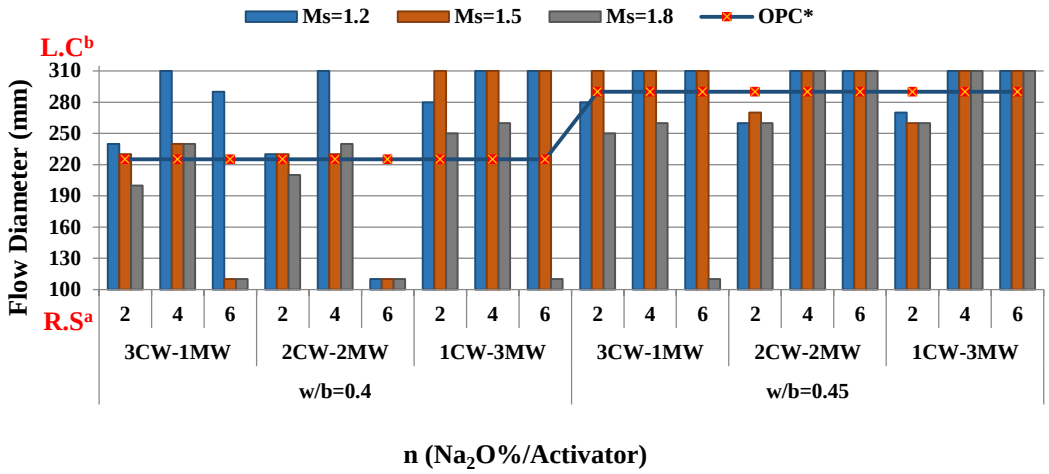


Figure 4.56. The flow values of CW/MW–BB samples according to "n" ratio (for "w/b=0.4" and for "w/b=0.45").

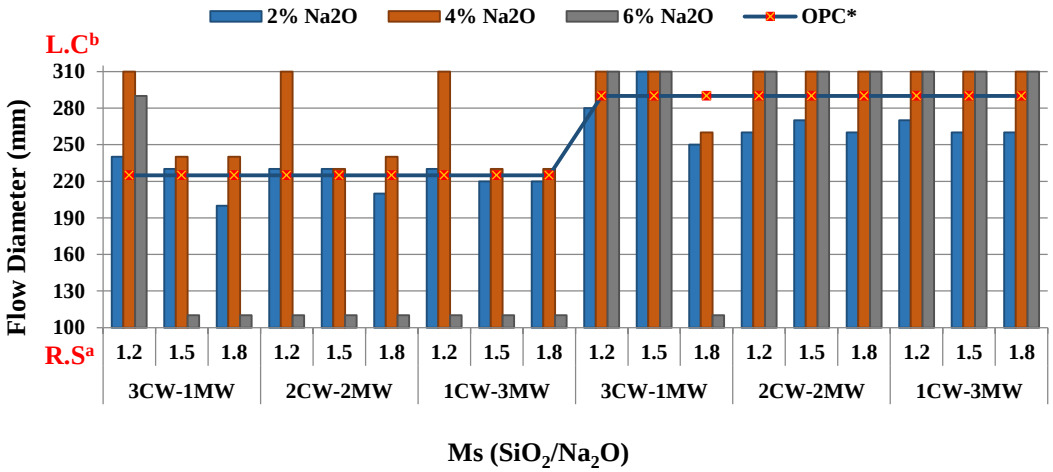


Figure 4.57. The flow values of CW/MW–BB samples according to "Ms" ratio (for "w/b=0.4" and for "w/b=0.45").

* The cement paste was formed only with water without using an alkaline activator.
[a] Below the flow radius of 100 mm is the "Rapid Setting (RS)" limit.
[b] Above flow radius of 300 mm is "Liquid Consistency (LC)" limit.

When the w/b ratio increased from 0.4 to 0.45, the flow diameter of the samples increased and their consistency became liquefied. For these binary mixture samples, the flow diameter of the samples having a value of 0.4 w/b generally remained within the experimental lower and upper limits. In terms of workability, the 0.4 w/b ratio was determined as a more significant ratio for this mixture. Therefore, the effects of "n" and

“Ms” ratios on the flow diameter were interpreted only for samples with a value a w/b of 0.4.

According to the test conditions in this binary mixing system, when MW is substituted at a rate equal to or less than mass in CW, the increase in “n” ratio from 2 to 4 has increased the flow diameter of the samples in Figure 4.56. However, it was found that the samples showed sudden solidification when the “n” ratio increased even more. When MW's substitution rate by mass exceeds CW, the flow diameter values were determined to be higher for each “n” ratio compared to other CW/MW-BB samples.

In Figure 4.57, changing the “Ms” ratio did not affect the flow diameter values of CW/MW-BB samples in the tendency to increase or decrease. However, especially for samples containing low and medium activator dosage (n=2 and n=4), the flow diameter values of the samples with 1.5 and 1.8 “Ms” values were observed similar to the cement sample.

✓ *Setting Time Test of CW/MW-BB*

In this experiment, initial and final setting time values of CW/MW-BB samples for both w/b ratios are given in Table 4.17.

Table 4.17. Setting time of CW/MW-BB samples (w/b=0.4 and w/b=0.45).

CODE	Initial Setting Time (min.)	Final Setting Time (min.)	Note	Code	Initial Setting Time (min.)	Final Setting Time (min.)	Note
3CW/1MW-2/1.2/0.4	169,0	178,7	SPD	**3CW/1MW-2/1.2/0.45**	>202	>312	
3CW/1MW-2/1.5/0.4	>202	>312		**3CW/1MW-2/1.5/0.45**	>202	>312	
3CW/1MW-2/1.8/0.4	149,0	153,0	SPD	**3CW/1MW-2/1.8/0.45**	>202	>312	
3CW/1MW-4/1.2/0.4	>202	>312		**3CW/1MW-4/1.2/0.45**	>202	>312	
3CW/1MW-4/1.5/0.4	>202	>312		**3CW/1MW-4/1.5/0.45**	>202	>312	
3CW/1MW-4/1.8/0.4	>202	>312	NS	**3CW/1MW-4/1.8/0.45**	>202	>312	NS
3CW/1MW-6/1.2/0.4	>202	>312	NS	**3CW/1MW-6/1.2/0.45**	>202	>312	NS
3CW/1MW-6/1.5/0.4	>202	>312	NS	**3CW/1MW-6/1.5/0.45**	>202	>312	NS
3CW/1MW-6/1.8/0.4	>202	>312	NS	**3CW/1MW-6/1.8/0.45**	>202	>312	NS
2CW/2MW-2/1.2/0.4	>202	>312		**2CW/2MW-2/1.2/0.45**	>202	>312	
2CW/2MW-2/1.5/0.4	>202	>312		**2CW/2MW-2/1.5/0.45**	>202	>312	
2CW/2MW-2/1.8/0.4	>202	>312		**2CW/2MW-2/1.8/0.45**	>202	>312	
2CW/2MW-4/1.2/0.4	>202	>312		**2CW/2MW-4/1.2/0.45**	>202	>312	
2CW/2MW-4/1.5/0.4	>202	>312		**2CW/2MW-4/1.5/0.45**	>202	>312	
2CW/2MW-4/1.8/0.4	>202	>312	NS	**2CW/2MW-4/1.8/0.45**	>202	>312	NS
2CW/2MW-6/1.2/0.4	>202	>312		**2CW/2MW-6/1.2/0.45**	>202	>312	
2CW/2MW-6/1.5/0.4	>202	>312	NS	**2CW/2MW-6/1.5/0.45**	>202	>312	NS
2CW/2MW-6/1.8/0.4	>202	>312	NS	**2CW/2MW-6/1.8/0.45**	>202	>312	NS
1CW/3MW-2/1.2/0.4	>202	>312		**1CW/3MW-2/1.2/0.45**	>202	>312	
1CW/3MW-2/1.5/0.4	>202	>312		**1CW/3MW-2/1.5/0.45**	>202	>312	
1CW/3MW-2/1.8/0.4	>202	>312		**1CW/3MW-2/1.8/0.45**	>202	>312	
1CW/3MW-4/1.2/0.4	>202	>312		**1CW/3MW-4/1.2/0.45**	>202	>312	
1CW/3MW-4/1.5/0.4	>202	>312		**1CW/3MW-4/1.5/0.45**	>202	>312	
1CW/3MW-4/1.8/0.4	>202	>312	NS	**1CW/3MW-4/1.8/0.45**	>202	>312	NS
1CW/3MW-6/1.2/0.4	>202	>312	NS	**1CW/3MW-6/1.2/0.45**	>202	>312	NS
1CW/3MW-6/1.5/0.4	>202	>312	NS	**1CW/3MW-6/1.5/0.45**	>202	>312	NS
1CW/3MW-6/1.8/0.4	>202	>312	NS	**1CW/3MW-6/1.8/0.45**	>202	>312	NS

RS: Rapid Setting SPD: Short Period Difference NS: No setting (after 48 h)

As a result of this experiment, it was determined that as the w/b ratio of BFS/MW-BB samples increased, Initial and final setting times increased. For all samples, it was observed that samples with "n" ratio of 6 did not complete their settings even after 48 hours. The flow diameter values of almost all samples were larger than the spreading diameter values determined for the same w/b values of the cement sample.

The change in the initial and final setting times of the samples according to the "n" ratio for both w/b ratios was shown in Figure 4.58.

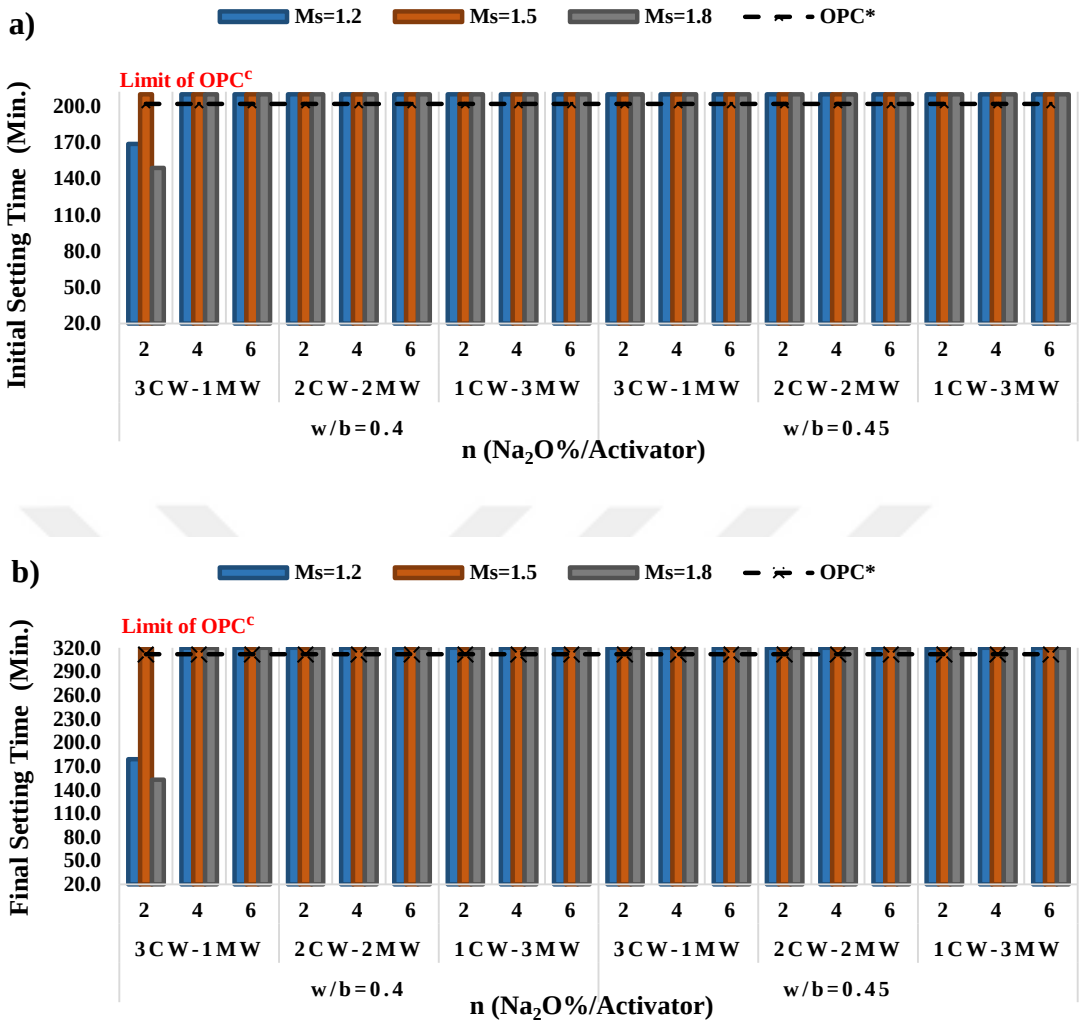


Figure 4.58. The setting time of CW/MW-BB Samples according to "n" ratio a) Initial setting time b) Final setting time.

* The cement paste is formed only with water without using an alkaline activator.
[c] These limit values are defined in ASTM C 191-13 Standard.

The initial and final setting times of the samples according to the "Ms" ratio was shown in Figure 4.59.

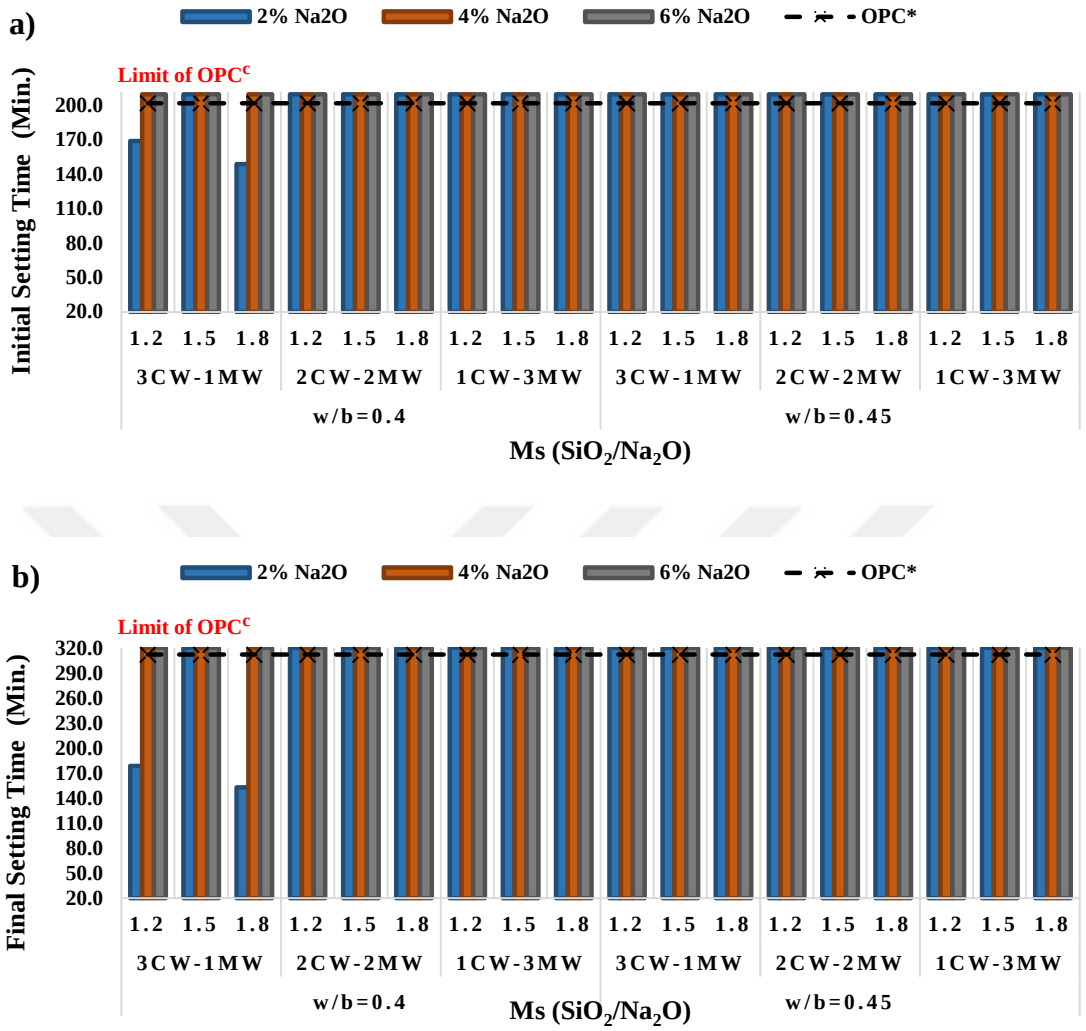


Figure 4.59. The setting time of CW/MW-BB Samples according to "Ms" ratio a) Initial setting time b) Final setting time.

* The cement paste is formed only with water without using an alkaline activator.
[c] These limit values are defined in ASTM C 191-13 Standard.

There was no significant effect of changing the rates of "n" and "Ms" on the setting times of the CW/MW-BB samples, since the initial and final setting of almost all samples was higher than the limit values determined in accordance with ASTM standards of the cement sample. However, unlike other unary and binary component samples, it was found that the samples could not complete their settings even after 48 hours, even if the transition from liquid consistency to solid consistency occurred. Compared to other binary component samples, the number of samples that could not

complete the settings at the end of 48 hours occurred within this binary activation system.

- ✓ *Workability Properties of CW/MW-BB*

It was observed that the workability and setting time values for this binary system did not change significantly with increasing MW substitution in CW. In fact, at the rate of 25, 50 and 75 % MW substituted in CW samples for "n" ratio of 4 and 6, no setting was observed even after 48 hours. Therefore, much lower strength values were obtained when other binary systems were compared. It was determined that, when alkali-activated CW-UB samples compared to MW containing samples sudden setting behavior prevented especially for high "n" rates. No publication of the alkali activation of marble waste with ceramic waste could be detected in the literature. However, limestone, which has a very similar chemical content to marble waste, found to improve the workability properties of Halloysite clay, which has a high SiO_2 and Al_2O_3 ratio, like ceramic waste. In study of Bayiya et al [105], as the limestone addition in the Halloysite activated with different concentrations of NaOH increased, the setting start time and workability properties increased. This increase was less for high NaOH concentrations than for sample having low NaOH concentrations. This study results were consistent with our study results. But, in other studies, it was stated that the addition of limestone used in alkali activation of metakaolin, which is rich in SiO_2 and Al_2O_3 minerals such as ceramic waste, decreases the consistency and increases the fluidity [106, 107].

4.2.3.2. Flexural and compressive strength properties of CW/MW-BB samples

In this binary activation system consisting of a mixture of CW and MW, MW has been replaced in CW in 3 different masses. The selected flexural and compressive strength values CW/MW-BB systems for each mix proportion was shown in Figure 4.60. Accordingly, the selected flexural strength value achieved for the 2CW/2MW composition, in which MW was substituted in the CW in a 2:2 ratios. The highest compressive strength value was also for the 2CW/2MW composition in which MW was substituted in the CW in a 2:2 ratios. Therefore, flexural and compressive strengths in

binary component systems evaluated over the combinations that gave the selected values among the samples.

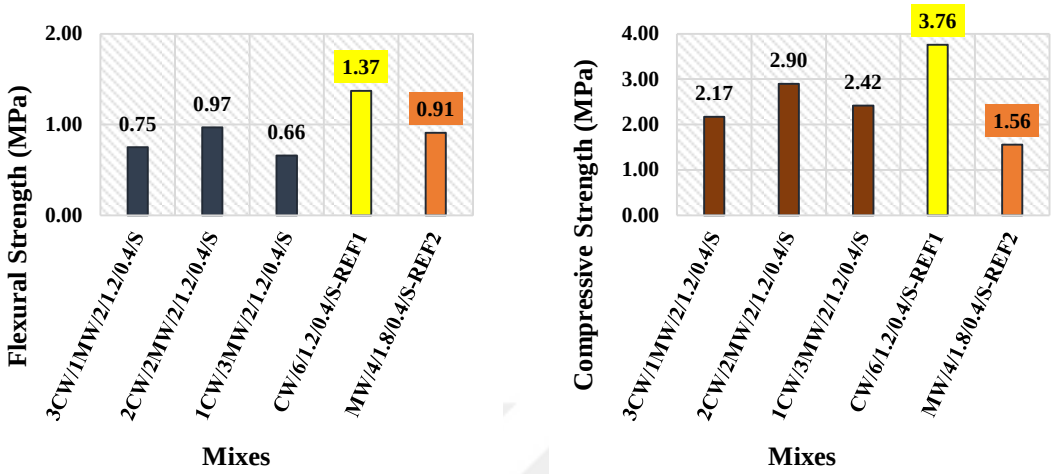
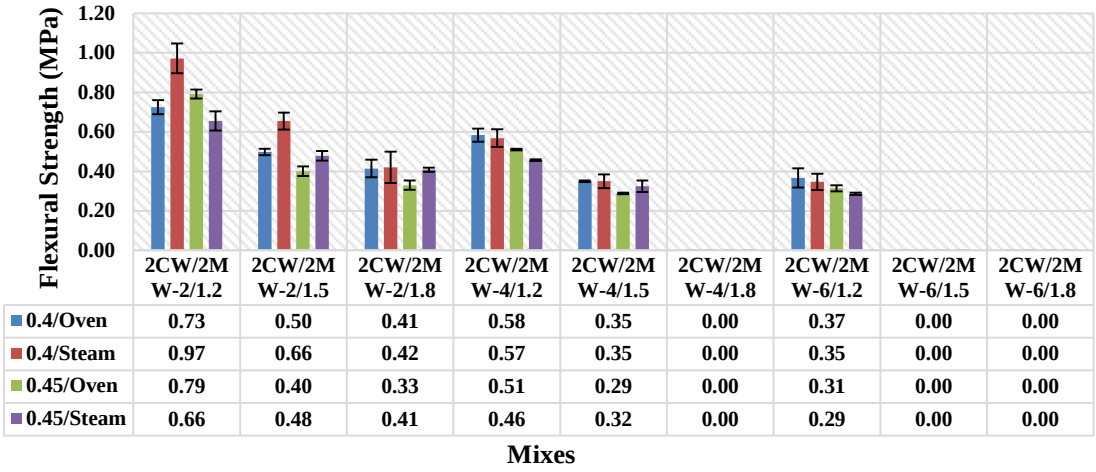


Figure 4.60. The selected flexural and compressive strength values CW/MW-BB systems for each mix proportion.

✓ *Flexural Strength Test*

The flexural strength values of the 2CW/2MW-BB samples were given in Figure 4.61 for both w/b ratios (0.4 and 0.45) and for both curing conditions (oven and steam curing).

The highest flexural strength value for CW/MW-BB sample set was for the "2CW/2MW/2/1.2/0.4/Steam" sample. Thus, the highest flexural strength value was determined for w/b = 0.4 ratio and steam curing.



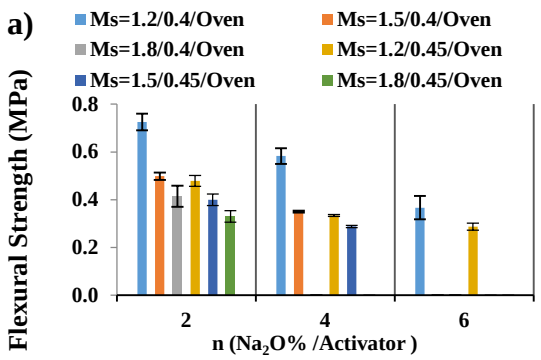
	2CW/2MW-2/1.2	2CW/2MW-2/1.5	2CW/2MW-2/1.8	2CW/2MW-4/1.2	2CW/2MW-4/1.5	2CW/2MW-4/1.8	2CW/2MW-6/1.2	2CW/2MW-6/1.5	2CW/2MW-6/1.8
0.4/Oven	0.73	0.50	0.41	0.58	0.35	0.00	0.37	0.00	0.00
0.4/Steam	0.97	0.66	0.42	0.57	0.35	0.00	0.35	0.00	0.00
0.45/Oven	0.79	0.40	0.33	0.51	0.29	0.00	0.31	0.00	0.00
0.45/Steam	0.66	0.48	0.41	0.46	0.32	0.00	0.29	0.00	0.00

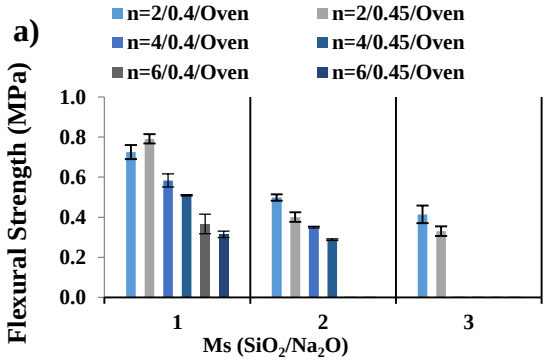
Figure 4.61. Flexural strength of 2CW/2MW-BB samples

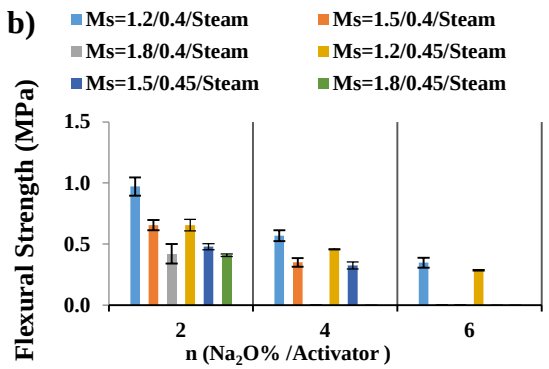
In this test set, when the w/b ratio increased from 0.40 to 0.45, there was a decrease for the flexural strength value for all samples in general. Some examples increased and others decreased. However, it was found that substitution of MW in CW containing samples did not improve the flexural strength values obtained for alkaline activation of CW-UB. However, the results obtained for this binary mixing system were higher than the flexural strength values of the MW-UB system. However, unlike CW-UB and MW-UB systems, there were examples with high activator levels in this system that did not complete the setting even after 48 hours (for example 2CW/2MW/4/1.8, 2CW/2MW/6/1.5 and 2CW/2MW/6/1.8). Therefore, the values on the y-axis of these combinations were zero and did not appear in the tables.

The variation of flexural strength values of 2CW/2MW-BB samples according to "n" ratio was given in Figure 4.62 for two different curing conditions. For this binary activation system, increasing the "n" ratio under both curing conditions caused decreasing in terms of flexural strength.

The changes in flexural strength values of 2CW/2MW-BB samples according to the "Ms" ratio are given in Figure 4.63 for two different curing conditions. The selected flexural strength value for this curing condition was formed for 1.2 "Ms". As the "Ms" value increased in this system, it was observed that the flexural strength values of the samples decreased for both cure conditions.







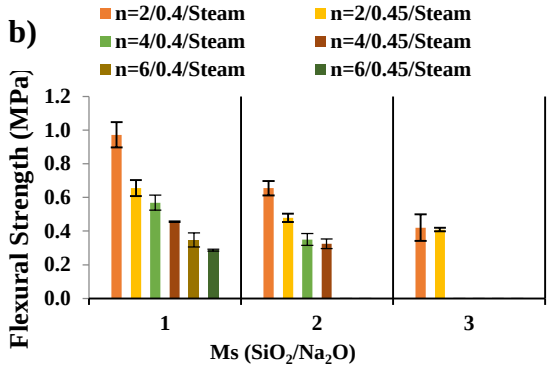


Figure 4.62. Change in flexural strength of 2CW/2MW-BB paste according to "n" ratio a) For oven cure b) For steam cure.

Figure 4.63. Change in flexural strength of 2CW/2MW-BB paste according to "M_s" ratio a) For oven cure b) For steam cure.

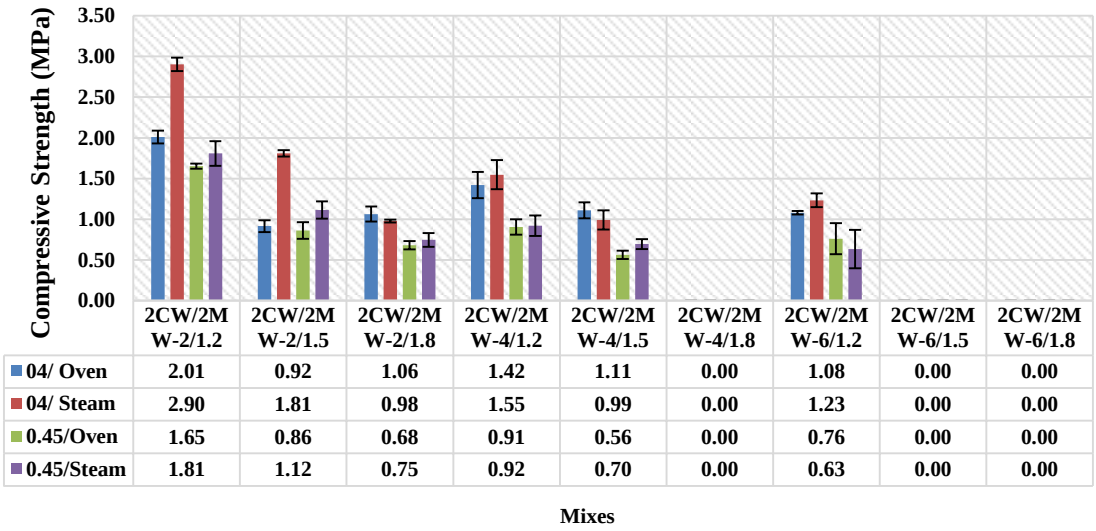
As a result, it was found that the selected flexural strength for this system has been achieved for the sample with the highest activator dosage (n=2), "Ms" value of 1.2 and steam cured for 2CW/2MW-BB samples.

✓ *Compressive Strength Test of CW/MW-BB*

The compressive strength values of 2CW/2MW-BB samples are given in Figure 4.64 for both w/b ratios (0.4 and 0.45) and both curing conditions (oven and steam).

The highest compressive strength value for CW/MW-BB sample set was for the "2CW/2MW-BB/2/1.2/0.4/Steam" sample. Thus, the highest compressive strength value was determined for w/b = 0.4 ratio and steam curing. When the w/b ratio increased from 0.40 to 0.45, the compressive strength values of the samples generally decreased for both curing conditions. The highest compressive strength value was

determined for the lowest “n” ratio in the CW/MW-BB system. However, it was understood that the samples in the system had the highest compressive strength value at the lowest “Ms” value for each “n” ratio. This means that for each activator dosage, the compressive strength value decreased as the amount of NaOH in the activator decreased.

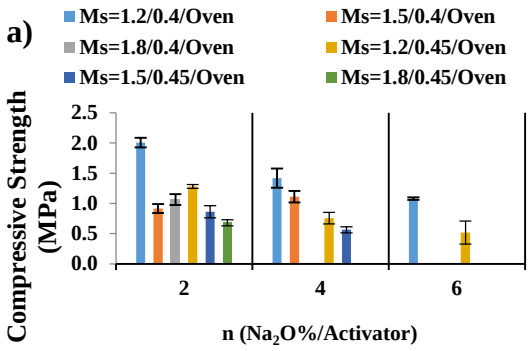


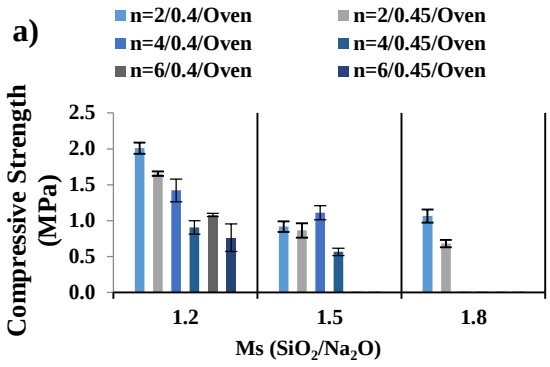
	2CW/2MW-2/1.2	2CW/2MW-2/1.5	2CW/2MW-2/1.8	2CW/2MW-4/1.2	2CW/2MW-4/1.5	2CW/2MW-4/1.8	2CW/2MW-6/1.2	2CW/2MW-6/1.5	2CW/2MW-6/1.8
04/ Oven	2.01	0.92	1.06	1.42	1.11	0.00	1.08	0.00	0.00
04/ Steam	2.90	1.81	0.98	1.55	0.99	0.00	1.23	0.00	0.00
0.45/Oven	1.65	0.86	0.68	0.91	0.56	0.00	0.76	0.00	0.00
0.45/Steam	1.81	1.12	0.75	0.92	0.70	0.00	0.63	0.00	0.00

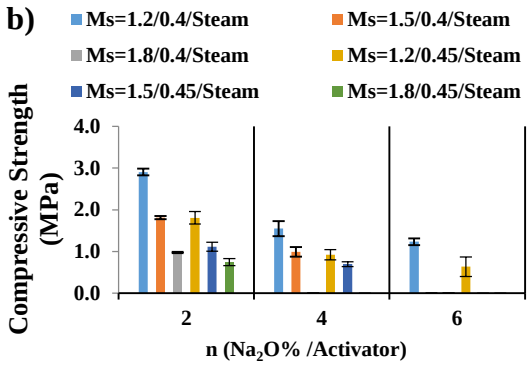
Figure 4.64. Compressive strength of 2CW/2MW-BB samples.

The variation of compressive strength values of 2CW/2MW-BB samples according to “n” ratio is given in Figure 4.65 for two different curing conditions. For both cure conditions, increasing the “n” ratio, that is, increasing the activator dosage, decreased the compressive strength value. The highest compressive strength value was realized for the lowest “n” ratio.

The variation of compressive strength values of 2CW/2MW-BB samples according to “Ms” ratio is given in Figure 4.66 for two different curing conditions. The increase in the “Ms” ratio decreased the compressive strength value. For both curing conditions, the highest compressive strength value was realized for the ratio with a “Ms” value of 1.2.







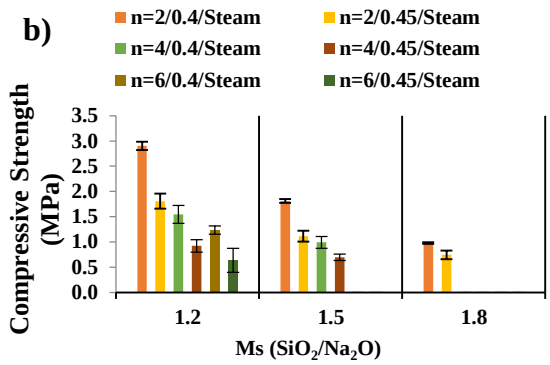


Figure 4.65. Change in flexural strength of 2CW/2MW-BB according to "n" ratio a) For oven cure b) For steam cure.

Figure 4.66. Change in flexural strength of 2CW/2MW-BB according to "M_s" ratio a) For oven cure b) For steam cure.

✓ *Strength Properties of CW/MW-BB*

The highest strength values (flexural and compressive) obtained in the CW/MW-BB two-component activation system were found to be lower than the alkali activation product of the CW-UB. This decrease was approximately 30% in terms of flexural strength and approximately 23% in terms of compressive strength for the sample CW/MW-BB with the highest flexural and compressive strength (2CW/2MW-BB). However, when the addition of MW in CW increased from 25% to 50%, it was observed that the strength values increased in terms of both flexural and compressive strength compared to the sample containing 25% marble waste replacement. In this case, it could be said that as the amount of CaO in the ceramic waste increased, the interaction of CW and MW increased. As the microstructural analyzes revealed in the following sections, it was observed that the "quartz" phase in the CW-MW-BB system decreased compared to the CW-UB system, thus the quartz phase joined the reaction

(see Figure 4.124). With the FTIR analysis, an absorption peak, which was thought to belong to a reaction product of (See 4.126) at 972 cm^{-1} wavelengths, was obtained. There was no publication in the literature involving the combined alkali activation of CW and MW. However, there were studies involving alkali activation of materials such as fly ash, metakaolin and clay rich in SiO_2 and Al_2O_3 oxides, together with CaO rich slag and limestone [105-110]. Very similar results from these studies to our study results reported by Bayiha et al. [109]. In their study, it was determined that the addition of limestone up to 45% contributes to the formation of the geopolymerization product within the activation of Halloysite type clay and thus improved the compressive strength [105].

✓ *Determination of the Selected CW/MW-BB Sample*

At the end of the second set of experiments including workability and strength tests, one samples that selected represent this test set were determined for CW/MW-BB in terms of both flexural and compressive strength. The experimental parameters of the selected samples were given in Table 4.18. The selection criterion applied during the sample selection was applied to determine the samples having the highest values in terms of flexural and compressive strengths and which were not problematic in the process of mixing, molding and setting in terms of workability.

Table 4.18. Experimental parameters of the selected samples of CW/MW-BB.

CW/MW-BB Parameters	**The Selected Sample**	
	Compressive Strength	**Flexural Strength**
Mixture Ratio (%)	50-50	50-50
"n" Rate	2	2
"Ms" Rate	1.2	1.2
"w/b" Rate	0.4	0.4
Cure Cond.	Steam	Steam

4.3. Third Stages: Determination The Optimum Parameters of the Ternary Binders

4.3.1. Blast furnace slag/ceramic waste/marble waste-ternary binders (BFS/CW/MW-TB)

4.3.1.1. Workability properties of BFS/CW/MW-TB samples

In the three-component (ternary) alkaline activation process, CW and MW was substituted in 4 different rates of BFS. The ratio of BFS/CW/MW samples to mass is 1:1:1, 2:1:1, 1:2:1 and 1:1:2 respectively. For example, for the "BFS/CW/MW" sample, the BFS, CW and MW samples have a mass ratio of 1:1:1. For the "2BFS/1CW/1MW" sample also, the BFS, CW and MW samples have a mass ratio of 2:1:1.

✓ *Flow Table Test of BFS/CW/MW-TB*

For all BFS/CW/MW-TB samples, flow diameter (mm) values were given in Table 4.19. BFS/CW/MW-TB samples, the increase in water/binder (w/b) value from 0.4 to 0.45 naturally increased the flow diameter (consistency). It has been determined that BFS/CW/MW-TB samples, in which all components are added in equal proportions by mass, have much higher values than the other ternary binder samples. Increasing the amount of ceramic waste in the content of the ternary binder systems has reduced the workability properties of the samples in terms of flow diameter. For all ternary binder samples, it has been determined that the samples with low activator dosage (n=2) at both w/b values are close to the flow diameter value of the cement sample. The high activator dosage (n=6) reduced the transition speed of the samples from liquid consistency to solid consistency.

Table 4.19. Flow diameter values (mm) of BFS/CW/MW-TB samples for w/b=0.4 and w/b=0.45.

BFS/CW/MW	**M_s**					
Na_2O (%)	**(w/b=0.4)**			**(w/b=0.45)**		
	1.2	**1.5**	**1.8**	**1.2**	**1.5**	**1.8**
2	260	270	240	L	L	L
4	280	270	L	L	L	L
6	RS	RS	RS	L	L	L
2BFS/1CW/1MW	**M_s**					
Na_2O (%)	**(w/b=0.4)**			**(w/b=0.45)**		
	1.2	**1.5**	**1.8**	**1.2**	**1.5**	**1.8**
2	240	230	220	L	L	260
4	280	270	260	L	L	RS
6	RS	RS	RS	L	L	L
1BFS/2CW/1MW	**M_s**					
Na_2O (%)	**(w/b=0.4)**			**(w/b=0.45)**		
	1.2	**1.5**	**1.8**	**1.2**	**1.5**	**1.8**
2	230	230	210	250	260	250
4	L	220	230	L	L	L
6	RS	RS	RS	L	L	L
1BFS/1CW/2MW	**M_s**					
Na_2O (%)	**(w/b=0.4)**			**(w/b=0.45)**		
	1.2	**1.5**	**1.8**	**1.2**	**1.5**	**1.8**
2	240	230	220	260	280	270
4	L	240	260	L	L	L
6	RS	RS	RS	L	L	L

L: Liquid R.S: Rapid Setting

The changes in the flow diameter according to the “n” and “Ms” ratios for both “w/b” values of BFS/CW/MW-TB samples were given in Figure 4.67 and Figure.4.68.

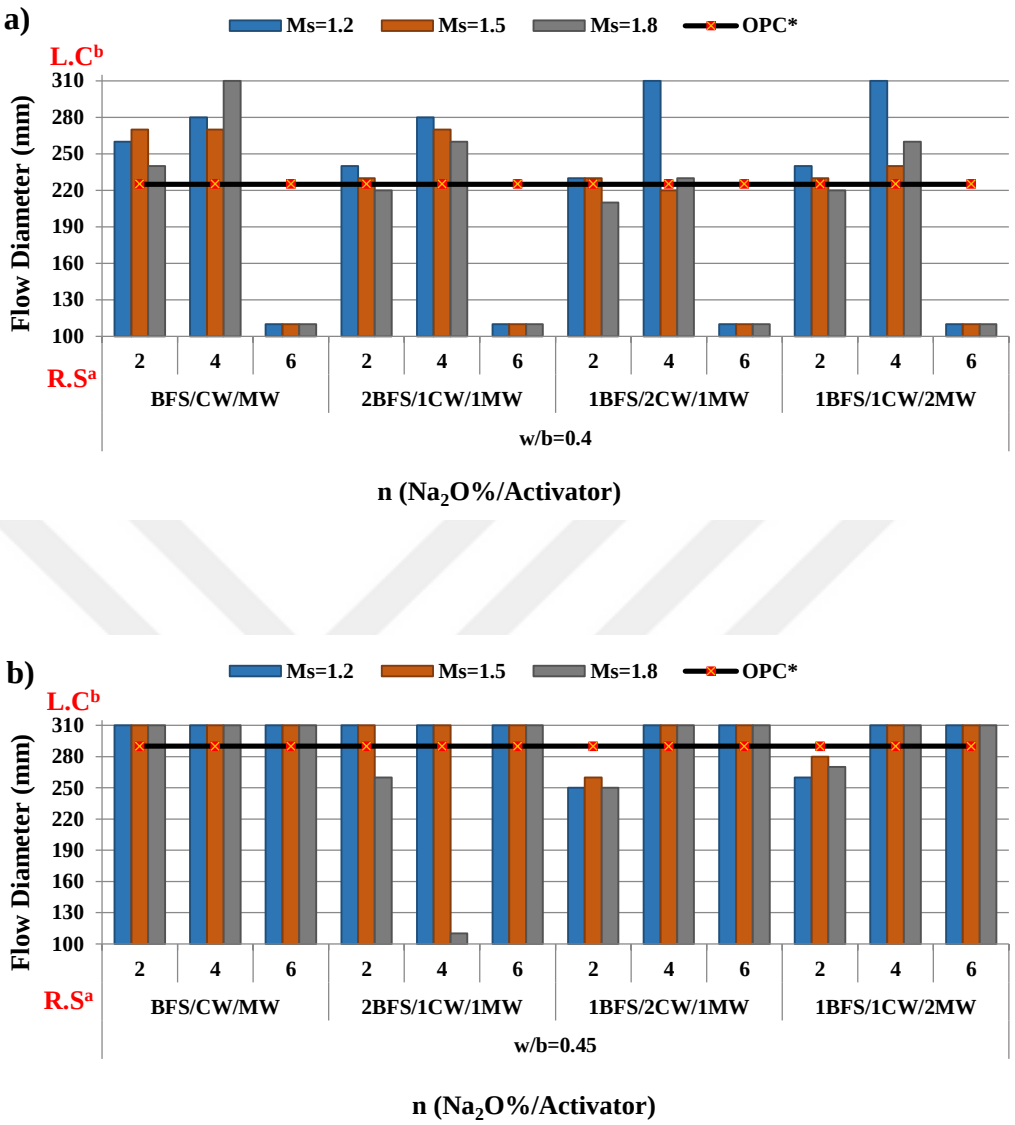


Figure 4.67. The flow values of BFS/CW/MW-TB samples according to "n" ratio a) for "w/b=0.4" b) for "w/b=0.45"

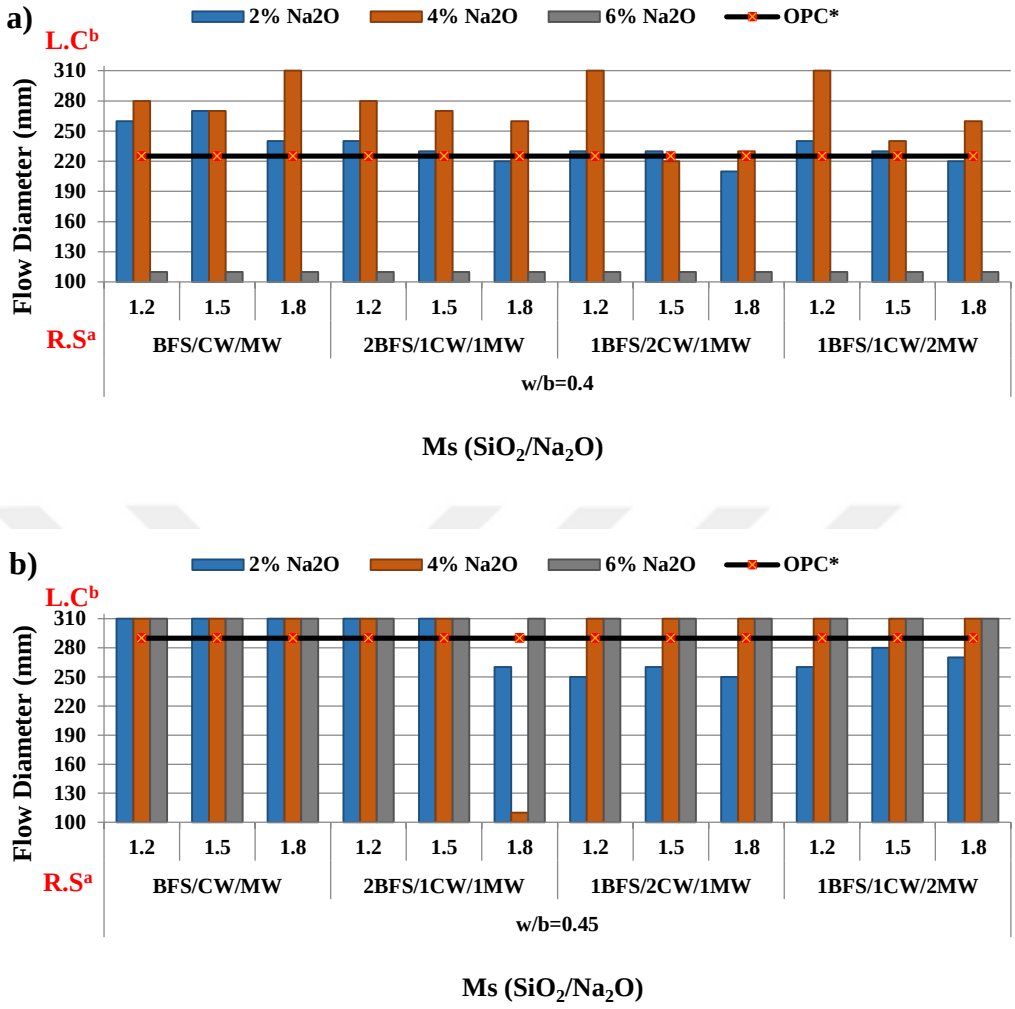


Figure 4.68. The flow values of BFS/CW/MW-TB samples according to "Ms" ratio a) for "w/b=0.4" b) for "w/b=0.45"

* The cement paste was formed only with water without using an alkaline activator.
[a] Below the flow radius of 100 mm is considered as "Rapid Setting (RS)" limit.
[b] Above flow radius of 300 mm is considered as "Liquid Consistency (LC)" limit.

When the w/b ratio increased from 0.4 to 0.45, the flow diameter of the samples increased and their consistency became liquefied. For these binary mixture samples, the flow diameter of the samples having a value of 0.4 w/b generally remained within the experimental lower and upper limits. In terms of workability, the 0.4 w/b ratio was determined as a more significant ratio for this mixture. Therefore, the effects of "n" and "Ms" ratios on the flow diameter were interpreted only for samples with a w/b value of 0.4.

According to the test conditions in the Figure 4.67, increasing the “n” value in the ternary samples increased the consistency up to a point and then decreased it. This point is the ratio of n=4. This means that as the dosage of activator solution (total amount of mixture of sodium silicate and sodium hydroxide / “n” ratio) used for the activation of the samples increased up to n=4, the consistency of the samples increased and then decreased. That is, for the ratio n=4, the flow diameter of the samples has reached the maximum value. However, when the n=6, the transition from liquid to solid consistency was rapid.

In Figure 4.68, the increase in “Ms” ratio generally reduced the flow diameter values of the samples for all substitution rates of CW and MW in the BFS. This means that the amount of sodium silicate in the activator solution increased whereas the decreased in the amount of sodium hydroxide hence it reduced the workability of the samples. Consequently “n” ratio was more effective than “Ms” ratio on the workability of all samples in this mixture.

✓ *Setting Time Test of BFS/CW/MW-TB*

In this experiment, initial and final setting time values of BFS/CW/MW-TB samples for both w/b ratios were given in Table 4.20.

Table 4.20. Setting time of BFS/CW/MW-TB samples (w/b=0.4 and w/b=0.45).

Code	İnitial Setting Time (min.)	Final Setting Time (min.)	Note	Code	İnitial Setting Time (min.)	Final Setting Time (min.)	Note
BFS/CW/MW-2/1.2/0.4	181.7	193.7	SPD	**BFS/CW/MW-2/1.2/0.45**	>202	>312	
BFS/CW/MW-2/1.5/0.4	166.3	174.7	SPD	**BFS/CW/MW-2/1.5/0.45**	>202	>312	
BFS/CW/MW-2/1.8/0.4	192.3	207.7	SPD	**BFS/CW/MW-2/1.8/0.45**	>202	>312	
BFS/CW/MW-4/1.2/0.4	>202	>312		**BFS/CW/MW-4/1.2/0.45**	>202	>312	
BFS/CW/MW-4/1.5/0.4	>202	>312		**BFS/CW/MW-4/1.5/0.45**	>202	>312	
BFS/CW/MW-4/1.8/0.4	>202	>312	NS	**BFS/CW/MW-4/1.8/0.45**	>202	>312	NS
BFS/CW/MW-6/1.2/0.4	72.3	175.0		**BFS/CW/MW-6/1.2/0.45**	>202	>312	
BFS/CW/MW-6/1.5/0.4	88.0	192.7		**BFS/CW/MW-6/1.5/0.45**	>202	>312	
BFS/CW/MW-6/1.8/0.4	98.3	>312	HS	**BFS/CW/MW-6/1.8/0.45**	>202	>312	
2BFS/1CW/1MW-2/1.2/0.4	136.7	144.0	SPD	**2BFS/1CW/1MW-2/1.2/0.45**	>202	>312	
2BFS/1CW/1MW-2/1.5/0.4	154.0	168.0	SPD	**2BFS/1CW/1MW-2/1.5/0.45**	>202	>312	
2BFS/1CW/1MW-2/1.8/0.4	147.0	155.0	SPD	**2BFS/1CW/1MW-2/1.8/0.45**	>202	>312	
2BFS/1CW/1MW-4/1.2/0.4	>202	>312		**2BFS/1CW/1MW-4/1.2/0.45**	>202	>312	
2BFS/1CW/1MW-4/1.5/0.4	>202	>312		**2BFS/1CW/1MW-4/1.5/0.45**	>202	>312	
2BFS/1CW/1MW-4/1.8/0.4	>202	>312	NS	**2BFS/1CW/1MW-4/1.8/0.45**	>202	>312	NS
2BFS/1CW/1MW-6/1.2/0.4	59.0	134.3		**2BFS/1CW/1MW-6/1.2/0.45**	>202	>312	
2BFS/1CW/1MW-6/1.5/0.4	70.7	163.0		**2BFS/1CW/1MW-6/1.5/0.45**	>202	>312	
2BFS/1CW/1MW-6/1.8/0.4	48.0	127.7		**2BFS/1CW/1MW-6/1.8/0.45**	>202	>312	
1BFS/2CW/1MW-2/1.2/0.4	>202	>312		**1BFS/2CW/1MW-2/1.2/0.45**	>202	>312	
1BFS/2CW/1MW-2/1.5/0.4	>202	>312		**1BFS/2CW/1MW-2/1.5/0.45**	>202	>312	
1BFS/2CW/1MW-2/1.8/0.4	>202	>312		**1BFS/2CW/1MW-2/1.8/0.45**	>202	>312	
1BFS/2CW/1MW-4/1.2/0.4	>202	>312		**1BFS/2CW/1MW-4/1.2/0.45**	>202	>312	
1BFS/2CW/1MW-4/1.5/0.4	>202	>312		**1BFS/2CW/1MW-4/1.5/0.45**	>202	>312	
1BFS/2CW/1MW-4/1.8/0.4	>202	>312	NS	**1BFS/2CW/1MW-4/1.8/0.45**	>202	>312	NS
1BFS/2CW/1MW-6/1.2/0.4	>202	>312		**1BFS/2CW/1MW-6/1.2/0.45**	>202	>312	
1BFS/2CW/1MW-6/1.5/0.4	>202	>312		**1BFS/2CW/1MW-6/1.5/0.45**	>202	>312	
1BFS/2CW/1MW-6/1.8/0.4	>202	>312		**1BFS/2CW/1MW-6/1.8/0.45**	>202	>312	
1BFS/1CW/2MW-2/1.2/0.4	>202	>312		**1BFS/1CW/2MW-2/1.2/0.45**	>202	>312	
1BFS/1CW/2MW-2/1.5/0.4	>202	>312		**1BFS/1CW/2MW-2/1.5/0.45**	>202	>312	
1BFS/1CW/2MW-2/1.8/0.4	>202	>312		**1BFS/1CW/2MW-2/1.8/0.45**	>202	>312	
1BFS/1CW/2MW-4/1.2/0.4	>202	>312		**1BFS/1CW/2MW-4/1.2/0.45**	>202	>312	
1BFS/1CW/2MW-4/1.5/0.4	>202	>312		**1BFS/1CW/2MW-4/1.5/0.45**	>202	>312	
1BFS/1CW/2MW-4/1.8/0.4	>202	>312	NS	**1BFS/1CW/2MW-4/1.8/0.45**	>202	>312	NS
1BFS/1CW/2MW-6/1.2/0.4	>202	>312		**1BFS/1CW/2MW-6/1.2/0.45**	>202	>312	
1BFS/1CW/2MW-6/1.5/0.4	>202	>312		**1BFS/1CW/2MW-6/1.5/0.45**	>202	>312	
1BFS/1CW/2MW-6/1.8/0.4	>202	>312		**1BFS/1CW/2MW-6/1.8/0.45**	>202	>312	

RS: Rapid Setting SPD: Short Period Difference NS: No setting (after 48 h) HS: Half Setting

As a result of this experiment, it was determined that as the w/b ratio of BFS/CW/MW-TB samples increased, initial and final setting times increased. For samples which ceramic and marble waste is much higher by mass, the initial and final setting times were prolonged according to the ASTM standards of the cement sample. For all three component samples, the setting time did not occur even after 48 hours in samples with a "n" ratio of 4 and a ratio of 1.8 "Ms". As with the other unary and binary component

binder samples, when the ratio of "n" increased from 2 to 4, setting times increased for all ternary component samples. The change in the initial and final setting times of the samples according to the "n" ratio for both w/b ratios is shown in Figure 4.69 and Figure 4.70, respectively.

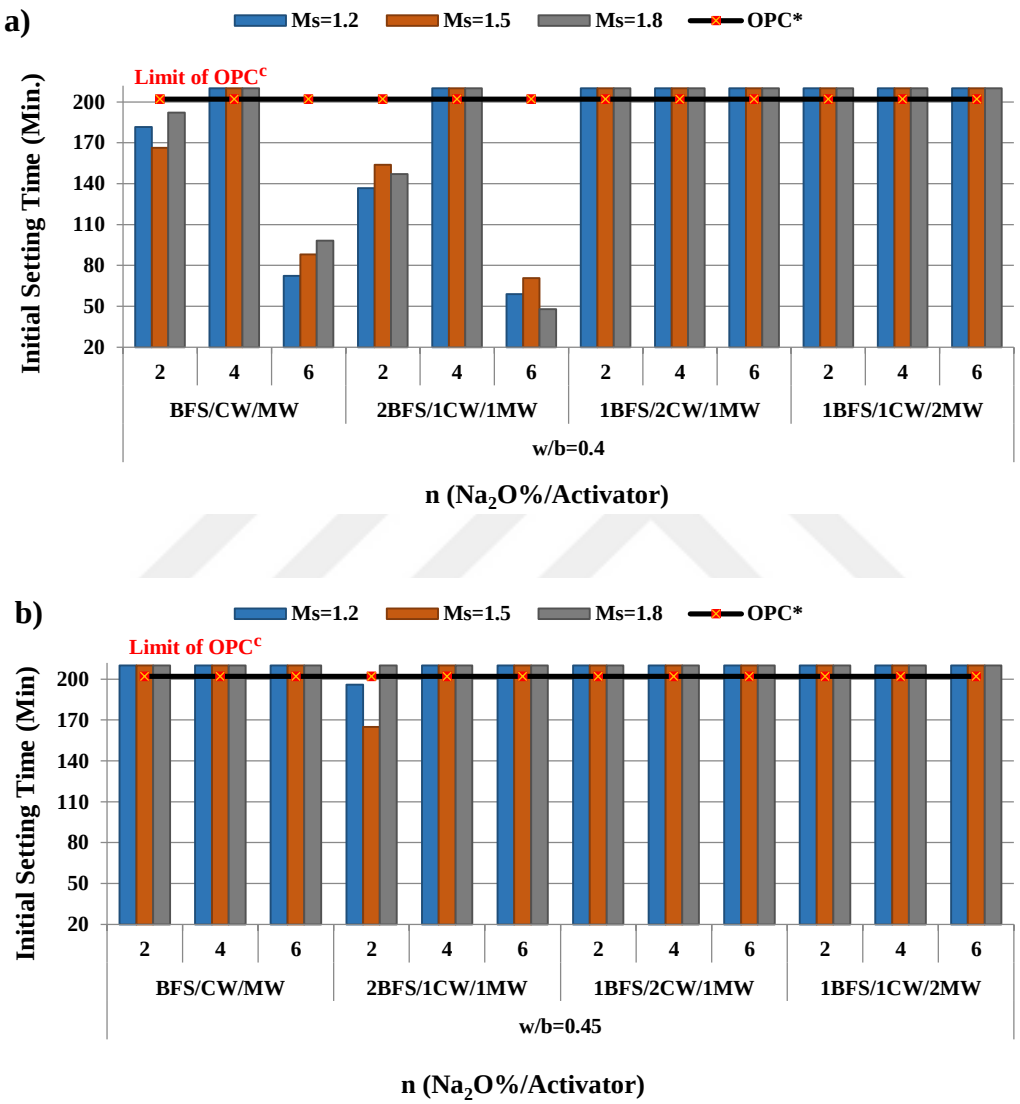


Figure 4.69. The initial setting time of BFS/CW/MW-TB samples according to "n" ratio a) for "w/b=0.4" b) for "w/b=0.45".

* The cement paste is formed only with water without using an alkaline activator.
[c] These limit values are defined in ASTM C 191-13 Standard.

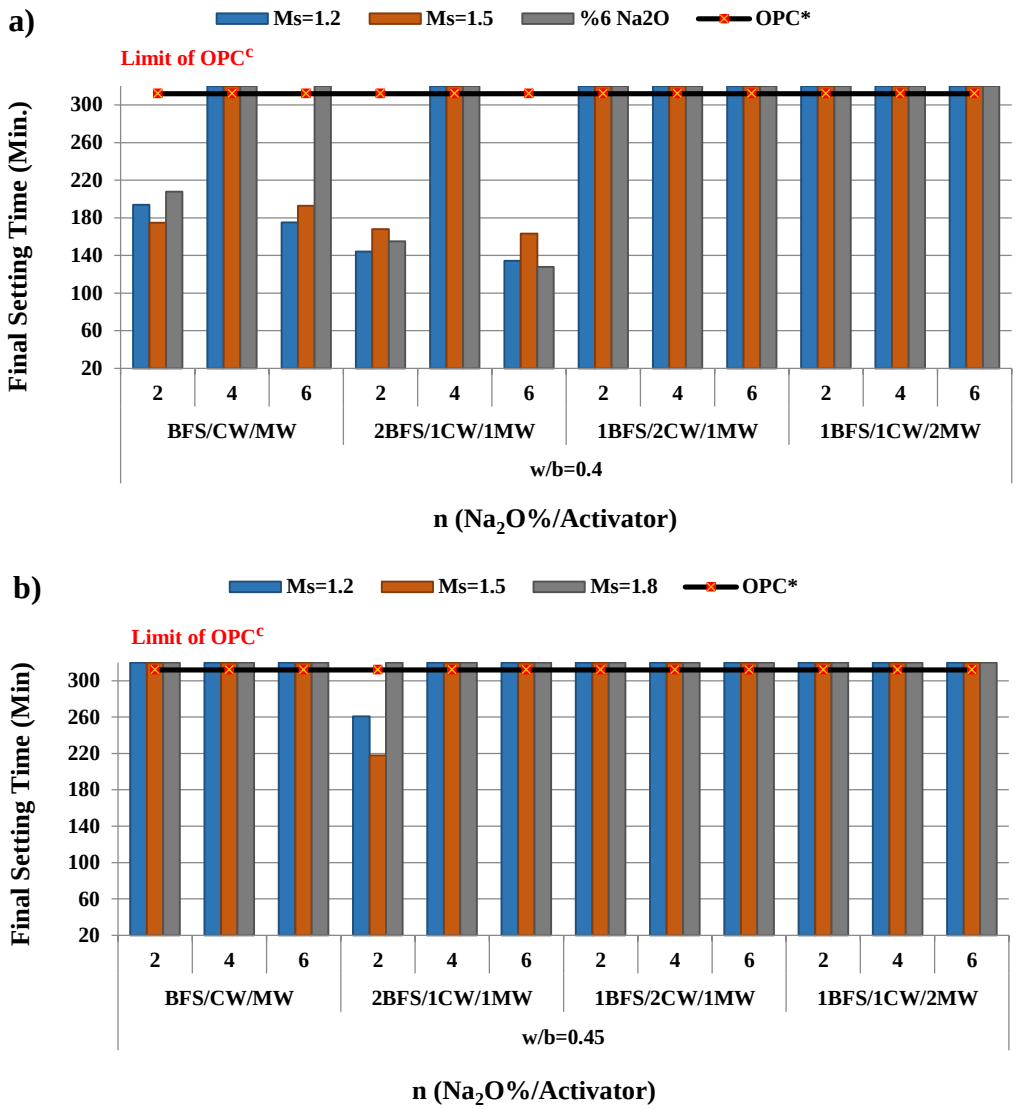


Figure 4.70. The final setting time of BFS/CW/MW-TB samples according to "n" ratio a) for "w/b=0.4" b) for "w/b=0.45".

* The cement paste is formed only with water without using an alkaline activator.
[c] These limit values are defined in ASTM C 191-13 Standard.

When the w/b ratio increased from 0.4 to 0.45, the flow diameter of the samples increased and their consistency became liquefied. For these ternary mixture samples, the flow diameter of the samples having a value of 0.4 w/b generally remained within the experimental lower and upper limits. In terms of workability, the 0.4 w/b ratio was determined as a more significant ratio for this mixture. Therefore, the effects of "n" and "Ms" ratios on the flow diameter were interpreted only for samples with a value a w/b value of 0.4.

When the ratio of "n" was equal to 4 for all ternary component samples, both the initial and final setting times were above the cement setting time limits. In these examples,

where the BFS was equal or higher by mass with CW and MW, when the rate of settings was 2 and 6, it is much lower than cement. As the CW and MW mass in the mixes increased, the setting time was prolonged and exceeded limits of the cement sample. The change in the initial and final setting times of the samples according to the "Ms" ratio for both w/b ratios was shown in Figure 4.71 and Figure 4.72, respectively. The change of "Ms" ratio in ternary component systems did not cause a general increase or decrease tendency in changing the setting time. For compositions where the BFS was equal to and greater than the other two components, less setting times were determined in sample with the highest and lowest activator dosage for all "Ms" values compared to the cement sample.

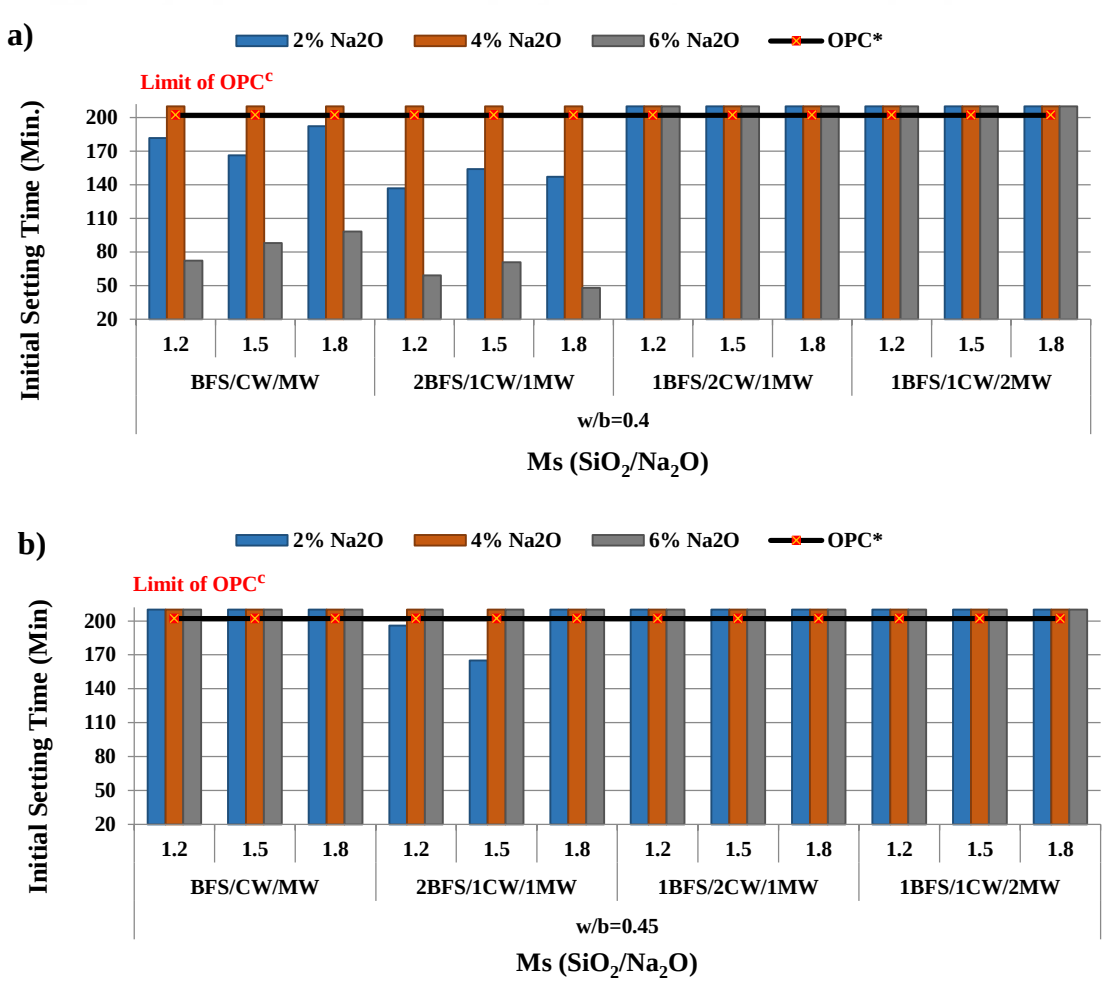


Figure 4.71. The initial setting time of BFS/CW/MW-TB samples according to "Ms" ratio a) for "w/b=0.4" b) for "w/b=0.45".

* The cement paste is formed only with water without using an alkaline activator.
[c] These limit values are defined in ASTM C 191-13 Standard.

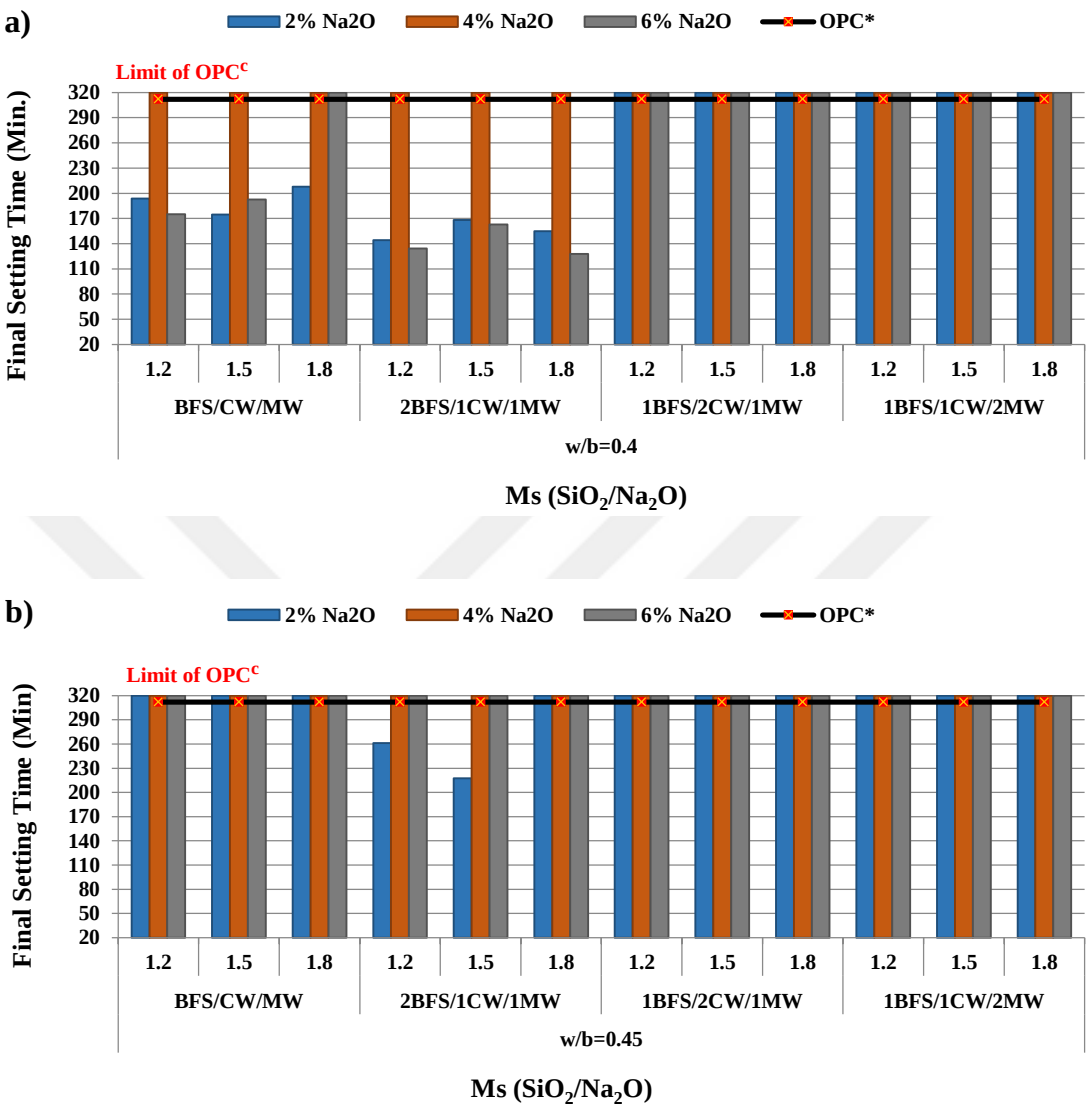


Figure 4.72. The final setting time of BFS/CW/MW-TB samples according to "Ms" ratio a) for "w/b=0.4" b) for "w/b=0.45".

* The cement paste is formed only with water without using an alkaline activator.
[c] These limit values are defined in ASTM C 191-13 Standard.

✓ *Workability Properties of BFS/CW/MW-TB*

Considering the workability properties in the ternary component alkaline activation system, as the substitution of BFS in this combination increased, both the flow diameter and setting time decreased. It was observed that the workability properties of the samples improved as the limestone powder with high CaO content such as marble waste percentage increased as reported in the literature [60]. This situation was similar to the

workability results in binary component systems. As the amount of CW increased in the ternary component system, the amount of BFS decreased at the same time and this combination had a much higher workability value than the BFS/CW-BB binary component system in terms of flow diameter and setting time, since it also contained marble waste. In this system, as the "n" ratio increased, there was a decrease in the workability properties as in the other systems, but no mixing and molding problems were observed for any sample.

4.3.1.2. Strength properties of BFS/CW/MW-TB samples

In this binary activated system consisting of a mixture of CW, MW and BFS, CW and MW have been replaced in BFS in 3 different masses. The selected flexural and compressive strength values BFS/CW/MW-TB systems for each mix proportion was shown in Figure 4.73. Accordingly, the selected flexural strength value among these samples achieved for the BFS/CW/MW/4/1.2/0.4/S composition, in which CW and MW were substituted in the BFS in a 1:1:1 ratio. The highest compressive strength value was also obtained for the 2BFS/1CW/1MW composition in which CW and MW were substituted in the BFS in a 2:1:1 ratio. Therefore, flexural and compressive strengths in ternary component systems evaluated over the combinations that gave the selected values among these samples.

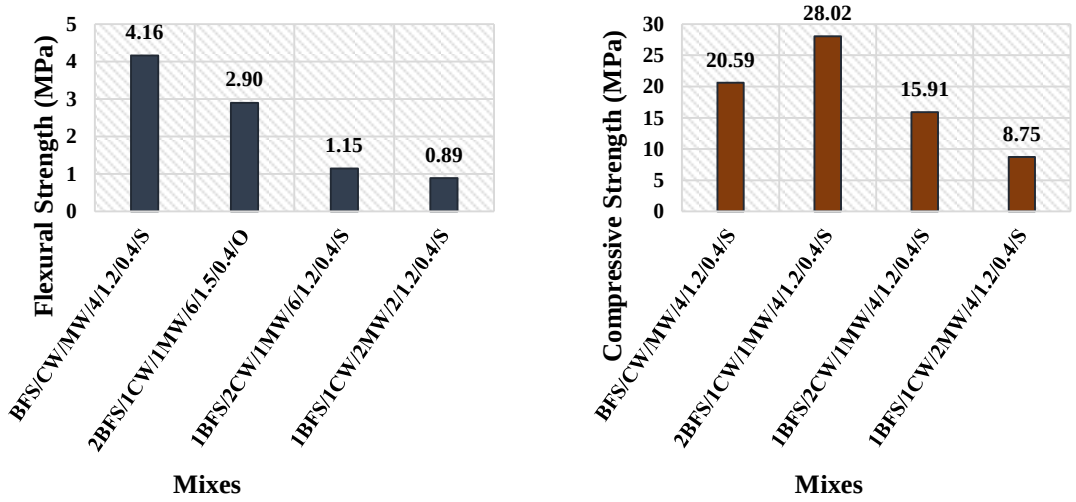
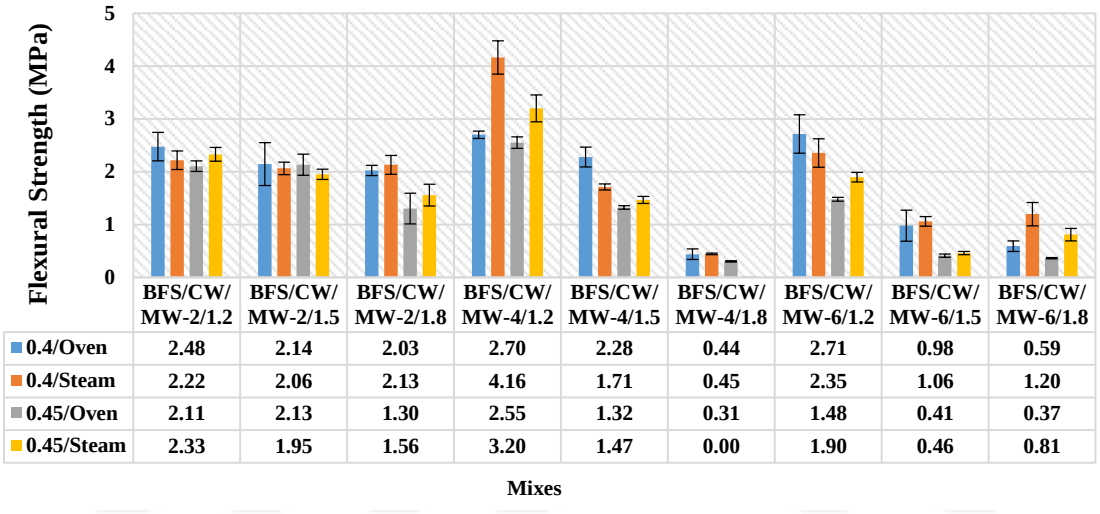


Figure 4.73. The selected flexural and compressive strength values among samples BFS/CW/MW-TB systems for each mix proportion.

✓ *Flexural Strength Test of BFS/CW/MW-TB*

The flexural strength values of the BFS/CW/MW-TB samples were given in Figure 4.74 for both w/b ratios (0.4 and 0.45) and for both curing conditions (oven and steam).

The highest flexural strength value for BFS/CW/MW-TB sample set was for the "BFS/CW/MW/4/1.2/0.4/Steam" sample. Thus, the highest flexural strength value was determined for w/b = 0.4 ratio and steam curing.



	BFS/CW/ MW-2/1.2	BFS/CW/ MW-2/1.5	BFS/CW/ MW-2/1.8	BFS/CW/ MW-4/1.2	BFS/CW/ MW-4/1.5	BFS/CW/ MW-4/1.8	BFS/CW/ MW-6/1.2	BFS/CW/ MW-6/1.5	BFS/CW/ MW-6/1.8
0.4/Oven	2.48	2.14	2.03	2.70	2.28	0.44	2.71	0.98	0.59
0.4/Steam	2.22	2.06	2.13	4.16	1.71	0.45	2.35	1.06	1.20
0.45/Oven	2.11	2.13	1.30	2.55	1.32	0.31	1.48	0.41	0.37
0.45/Steam	2.33	1.95	1.56	3.20	1.47	0.00	1.90	0.46	0.81

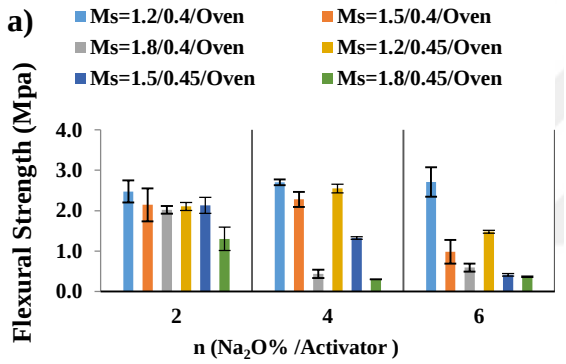
Figure 4.74. Flexural strength of BFS/CW/MW-TB samples.

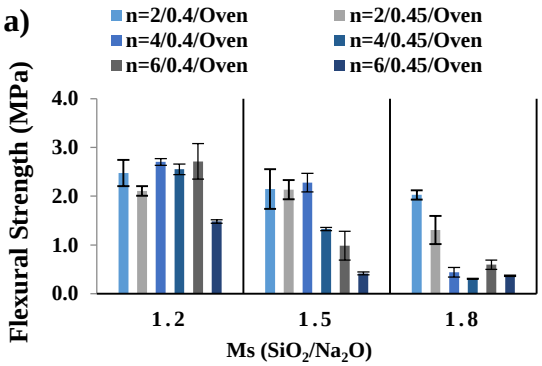
In this test set, when the w/b ratio increased from 0.40 to 0.45, there was tendency for the flexural strength value to decrease for more samples in general. The highest flexural strength value obtained for this test set was approximately 25% lower than the highest flexural strength value obtained for the BFS/CW-BB binary test set. Therefore, it can be said that marble waste addition negatively affects the flexural strength.

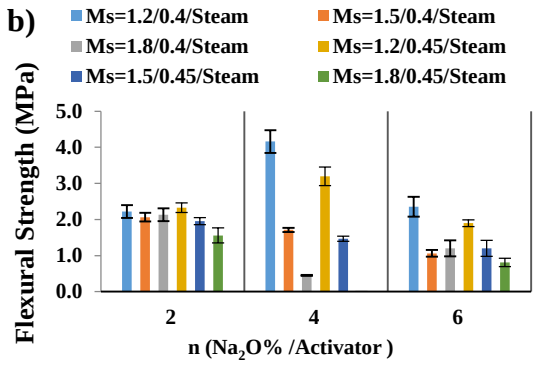
The variation of flexural strength values of BFS/CW/MW-TB samples according to "n" ratio was given in Figure 4.75 for two different curing conditions. For samples with low activator dosage (n=2), it was determined that most of the samples had much higher flexural strength values than the samples that contain moderate and high activator dosage (n=4 and n=6) for oven cure conditions. However, the samples with moderate activator dosage for both w/b ratios had the highest flexural strength value, especially in samples with low "Ms" value for steam curing.

The changes in flexural strength values of BFS/CW/MW-TB samples according to the "Ms" ratio are given in Figure 4.76 for two different curing conditions. The selected flexural strength value for this curing condition was formed for "Ms" value of 1.2 Especially, increasing the ratio of Ms for the oven cure decreased the flexural strength value. For the steam cure, the lowest flexural strength values were obtained for the highest Ms value (Ms=1.8).

As a result, it was found that the selected flexural strength for this system has been achieved for the sample with the highest activator dosage (n=4), "Ms" value of 1.2 and steam cured for BFS/CW/MW-TB samples. Additionally, the low "Ms" values and low and medium level "n" ratios for this ternary component series gave much higher results in terms of flexural strength.







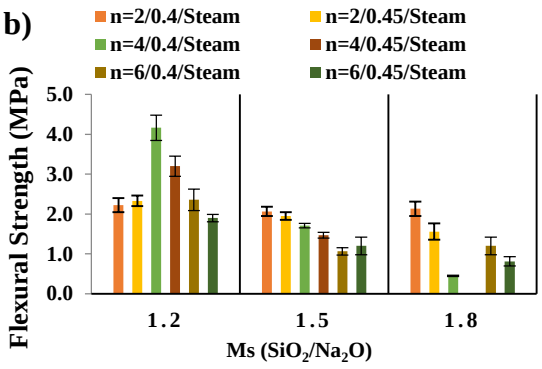


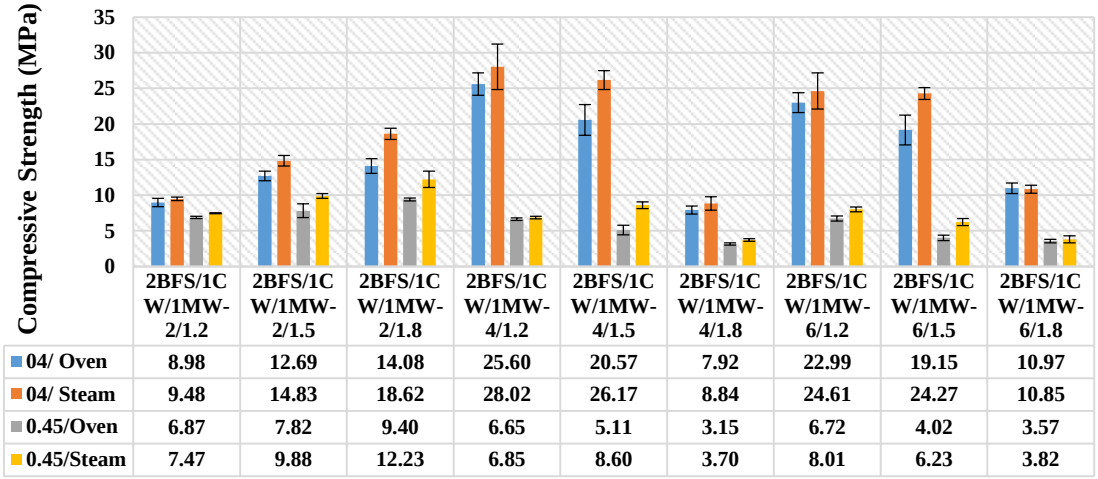
Figure 4.75. Change in flexural strength of BFS/CW/MW-TB paste according to "n" ratio a) For oven cure b) For steam cure.

Figure 4.76. Change in flexural strength of BFS/CW/MW-TB paste according to "M_s" ratio a) For oven cure b) For steam cure.

✓ *Compressive Strength Test of BFS/CW/MW-TB*

The compressive strength values of BFS/CW/MW-TB samples were given in Figure 4.77 for both w/b ratios (0.4 and 0.45) and both curing conditions (oven and steam).

The highest compressive strength value for BFS/CW/MW-TB sample set was for the "3BFS/1CW-BB/6/1.5/0.4/Steam" sample. Thus, the highest compressive strength value was determined for w/b = 0.4 ratio and steam curing. When the w/b ratio increased from 0.40 to 0.45, the compressive strength values of the samples generally decreased for both curing conditions. It was determined that the steam cured samples reached higher compressive strength values than the oven cured for both w/b ratios. It was found that substitution of CW in BFS improved the compressive strength values obtained for alkaline activation of both BFS-UB and CW-UB. It can be said that the compressive strength value increased as the activator dosage increased for samples that have been cured to a steam curing ratio of 0.4 w/b.



	2BFS/1CW/1MW-2/1.2	2BFS/1CW/1MW-2/1.5	2BFS/1CW/1MW-2/1.8	2BFS/1CW/1MW-4/1.2	2BFS/1CW/1MW-4/1.5	2BFS/1CW/1MW-4/1.8	2BFS/1CW/1MW-6/1.2	2BFS/1CW/1MW-6/1.5	2BFS/1CW/1MW-6/1.8
04/ Oven	8.98	12.69	14.08	25.60	20.57	7.92	22.99	19.15	10.97
04/ Steam	9.48	14.83	18.62	28.02	26.17	8.84	24.61	24.27	10.85
0.45/Oven	6.87	7.82	9.40	6.65	5.11	3.15	6.72	4.02	3.57
0.45/Steam	7.47	9.88	12.23	6.85	8.60	3.70	8.01	6.23	3.82

Figure 4.77. Compressive strength of 2BFS/1CW/1MW-TB samples

The variation of compressive strength values of 2BFS/1CW/1MW-TB samples according to "n" ratio is given in Figure 4.78 for two different curing conditions. For this ternary set of experiments, the increase in w/b ratio from 0.4 to 0.45 decreased the compressive strength values of the samples in both curing conditions. For samples with a w/b value of 0.4, when the value of "n" ratio increased from 2 to 4, the compressive strength values increased, but when the ratio "n" ratio increased to 6, the compressive strength decreased.

The variation of compressive strength values of 2BFS/1CW/1MW-TB samples according to "Ms" ratio is given in Figure 4.79 for two different curing conditions. Especially for samples containing medium and high activator dosage (n=4 and n=6), the increase in "Ms" ratio decreased the compressive strength values of the samples. For both curing conditions, the highest compressive strength value was realized for the ratio where the value of "Ms" was 1.2 for w/b of 0.4.

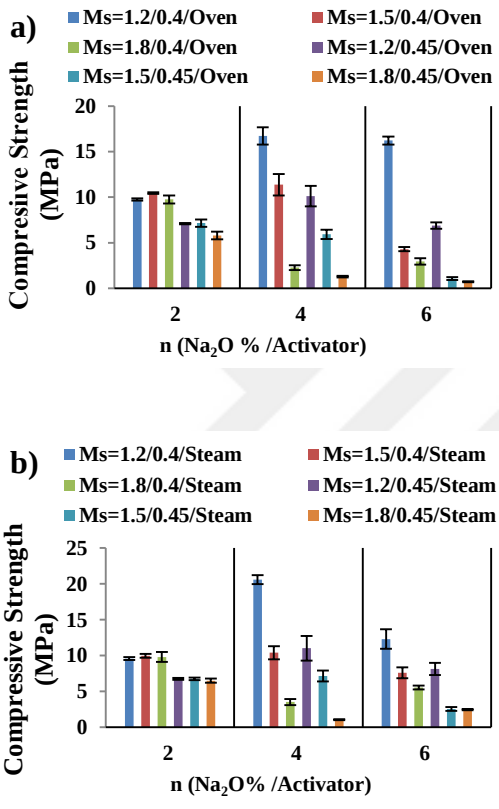


Figure 4.78. Change in compressive strength of 2BFS/1CW/1MW-TB according to "n" ratio a) For oven cure b) For steam cure.

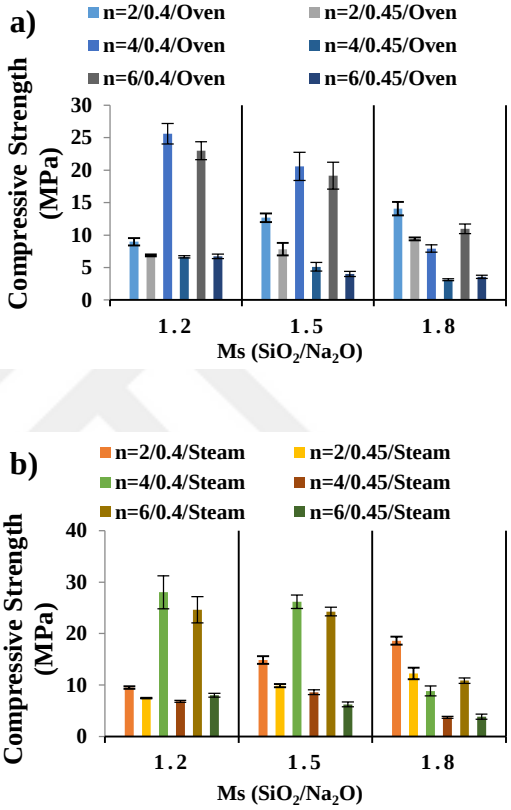


Figure 4.79. Change in compressive strength of 2BFS/1CW/1MW-TB according to "M_s" ratio a) For oven cure b) For steam cure.

✓ *Strength Properties of BFS/CW/MW-TB*

Considering the flexural strength values obtained for the ternary component system, the highest flexural strength was realized for the BFS/CW/MW-TB combination. In this combination, all components were present in equal proportions by mass. In fact, the highest flexural strength was determined for the BFS/CW/MW-TB combination after 90 days among all unary, binary and ternary component alkali activation systems applied

within the scope of this study (see Fourth Stage). When the microstructural examinations were performed in the following sections (sixth stage), a new crystal phase formed by these ternary component samples was not formed as like the binary component samples. A similar situation occurred for the example of 2BFS/ 1CW/ MW-TB, which was a ternary component joint with the highest compressive strength. In previous studies, it was stated that binary [21, 65, 111] or ternary [60, 74, 112] raw materials with high CaO and SiO_2 ratios showed much better strength and durability properties in alkali activated systems compared to single component systems. Therefore, in this ternary component mixture type carried out in this study. These three source materials such as BFS and MW with high CaO ratio with and CW with a high SiO_2 ratio improved the strength and durability properties of the hybrid mixture.

4.4. Determination of the Selected Samples in The First Three Stages

In the first three sections, a series of experiments were carried out to determine the processability properties, optimum activator combination rates ("n" and "Ms" ratio), water/binder ratio and the selected curing condition of unary, binary and ternary component for alkali-activated samples. As a result of these experiments, combinations that give the highest compressive and flexural strength values were selected for unary, binary and ternary component alkaline activation samples. These selected combinations were given in Table 4.21.

Table 4.21. Optimum combinations of the selected mixtures in the first three parts for mechanical properties

		The Selected Mıxtures			
		For Flexural Strength	**MPa**	**For Compressive Strength**	**MPa**
Unary Binders	**BFS**	BFS/4/1.5/0.4/S	3.36	BFS/6/1.5/0.4/S	40.53
	CW	CW/6/1.2/0.4/S*	1.37	CW/6/1.2/0.4/S	3.76
	MW	MW/4/1.8/0.4/S*	0,91	MW/4/1.8/0.4/S	1.56
Binary Binders	**BFS-CW**	2BFS/2CW/6/1.5/0.4/S	5.44	3BFS/1CW/6/1.5/0.4/S	55.63
	BFS-MW	2BFS/2MW/4/1.2/0.4/S	4.13	2BFS/2MW/6/1.2/0.4/S	50.93
	CW-MW	2CW/2MW/2/1.2/0.4/S*	0.97	2CW/2MW/2/1.2/0.4/S	2.90
Ternary Binders	**BFS/CW/MW**	BFS/CW/MW/4/1.2/0.4/S	4.16	2BFS/1CW/1MW/4/1.2/0.4/S	28.02

* In these examples, the same compositions were determined as the selected example for both flexural and compressive strength.

The abbreviations system of sample code for all samples showed in Figure 4.80.



Figure 4.80. Codes of samples.

As seen in Table 4.21, for all samples, 0.4 water/binder ratio and steam cure were determined as two of the experimental criteria giving the highest flexural and compressive strength. In terms of flexural and compressive strength, a total of 14 samples were determined in Table 4.21. However, since three (3) of these samples were determined with the same content in terms of both strengths, 11 binder samples with a total content were determined. After this stage, the experiments carried out in the four, five and six parts of the thesis were carried out on these selected examples identified in the first three stages. Ms value of 1.2 or 1.5 was found be optimum for most of the samples in terms of mechanical properties.

4.5. Fourth Stage-Determination of the Mechanical Properties of the Selected (Optimum) Binders

At this stage, determination of some physical and mechanical properties of the selected samples obtained for all binder types was carried out. For this purpose, curing period of 1, 7, 14, 28, 56 and 90 days were applied and then flexural and compressive strength tests were carried out to determine the early and late curing strength values of the samples. In order to determine the physical properties, a series of experiments including the determination of "dry and bulk density", "absorption (after immersion and boiling)", "volume of permeable pore space (voids)" and "water absorption" features were carried out.

4.5.1. Flexural and compressive strength of the selected binders among samples

In order to determine the selected flexural strength values of samples after 1, 7, 14, 28, 56 and 90 days curing period Figure 4.81 can be considered. As seen in the Figure 4.81,

the flexural strength value of the reference cement sample was higher than the flexural strength values of other samples for all test days. But for late curing times, the difference between the alkali solution activated samples and the flexural strength values of the cement sample had decreased much more than the early curing times.

Flexural strength values of all samples increased with curing time. When the flexural strength values of the samples were compared each other, it was determined that the ternary component alkaline solution activated "BFS/CW/MW/4/1.2/0.4/S" sample had the highest flexural strength value. In addition, the late or extended curing time strength values of these ternary component samples, especially on the 56th and 90th days, increased significantly compared to the early curing time strength values. The flexural strength increment rate of the ternary component BFS/CW/MW/4/1.2/0.4/S sample with the highest flexural strength value between days 56 and 90 was approximately 28%. This rate was very low for the cement sample as 0.6%. Therefore, it has been determined that the increase in late strength values for the ternary component BFS/CW/MW/4/1.2/0.4/S sample was much higher than the reference cement sample.

There was a rapid increase in flexural strength values between 57th and 90th days for the sample "2BFS/1CW/1MW/4/1.2/0.4/S", which was another ternary component sample.

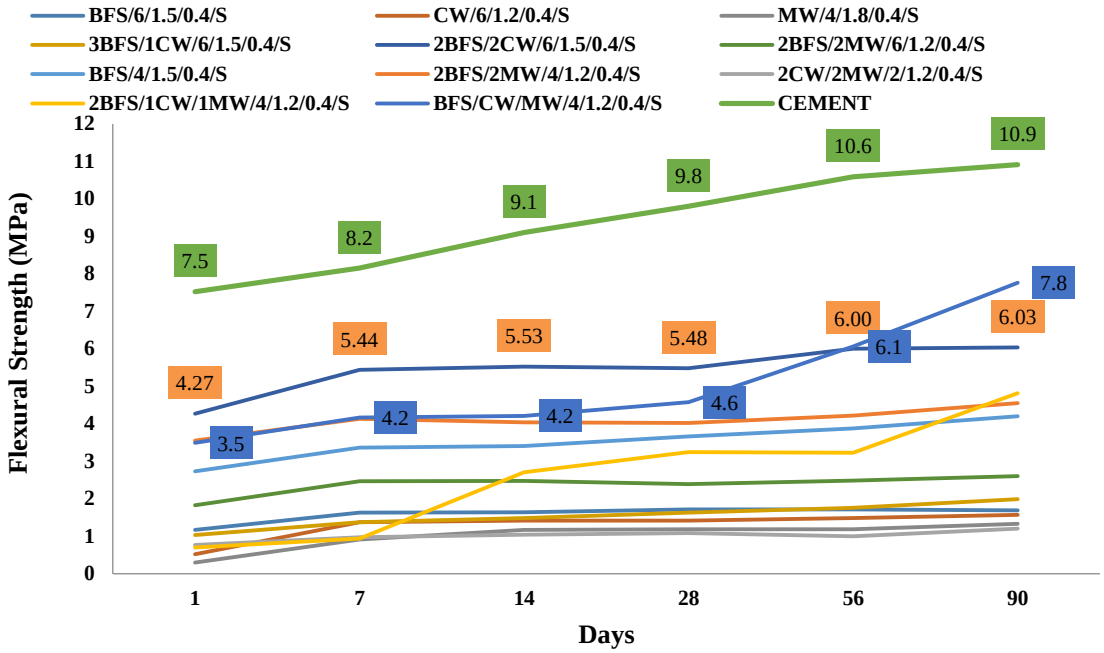


Figure 4.81. Flexural strength variation as a function of curing period.

Compressive strength values (after curing for 1, 7, 14, 28, 56 and 90 days) of the selected samples were given in Figure 4.82. As seen in the Figure 4.82, the compressive strength value of the cement sample is higher than the compressive strength values of the other alkaline solution activated samples for all test days. However, for extended curing times such as for 56 and 90 days, the difference between the alkali solution activated samples and the compressive strength values of the cement sample has almost closed compared to the early curing times.

When the compressive strength values of the samples were compared, it was observed that the one-component alkali activation sample of the blast furnace slag (BFS/ 6/1.5/0.4/S) almost reached the compressive strength value of the cement after 90 days of curing period. Compressive strength values of all samples increased in time.

In terms of compressive strength and flexural strength strengths, it would be useful to evaluate the early and late cured sample's strength values of unary, binary and ternary component samples among themselves. In Figure 4.83, early and late curing time strength properties of unary component samples were compared. According to this graph, it was found that the samples obtained as a result of the unary component alkali activation of CW and MW have lower strength values compared to the unary component samples of BFS in terms of both flexural and compressive strength.

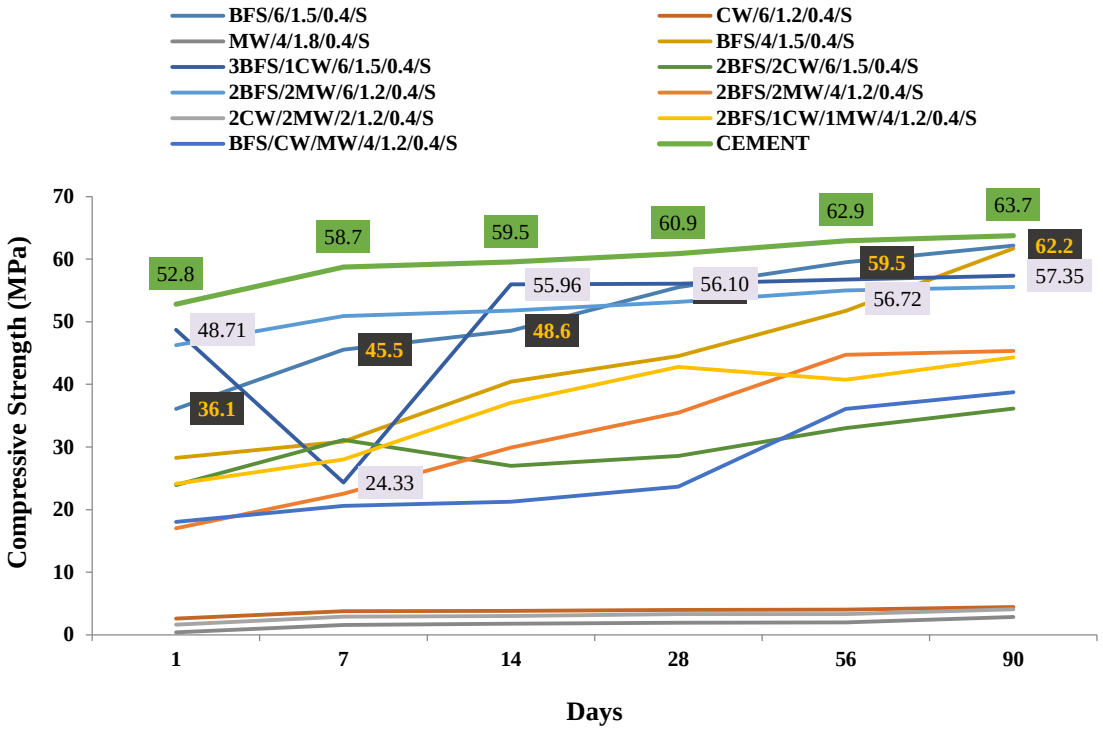


Figure 4.82. Compressive strength variation as a function of curing period.

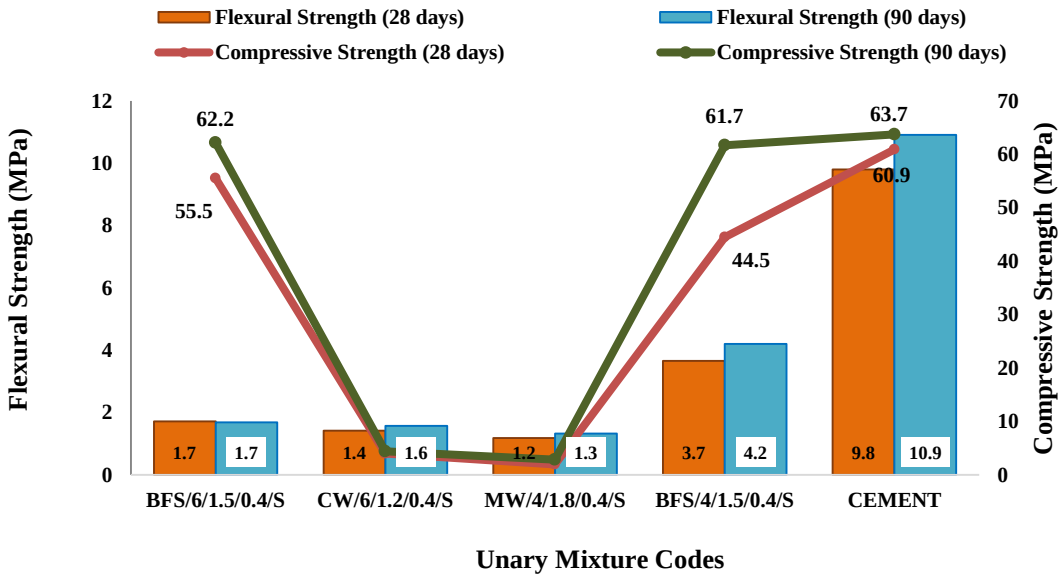


Figure 4.83. The effect of early and late curing on flexural and compressive strengths of the selected unary mixtures.

It was understood that for BFS-UB, while “n” value was 4, it had higher flexural strength than BFS-UB samples with other “n” ratios. It has also been determined that the increase in the compressive strength value of this sample over time was much higher than that of all other unary component samples. The 90-day compressive strength results of BFS were almost equal to cement. For the BFS with an "n" value of 6, the flexural strength value decreased over time, while the compressive strength value increased less than the BFS with n value of 4.

In Figure 4.84, early and late curing time strength properties of binary component samples were compared. According to this graph, the binary mixture, which gave the selected results in terms of flexural strength, was a sample of "2BFS/2CW/6/1.5/0.4/S" containing BFS and CW equal to mass. It was determined that CW increased the flexural strength of BFS more than three times compared to BFS-UB sample with same “n”, “Ms” and w/b values. Also, while the same experimental parameters were constant, the replacement of CW in the BFS by 1 in 3 by mass reduced the compressive strength value of the BFS-UB by only about 8%. Accordingly, when CW is substituted up to 50% in BFS, it was increased the flexural strength value by 3 times compared to the flexural strength of the BFS-UB sample.

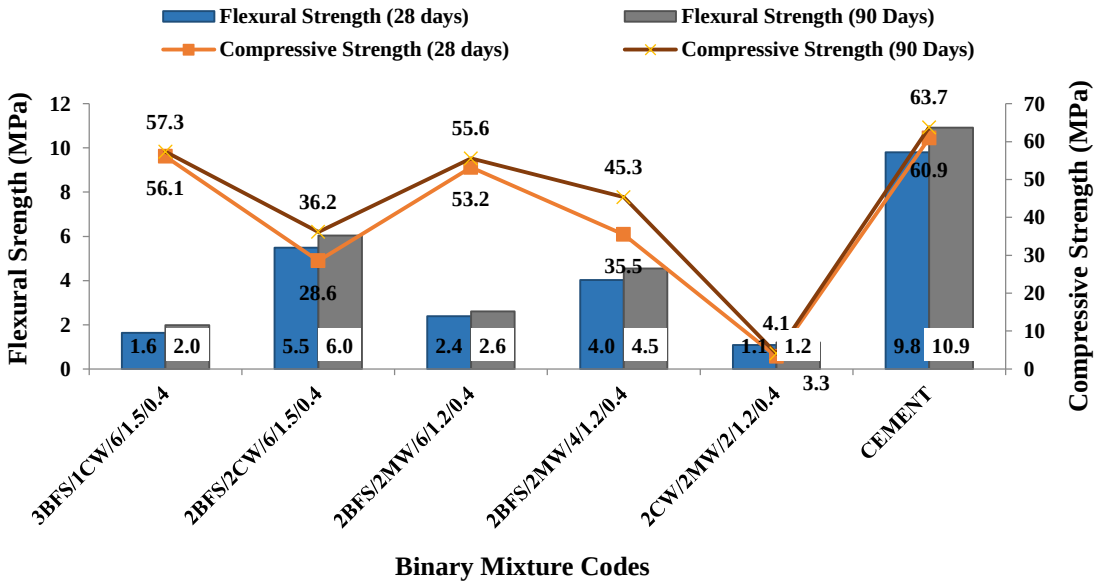


Figure 4.84. The effect of early and late curing on flexural and compressive strengths of the selected binary mixtures.

In binary component samples in which MW and BFS were mixed in equal proportions, for the same “n” value (n=4), the flexural strength increased slightly compared to the BFS-UB. On the other hand, the compressive strength value decreased by 15% for the same “n” ratio (n=6) compared to the BFS-UB. The highest flexural and compressive strength results for MW samples were realized for the smallest “Ms” value (Ms=1.2) within the scope of the study. It was shown that, just like in the CW containing sample, when MW is substituted up to 50% in BFS, the flexural strength value was increased compared to the flexural strength of the BFS-UB sample.

Consequently, it was determined that binary component mixture samples consisting of CW and MW had higher flexural and compressive strength values when compared to unary component samples of MW and slightly lower than unary component samples of CW. Binary component mixture samples formed by CW and MW were the lowest samples of the binary component alkali activated series in terms of strength values.

In Figure 4.85, strength properties of ternary component samples at early and late curing time were compared. In ternary component binder systems, the highest strength values were achieved for the medium level activator dosage (n=4). The flexural strength of the ternary component alkali activated samples increased compared to the flexural strength values of the binary component samples. Thus, the highest compressive strength value of all samples was realized for the BFS/CW/MW/4/1.2/0.4/S (90 days) sample. The compressive strength values of these samples decreased compared to the selected binary component samples of BFS and MW. When the binary and ternary component samples were compared, as the replacement percentage of CW increased in the sample, more loss of strength was observed compared to the replacement percentage of MW in the sample.

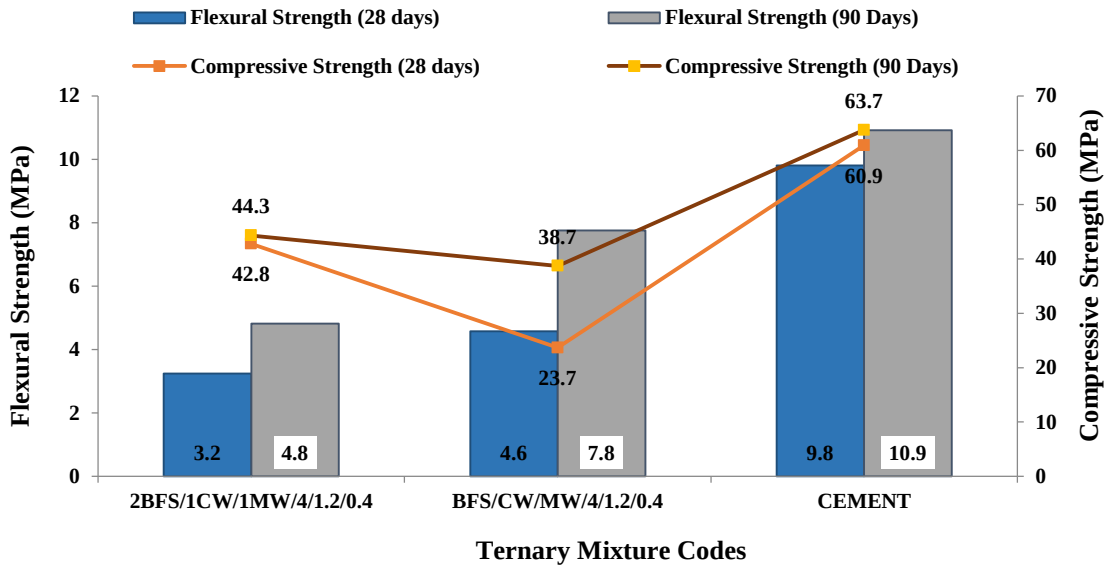


Figure 4.85. The effect of early and late curing on flexural and compressive strengths of the selected ternary mixtures.

As a result, samples formed by CW-UB and MW-UB had much lower strength properties compared to the strength properties of BFS-UB and cement paste samples. However, the significant impact of that these two industrial wastes (CW and MW) which was replaced high amounts (up to 50%) in the BFS while improving the flexural strength feature of the slag, caused a slight decrease in compressive strength.

By mixing the samples where the BFS was replaced individually and with CW or MW, higher flexural strength results were obtained for the medium level activator dosage (n=4). But when the activator dosage was increased to (n=6), the compressive strength was increased up to the highest values. However, high activator dosage (high "n" ratio) negatively affected the workability properties of the samples.

4.5.2. Dry bulk density, apparent density and volume of voids (permeable pore space) measurement results

In the context of this part, dry bulk density, apparent density and volume of permeable pore space (voids) parameters were measured on the selected samples selected as unary, binary and ternary components in the first three parts. All experiments were carried out on samples that were cured for 28 days. Experimental results of the selected samples

(dry bulk density, apparent density and volume of permeable pore space values) compared with the results of in Table 4.22 and Figure 4.86.

As can be seen in Figure 4.86, no results were obtained for MW/4/1.8/0.4 sample in this test system. Because, during the density test measurement the samples dissolved in water in soaking step of the test. Therefore, it was not possible to determine these parameters for the MW-UB sample.

Apparent density values of all samples vary between 2.25 and 2.49 g/cm^3 whereas bulk density values were observed to vary between 1.3 and 1.73 g/cm^3. The combination with the largest ratio of voids was obtained for the 2CW/2MW/2/1.2/0.4 sample, while the lowest percentage of voids was obtained for the BFS/4/1.5/0.4 sample. In order to better analyze the effects of raw material types and alkali activator ratios on the physical properties in this test system, the results were plotted separately for unary, binary and ternary component samples.

Table 4.22. Dry bulk density, apparent density and volume of voids of selected sample.

NO	MIXTURE CODES	Bulk density, dry	Apparent density	Volume of permeable pore space (Voids), %
1	BFS/6/1.5/0.4	1.68	2.32	27.6
2	CW/6/1.2/0.4	1.33	2.46	45.8
3	MW/4/1.8/0.4	0.00	0.00	0.0
4	2BFS/2MW/6/1.2/0.4	1.61	2.28	29.2
5	3BFS/1CW/6/1.5/0.4	1.62	2.30	29.4
6	2CW/2MW/2/1.2/0.4	1.30	2.49	47.8
7	2BFS/1CW/1MW/4/1.2/0.4	1.58	2.36	33.0
8	P/BFS/4/1.5/0.4	1.73	2.32	25.6
9	2BFS/2MW/4/1.2/0.4	1.58	2.25	29.6
10	2BFS/2CW/6/1.5/0.4	1.53	2.30	33.3
11	BFS/CW/MW/4/1.2/0.4	1.50	2.34	35.6
12	CEMENT	1.62	2.46	34.4

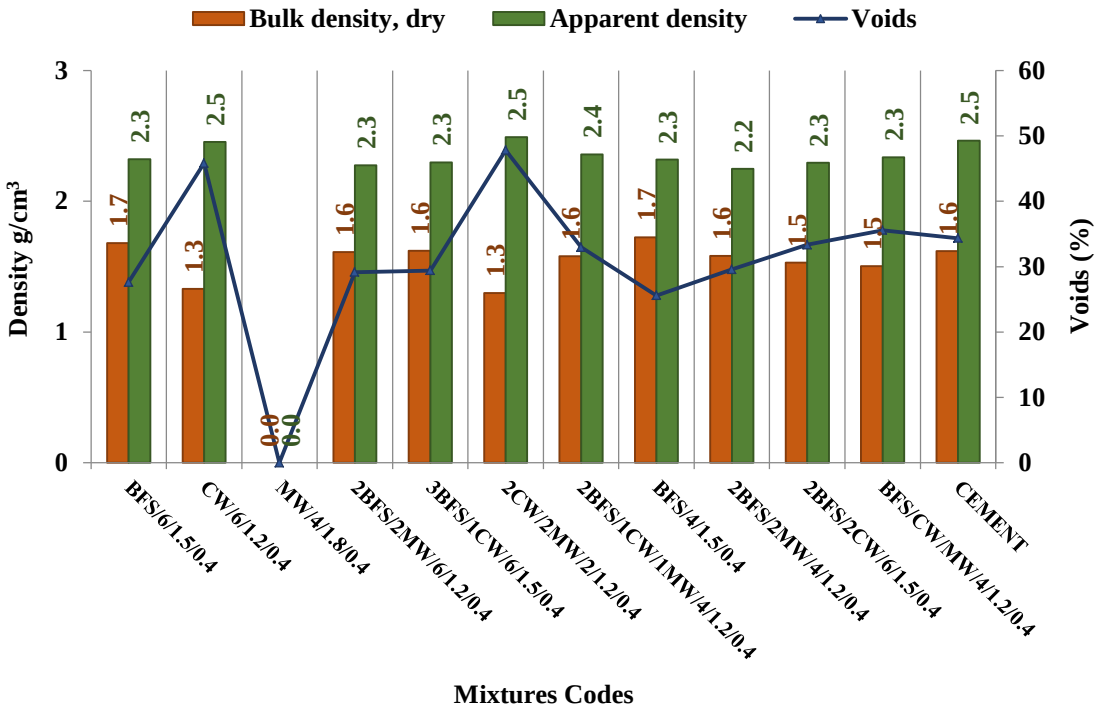


Figure 4.86. Bulk, apparent densities and voids results of the all selected samples.

Apparent density and voids results for selected unary samples were shown in Figure 4.87.

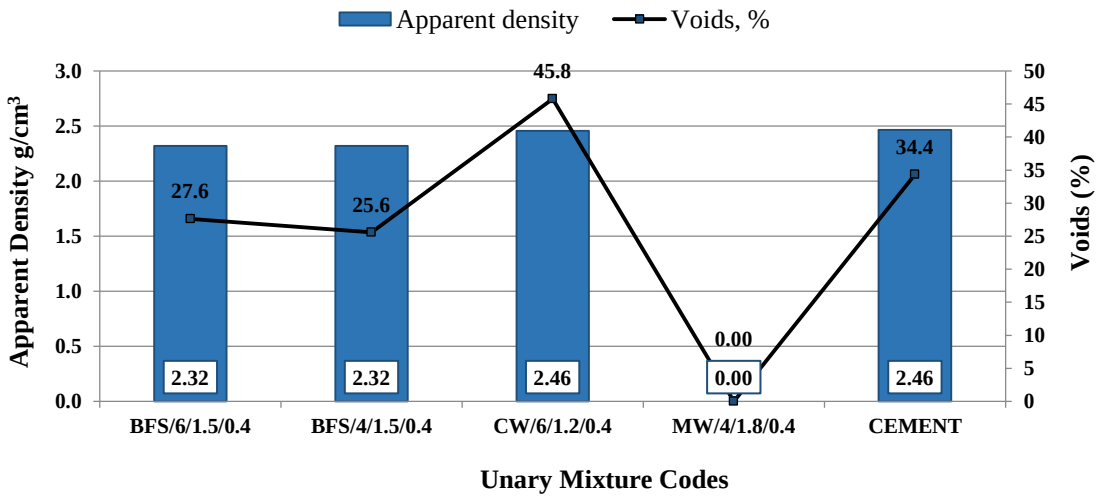


Figure 4.87. Apparent density and voids results of selected unary samples.

According to Figure 4.87, CW-UB and cement sample's apparent density values were the same. However, it was determined that the CW-UB had a 33% more void structure

than the cement in terms of the vacancy rate they contain. The density results were found for BFS-UB are lower than the cement and CW-UB sample. However, BFS-UB samples were found to have a much lower void ratio than both cement and CW-UB samples. The highest void ratio was determined for the CW-UB sample.

CW-UB sample, which has the highest void ratio among single component samples, had a much lower strength compared to other samples. The low void percentage for BFS-UB samples can also be explained by its better properties in terms of durability compared to cement.

Apparent density and voids results for binary component samples were shown in Figure 4.88. For binary component samples, density and voids percentages were lower than cement for all alkali activated samples except only 2CW/2MW/2/1.2/0.4 sample. CW and MW substitution in BFS decreased density values compared to BFS-UB sample. CW and MW substitution in BFS increased the void percentage of the binary component samples compared to the BFS-UB sample. However, CW substitution increased the void percentage of BFS more than MW substitution.

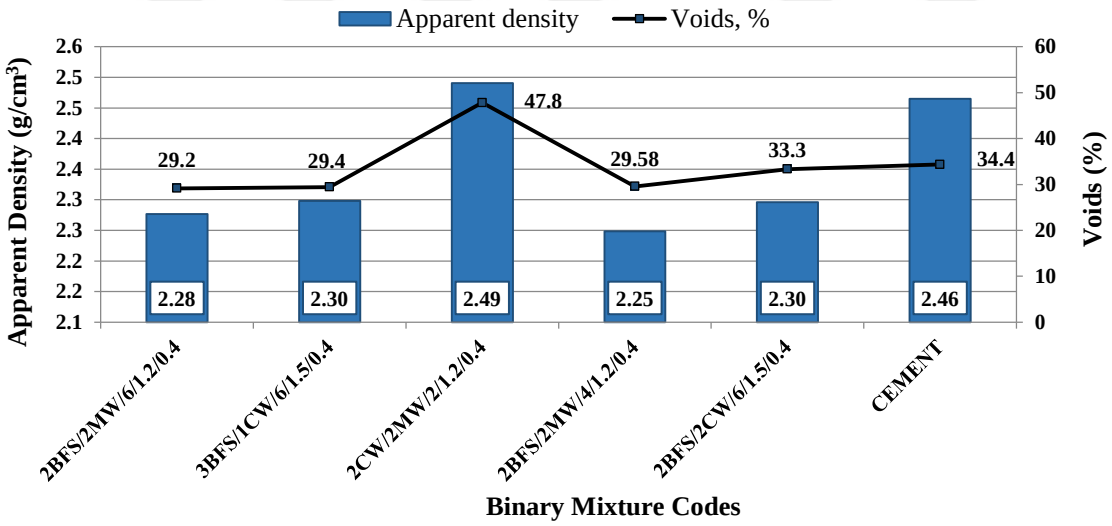


Figure 4.88. Apparent density and voids results of the selected binary mixtures.

Considering the void ratios of BFS-BB, BFS/CW-BB and BFS/MW-BB samples which exhibited lower void ratios than the cement sample, which suggest that these components showed superior properties in terms of durability.

Apparent density and void ratio results of the ternary component samples were shown in Figure 4.89. According to this Figure 4.89, it was found that as the total "CW+MW" ratio in the BFS increased, the percentage of void of ternary samples increased (these void ratios were exceeded the cement sample's). As a result, it was determined that the percentage of voids and apparent density in the ternary component mixtures in which CW and MW waste substitution was performed together in BFS, had greater voids and apparent density ratios than the binary component samples in which CW and MW wastes were substituted uniquely in the BFS.

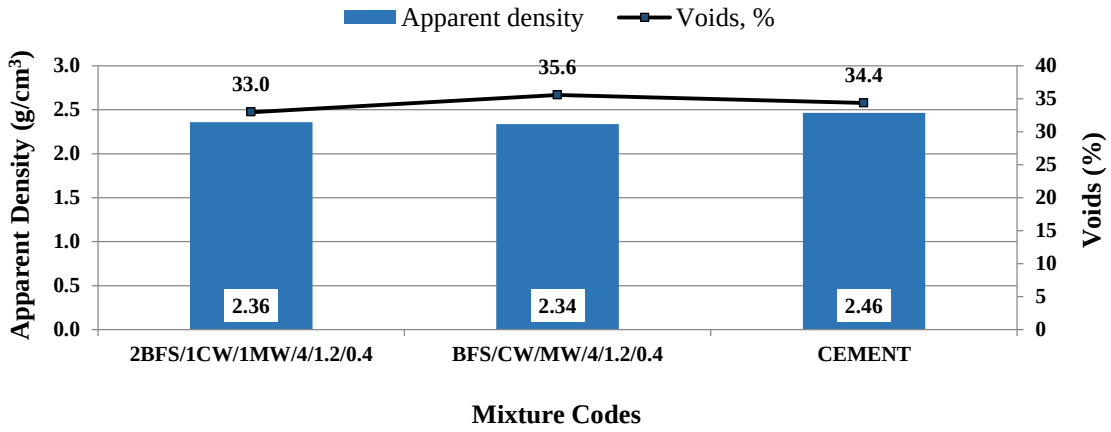


Figure 4.89. Apparent density and voids of the selected ternary mixtures.

4.2.3. Determination of the selected samples for the rate of water absorption

In Figure 4.90, water absorption measurement results (for 15 min, 1 h, 4 h and 24 h) were given for unary, binary and ternary component samples.

According to these results, the sample coded MW-UB was disintegrated after some hour and therefore no water absorption result was obtained for 24 hours. At the end of 24 hours, it was determined that CW-UB had the highest water absorption value. Similarly, it was observed that the water absorption value of the CW/MW-BB sample, in which CW and MW were added in equal proportions, was very high. But, it was observed that the water absorption values at the end of 24 hours for all other samples were much lower than the cement sample.

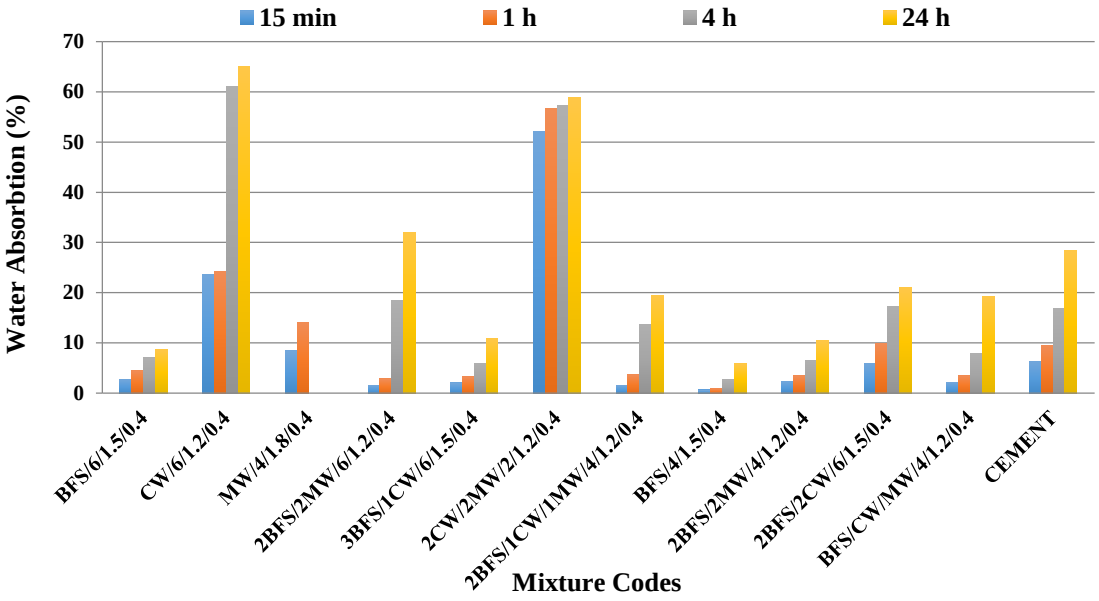
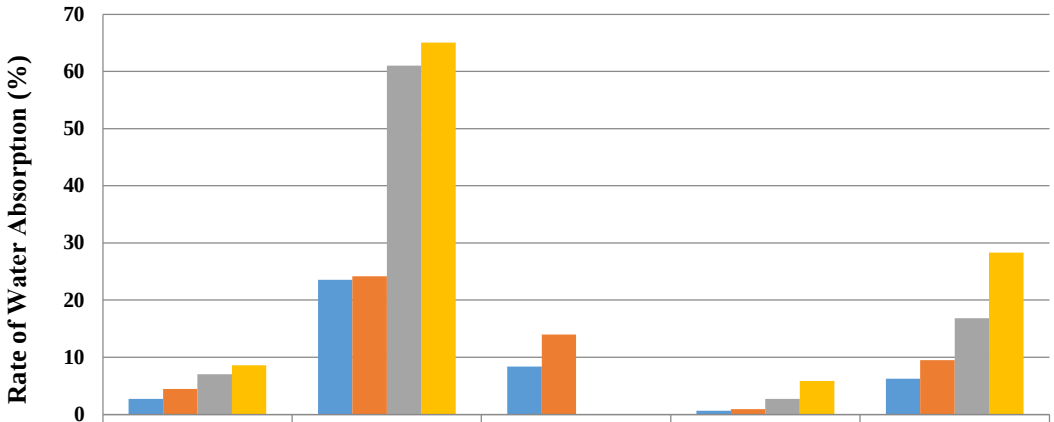


Figure 4.90. Comparison of the rate of water absorption for all the selected samples.

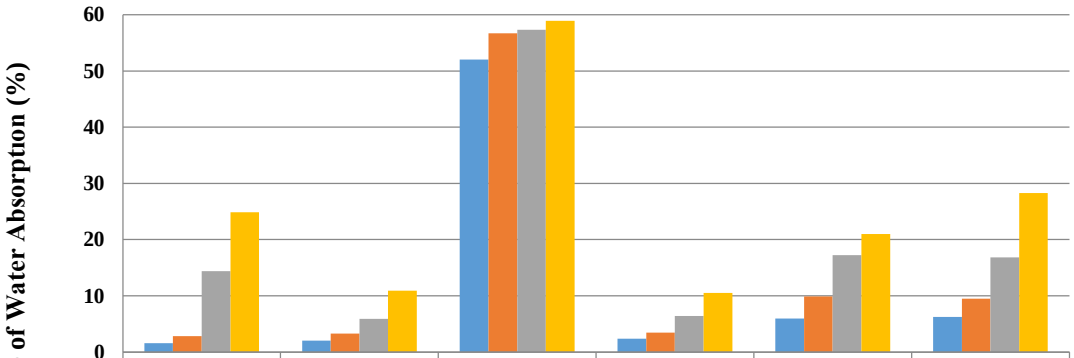
Water absorption rates of unary component samples were given in Figure 4.91. Accordingly, BFS-UB had the lowest water absorption values. Considering the water absorption rates at the end of 24 hours, for the BFS-UB sample with medium activator dosage (n=4), 45% less water absorption value was obtained compared to the BFS-UB with high activator dosage (n=6). At the end of 24 hours, water absorption rates of CW-UB were 2-3 times higher than cement's water absorption rate and 8-10 times higher than the water absorption rate of BFS-UB.



	BFS/6/1.5/0.4	CW/6/1.2/0.4	MW/4/1.8/0.4	BFS/4/1.5/0.4	CEMENT
15 min	2.7	23.6	8.4	0.6	6.2
1 h	4.5	24.2	14.0	0.9	9.5
4 h	7.0	61.0	0.0	2.7	16.8
24 h	8.6	65.1	0.0	5.9	28.3

Figure 4.91. Comparison of the rate of water absorption of the selected unary samples.

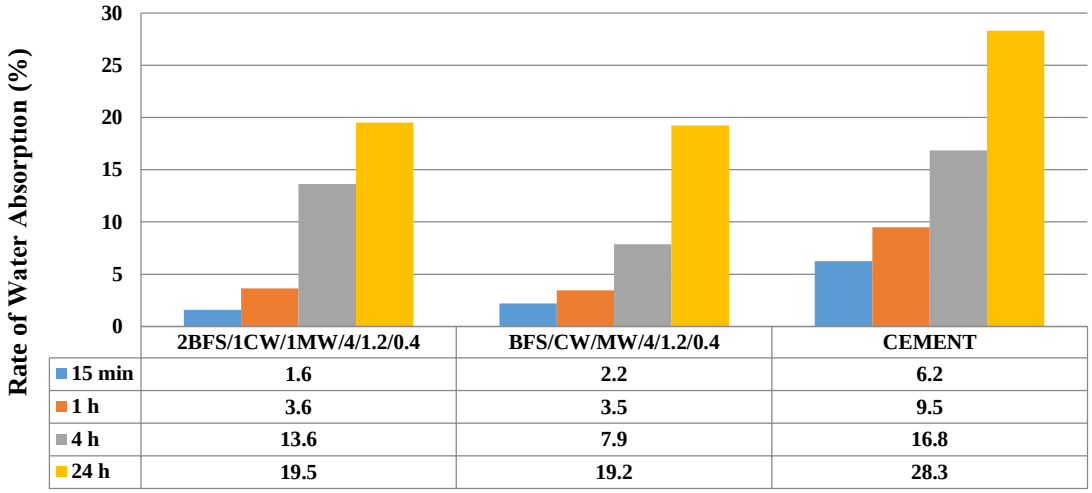
Water absorption rates of binary component samples were given in Figure 4.92. According to these results, the water absorption value of all other samples were lower compared to cement sample, except for 2CW/2MW/2/1.2/0.4/S sample after 24 hours. It was determined that the addition of CW and MW increased the water absorption value of binary samples compared to the BFS-UB.



	2BFS/2MW/6/1.2/0.4	3BFS/1CW/6/1.5/0.4	2CW/2MW/2/1.2/0.4	2BFS/2MW/4/1.2/0.4	2BFS/2CW/6/1.5/0.4	CEMENT
15 min	1.6	2.0	52.1	2.4	6.0	6.2
1 h	2.8	3.3	56.7	3.5	9.9	9.5
4 h	14.4	5.9	57.3	6.4	17.3	16.8
24 h	24.9	10.9	58.9	10.5	21.0	28.3

Figure 4.92. Comparison of the rate of water absorption of the selected binary samples.

Similar to the binary component sample results, water absorption values for ternary component samples after 24 hours were found to be approximately 40% lower than the cement sample (Figure 4.93).



	2BFS/1CW/1MW/4/1.2/0.4	BFS/CW/MW/4/1.2/0.4	CEMENT
15 min	1.6	2.2	6.2
1 h	3.6	3.5	9.5
4 h	13.6	7.9	16.8
24 h	19.5	19.2	28.3

Figure 4.93. Comparison of the rate of water absorption of the selected ternary samples.

For samples whose water absorption value were determined less than the cement sample, the void rates were determined also lower than the cement sample. Therefore, as the sample's void ratio increased, the water absorption rate also increased suggesting that there is direct correlation between void ratio and the water absorption rate.

4.6. Fifth Stage-Determination of the Durability Properties of the All Selected Binders

In this part, the durability properties of the selected unary, binary and ternary component specimens showing the selected performance in terms of physical and strength properties were determined and compared. These features were namely "drying shrinkage, high temperature effect, sulphate effect and sulphuric acid effect".

4.6.1. Drying shrinkage of the selected binders

In the first three parts of this thesis strength properties of samples determined. In this part, the drying shrinkage ratio results of the samples with the selected performance of mechanical properties were given in Figure 4.94.

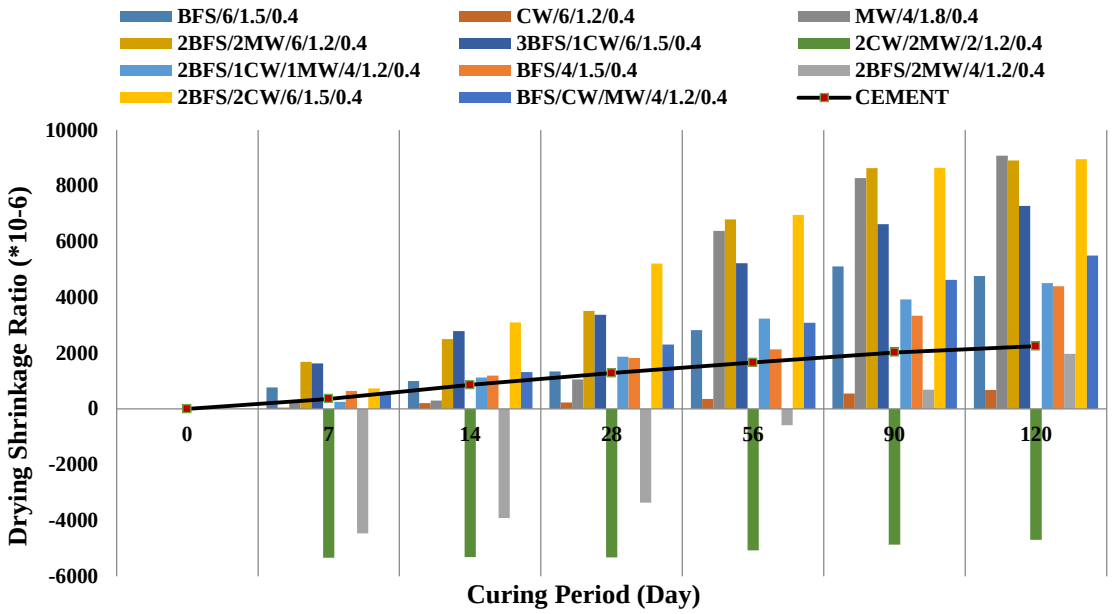


Figure 4.94. Comparison of drying shrinkage results of the all selected binders.

According to Figure 4.94, expansion rather than shrinkage was observed for 2CW/2MW/2/1.2/0.4 and 2BFS/2MW/4/1.2/0.4 samples. Drying shrinkage values were determined for all samples except these two samples. The maximum drying shrinkage value after 120 days was determined for the sample MW/4/1.8/0.4. The shrinkage values determined for CW/6/1.2/0.4, 2CW/2MW/2/1.2/0.4 and 2BFS/2MW/4/1.2/0.4 samples at the end of 120 days were smaller than the cement sample's.

The drying shrinkage values of the samples with unary component were given in Figure 4.95. According to this Figure 4.95, the highest shrinkage value was realized for the unary component MW-UB sample, while the smallest shrinkage value was determined for the unary component CW-UB sample. For the MW-UB sample, there was a significant increase in the drying shrinkage value, especially between curing period of 28 day and 56 day. In this example, this dramatic increase in drying shrinkage after 28 days could be attributed to the $CaCO_3$ content in the marble waste that may be react with physical water forming first turned into Ca $(OH)_2$, which could lead to volumetric expansion, and then $Ca(OH)_2$ is shrunk as it loosed water over time. Therefore, as the MW-UB sample subjected to steam curing resulting in lost its moisture content after 28 days and then its shrinkage values increased dramatically. This result is in agreement with the literature. In the literature, it was reported that for the activation of marble waste, especially water vapor curing reduced the drying shrinkage values of marble

more than in air or in water [51]. In the same study, it was determined that glass waste dust used in marble waste at a rate of 2.5-5% also reduced the drying shrinkage value of marble. In the same paper, it was stated that the reduction of drying shrinkage by the incorporation of glass powder into marble matrix was due to the fact that insoluble glass powder wastes act as a rigid aggregate, reducing shrinkage or improving the strength properties [51]. There was no published information in the literature about drying shrinkage of ceramic waste for alkali activation. Abdollahnejad et al. studied alkali activation of mixture of slag and fly ash [113]. They used as a fine aggregate of porcelain ceramic waste in an alkaline activation system. In this study, the drying shrinkage values decreased in the samples using ceramic waste compared to the samples using standard sand. It was emphasized that this situation might be caused by the fact that i) the ceramic waste gave different chemical reactions in the activation system due to its chemical composition, ii) because it had a more porous structure than natural sand, it absorbed the mixing water and thus the environment decreased the pH value and increased the strength [113]. Drying shrinkage values of unary component samples of blast furnace slag (BFS-UB) were found approximately 2 times higher than the cement sample. This result was consistent with the previous studies that alkaline solution activated blast furnace slag had a much higher ultimate drying shrinkage magnitude than cement sample [114-116].

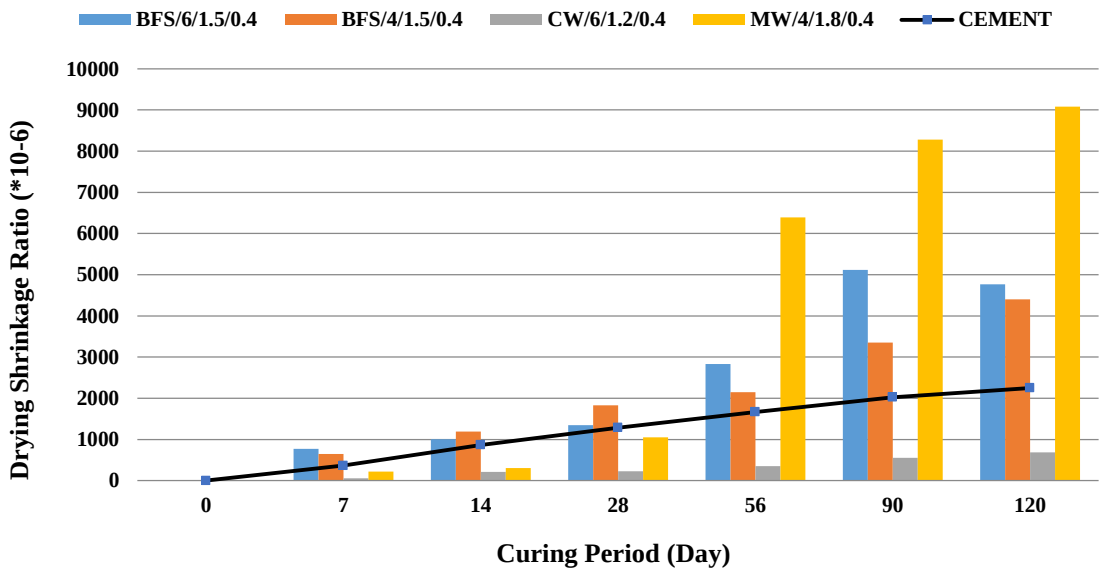


Figure 4.95. Comparison of drying shrinkage of the selected unary binders.

The drying shrinkage ratio values of the samples with binary components were given in Figure 4.96.

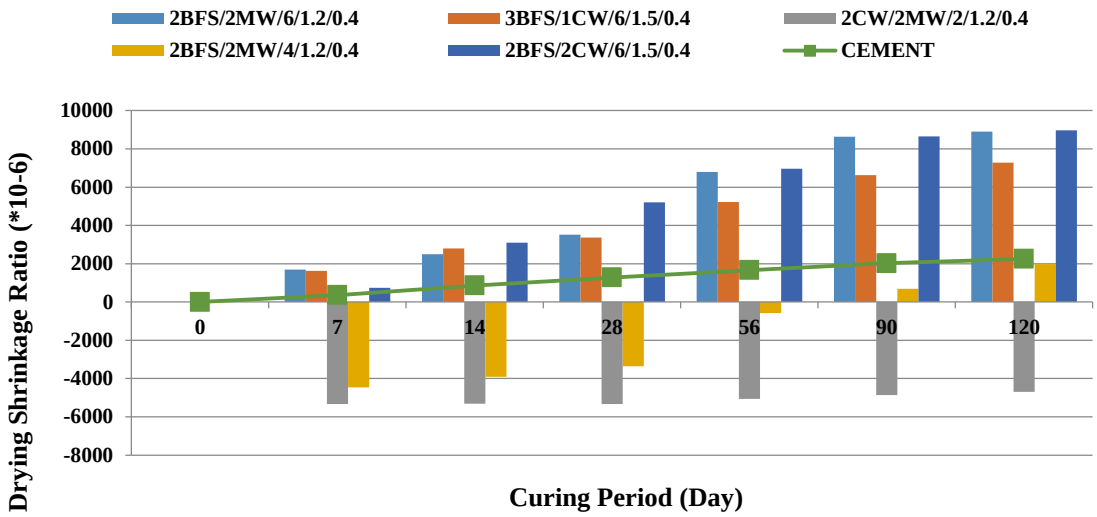


Figure 4.96. Comparison of drying shrinkage of the selected binary binders.

According to these results, while the activator ratio of the samples was 4 in the BFS/MW-BB system, expansion instead of shrinkage was observed until the curing period of 90th day. However, when the activator ratio increased to 6, the drying shrinkage value for the BFS/MW-BB sample was determined to be much higher than the other binary component samples after 120 days. Therefore, as the alkali activator ratio in the samples in the BFS/MW-BB system increased (as the n ratio increased), the shrinkage values increased. Likewise, it was determined that the presence of CW increased the drying shrinkage values in BFS/CW samples when compared to BFS-UB samples. For the CW/MW-BB samples, only expansion values were obtained during the drying shrinkage test period.

The drying shrinkage ratio values of the ternary component samples over time were given in Figure 4.97.

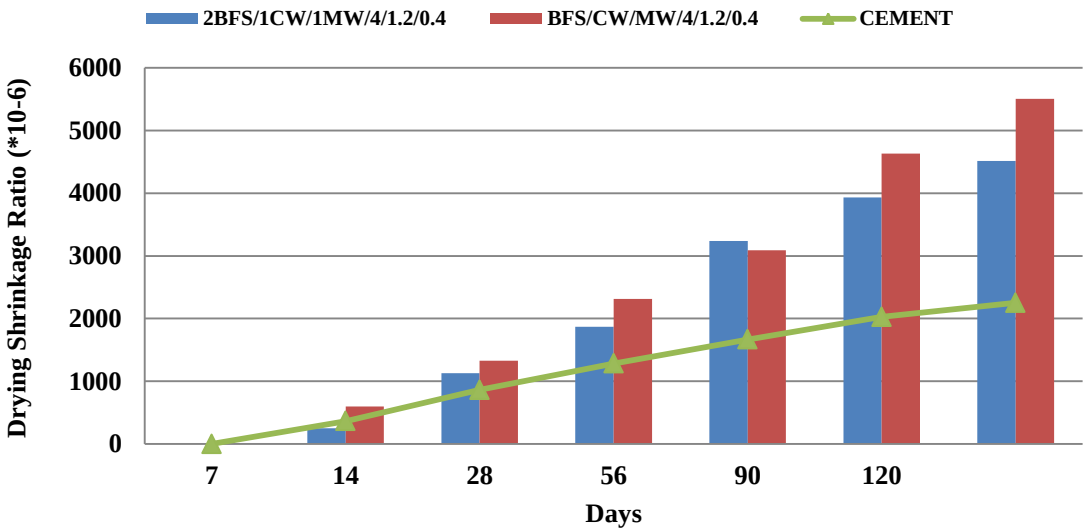


Figure 4.97. Comparison of drying shrinkage of the selected ternary binders.

The drying shrinkage values determined in both of the ternary component samples were approximately 2-2.5 times higher than the cement sample after 120 days. However, the drying shrinkage values of the ternary component samples were lower than the binary component BFS/CW-BB and BFS/MW-BB samples with high activator dosage.

4.3.2. High temperature effect on the selected binders

Strength and weight changes of samples at 200, 400, 600 and 800ºC for high temperature effect on unary, binary and ternary component containing samples were determined. Accordingly, flexural/ compressive strength and weight changes were plotted in Figure 4.98 for unary component samples.

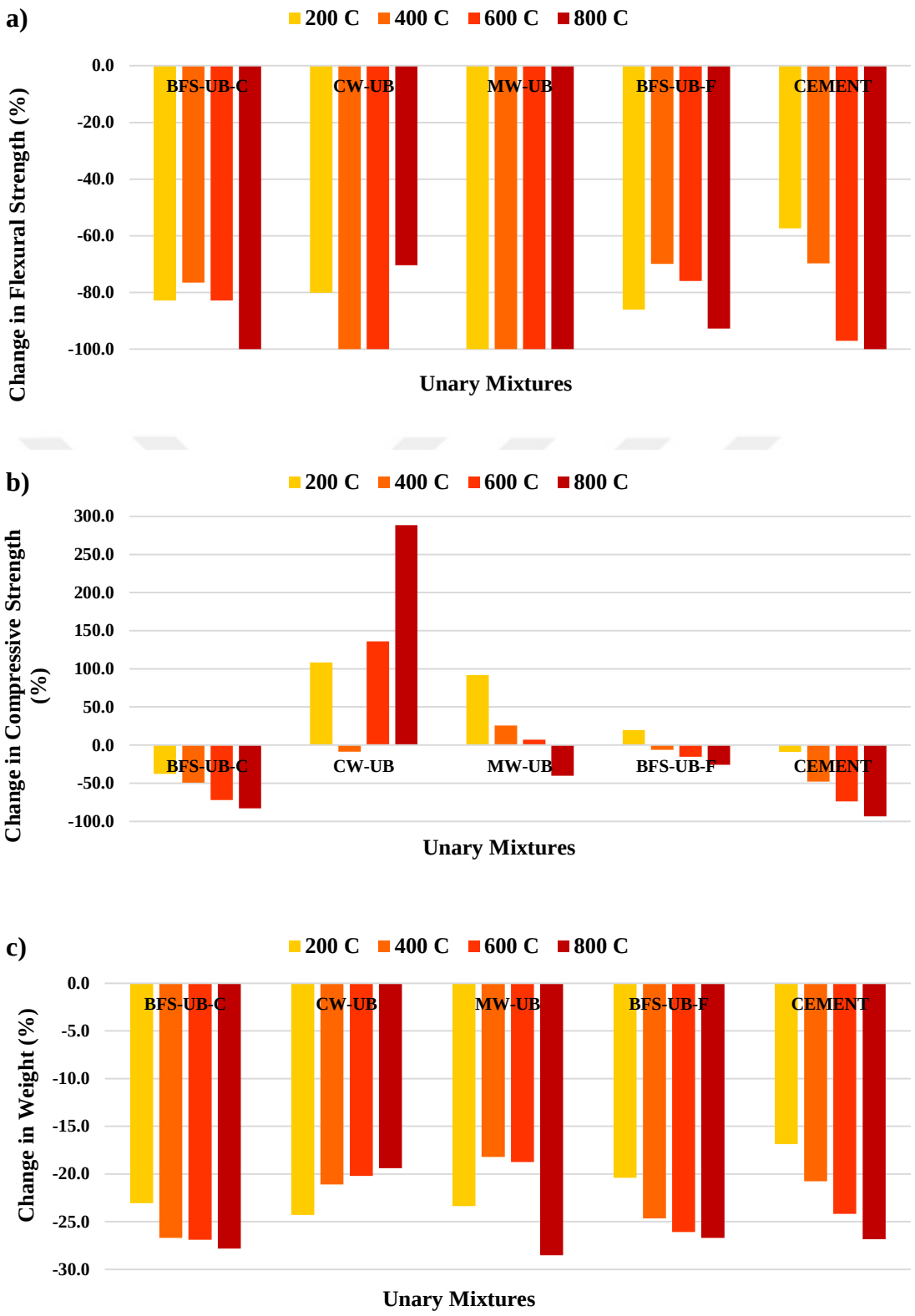


Figure 4.98. Change in a) flexural b) compressive strength and c) weight of the selected unary samples with temperature.

According to the results in Figure 4.98, the flexural strength values of the unary component samples under the effect of high temperature decreased significantly. The loss of flexural strength of cement at 200ºC was found to be less than all other unary component samples. However, as the temperature values increased, the flexural strength loss for cement continued increasingly. When reaching at 600ºC, BFS-UB-F samples lost less flexural strength than cement sample. When the last 800ºC was reached, the resistance to flexural strength was completely lost in all samples except the CW-UB. In the CW-UB example, the flexural strength value increased by 30% suggesting that a sintering event occurred for the CW-UB sample at between 600-800ºC.

Considering the compressive strength values of the unary component samples under the effect of high temperature, an increase was observed in the compressive strength values of unary component samples except BFS-UB-C and cement samples for 200ºC. However, when the temperature rises to 400ºC, the compressive strength values of all samples decreased. For 600ºC, the compressive strength value increased for the CW-UB samples, while the decrease continued for the other samples. Strength losses of all other single component samples for 800ºC were less than the cement sample. This showed that unary component samples had better durability properties under the effect of high temperatures compared to cement sample.

The XRD analysis of unary component sample, which changes with the effect of high temperature, was shown in Figure 4.99. For both BFS-UB-C samples, the strength loss increased at high temperature (≥ 600ºC). The alkali activated slag paste consists mainly of an amorphous phase, which is partially depicted in the XRD pattern as a broad feature centered at 29ºC of 2θ at room temperature. [36]. However, under the influence of high temperature (≥ 600ºC), the amorphous phase crystallized and the main common crystalline phase detected as “akermanite”. [36]. The same results were obtained in our study. In addition, the secondary crystalline phase was determined as “wollastonite”.

In this section, it was necessary to explain the increase in strength under the influence of high temperature, especially for the CW-UB sample. Because for the CW-UB sample, when the temperature value increased 800ºC, an increase in strength approaching 300% was observed in terms of compressive strength. These result was highly consistent with the results of another study in the literature [46]. In this study, an increase was observed

in the compressive strength values of the alkali activated ceramic waste samples with the effect of high temperature [46]. As seen in Figure 4.99/c, the peaks of quartz, mullite and albite can be detected at all temperature in XRD analysis of CW-UB sample. The mullite phase has a low thermal expansion coefficient, low creep rate and good thermal stability [48]. In addition, it was observed that "nepheline" phase was formed in the CW-UB sample (as shown in 4.99/c) when the temperature increased to 800ºC may be formed a bonding phase between particles of CW matrix. This could explain the dramatic increase in compressive strength observed at 800ºC. Nepheline phase ($NaAlSiO_4$) can be obtained by thermally treating zeolite at approximately 1200ºC [117,118]. Therefore, for the CW-UB sample, it supported the formation of zeolite structure as a reaction product as a result of alkali activation process of materials with high SiO_2 ratio in their chemical composition (such as ceramic waste, fly ash and metakaolin). As a result, it could be said that the reason for the increase in strength under the effect of high temperature for the CW-UB sample was the effect of the conversion of zeolite to nepheline mineral.

For the MW-UB example, calcite continued to exist as the primary structure at 800ºC, as in other temperatures (23ºC and 400ºC). However, at this temperature, the "gehlenite" mineral began to be observed. This showed that the formation of amorphous phase would increase as the temperature continued to increase. Similar results were obtained for a study in the literature [119]. At 900 °C, limestone decomposes and forms calcium oxide. In addition, a large gehlenite crystalline phase ($Ca_2Al_2SiO_7$) was found in the samples with added SiO_2 [119]. In our study, CaO from marble waste and sodium silicate activator combined with the SiO_2 ion to form the "gehlenite" structure.

When the weight or mass losses were evaluated, similar results were obtained. As the temperature increased, mass loss was observed in all samples, but when heating at 800ºC, the biggest loss occurred for the MW-UB sample. For the CW-UB sample, it was determined that as the temperature value increased, the mass loss decreased. A similar situation occurred in the sample of MW-UB at 400 and 600ºC. However, when the temperature increased to 800ºC, a mass loss of approximately 10% occurred in the MW-UB sample. This value was the highest mass loss value recorded for unary samples.

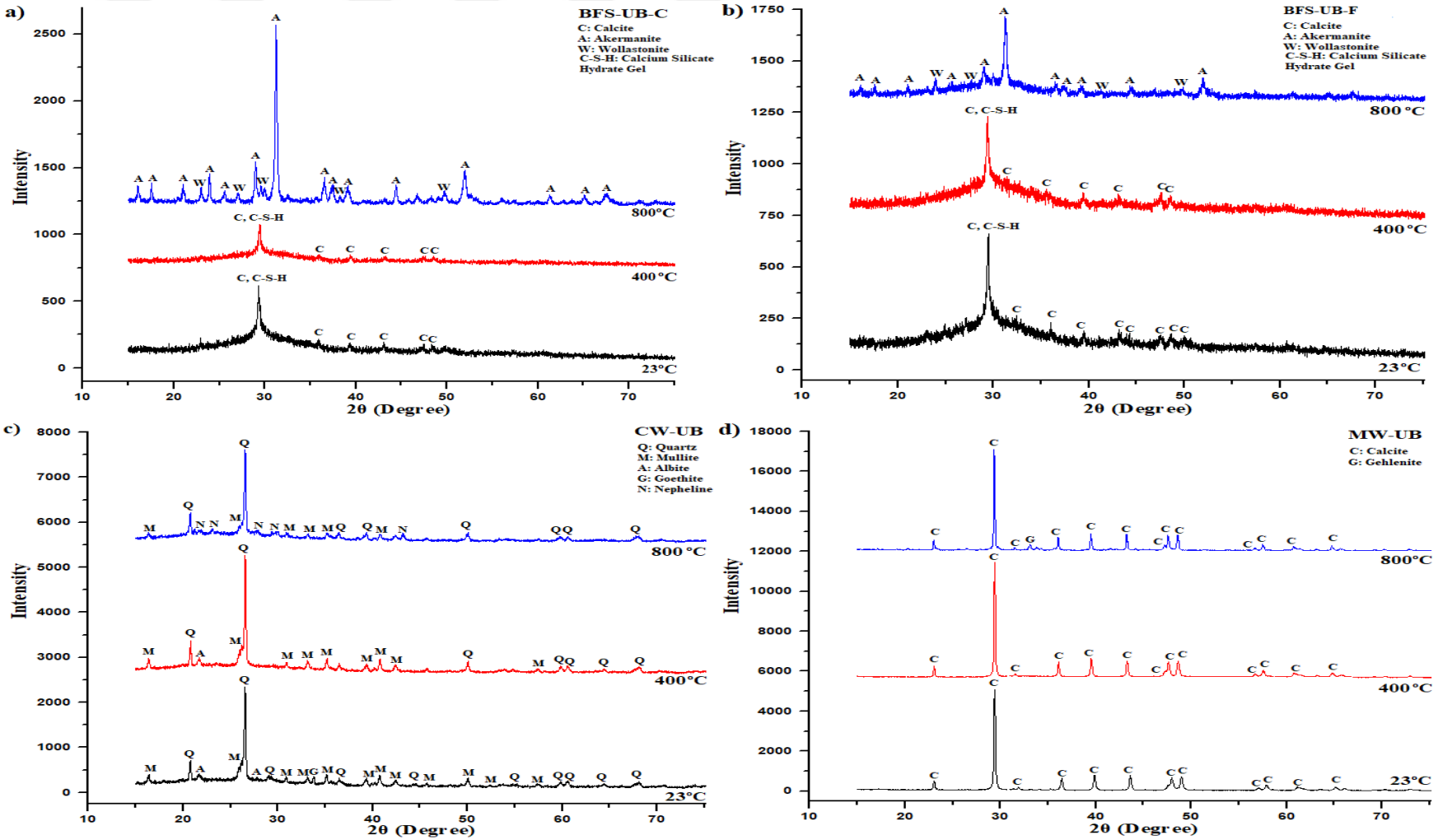


Figure 4.99. XRD analysis of the selected unary sample with temperature **a)** BFS-UB-(C) **b)** BFS-UB (F) **c)** CW-UB **d)** MW-UB

For binary component samples, flexural & compressive strength and weight changes were plotted in Figure 4.100. According to the results in Figure 4.100, the flexural strength values of the binary component samples under the effect of high temperature decreased significantly. At 200ºC, only 3BFS/1CW-BB-C sample increased flexural strength value and decreased in all other samples.

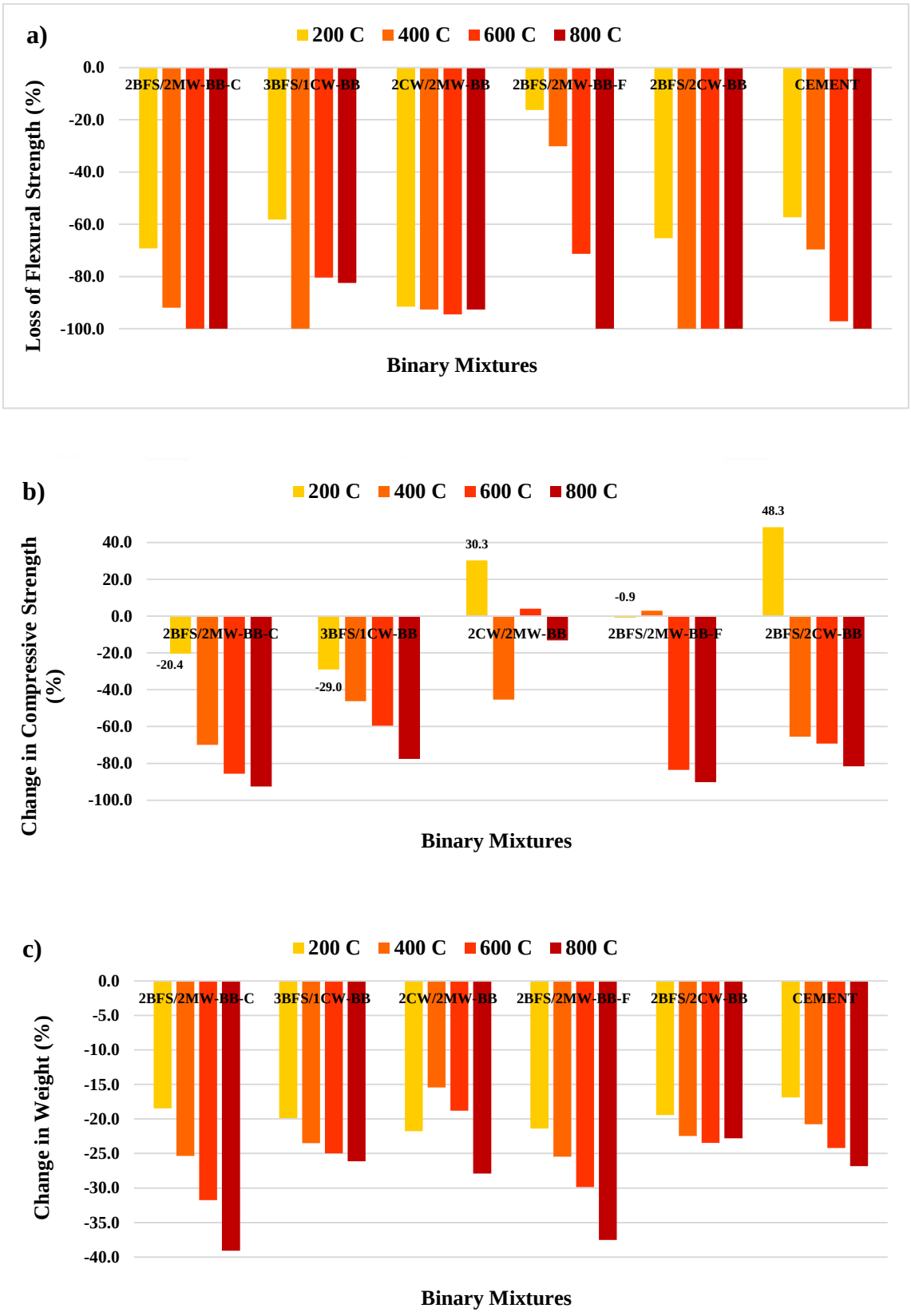


Figure 4.100. Change in a) flexural b) compressive strength and c) weight of the selected binary samples with temperature.

For the 2BFS/2MW-BB-F sample, the loss of flexural strength was less than the cement sample at all temperatures. It was observed that MW reduced the flexural strength loss of BFS under the influence of temperature. In addition, it was determined that the 2BFS/2MW-BB-F sample had approximately 30% less strength loss compared to cement at all temperature values (except 800ºC). It was observed that CW substituted in BFS increased the flexural strength resistance for high temperature values. For the 3BFS/1CW-BB-C sample, less flexural strength loss occurred than the cement sample at 600 and 800ºC.

While the flexural strength values of some of the binary component samples increased under the effect of 200ºC temperature, some of them decreased. The samples with increased strength were BFS and MW samples with high CW content. For the sample of 2BFS/2MW-BB-F with high MW substitution, there was a very small (1%) decrease in the compressive strength value. When the temperature increased to 400 ºC, the compressive strength values of the other samples, except for the 2BFS/2MW-BB-F sample, decreased by 50% or more. Compressive strength of the 2BFS/2MW-BB-F sample increased by 3%. When the temperature increased to 600 ºC, there was a dramatic decrease over 80% in the strength value of the 2BFS/2MW-BB-F sample. For this temperature value (600ºC), the only sample whose compressive strength value increased was the combination of CW and MW (CW/MW-BB). The compressive strength values of all samples except BFS samples containing CW were higher compared to cement. When the temperature reached at 800ºC, all samples except the 2BFS/2MW-BB-F sample lost their compressive strength by 75% or more. The biggest strength loss was in the cement sample with 93.6%.

When the weight or mass losses for binary component samples were evaluated, it was determined that similar results were obtained. As the temperature values increased, the mass loss of all samples increased. It was observed that mass loss decreased at 400 and 600ºC for only 2CW/2MW-BB sample. However, when heated at 800 ºC, it was observed that all samples lost about 25% mass, especially both BFS-UB samples containing marble waste (BFS/MW-BB-F and BFS/MW-BB-C.

The XRD analysis of binary component sample, which changes with the effect of high temperature, was shown in Figure 4.101. Two main phases were observed as the

temperature increased in the BFS/CW binary system. These phases were the "akermanite" and "wollastonite" phases. In the previous sections, it was stated that akermanite and wollastonite structures were detected in BFS-UB selected unary samples under the influence of high temperature (see section 4.3.2). In other words, these two structures ("akermanite" and "wollastonite" phases) were the structures formed by BFS-UB when it was under the influence of high temperature. However, the important point was that the "wollastonite" structure increased under the effect of high temperature as the amount of CW in the BFS/CW-BB samples increased. Wollastonite ($CaSiO_3$) is a mineral formed by the reaction of CaO and SiO_2 at 400-450 ºC [120]. This showed that as the amount of CW in BFS increased, the formation of reaction product rich in CaO and SiO_2 increased. Thus, the reason why BFS/CW binary samples suffer less strength loss under the effect of high temperature compared to other binary samples was explained. This result was also compatible with the results in the literature that the different uses of "wollastonite" structure in cement and concrete strengthen the thermal resistance of materials under the influence of high temperature [121, 122].

For both BFS/MW-BB samples (2BFS/2MW-BB-C and 2BFS/2MW-BB-F), it was determined that the "merwinite" phase was formed at 800 degrees (See Figure 4.101). However, when the XRD analyzes obtained after these two BFS/MW-BB samples were exposed to 800 ºC, different phase formations were also observed in the two samples. As seen in Figure 4.101/b, the intensity value of C_2S formation in the 2BFS/2MW-BB-C sample was higher and the phase appearance was more pronounced than in the BFS/MW-BB-F sample. C_2S and C_3S structures are the two main components of the cement, and when combined with water (during hydration), they form the C-S-H gel structure [124]. In this case, when the C-S-H gel structure was considered as the structure that gives the cement its strength, it can be said that the C_2S structure, which had a more pronounced and high intensity in XRD analysis, provided higher strength for the BFS/MW-BB-C sample.

For two 2BFS/2MW-BB samples, both flexural and compressive strength losses up to 400 ºC were very low compared to other binary samples. Because, as seen in Figure 4.102, the C-S-H gel structure maintained its existence at this temperature. However, when it is increased to 800 ºC, the "calcite" phase turns into "merwinite" phase and the strength loss increased dramatically at this temperature. Similar to our results, it was

reported that the formation of “merwinite”, “ettringite” and “portlandite” structures was observed under high temperature (800 ºC) as a result of the increase of Ca^{+} presence with the addition of phosphogypsum in BFS, and this improved the residual strength after the effect of high temperature [123].

In 2CW/2MW-BB binary sample, “quartz” and “calcite” structures were observed at 28 ºC and 400 ºC, while “alite” (C_3S) structure, which is one of the main components of cement, observed when the temperature increased to 800 ºC. C_3S is one of the main components of cement, and when it reacts with water, it creates the C-S-H gel structure of the cement, allowing it to gain strength [124]. This explains the reason why the CW/MW binary sample with C_3S phase structure had much less loss in compressive strength as the temperature increased compared to the other samples.

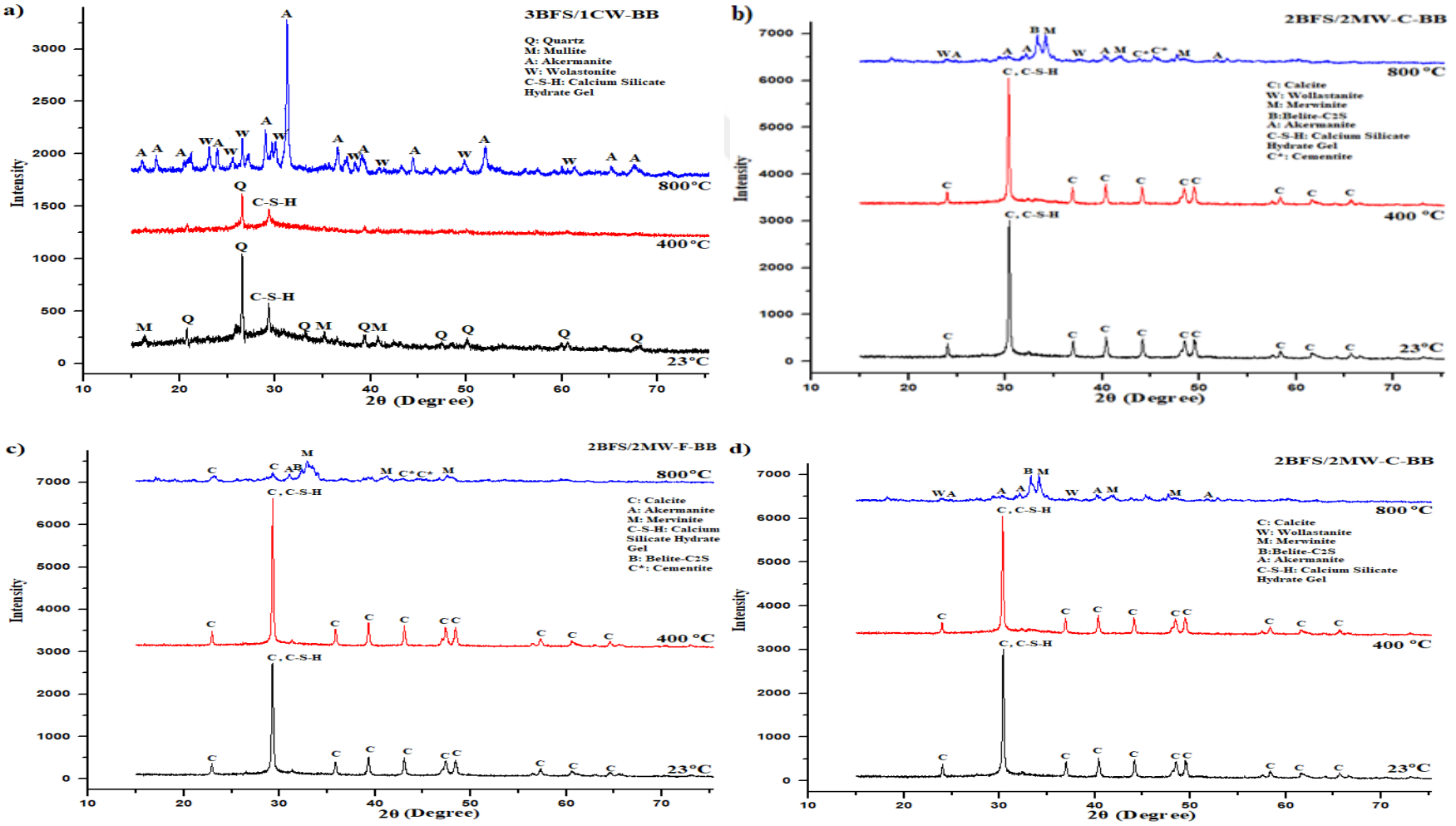


Figure 4.101. XRD analysis of the binary selected sample with temperature **a)** 3BFS/1CW-BB **b)** 2BFS/2CW-BB **c)** 2BFS/2MW-BB-F **d)** 2BFS/2MW-BB-C e)2CW/2MW-BB.

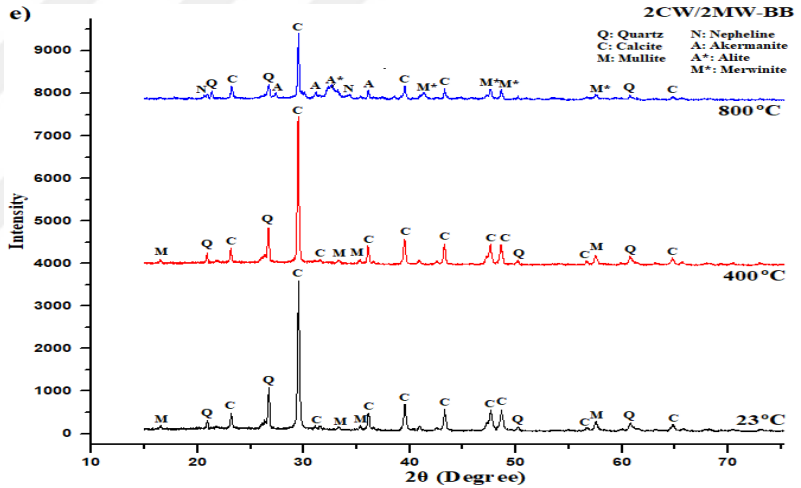


Figure 4.101. (continue) XRD analysis of the binary selected sample with temperature **a)** 3BFS/1CW-BB **b)** 2BFS/2CW-BB **c)** 2BFS/2MW-BB-F **d)** 2BFS/2MW-BB-C e)2CW/2MW-BB.

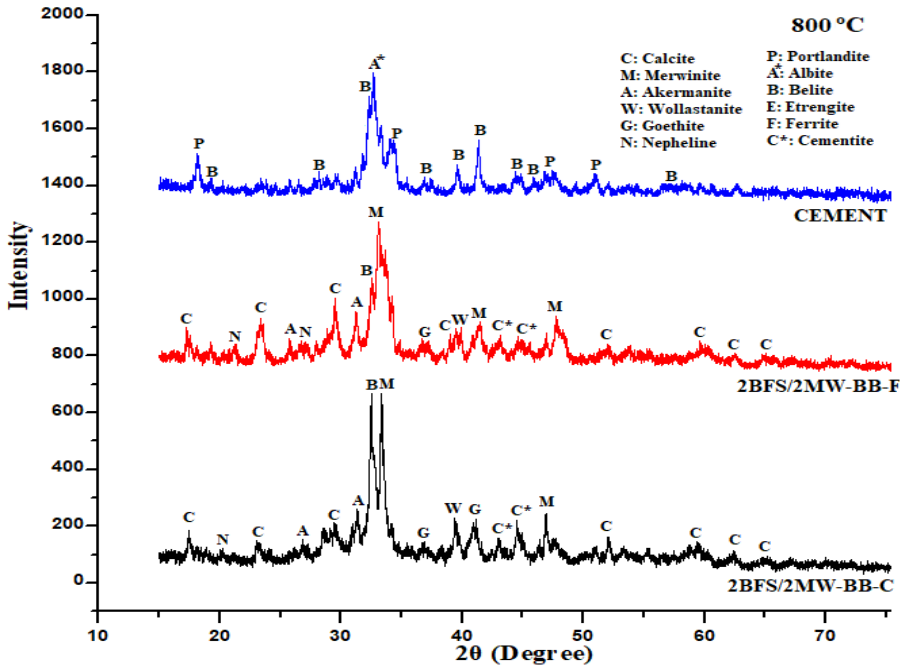


Figure 4.102. XRD analysis of the BFS/MW-BB selected samples and cement sample at 800 ºC

For the ternary component samples, flexural and compressive strength and weight changes were plotted in Figure 4.103. According to these results, the flexural strength values decreased as the temperature increased in these samples. Although it was observed that cement had less loss in flexural strength, when the loss compared to ternary component samples up to 400 ºC. When the temperature raised to 600 ºC, the cement sample lost more than 95% of its flexural strength feature. When reaching 800 ºC, all samples lost 95% or more of their flexural strength.

In terms of compressive strength, for sample coded BFS/CW/MW/4/1.2/0.4, there was an increase in strength at 200 and 400 ºC. However, the compressive strength values of the other ternary component sample (2BFS/1CW/1MW/4/1.2/0.4) and cement sample decreased as the temperature increased. It was understood that the cement sample had the highest loss in terms of compressive and flexural strength for all temperature values. When the temperature reached to 800 ºC, the BFS/CW/MW/4/1.2/0.4 sample lost only 60% of its compressive strength.

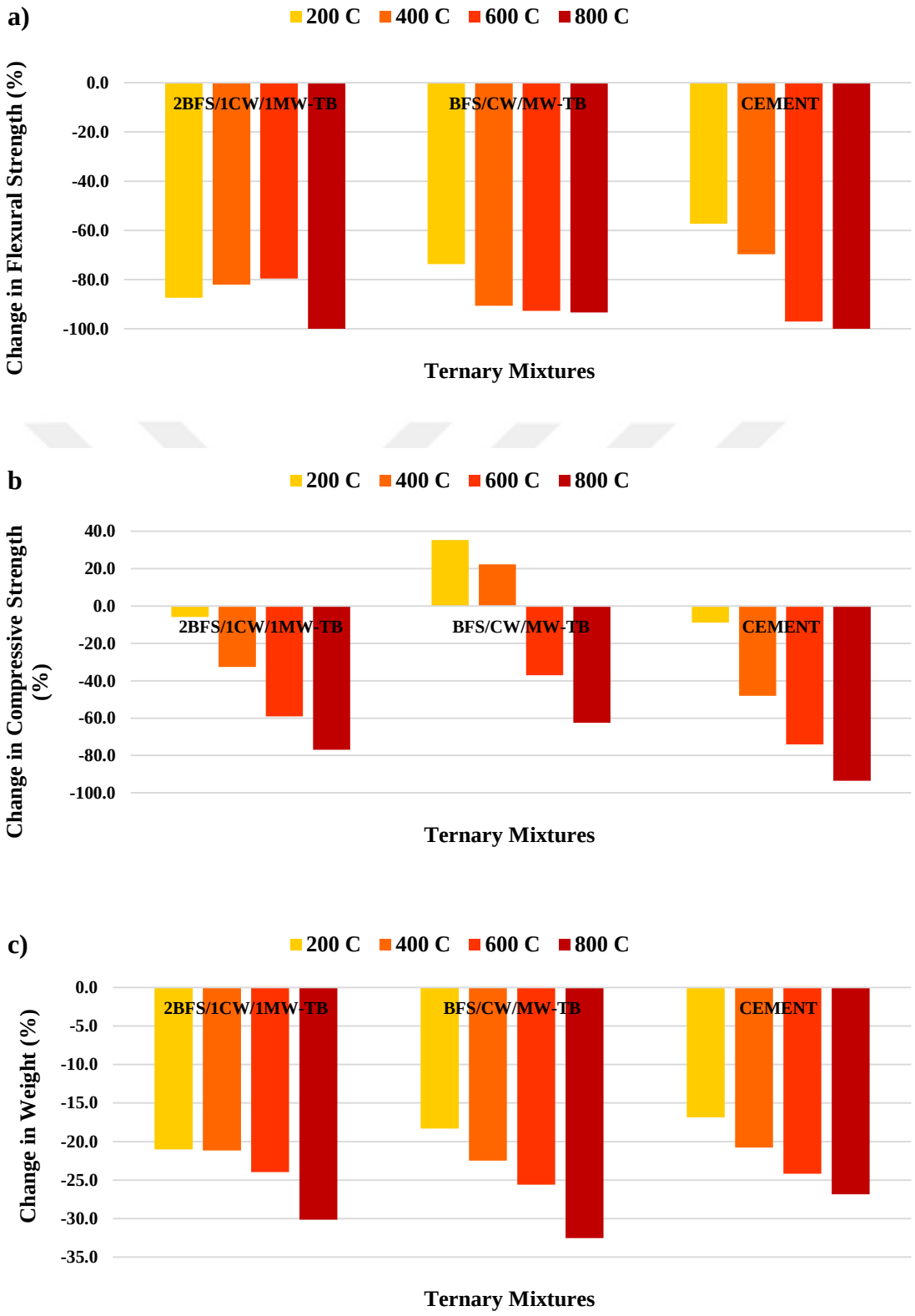


Figure 4.103. Change in a) Flexural b) Compressive strength and c) Weight of the ternary selected sample with temperature.

For the ternary component samples, the least mass loss was detected in the cement sample in contrast to the strength loss in terms of mass loss. In all samples, the loss in mass increased as the temperature value increased. At 800 ºC, the greatest mass loss occurred for the BFS/CW/MW/4/1.2/0.4 ternary component sample with the least loss of strength.

As a result, the substitution of CW and MW in the BFS increased the resistance of high temperature of the blast furnace slag. However, especially in terms of compressive strength, it was determined that all unary, binary and ternary component alkali activation samples were more durable compared to the cement sample under the influence of high temperature. It was found that especially the ternary component samples lost 30% less strength than the cement sample. Within the scope of this thesis, it was proved that all types of binders produced by alkali activation process show better mechanical properties than cement sample in terms of preserving their strength properties under high temperature.

The XRD analysis of ternary component sample, which changes with the effect of high temperature, was shown in Figure 4.104.

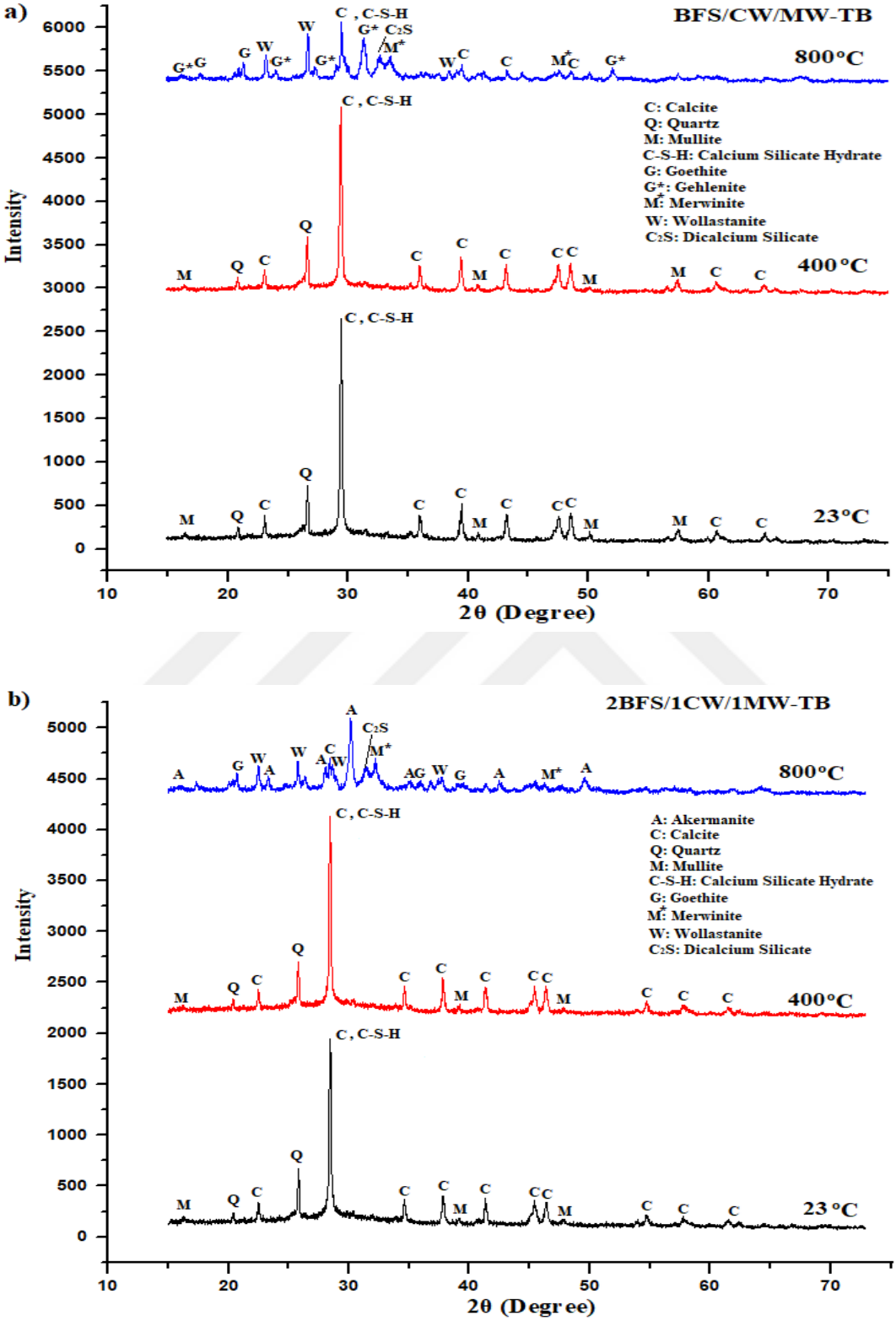


Figure 4.104. XRD analysis of the ternary selected sample with temperature a) BFS/CW/MW-TB b) 2BFS/1CW/1MW-TB

As seen in Figure 4.104, no change in phase structure was observed at 400 ºC in both of the ternary samples. However, when the temperature increased to 800 ºC, a change was observed in the phase structures in both samples. For the "BFS/CW/MW-TB" example, where all components were used equally by mass, much less loss of compressive strength was observed when the temperature was increased to 800 ºC compared to both the other ternary sample and cement (see Figure 4.103). When the phase change of this sample was examined at 800 ºC, it was observed that even at this temperature, some of the C-S-H gel structure was preserved. The C-S-H bond structure preserved at high temperature was an indication that the loss in compressive strength was less for this sample compared to other samples. However, for the "2BFS/1CW/1MW" example, where the BFS ratio was used twice as much as the other two components, it was observed that the entire phase structure changed when it was increased to 800 ºC. It was determined that structures such as akermanite, wollastonite and merwinite were formed under the effect of high temperature. These structures were similar to the phase structures formed under the high temperature effect of the two-component samples in the previous sections (see Figure 4.101).

In Figure 4.105, images of the selected samples at 200 and 800 ºC were given. It was observed that BFS samples containing CW and MW and ternary component samples (BFS/CW/MW-TB) preserved their dimensional properties better and less cracks and deformation formation were observed occurring compared to other samples.



Figure 4.105. Images of the selected samples fired to a) 200^{0}C and b) 800^{0}C.

In Figure 4.106, there were images of the cement sample fired at 200, 400, 600 and 800 ºC. Crack formation observed on all surfaces of the cement sample, especially after firing at 600 and 800 ºC. These images supported the loss of nearly 70% of the strength properties of the cement sample over 600 ºC.



Figure 4.106. Images of the cement samples fired to 200^0C, 400^0C, 600^0C and 800^0C.

When all these results were compared and evaluated, BFS-UB samples were more durable than cement samples under high temperature effect. There were also several publications in which blast furnace slag performs well under high temperature [36, 125, 126]. In this sense, the results obtained were in accordance with literature. In addition, in CW-UB single component alkaline activation system, approximately 300% strength gain was observed when fired and tested at higher temperatures.

It was also improved the resistance properties of CW added samples under high temperature in binary and ternary component systems. A similar result was confirmed by a study that the ceramic waste powder added to the slag/fly ash mixture improved the strength properties of the samples under the influence of high temperature [48].

4.6.3. Selected binders against sulphate attack test

In this experiment, the samples kept in 10% Na_2SO_4 solution for 90 days and then strength loss and mass loss of the samples were measured. According to these results, flexural and compressive strength losses of all samples exposed to sulfate effect at the end of 90 days were shown in Figure 4.107.

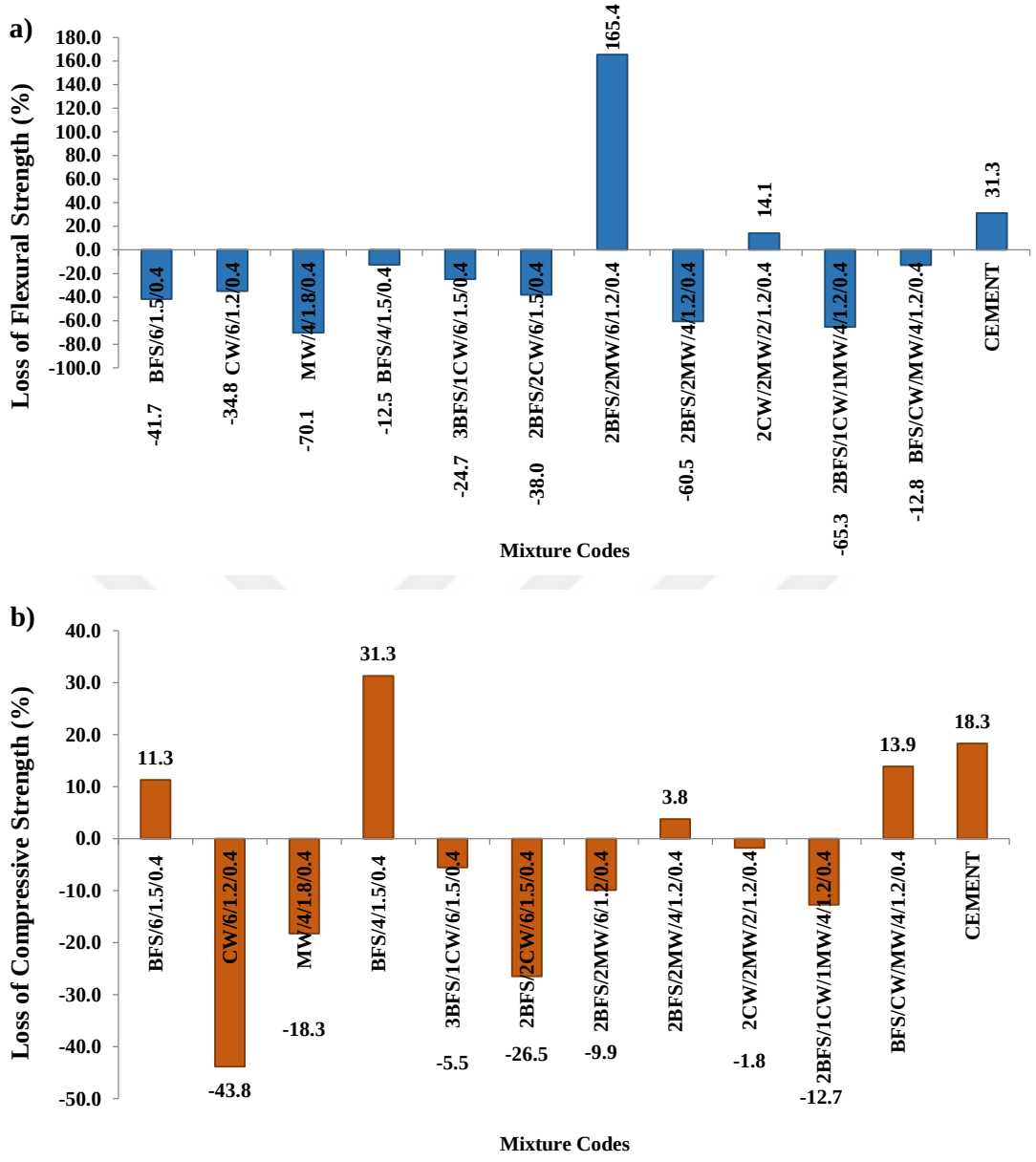


Figure 4.107. Loss of strengths of the selected binders exposed to sulphate effect a) Flexural b) Compressive.

According to Figure 4.107, it was observed that cement and BFS-UB samples did not suffer any loss under the effect of sulfate, especially in terms of compressive strength. Similar to these results of this study, it was reported that alkali activated slag samples exposed to sulphate effect in 5% Na_2SO_4 solution did not lose any strength compared to cement samples [82]. In this study, it was determined that CW-UB, MW-UB and binary component samples containing these wastes had more strength loss compared to cement and BFS-UB samples. This can be explained by the fact that BFS-UB samples and

cement samples have less void ratio and higher apparent density than other samples (see Figure 4.87-4.89). Thus, these examples exhibited a more impermeable structure and a more durability against external effects.

4.3.4. Sulphuric acid effect on the selected binders

In this experiment, the samples kept in 5% H_2SO_4 solution for 90 days and then strength loss and mass loss of the samples were measured. According to these results, flexural and compressive strength and mass losses of all samples exposed to sulfuric acid after 90 days were shown in Figure 4.108.

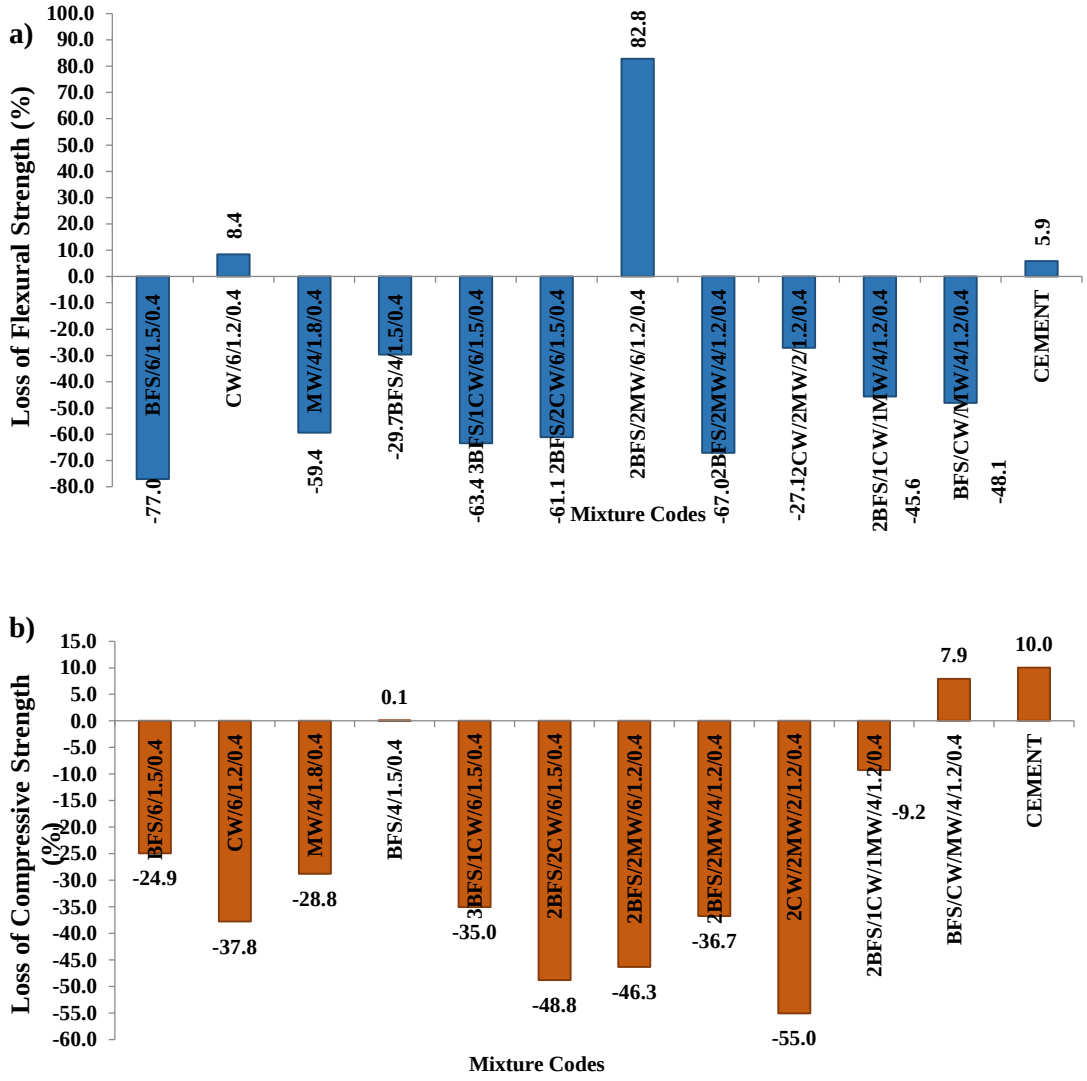


Figure 4.108. Loss of strengths of the selected binders exposed to sulphuric acid a) Flexural b) Compressive

When the experimental results were evaluated, it was determined that there was no decrease in the strength values of BFS-UB-F, BFS/CW/MW-TB and cement samples under the influence of sulfuric acid, especially in terms of compressive strength. In this part, it was determined that especially samples containing CW and MW were less resistant to chemical effects than BFS and cement.

4.7. Sixth Stage-Microstructural and Cost Analysis and Chemical Properties of the Selected Binders

In this section, the results of microstructural analysis conducted by SEM and EDS techniques that were carried out on the selected samples for unary, binary and ternary component samples. Also chemical characterization of the same sample's analyzes were performed by FTIR, XRD and SEM-EDS.

4.7.1. Microstructural analysis of the selected unary binders

4.7.1.1. Microstructural analysis of the BFS-UB samples

✓ *XRD Analysis of the BFS-UB*

In Figure 4.109, XRD phase analysis results of the raw materials of the BFS and the alkali activation samples of the selected BFS-UB for both flexural and compressive strengths (BFS 4/1.5/0.4/Steam (F) and BFS/6/1.5/0.4/Steam (C), respectively) were given.

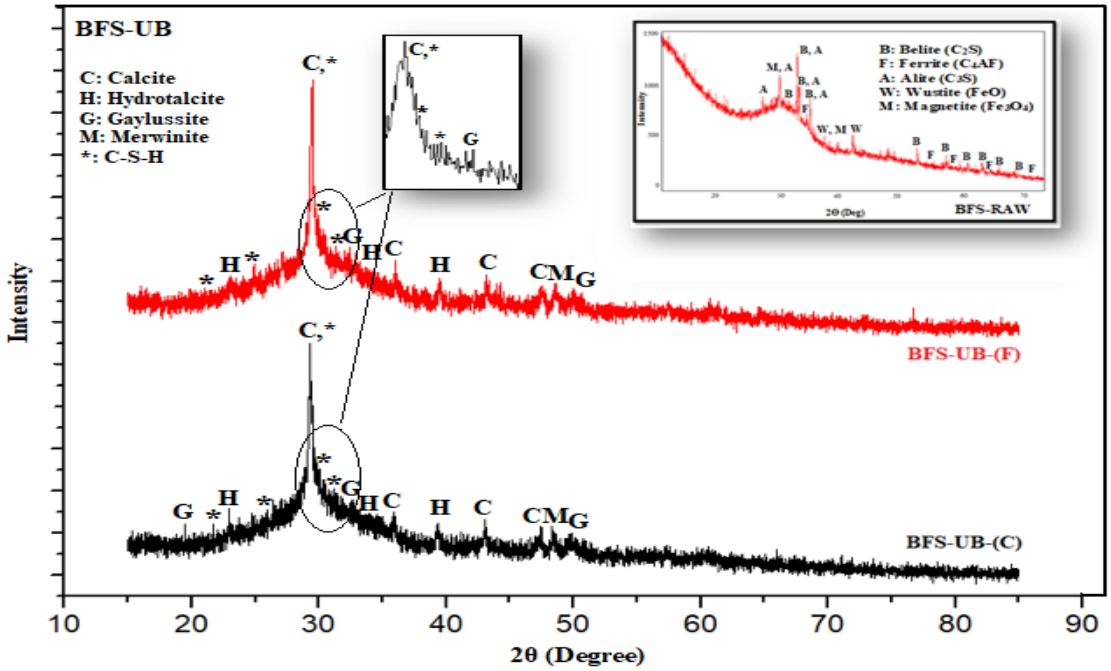


Figure 4.109. XRD patterns of the BFS-Raw and the selected BFS-UB (for both strengths) samples.

The raw Blast Furnace slag had an amorphous structure. Therefore, there was no significant main crystal phase peak other than some minor crystal phases (bellite, ferrite, alite etc.). In the several past studies it was also found that slag had an amorphous structure other than some different minor crystal phase structures and forms an amorphous hump at the 2θ ranges of 25-35^{o} [36, 99, 127].

In this study, two different BFS-UB samples with the highest value of flexural and compressive strength were obtained. For both samples, the ratios of "n" were different (4 and 6) but Ms ratio (1.5) was identical. This means that both samples had the same ratio of Sodium hydroxide/Sodium silicate in the activator solution, while the sample with "n" value of 6 had a total of 1.5 times more activator containing solution compared to the sample with "n" value of 4. The highest results were obtained in terms of flexural strength of the sample with "n" value of 4, and the compressive strength of the sample with the "n" value of 6.

When the XRD results for both samples were examined, the main peak for both samples were formed for the value of 2θ=29^{o} where the calcite and C-S-H peak overlap each other [99, 128-129]. Although a similar XRD pattern was obtained for both samples, the intensity value of this main peak of the sample with n values of 6 was determined more

than the sample with n values of 4. This increased the formation of C-S-H for the sample with n-value of 6 and a high alkalinity, thus resulting in a much higher compressive strength value [130-131].

Unlike calcite and C-S-H structure, structures such as hydrotalcite [99, 127, 129, 132], gaylusite [127,129,132] and merwinite [36] were formed for both samples.

✓ *FTIR Analysis of the BFS-UB*

In Figure 4.110, FTIR results of the raw materials of the BFS and the alkali activation samples of the selected BFS-UB for both flexural and compressive strengths (BFS 4/1.5/0.4/Steam-F and BFS/6/1.5/0.4/Steam-C, respectively) were given.

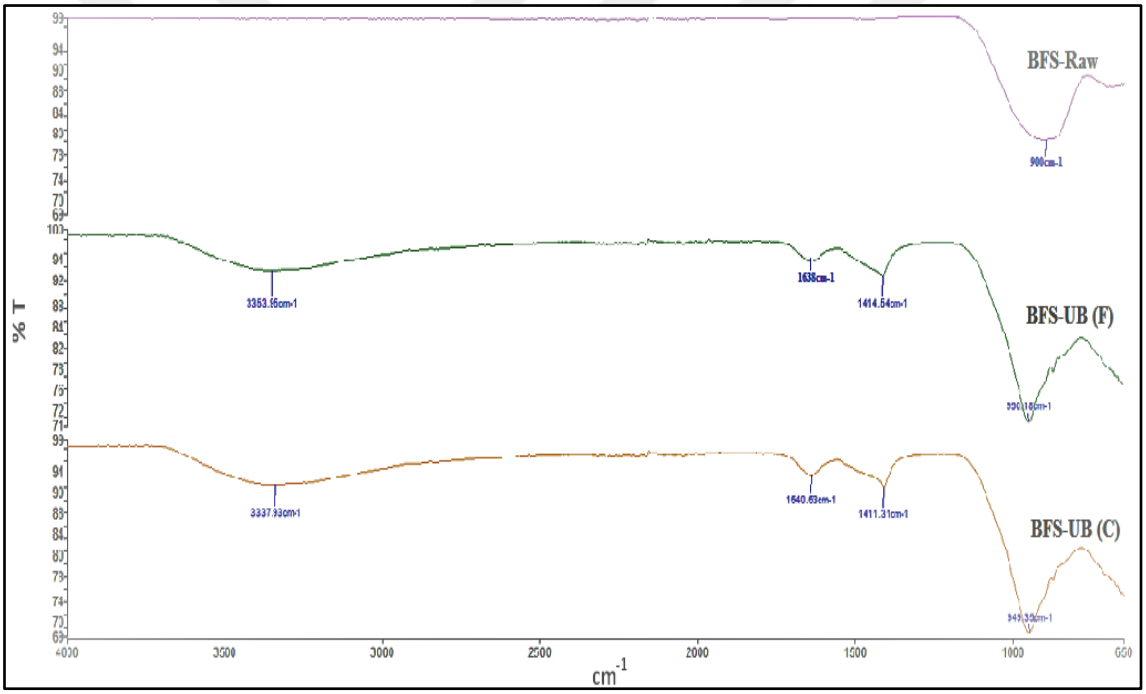


Figure 4.110. FTIR results of the BFS-Raw and the selected BFS-UB samples.

FTIR results obtained in this study and their comparisons with the literature were given in Table 4.22.

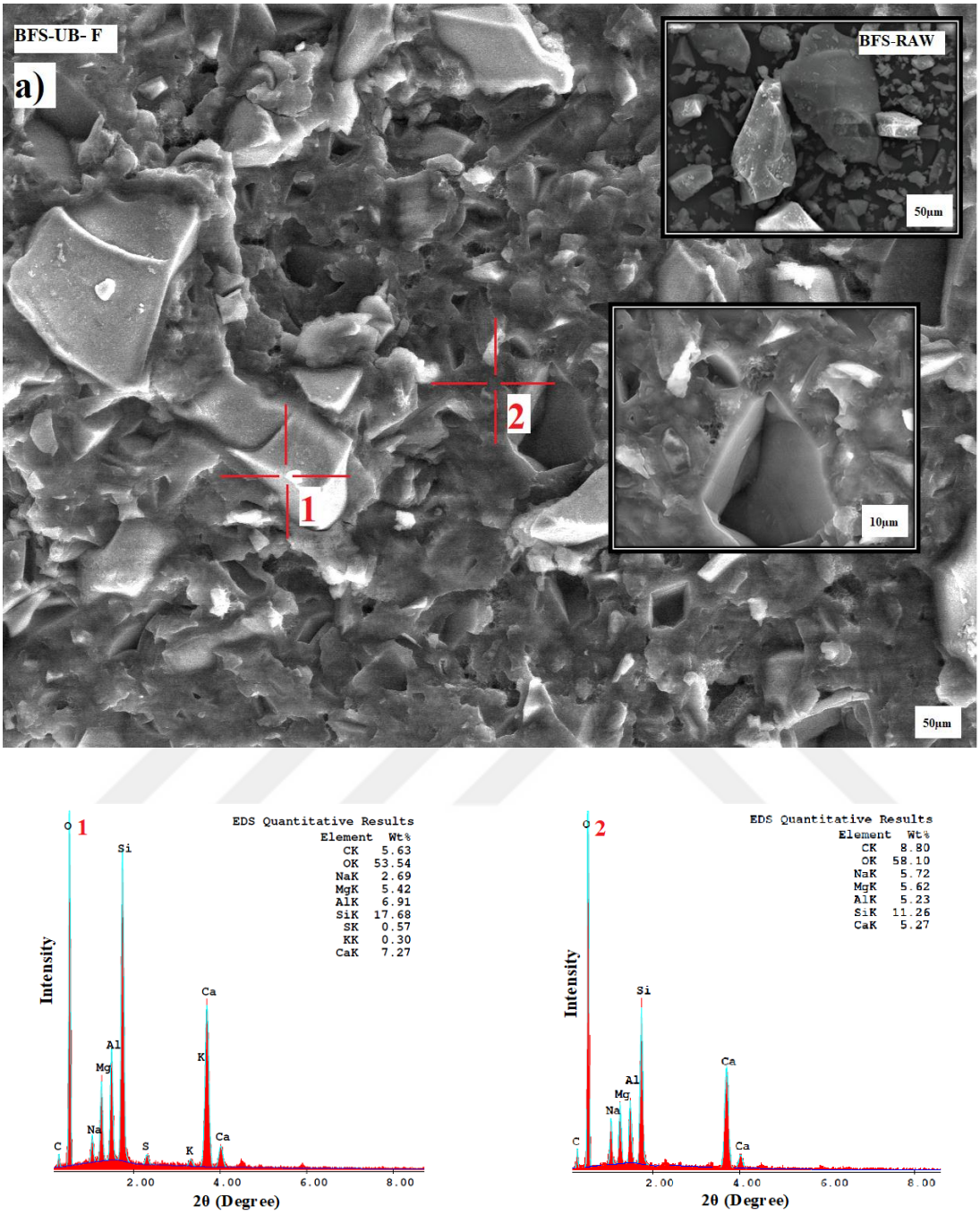
Table 4.22. FTIR results of BFS-Raw and both BFS-UB samples obtained in this study and their comparisons with the literature.

	BFS-UB			
	Band No	**Wavenumber cm^{-1}**	**Attribution**	**Reference**
BFS-Raw	1	900	Si-O-T asymmetric stretching	[129, 133-134]
BFS-UB-F	1	950	Si-O asymmetric stretching/C-S-H	[129, 133-134]
	2	1414	$v3[CO3]^{-2}$	[129, 133]
	3	1650	H-O-H Bending	[133-135]
	4	3353	O-H Stretching	[133-135]
BFS-UB-C	1	949	Si-O asymmetric stretching/C-S-H	[129, 133-134]
	2	1411	$v3[CO3]^{-2}$	[129, 133]
	3	1640	H-O-H Bending	[133-135]
	4	3337	O-H Stretching	[133-135]

Similar wavelengths were obtained for both samples obtained by activation of BFS-UB-F and BFS-UB-C samples. For the raw slag, the band of 900 cm-1 was related to the asymmetric stretching vibration mode of Si-O-T bonds, where T represents Si or Al, and the band position depended on the glass structures of the raw material [129-133-135]. The main binder gel band that appeared at 950-960 cm^{-1} was attributed to the Si-O asymmetric stretching bands in the SiO_4 tetrahedra [129, 134]. In general, for C–S–H and C–A–S–H systems, the Si–O–Si stretching bands were generally observed at a wavenumber of 950– 1000 cm^{-1}, associated with a silica network that is not highly polymerized [95, 130, 136]. The significant contain band around 1460-1410 cm^{-1} was ascribed to [CO_3^{-2}] [133], which were consistent with the gaylussite or calcite (mentioned with respect to the XRD results in Figure 4.109) [129]. The bands at 3300-3400 and 1640-1650 cm^{-1} were associated with the O-H stretching band and H-O-H bending band, respectively [129, 133, 135].

✓ *SEM-EDS Analysis of the BFS-UB*

In Figure 4.111, SEM-EDS image of the raw materials of the BFS and the alkali activated samples of the selected performance giving BFS-UB (BFS/4/1.5/0.4/Steam (F) and BFS/6/1.5/0.4/Steam (C)) were shown.



For the BFS-UB samples, SEM images of the samples with the highest strength values in terms of both flexural and compressive strength were obtained. In Figure 4.111, SEM-EDS analysis of the sample with the highest value in terms of flexural strength from the option was selected and performed. Here, darker and denser matrix regions and parts of a lighter colored appearance were identified. Even deep cavitation formations due to pull out of the particles from the matrix were observed on the surface of the

sample. SEM images of the slag in its unprocessed (raw) state consist of irregular dispersed particles. However, it was determined that the samples subjected to activation provide a much denser matrix formation. For example, Ca/Si ratio has increased as one goes from “region 1” to point “region 2” in the image in the part a). This suggests the formation of the C-S-H structure in the area “region 2”.

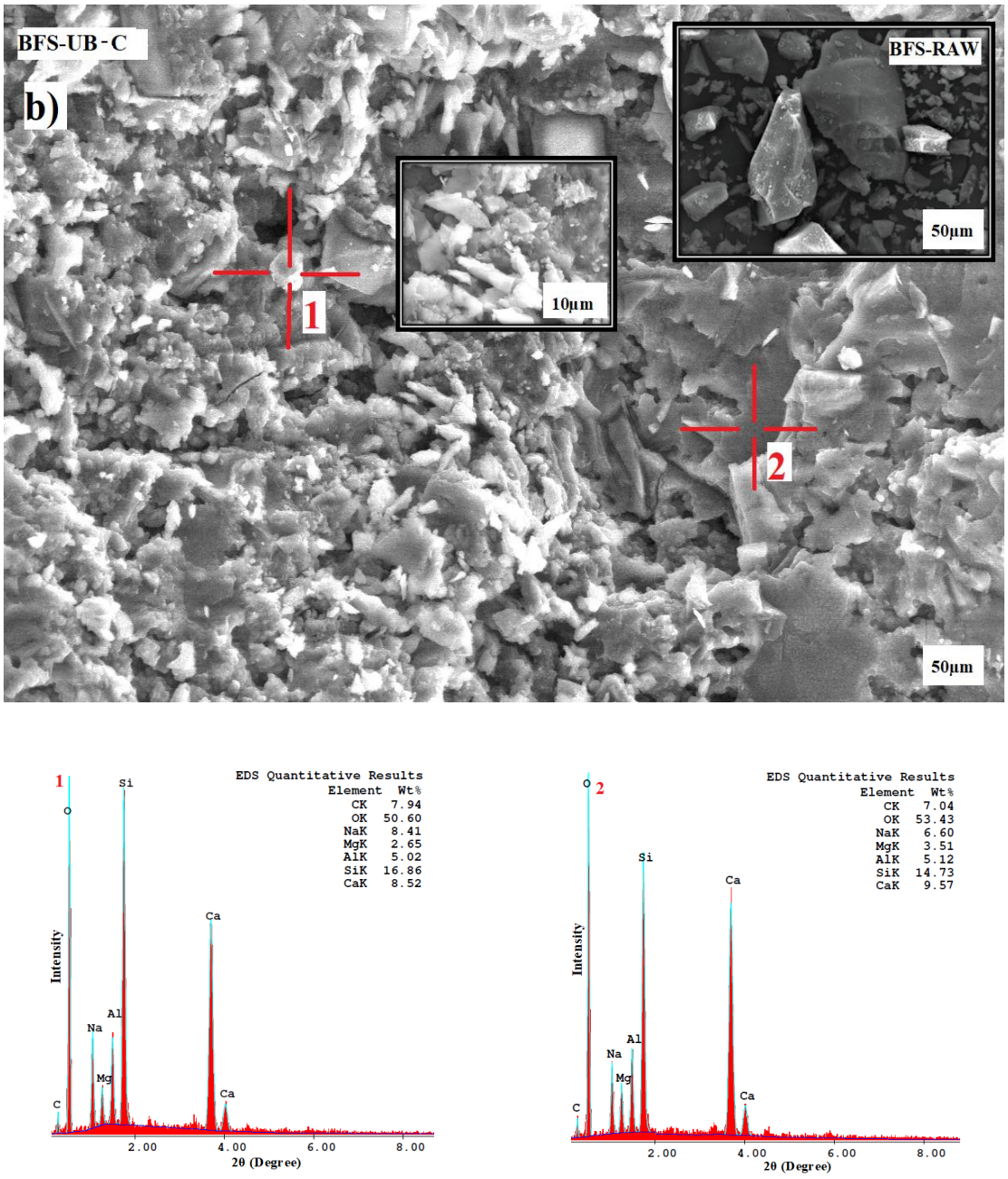


Figure 4.111. SEM-EDS images of the BFS-Raw and the selected samples **a)** BFS-UB-F **b)** BFS-UB-C.

4.7.1.2. Microstructural analysis of the CW-UB samples

✓ *XRD Analysis of the CW-UB*

In Figure 4.112, XRD results of the raw materials of the CW and the alkali activated selected performance giving sample of CW-UB (CW/6/1.2/0.4/Steam) were depicted.

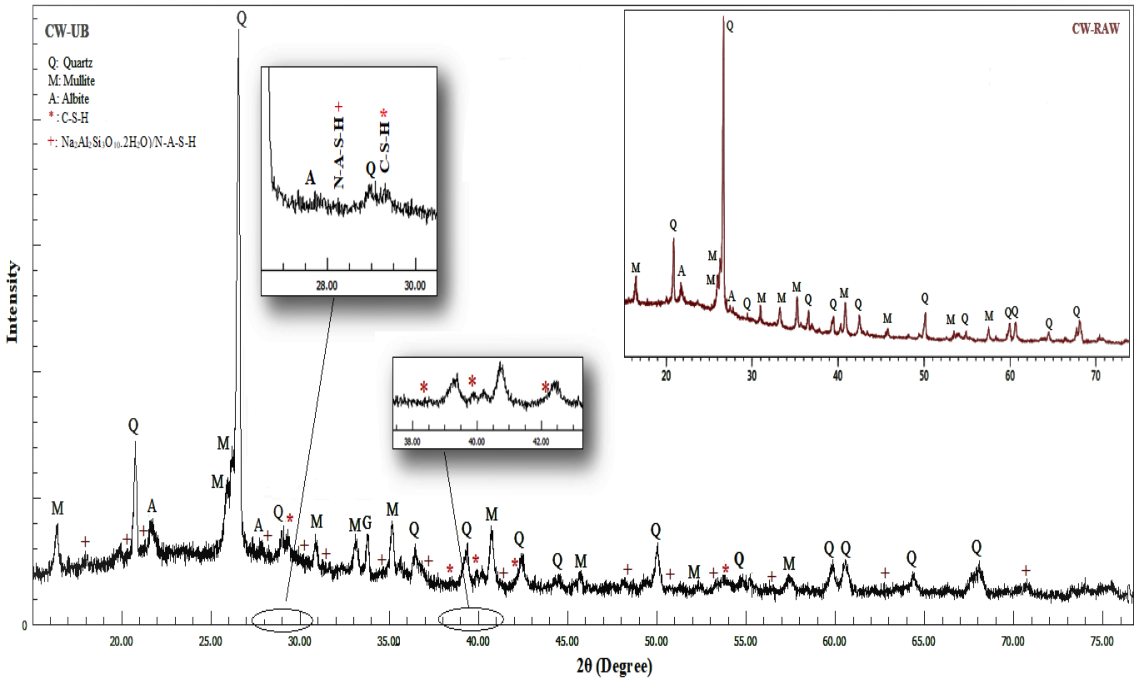


Figure 4.112. XRD pattern of the CW-Raw and selected CW-UB sample.

In the XRD results for raw material characterization of CW, main crystal structures such as quartz, mullite and albite have been identified [43, 46, 92]. The XRD results of the CW-UB sample subjected to alkali activation were also compatible with the crystal structures obtained during raw material characterization of CW and no new crystal phases formation were observed. This situation was quite normal. Because, during geopolymerization reaction, some of the crystalline structures transformed into amorphous inorganic alumina-silicates compounds or binding gel structure [137- 138]. In the alkali activation process, it was found that the peak intensity of the crystal phase detected in the raw material decreased and alkaline activation products were formed [138]. If the intensity of the crystalline phases had not decreased sufficiently, this indicated that the crystalline phases in the raw material were not dissolved enough to participate in the alkali activation process [41].

Alumina-silicate based materials with low Ca^{+2} content were expected to form a bond structure similar to “N-A-S-H” as a result of alkali activation [95]. Since the CW had an alumina-silicate structure, the bond structures expected to be formed as a result of alkaline activation for this example had been “N-A-S-H” bond structures. In our study, this structure manifested itself as the “Natrolite” structure. Natrolite, $Na_2[Al_2Si_3O_{10}].2H_2O$, is one of the fibrous zeolites with the framework constructed from the chains of corner-sharing Al and Si oxygen tetrahedral [139]. In the literature, as a result of alkali activation of ceramic waste, similar to the structure were found, structures rich in sodium, aluminum and silicon ions (wollastonite [41], plagioclases [96], albite [42], gismondine/zeolite [140]) were obtained. In our study, lime ($CaCO_3$) up to 2% of the raw material mass was used in all samples. This lime addition caused the formation of the "C-S-H" bond structure, which was the main bond structure formed during the alkali activation of the batch materials with high CaO ratio. It was determined that the alkaline activated ceramic waste sample created a C-S-H structure for the values of 2 theta degrees for "29.3^{o}", "38.5^{o}", "39.9^{o}", "42.3^{o}" and "54.2^{o}" [47, 88, 141].

✓ *FTIR Analysis of the CW-UB*

In Figure 4.113, FTIR results of the raw materials of the CW and the alkali activated sample of selected performance giving CW-UB (CW/6/1.2/0.4/Steam) were illustrated.

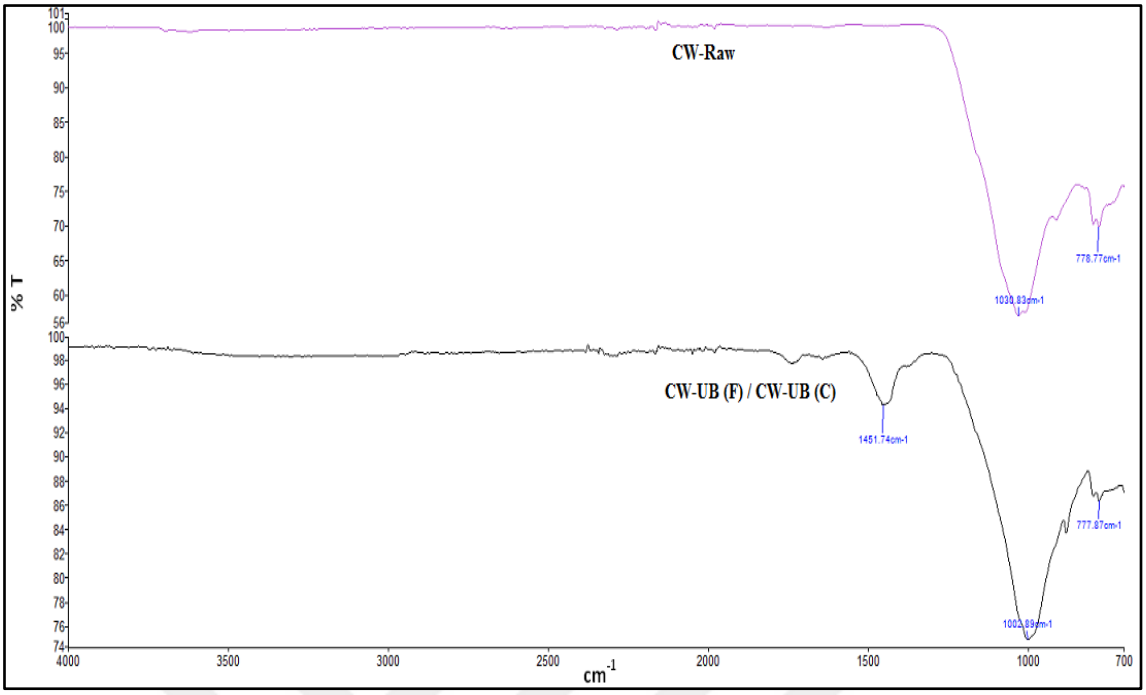


Figure 4.113. FTIR results of the CW-Raw and selected CW-UB sample.

FTIR results obtained in this study and their comparisons with the literature were given in Table 4.24.

Table 4.24. FTIR results of CW-Raw and CW-UB obtained in this study and their comparisons with the literature.

	CW-UB			
	Band No	**Wavenumber cm^{-1}**	**Attribution**	**Reference**
CW-Raw	1	1084	Si-O	[43, 88, 142]
	2	778	Si-O	[43, 88, 142]
	3	697	Si-O	[43, 88, 142]
	4	668	Si-O	[43, 88, 142]
CW-UB	1	1451	O-C-O/ Carbonates	[88, 143]
	2	1002	asymmetric stretching vibrations generated by the T–O–T bonds (T: Si or Al)/ N-A-S-H	[43, 46]
	3	777	Si-O	[43, 88, 142]

According to the FTIR results of the raw CW, four different IR bands were formed for the wavelengths of 1084, 778, 697 and 668 cm^{-1}. These bands for raw ceramic waste were a series of IR spectrum tapes that support the presence of quartz [43, 88, 142]. This supported the XRF analysis results (73% SiO_2 and 21% Al_2O_3) obtained during the

characterization of raw CW in our study and the presence of the quartz structure obtained for XRD analysis (see Table 3.2 and Figure 3.4).

As a result of the alkali activation of CW, three main IR bands were observed. These bands were realized in wavelengths of 1451, 1002 and 777 cm^{-1}, respectively. In this study, it was found that IR band formed in 1084 cm^{-1} band for raw ceramic waste shifted to 1002 cm^{-1} wavelength after alkaline activation of CW-UB. Similarly, in the literature, it was observed that the IR band formed at 1070 cm^{-1} wavelength for raw CW shifted to 1013 cm^{-1} wavelength after the alkali activation process [43]. In another study, it was reported that the IR band of 1080 cm^{-1} wavelength for raw CW shifted to 1000 cm^{-1} band after alkaline activation [46]. It was agreed that the IR bands, which slide into the 1000-1020 cm^{-1} wavelength range after ceramic activation, represented N-A-S-H bond structures formed as a result of activation of CW-UB [43, 46, 95]. This was considered to be caused by the addition of Al^{+4} ions in the Si-O-Si skeleton structure within the CW during the alkali activation process [144-145]. Therefore, it was determined that the N-A-S-H bond structure shown as a proof of polymerization of SiO_2 rich raw materials (fly ash, metakaolin etc.) was detected in alkali activation of the CW-UB used in our study [95].

In this study, three different Na_2O ratio (n ratio) was used for alkali activation of CW-UB and it was found that the selected mechanical properties were obtained for the highest percentage of Na_2O ratio (n=6). Similarly, in the literature, it has been reported that as the sodium concentration [Na^+] in the alkali activation process increased, the IR band was shifted to smaller wavelengths but showed better mechanical properties [46]. Finally, for the alkaline activation of CW-UB, it was thought that the IR band formed at 1452 cm^{-1} wavelength expresses a carbonate structure [92, 143].

✓ *SEM-EDS Analysis of the CW-UB*

In Figure 4.114, SEM-EDS image of the raw materials of the CW and the alkali activated sample of selected performance giving sample of CW-UB (CW/6/1.2/0.4/Steam) were shown.

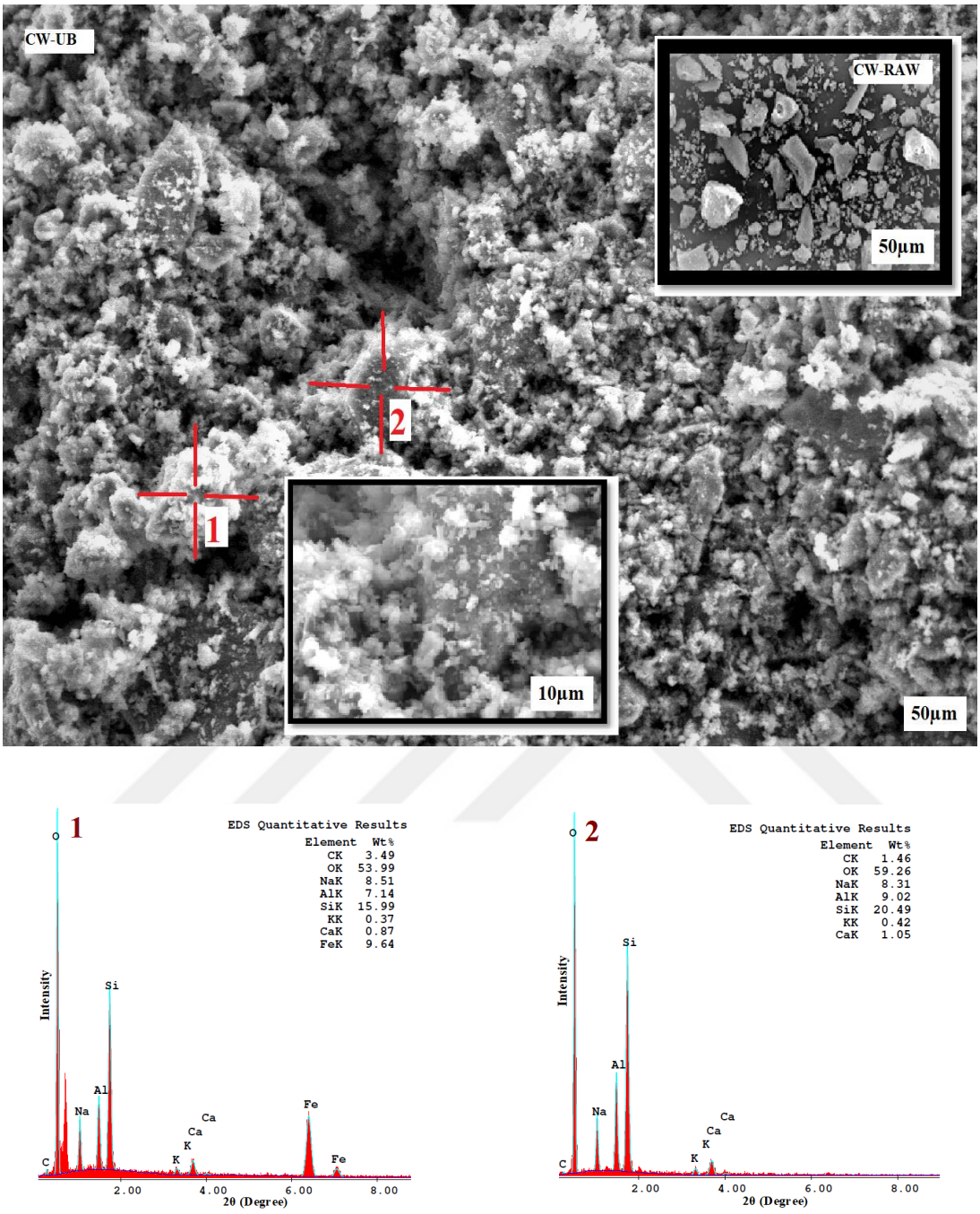


Figure 4.114. SEM-EDS images of the CW-Raw and selected CW-UB sample.

When the SEM image was taken and examined for characterization of the raw form of CW, it was observed that it had an irregular and relatively smooth structure [41, 46, 82, 146]. In addition, the line spectrum of the sample, determined by using EDS unit, indicated the presence of oxygen (O), silicon (Si) and aluminum (Al) as a main element in the sample with a trace of sodium (Na), calcium (Ca), and iron (Fe) as impurities

element [141]. It can be said that CW maintained its irregular or angular shape after the alkaline activation process. CW-UB samples disclosed dense and fragmented morphology with a high amount of unreacted starting powders [82]. In SEM images, dense structures (region 2) occupied much less space than other non-dense structures (region 1). It showed that Si, Al and Na contents of structures that appeared more densely as a result of EDS analysis were higher than structures that appeared less dense. This was confirmed in the study of Hwang et al [82]. It was stated that the formation of alumina-silicate gel was more in places where there was Si and Al increased in the structures and this situation supported the increase in strength of the samples [82, 141]. In our study, the low strength values obtained by alkali activation of CW-UB was due to the low occurrence of alumina-silicate gel structure and most of the ceramic particles did not appear to be reacted. Unlike the strength values obtained in this study, Sun et al. obtained higher strength values (about 60 MPa) for alkali activated of ceramic waste than value we obtained. In addition to the study conducted by Reig et al., alkali activated ceramic waste samples with high Na^+ content had high strength values and SEM images of these samples exhibited a much more compact structure compared to those with low sodium content [41].

4.7.1.3. Microstructural analysis of the MW-UB samples

✓ *XRD Analysis of the MW-UB*

In Figure 4.115, XRD results of the raw materials of the MW and the alkali activation sample of selected MW-UB (MW/4/1.8/0.4/Steam) were given.

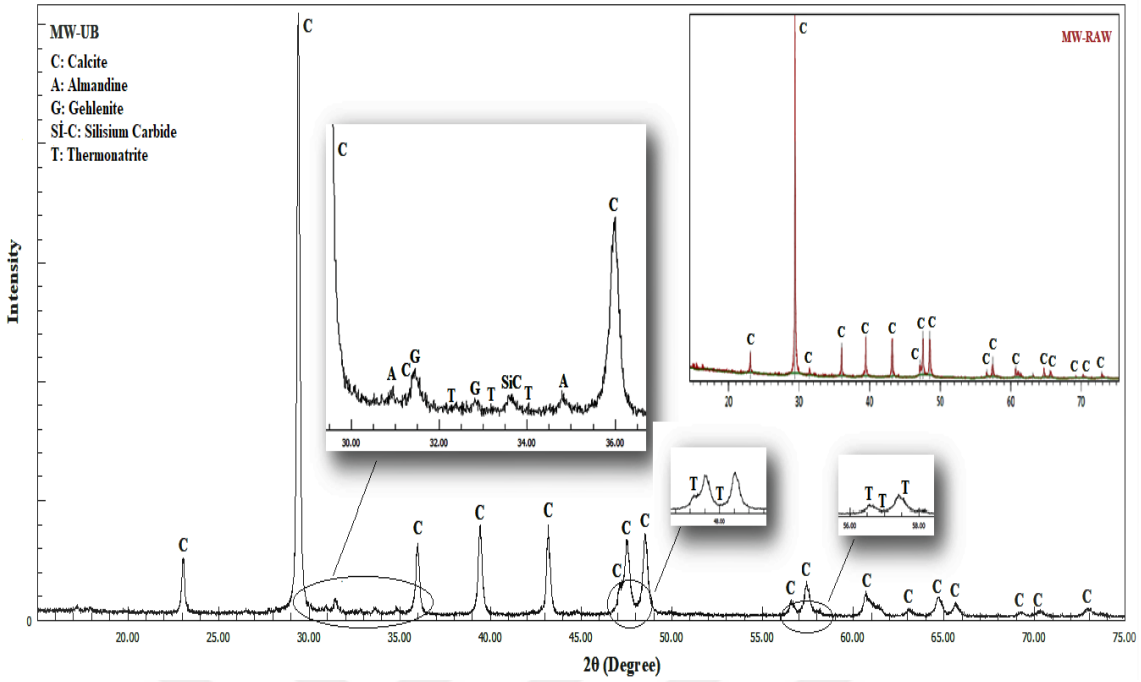


Figure 4.115. XRD pattern of the MW-Raw and selected MW-UB sample.

The MW used in this study was obtained by processing the marble mud formed by combining water and marble dust during the extraction and cutting of the large marble blocks in marble production areas. For this reason, a very large amount of calcite ($CaCO_3$) structure was dominant in the XRD pattern of raw marble waste as reported in the literature [51-52, 147]. XRF results were in line with XRD analysis, confirming the presence of calcium carbonate as main constituent (see Table 3.2).

The main phase peaks obtained as a result of XRD analysis of alkali activated marble waste did not differ much from the peaks obtained for raw marble waste. This results in the marble waste did not dissolve too much in the relevant activator solution and did not form a new phase [51, 53]. But some new phases had also been observed. These phases were Almandine ($Mg_3Al_2\ (SiO_4)_3$), Gehlenite ($Ca_2Al[AlSiO_7]$), Silicon Carbide (SiC), Thermonatrite ($Na_2CO_3H_2O$) [51, 53] structures. The presence of these phases indicated that some of the marble waste reacted with alkaline solutions.

In this study, the highest flexural and compressive strength values (1.33 and 2.83 MPa, respectively) for the alkaline activation of MW were found to be decrease in parallel with the phases contained in the MW-Raw which is not dissolved sufficiently in the alkaline activator solution and the new reaction products were not detected. In this study, after curing period of 1, 7, 14, 28 and 90-days, strength values were recorded. In

a very limited number of studies on the alkali activation process of the marble sludge in the literature, it was found that the strength increase in the alkaline activation process of the limestone powder (which is very close to marble waste in terms of chemical phase structure) increased considerably especially after 120 days. The strength increase of alkali activation of limestone powder at the end of 1 year (about 18 MPa) was approximately 8 times higher the strength value of 28 days (about 3 MPa) [52]. In this case, it was concluded that late strength values were higher than early strength's in alkali activation process for MW-UB.

✓ *FTIR Analysis of the MW-UB*

In Figure 4.116, FTIR results of the raw materials of the MW and the alkali activated sample of selected performance giving MW-UB (CW/4/1.8/0.4/Steam) were shown.

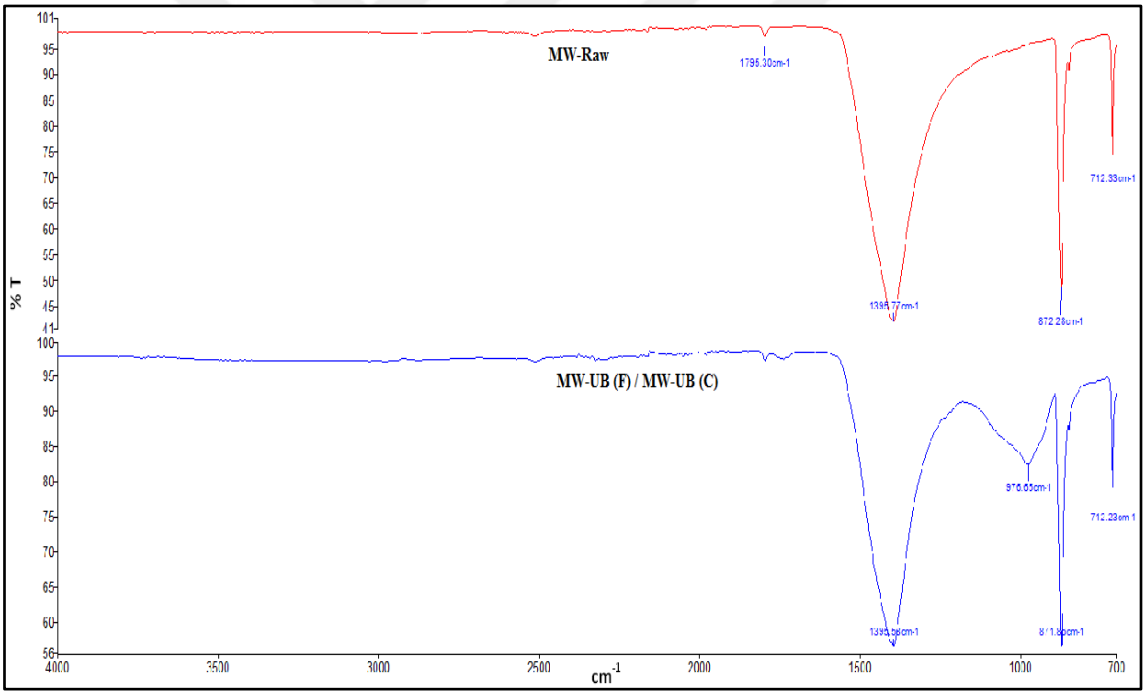


Figure 4.116. FTIR results of the MW-Raw and selected MW-UB sample.

Since there were a limited number of publications in the literature about the MW-UB, the number of studies involving the bond structure of MW-UB was also very few. FTIR results obtained in this study and their comparisons with the literature were given in Table 4.25.

Table 4.25. FTIR results of MW-Raw and MW-UB obtained in this study and their comparisons with the literature.

	MW-UB			
	Band No	**Wavenumber cm^{-1}**	**Attribution**	**Reference**
MW-Raw	1	1795	C=O / CO_3^{-2}	[148, 51]
	2	1395	C=O / Thermonatrite	[52]
	3	872	C=O / CO_3^{-2}	[148, 51, 149]
	4	712	C=O / CO_3^{-2}	[52]
MW-UB	1	1795	C=O / CO_3^{-2}	[148, 51]
	2	1395	C=O / Thermonatrite	[52]
	3	976	Si-O stretching vibrations/ C-S-H	[95,149-150]
	4	871	C=O / CO_3^{-2}	[148, 51, 149]
	5	712	C=O / CO_3^{-2}	[52]

In this study, it was observed that MW-Raw had 4 main IR bands as a result of FTIR analysis. These bands were IR bands that occur in wavelengths of 1795 [51,148], 1395 [52], 872 [51, 148-149] and 712 [52] cm^{-1}. They were formed as a result of symmetrical and asymmetrical vibrations of the carbonate ion [51]. According to the results of this analysis, the calcite structure of the marble sludge used in the study was confirmed by XRF and XRD analysis results (see Table 3.2 and Figure 3.5).

The IR bands obtained as a result of the MW-UB showed very similarity with the IR bands of the MW-Raw. This was in line with the XRD results, which showed that no new phase formation had occurred as a result of alkali activation of MW-UB. The formation of 4 main IR bands for raw marble waste after alkaline activation could be considered as an indication that the CO_3^{-2} existence continued. However, as a result of activation of MW-UB, an IR band with a wavelength of 976.65 cm^{-1} was observed, unlike the analysis results of MW-Raw. The band formed at this wavelength showed Si-O stretching vibrations bond structure, which was one of the most typical indicators of the main bonding structure of cement (C-S-H bond structure) [95, 149-150]. This proved that in the process of activation of MW-UB, there was a binding structure similar to the bond structure of cement.

✓ *SEM-EDS Analysis of the MW-UB*

In Figure 4.117, SEM-EDS image of the raw materials of the MW and the alkali activation sample of the selected performance giving MW-UB (CW/4/1.8/0.4/Steam) were depicted.

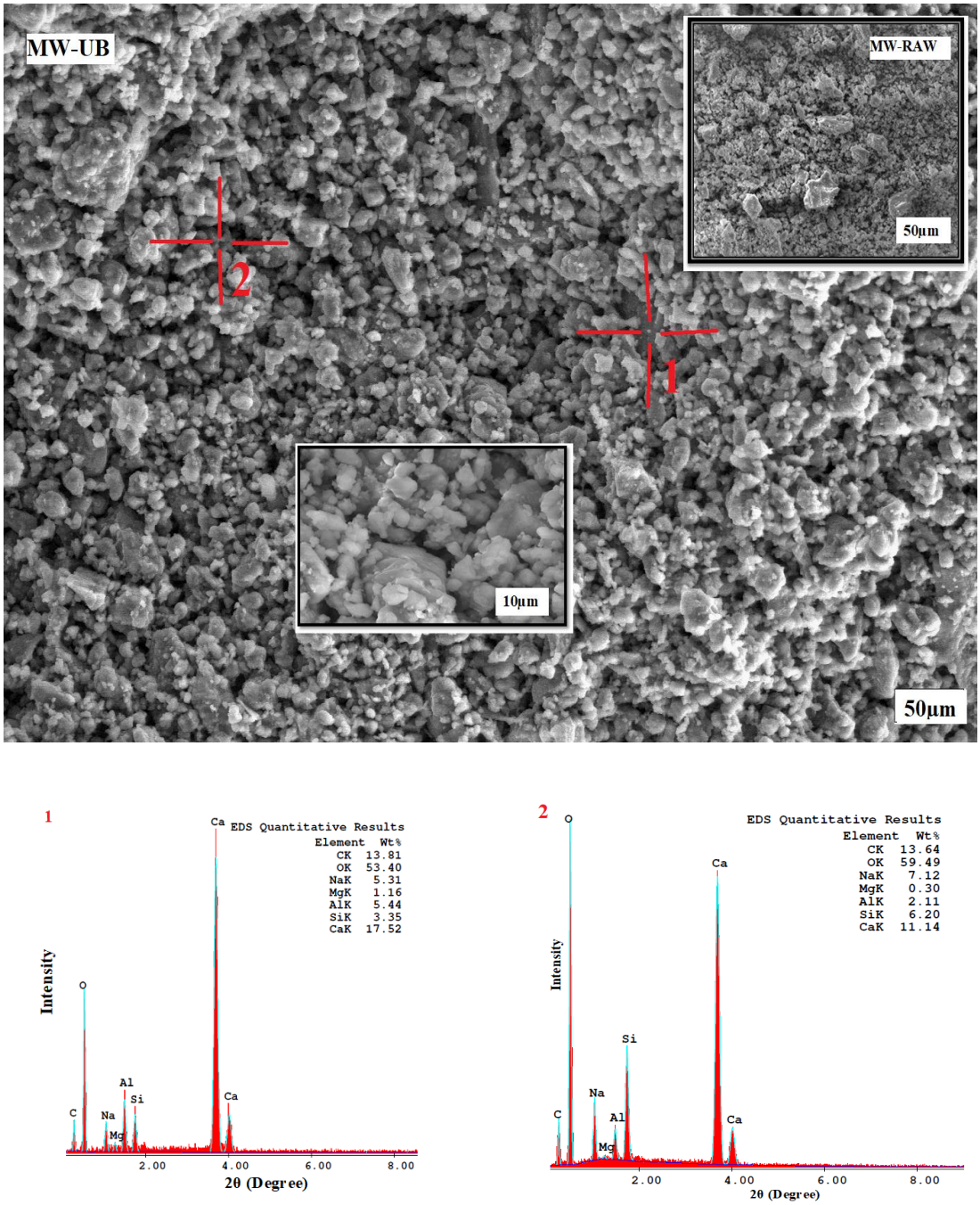


Figure 4.117. SEM-EDS images of the CW-Raw and selected CW-UB sample.

While the amount of Ca^{+2} was higher at the region "1" than the region "2", the amount of Na, Si and Al ions was much lower. Therefore, it could be attributed that region "1" belonged to unreacted marble waste particles. However, considering the region "2", it was observed that the Ca^{+2} ratio decreased but Na, Si and Al ions increased. This situation supported the increase of reaction products resulting from alkaline activation at these points. Similar to our study results, it was stated that the high Si, Ca and Na content obtained in EDS analysis supports the precipitation of silica gel and calcium silicate hydrates in the study carried out by Ortega-Zavala et al. In fact, if the amount of Na^{+} was high enough, it was stated that the C-S-H bond structure evolved into the N-A-S-H bond structure [52]. In addition to all these, it was emphasized in another study that Ca-Si matrix formation in the activation structure of the products formed as a result of activation of marble waste with sodium silicate and sodium hydroxide mixture solution [51].

4.7.2. Microstructural analysis of the selected binary binders

4.7.2.1. Microstructural analysis of the BFS/CW-BB samples

✓ *XRD Analysis of the BFS/CW-BB*

In Figure 4.118, XRD results of the alkali activated samples of selected BFS/CW-BB according to flexural (2BFS/2CW/6/1.2/0.4/Steam) and compressive strength (3BFS/1CW/6/1.2/0.4/Steam) were given.

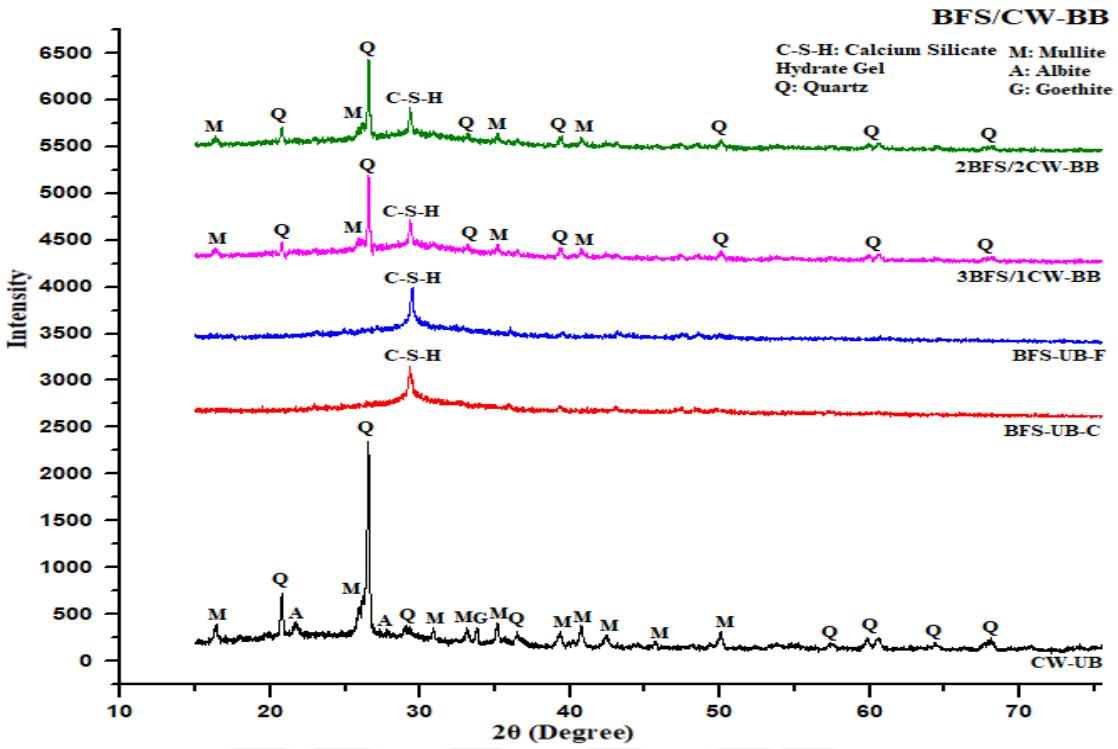


Figure 4.118. XRD pattern of the selected BFS/CW-BB sample.

Only the formation of an amorphous phase and a pronounced C-S-H peak in the BFS were remarkable. However, as the amount of CW in the BFS increased, a distinct Quartz peak occurred. This increases the density of the crystal peaks and caused a higher crystallization degree [103, 151]. Quartz peak had a greater intensity value in the 2BFS/ CW-BB sample where the CW is around 50% compared to the 3BFS/1CW-BB sample where the ceramic waste amount was 25%. This situation was caused by the increase in the amount of SiO_2 due to the increase in the amount of unreacted CW in the sample. This behavior was observed in a similar way due to the increase in the amount of CW where ceramic waste was replaced in ternary slag/fly ash systems [49] or in slag/fly ash binary component alkali activation systems [66].

✓ *FTIR Analysis of the BFS/CW-BB*

In Figure 4.119, FTIR results of the alkali activation samples of selected performance giving BFS/CW-BB according to flexural (2BFS/2CW/6/1.2/0.4/Steam) and compressive strength (3BFS/1CW/6/1.2/0.4/Steam) were illustrated.

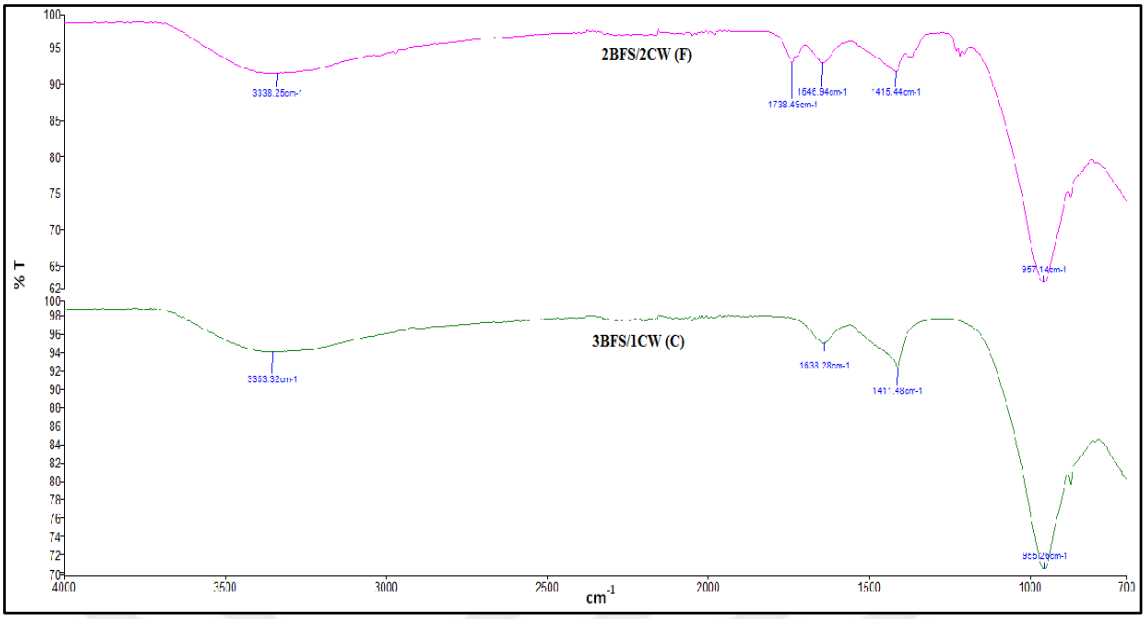


Figure 4.119. FTIR results of the selected BFS/CW-BB samples.

FTIR results obtained in this study and their comparisons with the literature were given in Table 4.26.

Table 4.26. FTIR results of BFS/CW-BB obtained in this study and their comparisons with the literature.

	BFS/CW-BB			
	Band No	**Wavenumber cm^{-1}**	**Attribution**	**Reference**
3BFS/1CW-BB	1	3353	O-H Stretching	[133-135]
	2	1638	H-O-H Bending	[133-135]
	3	1411	v3$[CO3]^{-2}$	[129, 133]
	4	955	Si-O asymmetric stretching/C-(N)-A-S-H	[129, 133-134]
2BFS/2CW-BB	1	3338	O-H Stretching	[133-135]
	2	1646	H-O-H Bending	[133-135]
	3	1415	v3$[CO3]^{-2}$	[129, 133]
	4	957	Si-O asymmetric stretching/ C-(N)-A-S-H	[129, 133-134]

When the results in Table 4.26 were evaluated, it represented the Si-O bond formed for the 955-957 cm^{-1} IR band, which was thought to belong to the reaction product. Considering the FTIR results of the single component BFS and CW samples, it was observed that the IR peak, where this reaction product was formed, increased as the amount of CW in the samples increased [47].

✓ *SEM-EDS Analysis of the BFS/CW-BB*

In Figure 4.120, SEM-EDS results of the alkali activation samples of selected BFS/CW-BB according to flexural (2BFS/2CW/6/1.2/0.4/Steam) and compressive strength (3BFS/1CW/6/1.2/0.4/Steam) were given.

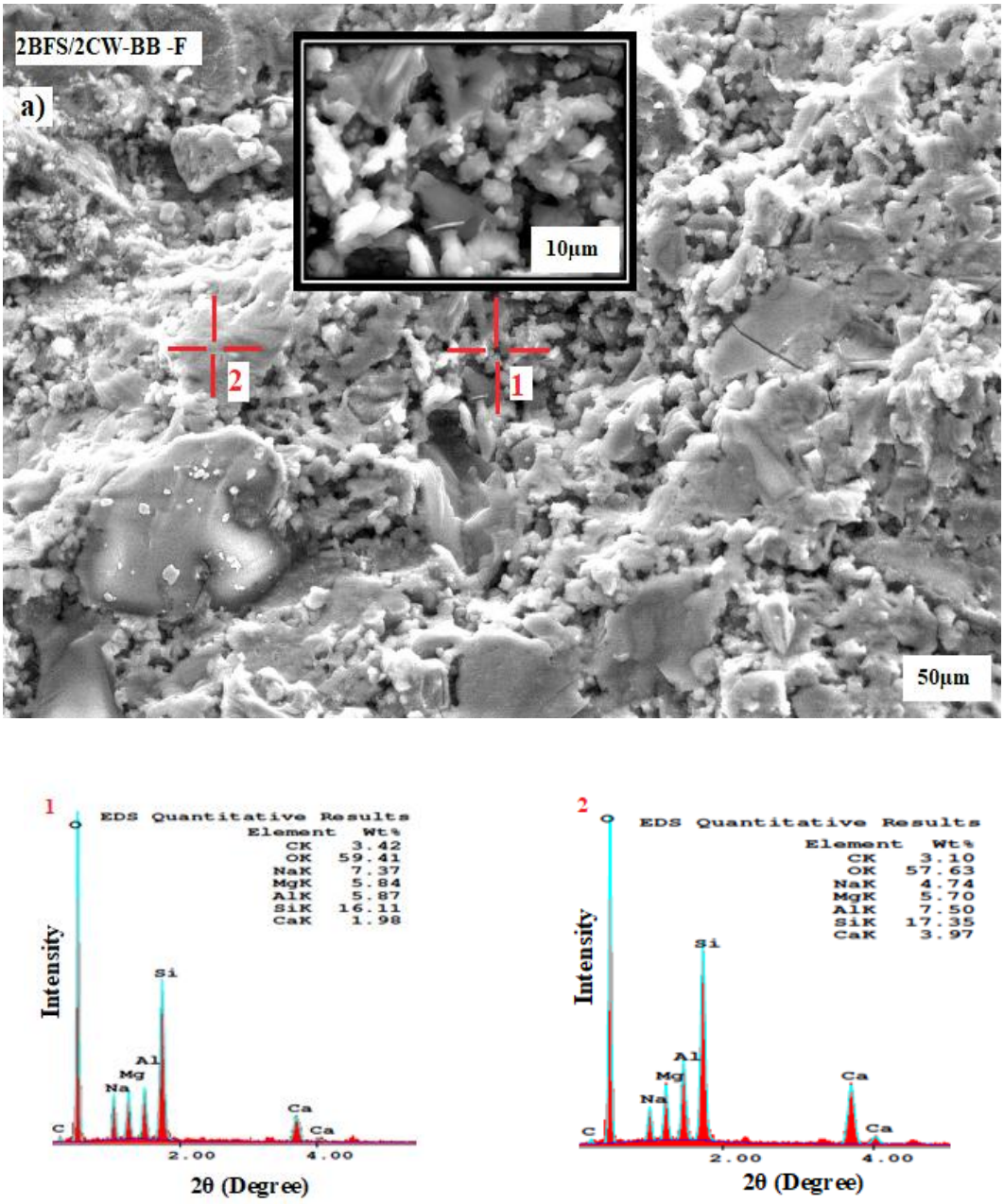


Figure 4.120. SEM-EDS images of the selected BFS/CW-BB samples a) BFS/CW-F b) BFS/CW-C

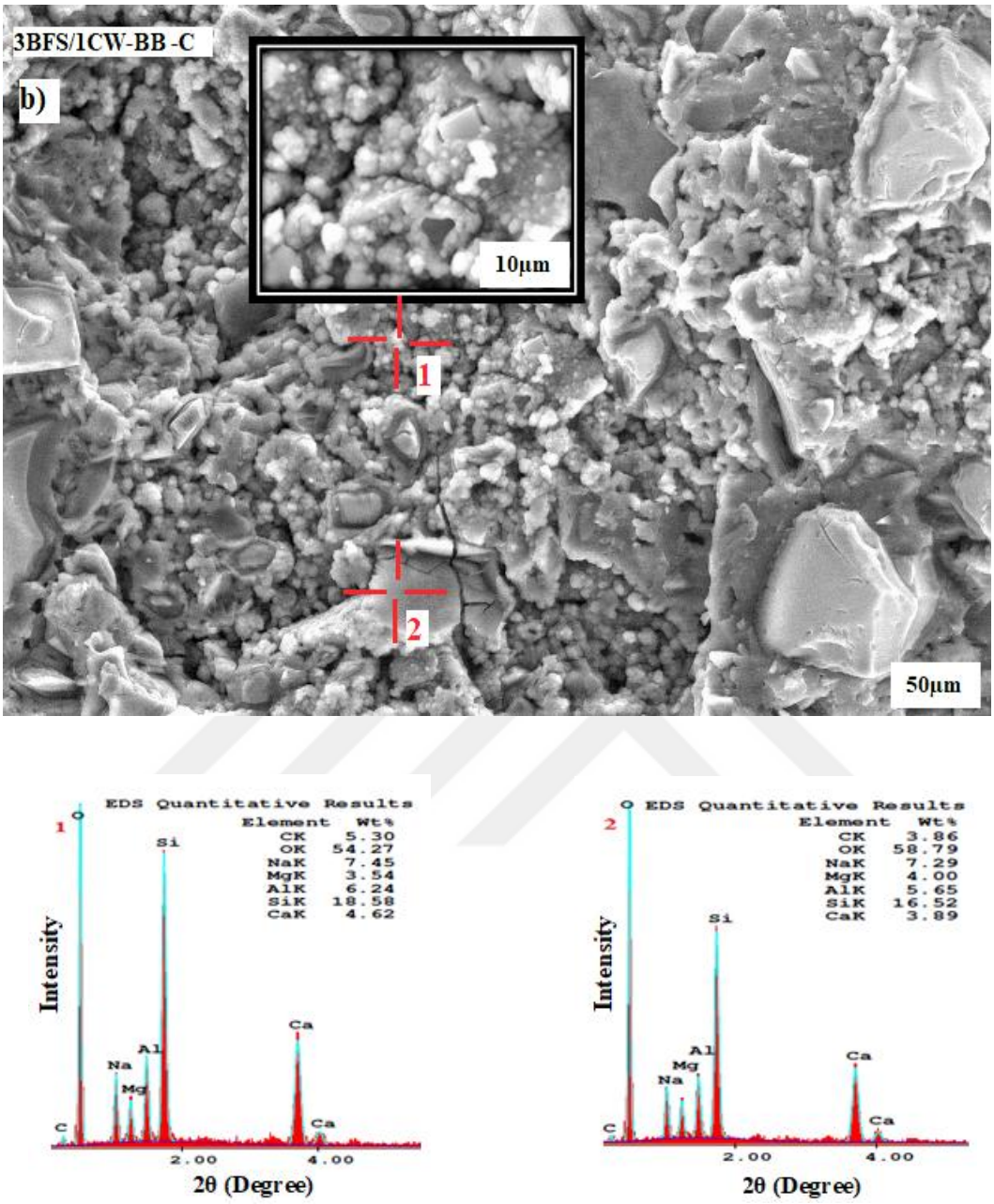


Figure 4.120. (continue) SEM-EDS images of the selected BFS/CW-BB samples a) BFS/CW-F b) BFS/CW-C

When Figure 4.120, was evaluated generally, the ratio of CaO/SiO_2 determined in Figure 4.120/a was approximately 30% less than Figure 4.120/b and the ratio of SiO_2/Al_2O_3 was almost the same. This situation was expected. Because the slag rate in the sample in Figure 4.120/a was 50% higher than Figure 4.120/b, and the CW rate was 50% less. Therefore, the presence of CaO increased and the presence of SiO_2 decreased in Figure 4.120/b. This increased the CaO/SiO_2 ratio in Figure 4.120/b. It was thought

that increasing this ratio increased the compressive strength value of the product as reported in the literature [151-152]. In both case, CaO and SiO_2 they were both matrix forming structures containing reaction products, partially reacted particles and unreacted particles in the microstructures [47]. In addition, it was determined that as the amount of ceramic waste in the samples increased, the amount of Si ions obtained as a result of EDS analysis increased. The main reason for this was the CW that did not react to BFS in the samples due to its inert phases present quartz and mullite. This behavior caused the samples to be more porous and therefore less resistant to chemical affect [47].

Considering Figure 4.120/a, the ratio of CaO/SiO_2 at point "number 2" was 45% higher than the ratio of CaO/SiO_2 at point "number 1". The increase in the CaO/SiO_2 ratio suggested that a reaction product such as (C-A-S-H) or (C, N) -A-S-H was formed at the point number 2 [152]. Similarly, since the ratio of CaO/SiO_2 and SiO_2/Al_2O_3 was higher in the region "1" in Figure 4.120/b, it was thought that a reaction product formed in that region that provides strength gain due to C-S-H phase presence confirmed by XRD analysis (Figure 4. 118).

4.7.2.2. Microstructural analysis of the BFS/MW-BB samples

✓ *XRD Analysis of the BFS/MW-BB*

In Figure 4.121, XRD results of the alkali activation samples of the selected performance giving samples (BFS/MW-BB) according to flexural (2BFS/2MW/4/1.2/0.4/Steam) and compressive strength (2BFS/2MW/6/1.2/0.4/Steam) were shown.

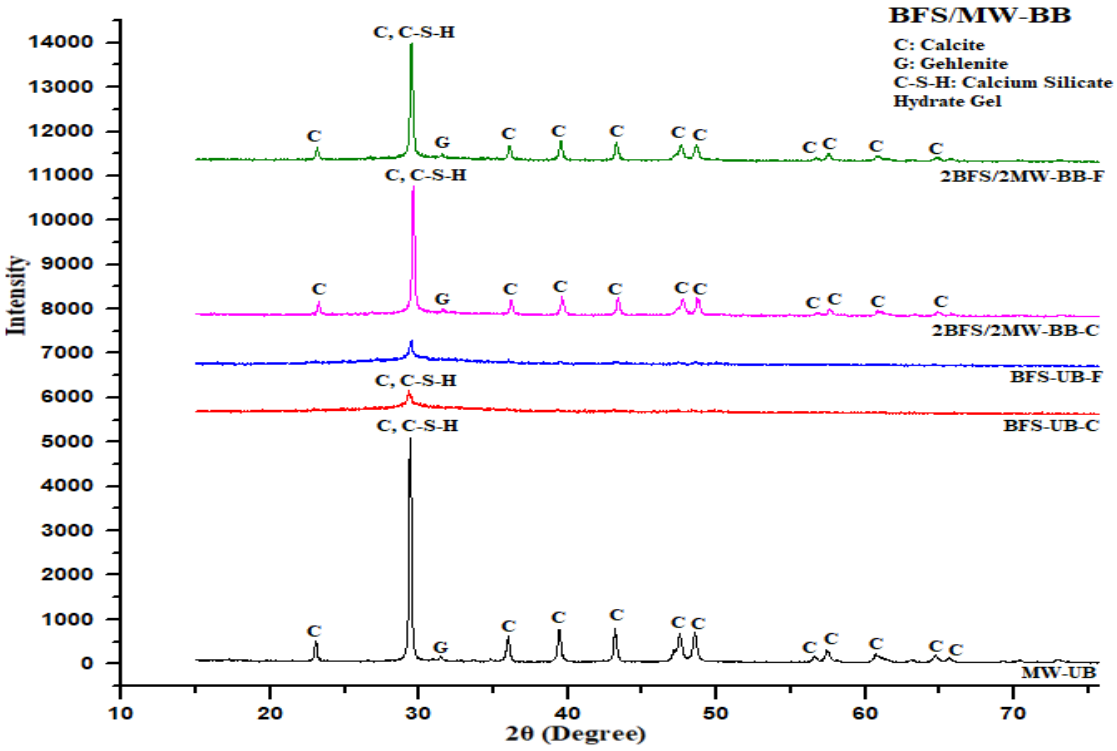


Figure 4.121. XRD pattern of the selected BFS/MW-BB sample.

The peaks obtained in the BFS/MW-BB binary component system were very similar to the peaks obtained in the one-component alkaline activation system of MW. The determination of the phases formed by MW and BFS as a single component during the alkali activation process has been detailed in the previous sections (see Figure 4.109 and Figure 4.115). Unlike these peaks, no crystal phase formation was observed. The most prominent and high intensity phase was the calcite phase. In addition to the calcite phase, other minor phases were formed and identified in the microstructure such as thermonatrite ($Na_2CO_3 \cdot H_2O$) and gehlenite ($Ca_2Al\ [AlSiO_7]$). According to the XRD results of blast furnace slag and MW, it was determined that a new phase was not formed in the system with these two components. Similarly, this result is in good agreement with the literature. It was reported that limestone and slag combinations did not react chemically and did not form a new phase according to XRD results [57]. In addition, it was stated that the formation of a crystalline phase could not be detected in alkali activated products consisting of a mixture of limestone, slag and fly ash [59]. In this case, it was understood that the MW did not react chemically with the blast furnace slag, but physically formed higher packing density by filling the micro cracks in the BFS [57, 59]. It was known that limestone refined particle packing by reducing the pore

volume in the slag/fly ash mixture and thus provides strength increase [60]. This cause one of the reasons to increase in flexural and compressive strength for the samples in our study which can be attributed to "higher packing effect" because of the presence of limestone in the samples.

In the XRD patterns (Figure 4.121) obtained in this study, it was observed that calcite and C-S-H peak overlap each other. It was thought that MW contributed to the formation of the C-S-H bond structure. Because of the Ca/Si ratio in the system increased with the addition of MW into the system. It was thought that this situation increased the pH value of the environment and decreased the polymerization compared to alkaline environments with high Si ratio [95]. This was confirmed by FTIR results in the following sections (see Figure 4.122). As a result, the FTIR absorption peak that occurred around 975-978 cm^{-1} in environments with high SiO_2 shifts to lower wavelengths (950-955 cm^{-1}) as the CaO ratio in the structure increased. In this study, FTIR absorption peak for BFS/MW-BB samples were formed at approximately 955 cm^{-1} wavelengths.

✓ *FTIR Analysis of the BFS/MW-BB*

In Figure 4.122, FTIR results of the alkali activation samples of selected performance giving sample BFS/MW-BB according to flexural (2BFS/2MW/4/1.2/0.4/Steam) and compressive strength (2BFS/2MW/6/1.2/0.4/Steam) were shown.

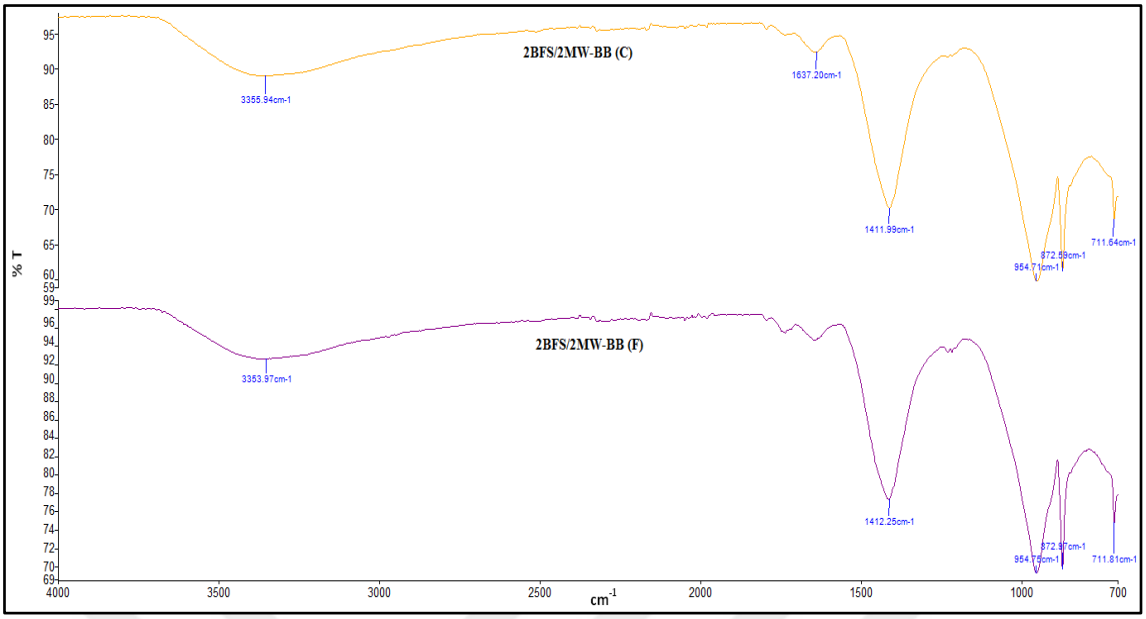


Figure 4.122. FTIR results of the selected BFS/MW-BB samples.

FTIR results obtained in this study and their comparisons with the literature were given in Table 4.27.

Table 4.27. FTIR results of BFS/MW-BB obtained in this study and their comparisons with the literature.

	BFS/MW-BB			
	Band No	**Wavenumber cm^{-1}**	**Attribution**	**Reference**
BFS/MW-BB -F	1	3553	O-H Stretching	[133-135]
	2	1637	H-O-H Bending	[133-135]
	3	1412	v3$[CO3]^{-2}$	[129, 133]
	4	954	Si-O asymmetric stretching/C-S-H	[129, 133-134]
	5	872	C=O / CO_3^{-2}	[51, 148-149]
	6	711	C=O / CO_3^{-2}	[52]
BFS/MW-BB -C	1	3555	O-H Stretching	[133-135]
	2	1635	H-O-H Bending	[133-135]
	3	1411	v3$[CO3]^{-2}$	[129, 133]
	4	954	Si-O asymmetric stretching/C-S-H	[129, 133-134]
	5	872	C=O / CO_3^{-2}	[51, 148-149]
	6	711	C=O / CO_3^{-2}	[52]

All IR peaks in the Table 4.27 were similar to the peaks obtained in unary component alkaline activated systems of BFS and MW. The Si-O band, which was the indicator of the C-S-H bond structure occurring in the 950 cm^{-1} band only in BFS-UB systems,

shifted to the 954 cm^{-1} band for BFS/MW-BB systems. A new phase was not formed according to the XRD results (Fig. 4.121) for this binary system which was also confirmed by FTIR results.

✓ *SEM-EDS Analysis of the BFS/MW-BB*

In Figure 4.123, SEM-EDS results of the alkali activation samples of the selected performance giving samples BFS/MW-BB according to flexural (2BFS/2CW/4/1.2/0.4/Steam) and compressive strength (2BFS/2MW/6/1.2/0.4/Steam) were depicted.

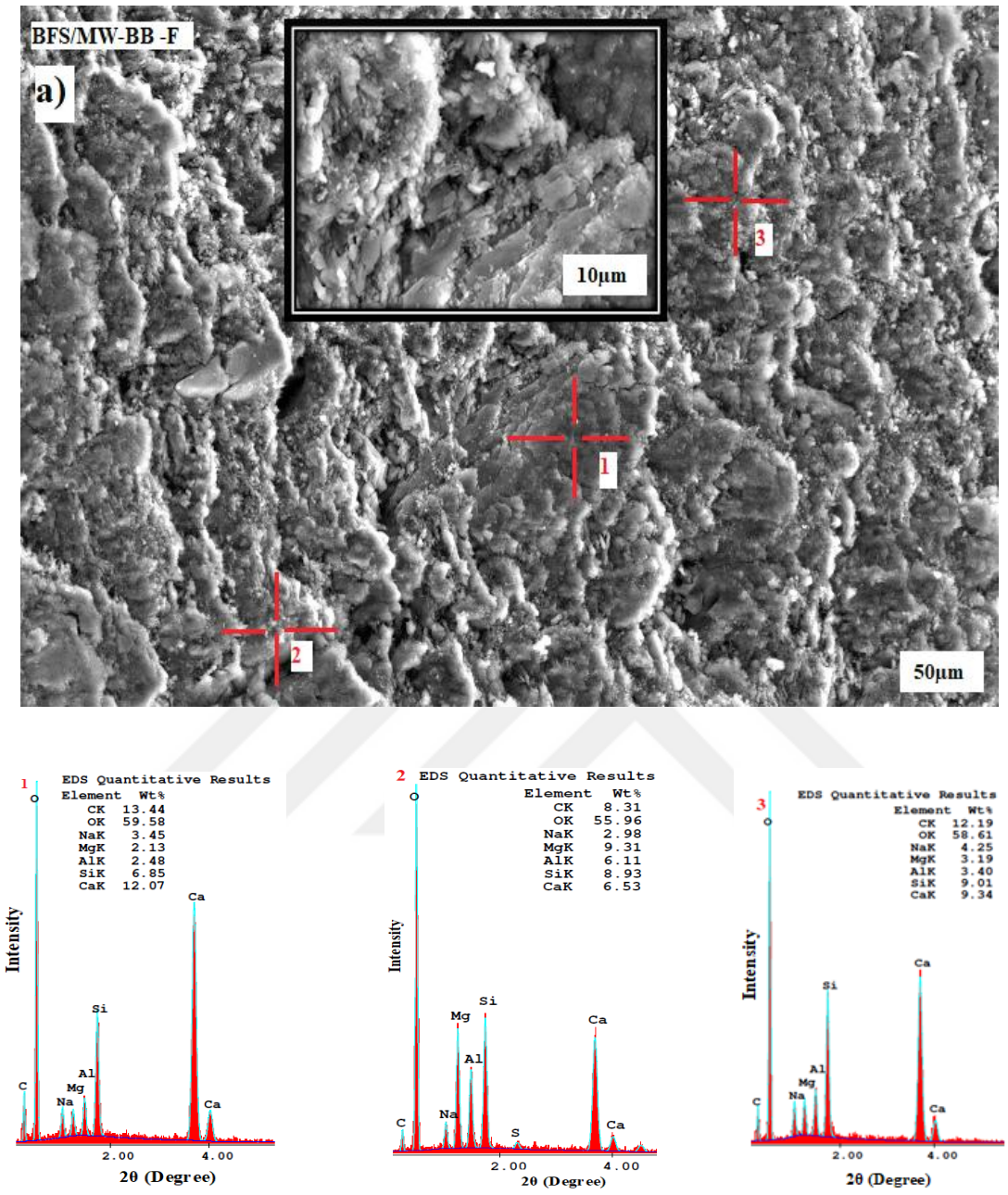


Figure 4.123. SEM-EDS images of the selected BFS/MW-BB samples a) BFS/MW-F b) BFS/MW-C.

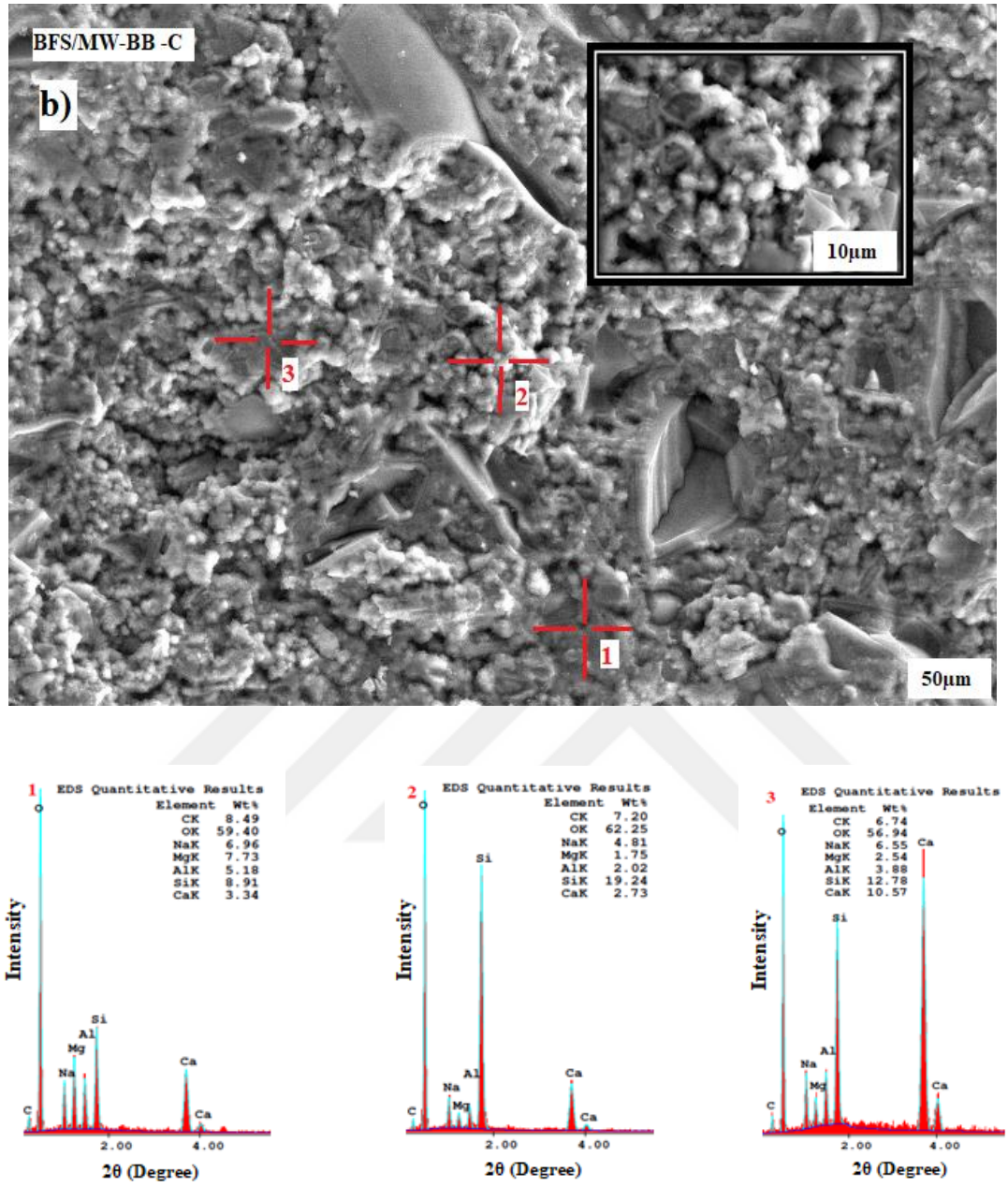


Figure 4.123. (continue) SEM-EDS images of the selected BFS/MW-BB samples a) BFS/MW-F b) BFS/MW-C.

In Figure 4.123/a, BFS-MW-BB (F) combination which gave the selected result in terms of flexural strength was given. In this combination, “regions 1 and 3” with high Ca/Si ratio were thought to be the regions containing the reaction product. In the literature, the mixture containing BFS and limestone was activated with sodium carbonate and it was stated that the Ca/Si ratio of the resulting reaction product C-S-H bond structure was greater than that of other alkali activated systems. It was stated that

this was due to the excessive calcite structure within the mixing [57]. The excess Si ion in the area “region 2” in Figure 4.123/a might be due to the concentration of unreacted sodium silicate activator.

Figure 4.123/b showed the BFS-MW-BB (C) combination that gave the selected result in terms of compressive strength. In this image, the regions that appeared darker and without spaces (region 3) were thought to be regions belonging to the reaction product. In these regions, the Ca/Si ratio was higher than other light-colored and granular structures. The granular and light gray areas (region 1 and 2) were thought to belong to non-reacting or partially reacting source materials and/or alkaline activators.

4.7.2.3. Microstructural analysis of the CW/MW-BB samples

✓ *XRD Analysis of the CW/MW-BB*

In Figure 4.124, XRD results of the alkali activation samples of the selected performance giving sample CW/MW-BB according to flexural and compressive strength (2CW/2MW/2/1.2/0.4/Steam) were given below.

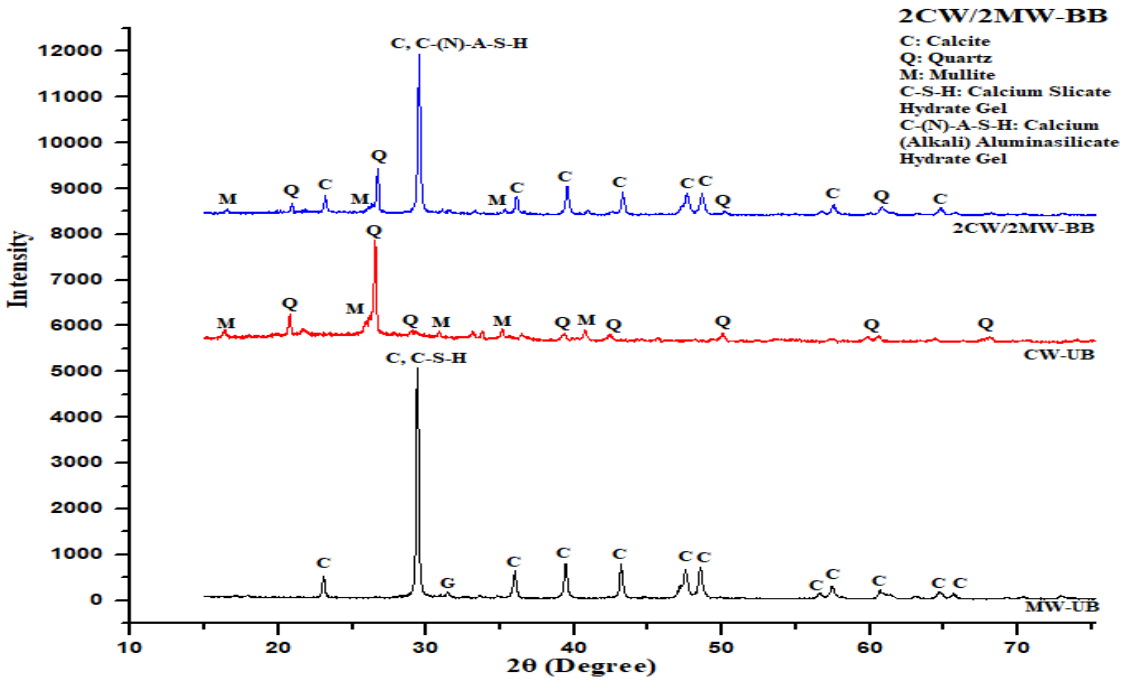


Figure 4.124. XRD pattern of the selected CW/MW-BB sample.

There was no publication in the literature involving the combined alkali activation of CW and MW. However, there were studies involving alkali activation of materials such as fly ash and metakaolin rich in oxides of SiO_2 and Al_2O_3 together with CaO rich slag. The products formed in these studies were expected to form a C-(N)-A-S-H type reaction product in these binary component systems in microstructural analysis [108-110]. The compositions of the C-A-S-H type gels formed in these cements (denoted C-(N)-A-S-H to reflect the increased alkali content in addition to the high levels of Al incorporated into this phase) vary depending on the activation conditions, but are typically close to Ca/Si = 1 [153]. In our study, as shown in Figure 4.125, the general EDS analysis result of the 2CW/2MW-BB sample was determined as Ca/Si = 0.76. Moreover, its 6.25% Al content also draws attention. Therefore, it was predicted that the bond structure that might occur in the 2CW/2MW-BB sample might be C-(N)-A-S-H. However, in this study, the strength values obtained as a result of binary component activation of CW and MW were found to be low compared to other binary component systems (BFS/CW-BB, BFS/MW-BB). It was thought that this behaviour might be due to the fact that the CW and MW did not completely react chemically. In the literature, the effects of limestone addition on the alkali activation process of Halloysite clay, which was very similar to the chemical structure of the ceramic waste used in our study, were investigated [105]. Especially, this study was very similar to the CW/MW-BB system in our study. In the study in question, only NaOH was chosen for the alkali activator, unlike our study. It was found that the XRD peaks obtained in this study were very similar to the XRD peaks obtained in our study. In addition, it was stated that even the partial dissolution of limestone in clay provided the formation of geopolymerization products and thus increased the strength [105]. In our study, it was determined that the intensity value of the quartz phase originating from SiO_2 within the unary component CW-UB was higher than the quartz phase in the CW/MW binary component system. However, similarly, it was observed that the calcite phase originating from CaO within the unary component MW-UB was also higher than the intensity of the calcite phase in the CW/MW binary component system. Therefore, these observations suggest that two products partially reacted with each other. According to the results of FTIR analysis, where these two products reacted with each other, there was a peak in 972 cm^{-1} IR band expressing the C-A-S-H bond structure (see Figure 4.126). Bayiha et al. [105] also

determined the peak at which the C-A-S-H bond, which was the main reaction product, was formed in the absorption band between 956–978 cm^{-1}. Therefore, our study results were compatible with the results of this study published in the literature. However, since the strength increase in CW/MW-BB binary system was much lower than in other two component systems, it could be said that most of the materials in this system did not actively participate in the chemical reaction.

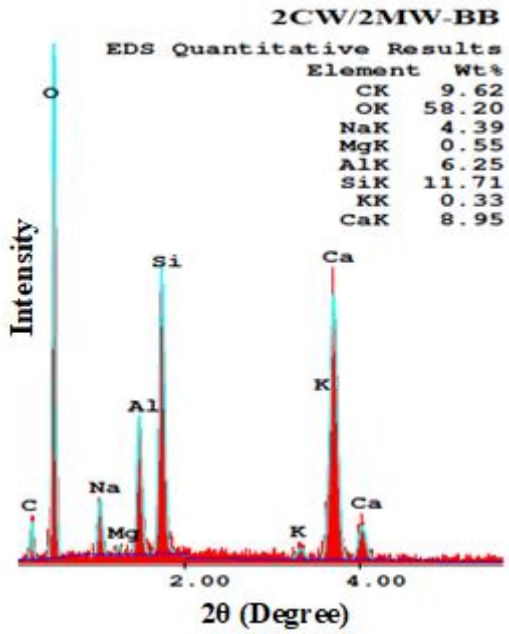


Figure 4.125. General EDS analysis of 2CW/2MW-BB sample.

✓ *FTIR Analysis of the CW/MW-BB*

In Figure 4.126, FTIR results of the alkali activation samples of selected performance giving sample CW/MW-BB according to flexural and compressive strength (2CW/2MW/2/1.2/0.4/Steam) were given below.

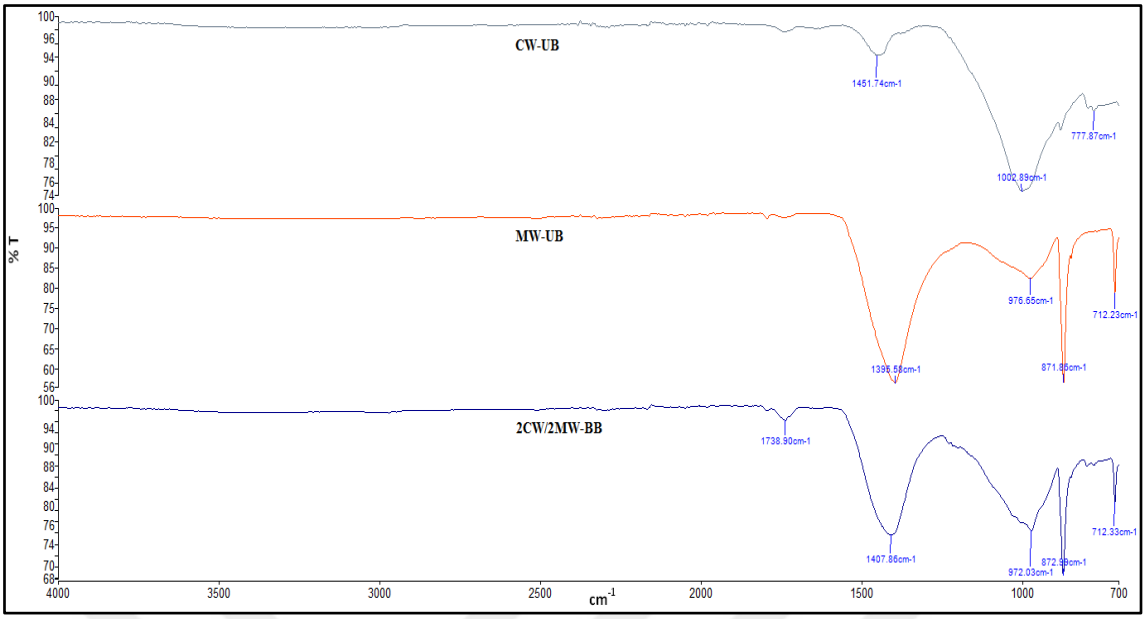


Figure 4.126. FTIR results of the selected CW/MW-BB sample.

FTIR results obtained in this study and their comparisons with the literature were given in Table 4.28.

Table 4.28. FTIR results of CW/MW-BB obtained in this study and their comparisons with the literature.

	CW/MW-BB			
	Band No	**Wavenumber cm^{-1}**	**Attribution**	**Reference**
CW/MW-BB	1	1738	C=O / CO_3^{-2}	
	2	1407	C=O / CO_3^{-2}	[129, 133]
	3	972	Si-O stretching vibrations/ C-A-S-H	[65, 110]
	4	872	C=O / CO_3^{-2}	[51, 148-149]
	5	712	C=O / CO_3^{-2}	[52]

When the results in the Table 4.28 were evaluated, IR bands were formed due to the formation of $CO3^{-2}$, similar to the alkali activation system of MW-UB (4 and 5). There was no publication in the literature involving the alkali-activated process of CW and MW together. Therefore, alkaline activation processes of source materials, which were similar to the chemical compositions of CW and MW, investigated. The IR bands of the main reaction products that provided strength in slag/fly ash two-component activation systems in the literature determined for the range of 950-980 cm^{-1} [110]. In another study, the main absorption peak that forms the C-A-S-H bond structure for the slag/fly

ash binary component alkali activation system was realized for the asymmetric stretching vibration of Si-O band [65]. Finally, the effects of limestone addition on the alkali activation process of Halloysite clay, which was very similar to the chemical structure of the CW used in our study, were investigated [105]. In this study, it was determined that the characteristic Si-O bond representing the reaction product of the "clay + limestone" mixture activated with 8 and 10 M NaOH was formed in the band of 956–978 cm^{-1} [105]. In this case, it could be said that the absorption peak for the 972 cm^{-1} band in our study determined the formation of C-(N)-A-S-H. However, the strength values found for this binary component system were lower than the strength values of the other binary component activation systems performed in this study. The IR bands obtained as a result of FTIR also confirmed the presence of unreacted CO_3^{-2} in the system. Therefore, it could be concluded that most of the materials did not actively participate in the chemical reaction in this system consisting of CW and MW.

✓ *SEM-EDS Analysis of the CW/MW-BB*

In Figure 4.127, SEM-EDS image of the selected performance giving sample CW/MW-BB (2CW/2MW/2/1.2/0.4/Steam) were given below.

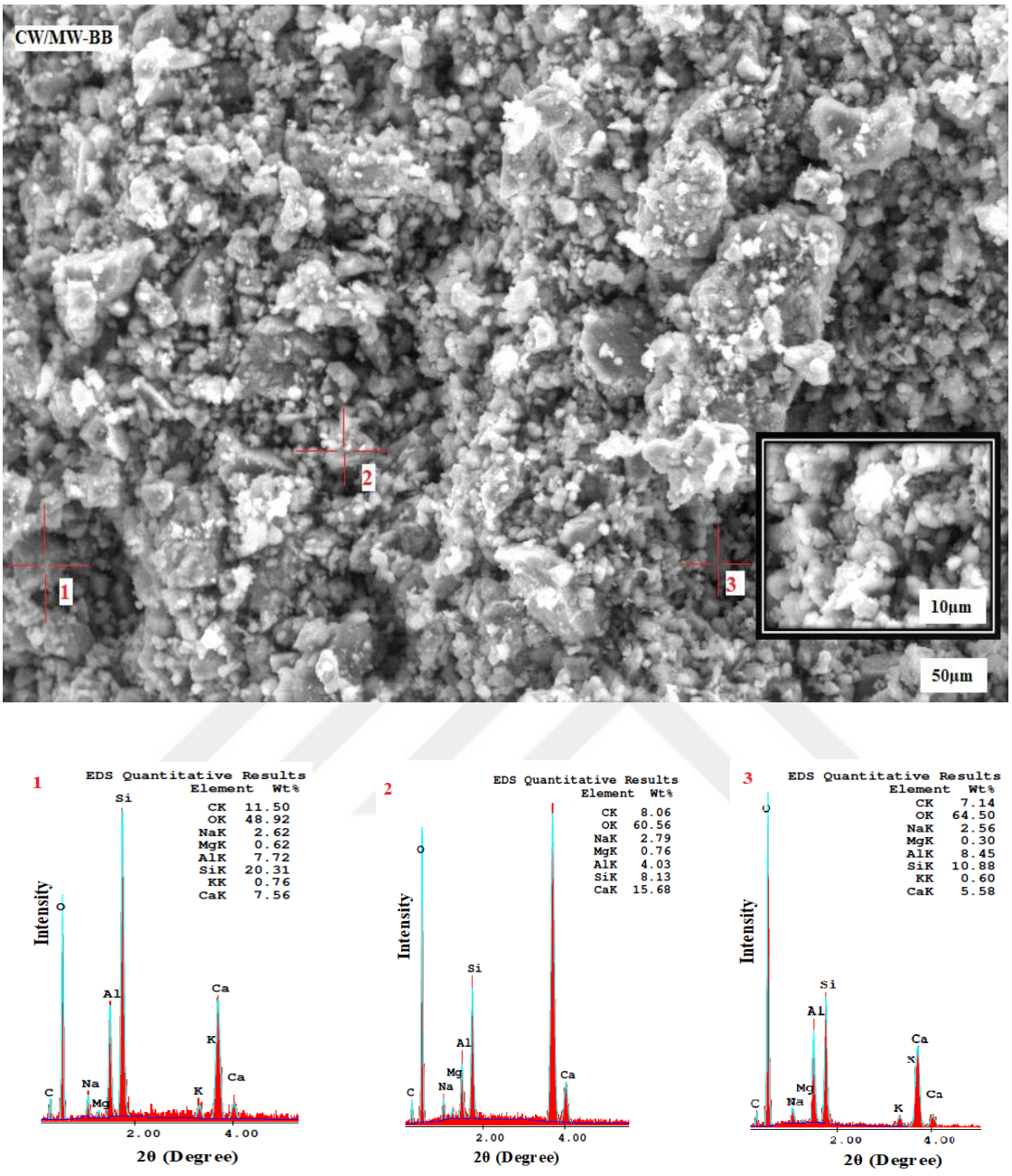


Figure 4.127. SEM-EDS images of the selected CW/MW-BB sample. Düzelttim

As can be seen in Figure 4.127, the data obtained as a result of the SEM-EDS analysis showed that there was unreactive CW and MW for this binary component system. In the EDS results region 1, the SiO_2 ratio was quite high. It was thought that the phase found here belongs to unreacted CW. Likewise, according to the result of the EDS analysis region 2, a phase with a high CaO ratio was determined. It was presumed that this phase also belongs to the MW. However, in the image region 3, it was determined that the

SiO_2 and CaO amounts similar to each other. This part was a phase of reaction products formed as a result of the chemical reaction of CW and MW. This phase was thought to be a C-A-S-H or hybrid C- (N)-A-S-H type phase. Similar to our study results, an EDS analysis revealed that CaO and SiO_2 ratios close to each other in a binary component alkali activation system consisting of a mixture of 50% slag and 50% fly ash [154]. Ismail et al was concluded that the reaction product formed was a C-A-S-H or hybrid C-(N)-A-S-H type product in this study [154]. Similar to the results obtained in this work, as a result of our EDS analysis of region 3, in the matrix developed around the waste ceramic particles in an alkali activation system, a mixture of ceramic and marble waste substituted by 50% each other, close amounts of Ca and Si ions were obtained. In the literature, it was stated that if the Ca/Si ratio was one or less (≤ 1) in the intermediate matrix formed around the main components in alkali-activated hybrid paste samples with main components containing a source of CaO and SiO_2, the presence of Na^+ in the environment caused C–N–(A)–S–H type gel formation [99, 155].

4.7.3. Microstructural analysis of the selected ternary binders

4.7.3.1. Microstructural analysis of the BFS/CW/MW-TB samples

✓ *XRD Analysis of the BFS/CW/MW-TB*

In Figure 4.128 and Figure 4.129, XRD results of the alkali activation samples of the selected performance giving sample BFS/CW-BB, BFS/MW-BB, CW/MW-BB and BFS/CW/MW-TB according to flexural (BFS/CW/MW-TB-F) and compressive strength (2BFS/1CW/1MW-TB-C) were given below, respectively. XRD analyzes of binary systems were also given in these graphs. Thus, it was aimed to compare and better understand the phases developing in the ternary systems with the phase analyzes of the binary systems.

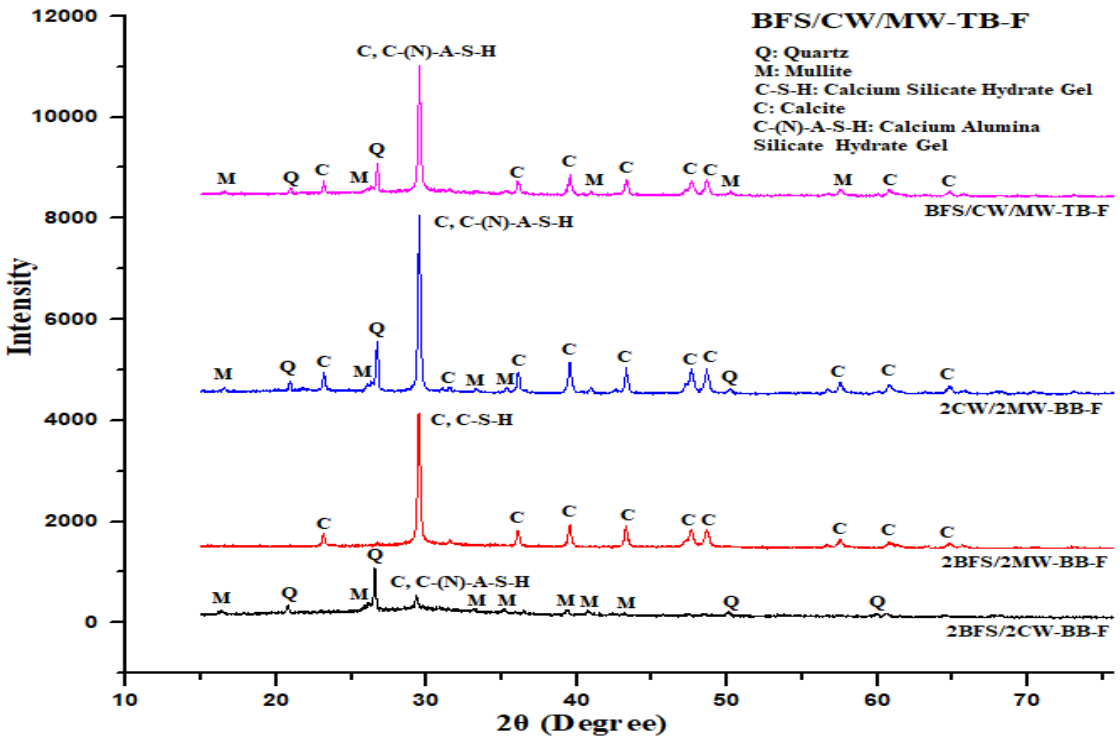


Figure 4.128. XRD pattern of the selected BFS/CW/MW-TB-F sample according to flexural strength.

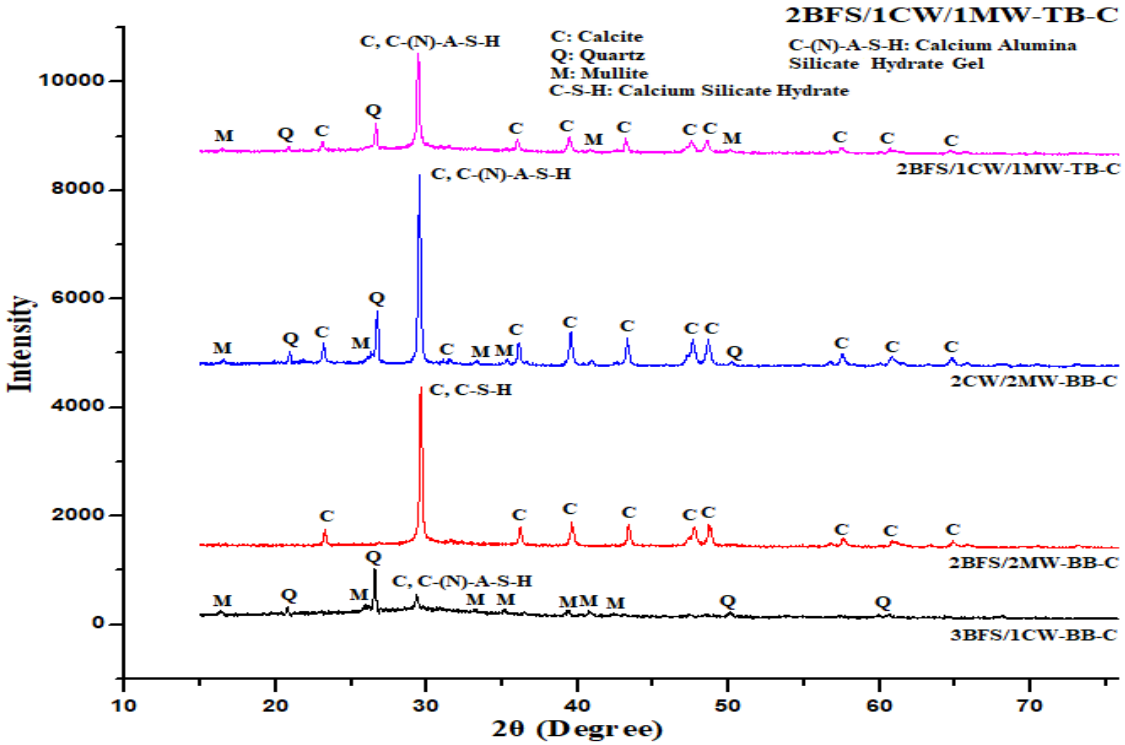


Figure 4.129. XRD pattern of the selected 2BFS/1CW/1MW-TB-C sample according to compressive strength.

As seen in Figure 4.128 and Figure 4.129, the C- (N) -A-S-H gel structure and calcite phase, which can be defined as the main reaction product, were superimposed as in other binary component and unary component systems. However, the intensity of the 2θ value around 29-30^0 of the BFS/CW/MW-TB (F) sample, which yielded much higher flexural strength, was higher than the other ternary component sample (2BFS/1CW/1MW-TB (C)). The reason for this intensity difference was thought to be the unreacted calcite phase in the BFS/CW/MW-TB sample. 2BFS/1CW/1MW-TB (C) composition was the ternary component sample with the highest result in terms of compressive strength. This situation suggested that the CW in the ternary component system did not chemically contribute to the formation of reaction products. There was even a study in the literature reporting that this event negatively affects the formation of C-S-H or C-A-S-H gel structure due to the increase in the amount of CW added to the slag/fly ash two-component system [47]. In addition, in another study, it was determined that substituting porcelain ceramic waste into blast furnace slag did not create any new crystalline phase formation according to XRD results [151]. It was understood that the addition of MW in the same slag did not contribute to the formation of a new crystal phase. However, it was determined that MW provides strength increase in alkali activated slag by filler effect without forming a new crystal phase [57, 59-60]. This situation was consistent with our study results for 28-day cured strength values.

✓ *FTIR Analysis of the BFS/CW/MW-TB*

In Figure 4.130, FTIR results of the alkali activation samples of selected performance giving sample BFS/CW/MW-TB according to flexural (BFS/CW/MW/4/1.2/0.4/Steam) and compressive strength (2BFS/1CW/1MW/4/1.2/0.4/Steam) were given below.

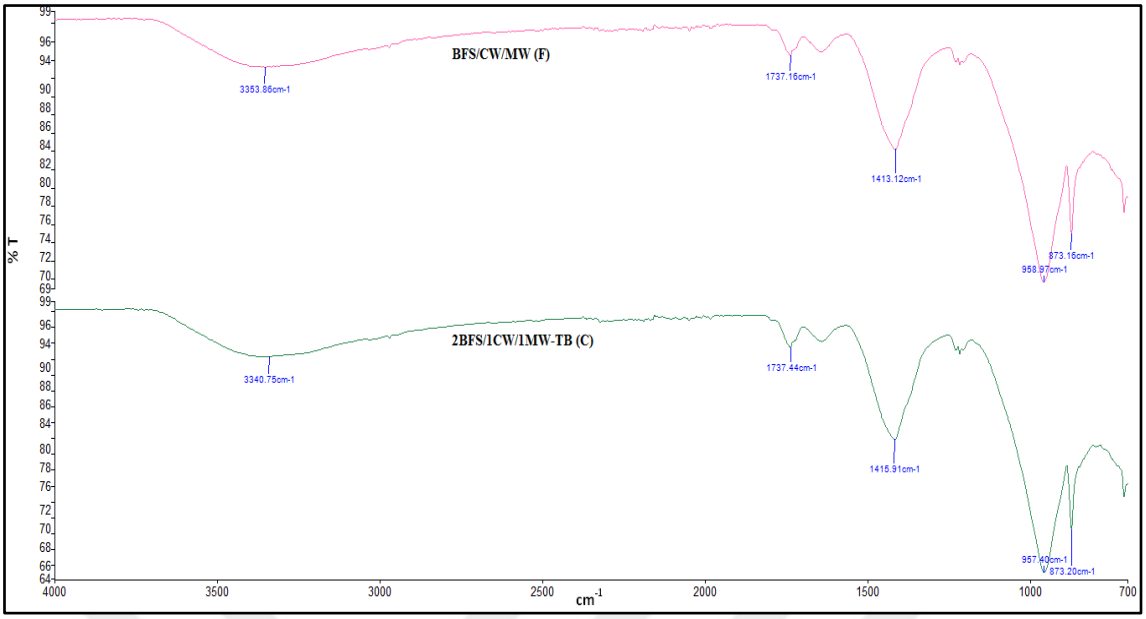


Figure 4.130. FTIR results of the selected BFS/CW/MW-TB samples.

FTIR results obtained in this study and their comparisons in literature were given in Table 4.29.

Table 4.29. FTIR results of BFS/CW/MW-TB obtained in this study and their comparisons with the literature.

	BFS/CW/MW-TB			
	Band No	**Wavenumber cm^{-1}**	**Attribution**	**Reference**
BFS/CW/MW-TB-F	1	873	C=O / CO_3^{-2}	[41, 148-149]
	2	958	Si-O asymmetric stretching/C-(N)-A-S-H	
	3	1413	v3$[CO3]^{-2}$	[129, 133]
	4	1737	C=O stretching	
	5	3353	O-H Stretching	[129, 133, 135]
2BFS/1CW/1MW-TB-C	1	873	C=O / CO_3^{-2}	[41, 148-149]
	2	957	Si-O asymmetric stretching/ C-(N)-A-S-H	
	3	1415	v3$[CO3]^{-2}$	[129, 133]
	4	1737	C=O stretching	
	5	3340	O-H Stretching	[129, 133, 135]

The wavelengths obtained in the Table 4.29 were similar to those obtained in unary component BFS, CW and MW alkali activated systems. The C- (N) -A-S-H gel IR peak, which provided strength gain in this ternary component activation system, was formed for the wavelength of 957-958 cm^{-1}. However, in the BFS-UB system, this bond

structure was formed around 950 cm^{-1} wavelengths as a C-S-H gel. From the aspect of source materials, the Si – O bond in slag was around 900 cm^{-1}; the increase in wavenumber indicated the formation of a higher polymerized Si– O network [109].

SEM-EDS Analysis of the BFS/CW/MW-TB

In Figure 4.131, SEM-EDS results of the alkali activated samples of selected performance giving sample BFS/CW/MW-TB according to flexural (BFS/CW/MW/4/1.2/0.4/Steam) and compressive strength (2BFS/1CW/1MW/4/1.2/0.4/Steam) were given below.

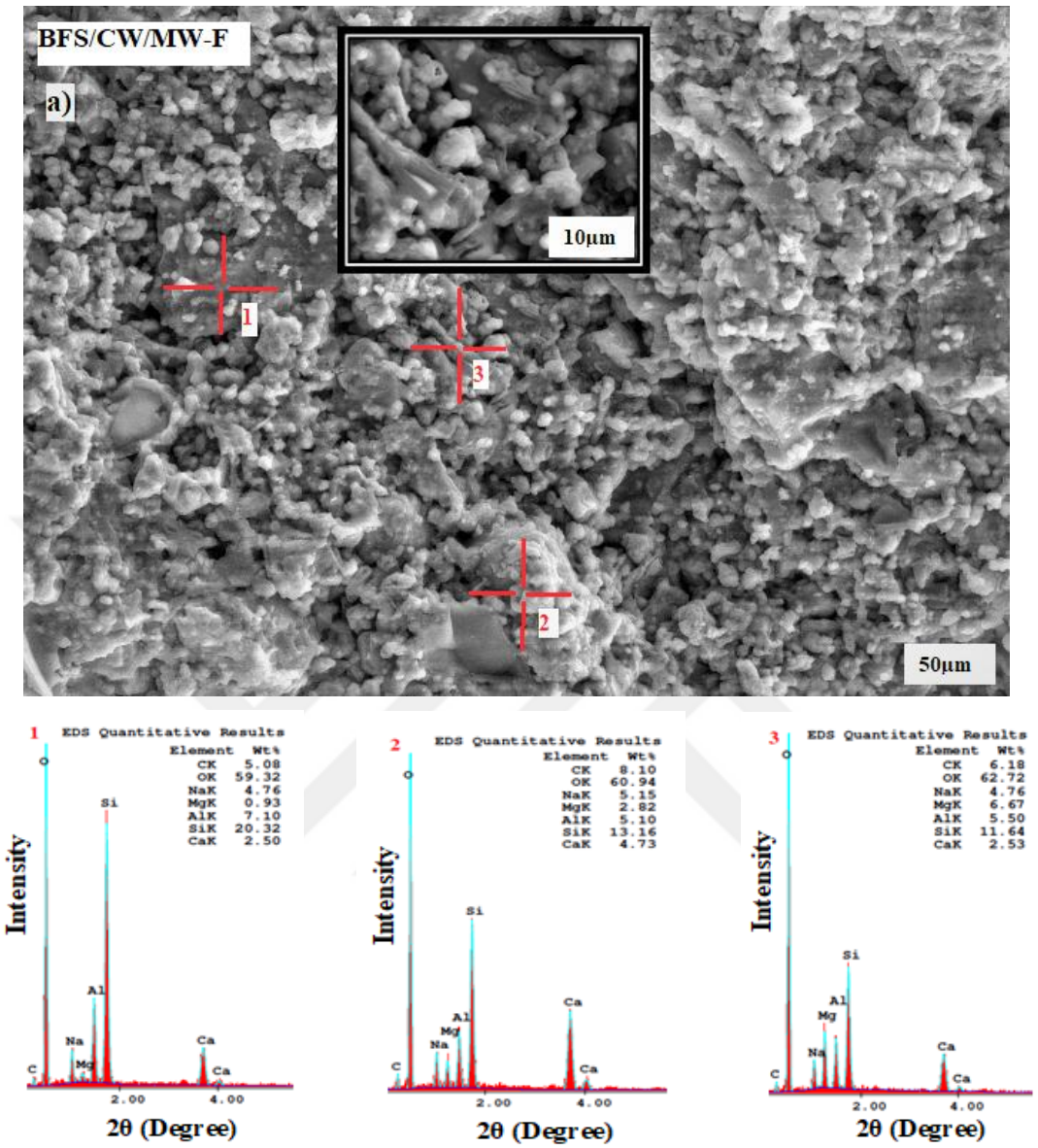


Figure 4.131. SEM-EDS images of the selected BFS/CW/MW-TB samples a) BFS/CW/MW-TB-F b) BFS/CW/MW-TB-C.

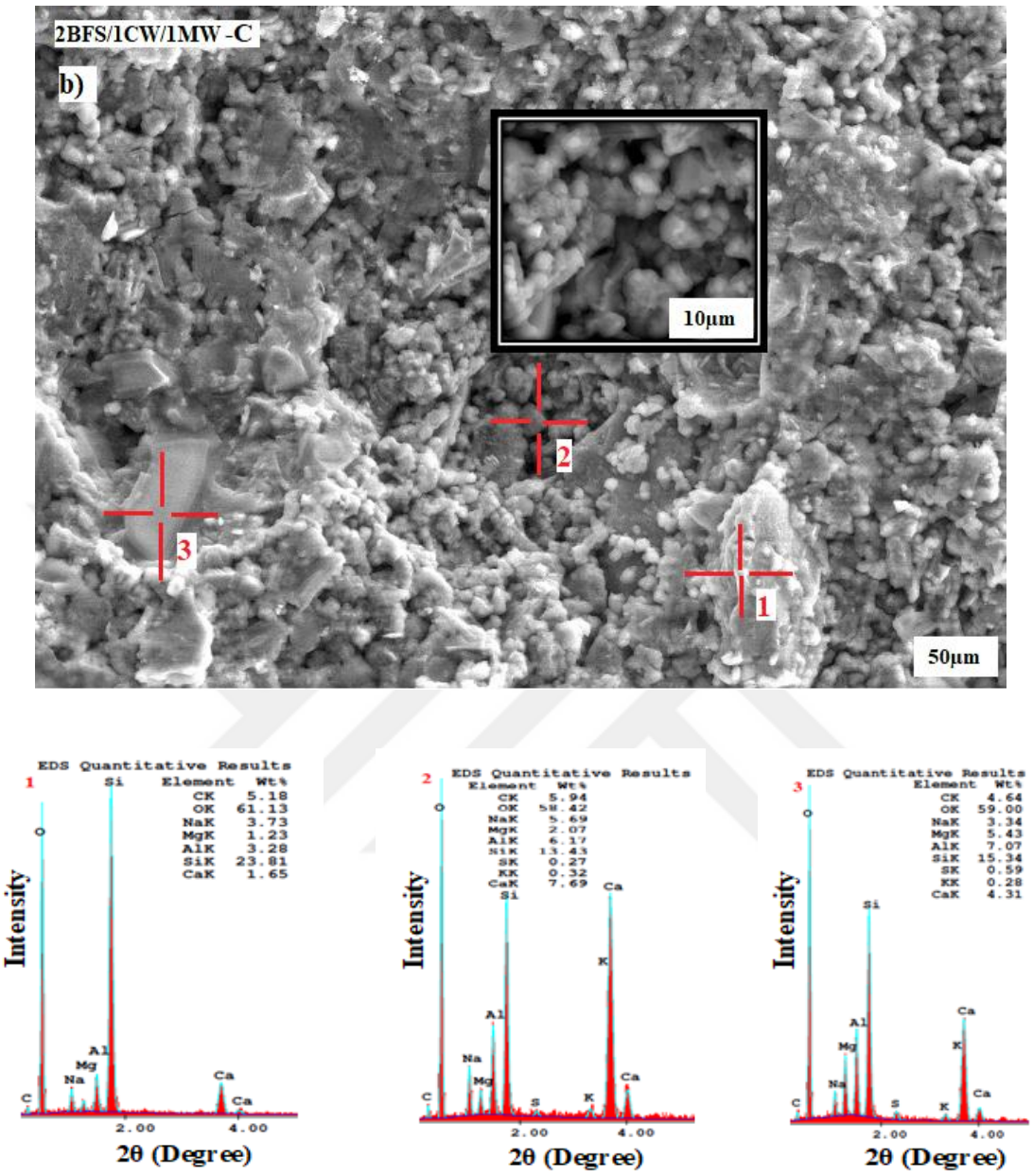


Figure 4.131. (continue) SEM-EDS images of the selected BFS/CW/MW-TB samples a) BFS/CW/MW-TB-F b) BFS/CW/MW-TB-C.

There was a more homogeneous and compact structure appearance in Figure 4.131/a and Figure 4.131/b compared to other unary and binary component systems. In these compositions, it was expected that the reaction product, which will be both CW and MW, will form a bond structure similar to C-A-S-H or C- (N) -S-H [60]. However, as a result of microstructure analysis, XRD and FTIR peaks were detected due to the presence of unreactive source materials. Considering the 90-day cured strength values

of these ternary component samples, it was observed that strength of these samples decreased than BFS-UB and cement samples. According to the EDS analysis, it was thought that there were mostly undissolved CW and sodium silicate in regions with high SiO_2 ratio. The regions with increased CaO/SiO_2 ratio were predicted to form those reaction products.

4.7.4. Cost Analysis Comparison

This simple cost analysis is based on 40*40*160 mm prismatic test samples produced under laboratory conditions. A cement of the same dimensions and a ternary component sample (BMS/CW/MW-TB-F) were compared in terms of cost. The result showed that the ternary component sample produced by the alkaline activation method price was 12.3 $ more than the cement sample. However, the cost of environmental impact is not included in this cost analysis. When the literature studies on this subject are examined, replacing Portland cement concrete with alkali –activated based concrete was reported to reduce CO_2 emissions by more than 25%. Furthermore, the use of waste-based aluminosilicates such as fly ash and slag in alkali activated binders will reduce the energy and the cost associated with managing these wastes by about 30%.

When all these are evaluated, taking into account the cost of environmental impact, alkali activated as construction materials can be considered as green binders with low-cost raw materials and sustainable technologies.

Table 4.30. Cost analysis of calculation table.

		Shape	Purchase Price ($/kg)	Transport ($/kg)	Drying (Electricity Cost) ($/kg)	Grinding (Electricity Cost) ($/kg)	TOTAL($)
Raw Material	Blast Furnace Slag ($/kg)	Powder	170.47	0.085	–	–	170.56
	Ceramic Waste ($/kg)	Powder	6.46	0.085	–	–	6.55
	Marble Waste ($/kg)	Mud	0.00	0.17	6.12	–	6.29
	Lime ($/kg)	Powder	20.40	–	–	–	20.40
Alkali Activator	Sodium Silicate ($/l)	Liquid	6.50	3.4	–	–	9.90
	Sodium Hydroxide ($/kg)	Pellet	425.00	3.4	–	–	428.40
Water	Distilled Water ($/l)	Liquid				6.17	6.17

Table 4.31. Cost values of cement and ternary sample binder.

Raw Material	Blast Furnace Slag	56.85
	Ceramic Waste	2.18
	Marble Waste	2.10
	Lime	0.98
Alkali Activator	Sodium Silicate	1.50
	Sodium Hydroxide	17.03
Water	Distilled Water	2.71
BFS/MW/CW	**TOTAL ($)**	**83.4**
CEMENT	**TOTAL($)**	**70.5**

5. CONCLUSIONS

Cement is still the most widely used binding material in the construction industry worldwide. Therefore, the production sector is one of the largest sectors in the world. However, it is an industrial product that has serious harm to nature and human health in terms of harmful gas emissions and high energy costs during its production. Considering the increasing CO_2 emissions throughout the world in recent years and the damages that such production processes cause to natural life, it was become inevitable to search for environmentally friendly and low energy cost products that replaced these production processes. In this context, alkali activated binder production processes became one of the most interesting research topics with almost nonexistent CO_2 emission values and low energy costs. Therefore, the raw materials used in this study were products used as by-products and/or waste in an industrial production process. In addition, unlike cement, a low-cost and low-CO_2 production process used. Considering all these values, this study contributed to the production of sustainable and environmentally friendly industrial products.

Within the scope of this study, three different industrial by-products/waste were activated using alkaline activator solutions. The product that came out after this process was aimed to form a cement-like binding material that acts as a binder in concrete. For this purpose, blast furnace slag, ceramic waste and marble waste were used as source material in this production process. Sodium silicate and sodium hydroxide were selected as the two types of activators forming the alkali activator mixture. Among these materials, especially BFS is a raw material that used frequently in the alkali activation process before. However, a very limited number of studies encountered in which CW and MW were used as source materials in the alkaline activation process. The effects of these two types of waste in the BFS in the alkaline activation process were also unknown. For this purpose, within the scope of this study, unary, binary and ternary component alkali activation processes of BFS, CW and MW studied and the potential of the products to be used as binders that could be used instead of cement evaluated. In this evaluation, strength, durability and microstructure analyzes were performed on the samples. All these obtained data were compared with the data obtained under the same production conditions of cement. Thus, the potential of these materials, which were

produced with the hope of being a new generation binder, to became a usable binding material instead of cement was investigated.

In order to ensure that all raw materials and alkali activators used in the study were products with the most optimum experimental parameters, different parameters were used in the alkali activation production system. These parameters were differentiated in terms of activator dosages used in activation, curing methods and water/binder ratios. For this reason, in the study, 3 different "n" ratios (total Na_2O ratio in the activator), different "Ms" ratio (SiO_2/Na_2O ratio in the activator), two different w/b ratios and two different cure types for each raw material. It was tested. A number of physical, strength, durability and microstructural analyzes were carried out on unary, binary and ternary component samples with the obtained optimum parameters. The results were presented within the samples and by comparing them with the values obtained in the same conditions.

In this section, the experimental results of the samples with unary, binary and ternary components summarized under separate headings.

BFS-UB

- In the BFS-UB system, the flow diameter values for samples with low and medium level of activator dosage (n=2 and n=4) were obtained 5-10% higher than the cement sample. However, as the activator dosage increased (n = 6), the rate of transition of the samples from fluid to solid consistency decreased to a few minutes. This situation shortened the mixing and molding times of the samples, thus reducing the workability values.
- The initial and final setting times of BFS-UB samples were shorter than cement samples. Only when the n ratio equals 4, long initial and final setting times were obtained from the cement sample. However, all BFS-UB samples completed their setting in 8-10 hours. After 24 hours, all samples were removed from the mold without any problems.
- In BFS-UB (BFS-UB-F and BFS-UB-C), which gave the best results in terms of flexural and compressive strength at the end of the 7-day strength period, had different experimental parameters from each other. While the best flexural strength value was realized for the "BFS/4/1.5/0.4" sample, the best compressive strength

result was obtained for the "BFS/6/1.5/0.4/S" sample. Thus, for the BFS-UB samples, increasing the activator dosage improved the compressive strength value of the sample.

- The bulk density, apparent density and porosity ratios of both BFS-UB samples, which gave the best results in terms of flexural and compressive strength, were almost the same as the cement sample. BFS-UB samples had higher bulk density and less void ratio compared to unary and cement samples. In this respect, it could be said that BFS-UB samples had a more compact and void-free structure compared to other unary component binder samples.
- It was determined that the BFS-UB (C) sample, which gave the highest value in terms of compressive strength, absorbed approximately 3.3 times less water than cement after 24 hours of water absorption test. This value was 4.8 times less for the BFS-UB (F) sample, which gave the highest result in terms of flexural strength. Therefore, it could be said that BFS-UB unary component binder structures had very low water absorption values compared to cement and thus were more resistant to aggressive environmental conditions consisting of water and harmful chemicals.
- The early flexural strength results (7 days) of the BFS-UB samples were found to be approximately 4.8MPa less for the BFS-UB (F) sample compared to the cement sample, while the late flexural strength value (90 days) was 6.7MPa less. This situation showed that the rate of gaining flexural strength of BFS-UB samples over time was slower than cement.
- The early compressive strength results (7 days) of the BFS-UB samples were found to be approximately 13.2MPa less for the BFS-UB (C) sample compared to the cement sample, while the late flexural strength value (90 days) was found to be 1.5MPa less. This showed that the rate of gaining compressive strength of BFS-UB samples over time was higher than that of cement.
- The drying shrinkage values found in both BFS-UB samples were determined approximately 2 times higher than the cement sample.
- For both BFS-UB samples, the strength loss under high temperature effect was much less than cement. Even the cement sample lost almost all of its strength under the effect of high temperature (800ºC), while the BFS-UB (F) sample lost only 26%.

- Both BFS-UB samples did not lose their compressive strength under the action of sulfate, on the contrary, an increase in compressive strength values was observed. There was an increase in compressive strength in the cement sample exposed to sulphate. However, the increase in the compressive strength of the BFS-UB (F) sample was higher than that of the cement sample.
- BFS-UB (F) sample also did not lose its compressive strength under the action of sulfuric acid, on the contrary, an increase in compressive strength values was observed. The BFS-UB (C) sample, on the other hand, experienced a strength loss of approximately 25% under the effect of acid. No loss of strength was observed in cement.
- The microstructure studies of the BFS-UB samples studied by XRD, FTIR and SEM-EDS analyzes that cement as the main reaction product forms the C-S-H bond structure as the main reaction product.
- It was determined that the unary component samples of BFS-UB samples were very close to or even superior to cement in terms of both strength and durability properties. In terms of strength and durability properties, it could be said that the BFS-UB combination could be used as a binder equivalent to the CEM I 42.5 R cement used for the production of cement paste in this study. Therefore, the usability of BFS-UB combinations for the production of structural products seemed appropriate.

CW-UB

- Flow diameter values of CW-UB sample were lower than both BFS-UB and cement samples. Similar to the results in the BFS-UB test set, the flow diameter values of the samples with "n" ratio equal to 2 or 4 were determined in this experiment set similar to the cement flexural diameter values. However, as the rate of activator in the content of the samples increased (n = 6), the transition speed of the samples from fluid to solid consistency was very high.
- The initial and final setting times of CW-UB samples were shorter than compared to the cement sample, especially for low and high activator dosages. When the "n" ratio was equal to 4, the setting times were prolonged, similar to the BFS-UB

examples. However, all BFS-UB samples completed their setting in 8-10 hours. After 24 hours, all samples were removed from the mold without any problems.

- CW-UB composition, which gave the best results in terms of flexural and compressive strength at the end of the 7-day strength period, was realized for the "CW/6/1.2/0.4" sample. However, the strength values obtained were quite low compared to the strength values of BFS-UB and cement samples. It was possible that this combination could be used industrially for the production of non-bearing products that did not require high strength.
- The bulk density, apparent density and void ratios of the CW-UB sample, which gave the best results in terms of both flexural and compressive strength, were almost the same as the cement sample. The bulk density value of CW-UB samples was lower and the void ratio was higher than the BFS-UB and cement samples. In this respect, it could be said that CW-UB samples had a more porous structure than other unary component binder samples.
- It was determined that the CW-UB sample, which gave the highest value in terms of flexural and compressive strength, absorbed approximately 2.2 times more water than cement sample after 24 hours in water absorption test. This situation might be due to the structure of the CW-UB sample which was more porous than BFS-UB and cement samples.
- The difference between early (7 days) and late (90 days) strength values of CW-UB samples was quite small. Therefore, the strength gain rate of CW-UB samples over time was determined to be quite small when compared with cement and BFS-UB samples.
- The drying shrinkage value of the CW-UB sample at the end of 120 days was found to be less than all other unary component binder and cement samples. This showed that the dimensional stability of the CW-UB sample was preserved much better than the other samples.
- CW-UB sample did not experience any loss of compressive strength under the influence of high temperature. When the temperature rises to 800 ºC, an increase of up to 300% was observed in its strength. This situation might have occurred as a result of the sintering of glassy phases in ceramic waste with the effect of high

temperature increase. Therefore, for the CW-UB sample, there was an increase in strength under the effect of high temperature.

- It had lost 34% of the flexural strength of the CW-UB sample under the effect of sulfate and approximately 44% of its compressive strength. CW-UB sample lost about 35% of its compressive strength under the effect of acid. Therefore, it was found to be less durable than the cement sample in terms of resistance to aggressive chemical environments.
- As a result of the microstructure studies of the CW-UB samples, it was determined that the "natrolite" structure was formed after activation and that this structure represented the N-S-H bond structure, unlike the raw material examinations. However, since the strength values obtained for the CW-UB combination were far below the cement and BFS-UB combinations, it was concluded that the CW did not react completely with the activators in the activation system. The phases in the ceramic waste that did not react were determined by microstructural analysis.
- CW-UB combination showed worse performance than cement and BFS-UB samples in terms of strength and durability properties. However, it was possible that this combination could be used industrially for the production of non-bearing products that did not require high strength.

MW-UB

- Flow diameter values of MW-UB sample were higher than both BFS-UB and cement samples. Similar to the results in the BFS-UB test set, the flow diameter values of the samples with "n" ratio equal to 2 or 4 were determined in this experiment set similar to the flow diameter values of cement sample. However, as the rate of activator in the content of the samples increased (n = 6), the fluidity of the samples increased. In the MW-UB sample, unlike the others, as the "n" ratio increased, there was no rapid transition from liquid to solid consistency.
- The initial and final setting times of MW-UB samples were found to be higher for all “n” ratios than cement and other unary binders when compared to the cement sample. MW-UB samples with a value of 0.4 w/b completed their setting in 8-10 hours. After 24 hours, all samples were removed from the mold without any problems.

- The MW-UB composition, which gave the best results in terms of flexural and compressive strength at the end of the 7-day curing period, was realized for the "MW/4/1.8/0.4" sample. However, the strength values obtained were quite low compared to the strength values of BFS-UB and cement samples. The lowest strength values for the unary component alkaline activation system were determined for the MW-UB binders. It was possible that this combination could be used industrially for the production of non-bearing products that did not require high strength.
- The bulk density, apparent density and void ratios of the MW-UB sample, which gave the best results in terms of both flexural and compressive strength, could not be measured. Because the samples, which had to remain in water for 24 hours due to experimental conditions, could not maintain their formal integrity within the 4th hour.
- The water absorption value of the MW-UB sample, which gave the highest value in terms of flexural and compressive strength, could not be measured. Because the samples, which had to remain in water for 24 hours due to experimental conditions, could not maintain their formal integrity within the 4th hour.
- The difference between early (7 days) and late (90 days) strength values of MW-UB samples was quite small. Therefore, the rate of gaining strength of MW-UB samples over time was determined to be very small when compared with cement and BFS-UB samples.
- The drying shrinkage values of the MW-UB sample obtained after 120 days was found to be 2 and 4 times higher, respectively, compared to all other unary component binders and cement samples. This showed that the dimensional stability of the CW-UB sample was not sufficiently maintained compared to other samples.
- For the MW-UB sample, there was no loss of compressive strength up to 600 ºC under the high temperature effect. When the temperature raised to 800 ºC, loss of strength observed. This value was lower than the cement sample. Therefore, it was observed that the MW-UB sample exhibited a better behavior than cement in terms of strength loss under high temperature effect.
- Under the effect of sulfate, 70% of the flexural strength of the MW-UB sample and about 18% of its compressive strength have been lost. The CW-UB sample lost

about 30% of its compressive strength under the influence of sulfuric acid. Therefore, it was found to be less durable than the cement sample in terms of resistance to aggressive chemical environments.

- As a result of microstructure studies of MW-UB samples, different from raw material examinations, it was determined that "gehlenite, thermonatrite, silicium carbide and almandine" structures were formed after activation. Since the strength values obtained for the MW-UB combination were far below the cement and BFS-UB binders, it was concluded that MW did not react completely with the activators in the activation system.
- MW-UB combination showed worse performance than cement and BFS-UB samples in terms of strength and durability properties. However, it was possible that this combination could be used industrially for the production of non-bearing products that did not require high strength.

BFS/CW-BB

- As the amount of CW in the BFS/CW-BB samples increased, the flow diameter values and the initial/final setting times decreased. In this case, it could be said that CW reduces the processability properties of BFS. For samples with high "n" ratios, the transition time from liquid to solid was short.
- For the BFS/CW-BB samples, the CW contents of the samples that gave the highest flexural and compressive strength were different from each other. While 25% CW substitution was the best sample in terms of compressive strength, the sample containing 50% CW gave the best result in terms of flexural strength. Therefore, as the amount of CW in BFS increased up to 50%, the compressive strength of the samples decreased while the flexural strength values increased.
- Activator variables (n and Ms) of the BFS/CW-BB samples, which gave the best results in terms of flexural and compressive strength, were equal to each other. It was determined that the BFS/CW-BB samples that gave the best results in terms of durability were formed for the samples containing the highest activator dosage (n=6).
- For the BFS/CW-BB sample containing 25% CW, the rate of increase in early and late flexural/compressive strengths was lower than the BFS/CW-BB sample

containing 50% CW. In this case, for the BFS/CW-BB sample, it could be said that as the amount of CW in its content increased, the strength gaining rate increased over time.

- As the CW content in BFS increased, the bulk and apparent density values of the samples decreased and the void ratios increased compared to the BFS-UB samples. However, the void ratios of both BFS/CW-BB samples were found to be less than the cement sample.
- As the CW content in BFS increased, the water absorption values of the samples increased compared to the BFS-UB samples. However, the water absorption values of both BFS/CW-BB samples were found to be less than the cement sample.
- The drying shrinkage value of the CW-UB sample at the end of 120 days was the lowest value in the whole test system. However, for BFS/CW-BB samples, as the amount of CW in the samples increased, the drying shrinkage values increased compared to the BFS-UB samples.
- It was found that BFS/CW-BB samples lost less strength under the influence of high temperature compared to BFS-UB (C) and cement samples.
- BFS samples where CW replaced had lost strength more than BFS-UB samples and cement under the influence of sulphate and sulfuric acid. As the CW substitution in the samples increased, the strength losses increased. It was predicted that this situation may be due to the fact that the vacancy rates of the CW substituted BFS samples were higher than the BFS-UB samples.
- The main reaction product (C-A-(N)-S-H) phase formed by the BFS/CW-BB samples was the same as the 29-30^{o} 2θ phase created by the BFS-UB (C) sample. However, the intensity value created by the BFS-UB (C) sample for this 2θ value was higher than the BFS/CW-BB samples. Therefore, it was compatible for the BFS-UB (C) sample to had a higher strength value. The intensity value of 2θ, representing the C-A-(N)-S-H bond of the BFS/CW-BB (C) sample, was greater than the BFS/CW-BB (F) sample. In addition, Quartz structures formed due to unreacted CW were determined in the microstructure analysis of BFS/CW-BB samples. This indicated that CW and BFS were not fully reacted.

BFS/MW-BB

- As the amount of MW in the BFS/MW-BB samples increased, the flow diameter values and the initial/final setting times increased. In this case, it could be said that MW improved the workability properties of BFS. For samples with high “n” ratios, the transition time from liquid to solid was prolonged.
- For the BFS/MW-BB samples, the MW amounts of the samples that gave the highest flexural and compressive strength were the same sample. The 50% MW replacement was the best sample in terms of flexural and compressive strength. Therefore, as the amount of MW in the BFS increased up to 50%, the flexural and compressive strength values of the samples increased.
- The "n" ratio was different from the activator variables of the BFS/MW-BB samples that give the best results in terms of flexural (BFS/MW (F)) and compressive strength, (BFS/MW (C)) but the "Ms" ratio was equal to each other. It was determined that the BFS/MW-BB samples, which gave the best results in terms of compressive strength, were formed for the samples containing the highest activator dosage (n=6). The highest flexural strength occurred in the sample containing a moderate dosage of alkaline activator (n = 4).
- For BFS/MW-BB samples containing 50% MW, the rate of increase between early and late flexural strengths was close to each other. However, for the BFS/MW (F) sample, the rate of increase between the early and late compressive strengths was higher than the rate of increase for the BFS/MW (C) sample.
- For both BFS/MW-BB samples, apparent density and void ratios were lower than cement samples. However, void ratios increased by approximately 6-7% compared to BFS-UB samples.
- Water absorption values of BFS/MW-BB samples increased compared to BFS-UB samples. That was, the substitution of MW in BFS increased the water absorption values of the BFS-UB samples. However, the water absorption values of both BFS/MW-BB samples were less than the cement sample.
- For the BFS/MW-BB (F) sample, the drying shrinkage value determined after 120 days was lower than the BFS-UB and cement samples. However, the drying shrinkage value of the BFS/MW-BB (C) sample was higher than the BFS-UB and cement samples. The BFS/MW-BB (F) sample with less activator ratio preserved its

longitudinal stability much better than the BFS/MW-BB (C) sample with high activator ratio.

- Under the effect of high temperature (800^{o}C), both BFS/MW-BB samples experienced more strength loss compared to BFS/UB samples. However, there were less strength losses than the cement sample at the same temperature.
- Both of the BFS/MW-BB samples had a greater loss of strength under the influence of sulphate and sulfuric acid than the BFS-UB and cement samples. However, as with the high temperature effect, the sample with a low "n" ratio experienced less strength loss than the high one. Therefore, it could be said that increasing the "n" ratio for the BFS/MW-BB binary component mixture had a negative effect on the flexural strength properties.
- In both BFS/MW-BB samples, the C-S-H bond structure determined in the microstructural analysis of BFS-UB samples was determined. However, in XRD analysis, there was also a calcite peak above the 2θ value representing this bond structure. The XRD peak of these two structures overlaps. Although the intensity value of the 2θ peak of the BFS/MW-BB samples was higher than the BFS-UB samples, the strength values were lower. This situation showed that the peak at the same 2θ value for BFS/MW-BB samples was due to the calcite structure. Therefore, in this binary mixture, BFS and MW did not react completely in the alkaline activation system.

CW/MW-BB

- As the amount of MW in the CW/MW-BB samples increased, the flow diameter values and the initial/final setting times increased. In this case, it could be said that MW improved the workability properties of BFS. For samples with high "n" ratios, no setting occurred even after 48 hours.
- For the CW/MW-BB sample, the sample giving the highest flexural and compressive strength was the same sample. The 50% MW replacement was the best sample in terms of flexural and compressive strength. Therefore, as the amount of MW in CW increased up to 50%, the flexural and compressive strength values of the samples increased. However, the highest flexural and compressive strength values obtained for the CW/MW-BB binary component binder system were lower

than the CW-UB sample. Therefore, the substitution of MW in CW negatively affected the strength properties.

- CW / MW-BB samples, which gave the best results in terms of flexural and compressive strength, had the lowest "n" ratio and "Ms" ratio. In other words, as the activator dosage increased, the strength properties of the samples decreased.
- For CW/MW-BB samples containing 50% MW, the rate of increase between early and late flexural strengths was close to each other. The system in which the lowest resistance values were obtained among the binary component activation systems applied in this study was the CW/MW-BB system.
- For the CW/MW-BB sample, the difference between the apparent and bulk density and void ratio were determined to be higher than other binary component activation systems and cement sample.
- The water absorption value for the CW/MW-BB sample was determined to be higher than the other binary component activation systems and cement sample. However, MW substituted by 50% in CW reduced the water absorption value by approximately 6-7% compared to the CW-UB sample.
- For CW/MW-BB sample, after 120 days, expansion was detected instead of shrinkage. The drying shrinkage value determined for the CW-UB sample was also lower than the other unary binder activation systems and cement sample. For the sample substituting 50% MW in CW, expansion was determined rather than shrinkage.
- The loss of compressive strength (13%) occurred under the effect of high temperature ($800^{o}C$) for CW/MW-BB samples. This value was considerably less than both other binary component activation systems and cement sample. However, the substitution of MW in CW increased the resistance loss at high temperature compared to the CW-UB sample.
- While the compressive strength loss of the CW/MW-BB sample under the effect of sulphate was approximately 2%, the compressive strength loss under the effect of sulfuric acid found to be over 50%. Substitution of MW in CW increased resistance to sulphate and decreased acid resistance.
- The strength properties of the CW/MW-BB sample were found to be quite low compared to other binary binder systems and cement sample. This situation

confirmed that no new reaction product formed for the CW/MW-BB system and these two wastes did not react with each other as a result of microstructure analysis.

BFS/CW/MW

- Two different combinations gave the best results in terms of flexural and compressive strength in ternary binder samples. The mass value of the BFS ratio in the ternary binder (2BFS/1CW/1MW/4/1.2/0.4) which gave the best result in terms of compressive strength was 2 times more than the value of the other binary components (CW and MW). In the ternary binder (BFS/CW/MW/4/1.2/0.4), which gave the best results in terms of flexural strength, ternary components were used in equal proportions by mass.
- Both BFS/CW/MW-TB samples reached the highest strength values for the same "n" and "Ms" (4 and 1.2) ratios.
- The flow diameter and setting times of BFS/CW/MW-TB (F) sample were larger than the BFS/CW/MW-TB (C) sample due to the amount of BFS was more.
- The strength increase rate between the early and late flexural and compressive strength of the BFS/CW/MW-TB (F) sample was higher than the BFS/CW/MW-TB (C) sample.
- The apparent density value of the BFS/CW/MW-TB (F) sample was lower than the BFS/CW/MW-TB (C) sample and therefore the vacancy rate was higher. But the void ratio of both samples was similar to the cement sample.
- The water absorption value of the BFS/CW/MW-TB (F) sample was lower than the BFS/CW/MW-TB (C) sample. As the "CW + MW" substitution increased in the ternary component samples, the water absorption rate decreased. However, the water absorption values of both ternary binder samples were lower than the cement sample.
- The drying shrinkage value of the BFS/CW/MW-TB (F) sample at the end of 120 days was greater than the BFS/CW/MW-TB (C) sample. The higher "CW + MW" content in BFS/CW/MW-TB (F) sample increased the value of drying shrinkage. The drying shrinkage values of both ternary binder samples were determined to be higher than the cement sample.

- It was determined that the BFS/CW/MW-TB (F) sample did not lose compressive strength for 200 and 400^{o}C, and had less strength loss for 800^{o}C than both BFS/CW/MW-TB (C) and cement samples. Increasing "CW + MW" content in BFS decreased the strength losses of the samples under high temperature effect.
- The BFS/CW/MW-TB (F) sample did not lose any compressive strength under the influence of both sulphate and sulfuric acid. Increasing "CW + MW" content in BFS decreased the strength losses of the samples under the effect of aggressive chemical environments.
- In both of the BFS/CW/MW-TB samples, it was determined that the substitution of "CW + MW" in BFS did not increase the strength properties of the ternary component samples compared to the BFS-UB binders. In the microstructure analysis, a different reaction phase was not detected from the BFS-CW and BFS-MW binary binder systems. This confirmed that in this ternary binder activation system, all source materials and activators did not react completely with each other.

In the comparison of the simple cost analysis performed for the cement and the ternary component BFS/CW/MW-TB-F sample within the scope of the thesis, it was understood that the alkali-activated binder method is a slightly more expensive system than cement. However, in this cost analysis, the cost of the environmental impact factors that occurred during the production of the two products was not calculated. Considering all these environmental factors during the operational life, the necessity of increasing green and sustainable materials has arisen in the globalizing and industrializing world order, both in terms of economic and human and environmental health. The binder systems can be produced within the scope of the thesis were obtained as sustainable materials and green binders that serve this requirement.

When all these results were evaluated, BFS, CW and MW source materials were activated with the alkaline activator (with different concentrations and combination ratios of sodium hydroxide and sodium silica). The most suitable production conditions for unary, binary and ternary component systems of all these materials determined. It was studied that these source materials could be produced as a bearing and non-bearing binder material by activating with alkali activators.

Contrary to cement production, in this study variety of binder materials were produced that had cement-like strength and durability with a low energy cost production method without CO_2 and other harmful gas emissions.

It could be concluded that this work enabled the reuse of waste materials, produced as binding material that can be used instead of cement with very low harmful gas emissions and energy, and contributed to the production of environmentally friendly and sustainable materials.

REFERENCES

[1] Habert, G., d'Espinose de Lacaillerie, J-B., Roussel, N. 2011. "An environmental evaluation of geopolymer based concrete production: reviewing current research trends." Journal of Cleaner Production, 19(11), 1229-1238.

[2] Paris, J.M., Roessler, J.G., Ferraro, C.C., DeFord, H.D., Townsend, T.G. 2016. "A review of waste products utilized as supplements to Portland cement in concrete." Journal of Cleaner Production, 121, 1-18.

[3] World Business Council for Sustainable Development (WBCSD)/International Energy Agency (IEA). Technology Roadmap - Low-Carbon Transition in the Cement Industry. Available from: https://www.iea.org/news/cement-technology-roadmap-plots-path-to-cutting-co2-emissions-24-by-2050 release date: April 6, 2018.

[4] Shi, C., Fernández Jiménez, A., Palomo, A. 2011. "New cements for the 21st century: The pursuit of an alternative to Portland cement." Cement and Concrete Research, 41(7), 750-763.

[5] Shi, C., Roy, D.M., Krivenko, P.V. 2006. "Alkali-activated Cements and Concretes", Ed. Taylor & Francis, London.

[6] Lehne, J., Preston, F. 2018. "Making Concrete Change Innovation in Low-carbon Cement and Concrete". Chatham House Report, iv, p:138.

[7] Oh, D-Y., Noguchi, T., Kitagaki, R., Park, W-J. 2014. "CO_2 emission reduction by reuse of building material waste in the Japanese cement industry". Renewable and Sustainable Energy Reviews, 38, 796-810.

[8] Deja, J., Uliasz-Bochenczyk, A., Mokrzycki, E. 2010. "CO_2 emissions from Polish cement industry". International Journal of Greenhouse Gas Control, 4(4), 583–588.

[9] Barker, D.J., Turner, S.A., Napier-Moore, P.A., Clark, M., Davison, J.E. 2009. "CO_2 capture in the cement industry". Energy Procedia, 1(1), 87–94.

[10] Aydın, S. 2010. “Development of a Fiber Reinforced Composite with Alkali Activated Ground Granulated Blast Furnace Slag", Doctoral dissertation, Dokuz Eylül University, Graduate School of Natural and Applied Sciences, İzmir.

[11] Olivier, J., Janssens-Maenhout, G., Muntean, M. and Peters, J. (2016), Trends in global CO2 emissions: 2016 Report, The Hague: PBL Netherlands Environmental Assessment Agency, http://edgar.jrc.ec.europa.eu/news_docs/jrc-2016-trends-inglobal-co2-emissions-2016-report-103425.pdf (accessed 27 Nov. 2017).

[12] Aydin, S., Baradan, B. 2012. “Mechanical and microstructural properties of heat cured alkali-activated slag mortars”. Materials & Design, 35(3), 374–383.

[13] Davidovits, J. 1991. “Geopolymers: inorganic polymeric new materials”. Journal of Thermal Analysis, 37(8), 1633–1656.

[14] Wongpa. J., Kiattikomol, K., Jaturapitakkul, C., Chindaprasirt, P. 2010. “Compressive strength, modulus of elasticity, and water permeability of inorganic polymer concrete”. Materials & Design, 31(10), 4748–4754.

[15] Fernando, P.T., João, C.G., Said, J. 2008. “Alkali-activated binders: A review. Part 2. About materials and binders manufacture”. Construction and Building Materials, 22(7), 1315–1322.

[16] Shi, C., Krivenko, P.V., Roy, D. 2006. “Alkali-activated cements and concretes”, First Edition, USA and Canada: Taylor&Francis.

[17] Bondar, D., Lynsdale, C.J., Milestone, N.B., Hassani, N., Ramezanianpour, A.A. 2011. “Effect of type, form, and dosage of activators on strength of alkali-activated natural pozzolans”. Cement and Concrete Composites, 33(2), 251–260.

[18] Fernández-Jiménez, A., Palomo, J.G., Puertas, F. 1999. “Alkali-activated slag mortars Mechanical strength behaviour”. Cement and Concrete Research, 29(8), 1313–1321.

[19] Yang, K-H., Song, J-K., Song, K-II. 2013. “Assessment of CO_2 reduction of alkali-activated concrete”. Journal of Cleaner Production, 39, 265-272.

[20] Turner, L.K, Collins, F.G. 2013. “Carbon dioxide equivalent (CO_2-e) emissions: A comparison between geopolymer and OPC cement concrete”. Construction and Building Materials, 43, 125-130.

[21] Bernal, S.A., Mejía de Gutierrez, R. Provis, J.L. 2012. “Engineering and durability properties of concretes based on alkali-activated granulated blast furnace slag/metakaolin blends”. Construction and Building Materials, 33, 99–108.

[22] Juenger, M.C.G., Winnefeld, F., Provis, J.L., Ideker, J.H. (2011). “Advances in alternative cementitious binders”. Cement and Concrete Research, 41, 1232-1243.

[23] Pacheco-Torgal, F., Castro-Gomes, J., Jalali, S. 2008. “Alkali-activated binders: A review Part 1. Historical background, terminology, reaction mechanisms and hydration products”. Construction and Building Materials, 22, 1305–1314.

[24] Roy D. M. 1999. “Alkali-activated cements. Opportunities and challenges” Cement Concrete Research, 29, 249–254.

[25] Kuo, W.T., Hou, T.C. 2014. “Engineering properties of alkali-activated binders by use of desulfurization slag and GGBFS”. Construction and Building Materials, 66, 229–234.

[26] Collins, F., Sanjayan, J.G. 1998. “Early age strength and workability of slag pastes activated by NaOH and Na_2CO_3”. Cement and Concrete Research, 28, 655–664.

[27] Collins, F.G., Sanjayan, J.G. 1999. “Workability and mechanical properties of alkali activated slag concrete”. Cement and Concrete Research, 29, 455–458.

[28] Collins, F.G., Sanjayan, J.G. 1999. “Effects of ultra-fine materials on workability and strength of concrete containing alkali-activated slag as the binder”. Cement and Concrete Research, 29(3), 459–462.

[29] Collins, F.G., Sanjayan, J.G. 1999. “Strength and shrinkage properties of alkali-activated slag concrete containing porous coarse aggregate”. Cement and Concrete Research, 29(4), 607–610.

[30] Bakharev, T., Sanjayana, J.G., Cheng, Y-B. 2000. “Effect of admixtures on properties of alkali-activated slag concrete”. Cement and Concrete Research, 30(9), 1367–1374.

[31] Bakharev, T., Sanjayana, J.G., Cheng, Y-B. 1999. “Alkali activation of Australian slag cements”. Cement and Concrete Research, 29(1), 113–120.

[32] Fernández-Jiménez, A., Palomo, J.G., Puertas, F. 1999. “Alkali-activated slag mortars: Mechanical strength behaviour”. Cement and Concrete Research, 29(8), 1313–1321.

[33] Palacios, M., Puertas, F. 2007. “Effect of shrinkage-reducing admixtures on the properties of alkali-activated slag mortars and pastes”. Cement and Concrete Research, 37(5), 691–702.

[34] Bakharev, T., Sanjayana, J.G., Cheng, Y-B. 2002. “Sulfate attack on alkali-activated slag concrete”, Cement and Concrete Research, 32(2), 211-216.

[35] Bakharev, T., Sanjayana, J.G., Cheng, Y-B. 2001. “Resistance of alkali-activated slag concrete to carbonation”. Cement and Concrete Research, 31(9), 1277-1283.

[36] Rovnanik, P., Bayer, P., Rovnanikova, P. 2013. “Characterization of alkali activated slag paste after exposure to high temperatures”. Construction and Building Materials, 47, 1479–1487.

[37] Chi, M. 2012. “Effects of dosage of alkali-activated solution and curing conditions on the properties and durability of alkali-activated slag concrete”. Construction and Building Materials, 35, 240-245.

[38] Brough, A.R., Atkinson, A. 2002. “Sodium silicate-based, alkali-activated slag mortars Part I. Strength, hydration and microstructure”. Cement and Concrete Research, 32(6), 865-879.

[39] Bakharev, T., Sanjayan, J.G., Cheng Y-B. 1999. “Effect of elevated temperature curing on properties of alkali-activated slag concrete”. Cement and Concrete Research, 29, 1619–1625.

[40] Zivica, V. 2006. “Effectiveness of new silica fume alkali activator”. Cement and Concrete Composites, 28(1), 21–25.

[41] Reig, L., Tashima, M.M., Soriano, L., Borrachero, M.V., Monzo, J., Paya, J. 2013. “Alkaline Activation of Ceramic Waste Materials”. Waste and Biomass Valorization, 4(4), 729-736.

[42] Reig, L., Tashima, M.M., Borrachero, M.V., Monzó, J., Cheeseman, C.R., Payá, J. 2013. “Properties and microstructure of alkali-activated red clay brick waste”. Construction and Building Materials, 43, 98-106.

[43] Reig, L., Soriano, L., Borrachero, M.V., Monzó, J., Payá, J. 2014. “Influence of the activator concentration and calcium hydroxide addition on the properties of alkali-activated porcelain stoneware”. Construction and Building Materials, 63, 214-222.

[44] Reig, L., Soriano, L., Borrachero, M.V., Monzó, J., Payá, J. 2016. “Influence of calcium aluminate cement (CAC) on alkaline activation of red clay brick waste (RCBW)”. Cement and Concrete Composites, 65, 177-185

[45] Reig, L., Sanz, M.A., Borrachero, M.V., Monzó, J., Soriano, L., Payá, J. 2017. “Compressive strength and microstructure of alkali-activated mortars with high ceramic waste content”. Ceramics International, 43, 13622–13634.

[46] Sun, Z., Cui, H., An, H., Tao, D., Xu, Y., Zhai, J., Li, Q. 2013. “Synthesis and thermal behavior of geopolymer-type material from waste ceramic”. Construction and Building Materials, 49, 281-287.

[47] Huseien, G.F., Sam, A.R.M., Shah, K.W., Asaad, M.A., Tahir, M.M., Mirza, J. 2019. “Properties of ceramic tile waste based alkali-activated mortars incorporating GBFS and fly ash”. Construction and Building Materials, 214, 355–368.

[48] Huseien, G.F., Sam, A.R.M., Mirza, J., Tahir, M.M., Asaad, M.A., Ismail, M., Shah, K.W. 2018. “Waste ceramic powder incorporated alkali activated mortars exposed to elevated Temperatures: Performance evaluation” Construction and Building Materials, 187, 307–317.

[49] Huseien, G.F., Sam, A.R.M., Shah, K.W., Mirza, J., Tahir, M.M. 2019. Evaluation of alkali-activated mortars containing high volume waste ceramic powder and fly ash replacing GBFS. Construction and Building Materials, 210, 78–92.

[50] Abdollahnejad, Z., Mastali, M., Luukkonen, T., Kinnunen, P., Illikainen, M. 2018. "Fiber-reinforced one-part alkali-activated slag/ceramic binders". Ceramics International, 44, 8963–8976.

[51] Coppola, B., Palmero, P., Montanaro, L. Tulliani, J.M. 2019. "Alkali-activation of marble sludge: influence of curing conditions and waste glass addition". Journal of the European Ceramic Society, https://doi.org/10.1016/j.jeurceramsoc.2019.11.068.

[52] Ortega-Zavala, D.E., Santana-Carrillo, J.L., Burciaga-Díaz, O., Escalante-García, J.I. 2019. "An initial study on alkali activated limestone binders". Cement and Concrete Research, 120, 267–278.

[53] Yip, C.K., Provis, C.L., Lukey, G.C., van Deventer, J.S.J. 2008. "Carbonate mineral addition to metakaolin-based geopolymers". Cement and Concrete Composites, 30(10), 979-985.

[54] Suhong, Y., Ziyun, W., Qijun, Y., Yuwei, M., Jie, H. 2015. "Investigation on the Thermo-dynamics of Alkali-activated Carbonatite". Journal of Wuhan University of Technology- Materials Science Edition, 30 (4), 774-780.

[55] Tekin, İ. 2016. "Properties of NaOH activated geopolymer with marble, travertine and volcanic tuff wastes". Construction and Building Materials, 127, 607–617.

[56] Moseson, A.J., Moseson, D.E., Barsoum, M.W. 2012. "High volume limestone alkali-activated cement developed by design of experiment". Cement & Concrete Composites, 34, 328–336.

[57] Rakhimova, N.R., Rakhimov, R.Z., Naumkina, N.I., Khuzin, A.F., Osin, Y.N. 2016. "Influence of limestone content, fineness, and composition on the properties and microstructure of alkali-activated slag cement". Cement and Concrete Composites, 72, 268-274.

[58] Yang, W-H., Ryu, D-W., Park, D-C., Kim, W-J., Seo, C-H. 2014. “A study of the effect of light-burnt dolomite on the hydration of alkali-activated Portland blast-furnace slag cement”. Construction and Building Materials, 57, 24–29.

[59] Gao, X., Yu, Q.L., Brouwers H.J.H. 2015. “Properties of alkali activated slag–fly ash blends with limestone addition”. Cement & Concrete Composites, 59, 119–128.

[60] Xiang, J., Liu, L., Cui, X., He, Y., Zheng, G., Shi, C. 2018. “Effect of limestone on rheological, shrinkage and mechanical properties of alkali – Activated slag/fly ash grouting materials”. Construction and Building Materials, 191, 1285–1292.

[61] Cwirzen, A., Provis, J.L., Penttala, V., Habermehl-Cwirzen, K. 2014. “The effect of limestone on sodium hydroxide-activated metakaolin-based geopolymers”. Construction and Building Materials, 66, 53–62.

[62] Valentini, L., Contessi, S., Dalconi, M.C., Zorzi, F., Garbin, E. 2018. “Alkali-activated calcined smectite clay blended with waste calcium carbonate as a low-carbon binder”. Journal of Cleaner Production, 184, 41-49.

[63] Zhaoa, F-Q., Ni, W., Wang, H-J., Liu, H-J. (2007). “Activated fly ash/slag blended cement”. Resources, Conservation and Recycling, 52, 303–313.

[64] Puertas, F., Martínez-Ramírez, S., Alonso, S., Vázquez, T. 2000. “Alkali-activated fly ash/slag cements: Strength behaviour and hydration products”. Cement and Concrete Research, 30(10), 1625-1632.

[65] Gao, X., Brouwers, H.J.H. 2015. “Reaction kinetics, gel character and strength of ambient temperature cured alkali activated slag–fly ash blends”. Construction and Building Materials, 80, 105–115.

[66] Lee, N.K., Lee, H.K. 2015. “Reactivity and reaction products of alkali-activated, fly ash/slag paste”. Construction and Building Materials, 81, 303–312.

[67] Bernal, S.A., Provis, J.L., Rose, V., Mejía de Gutierrez, R. 2011. “Evolution of binder structure in sodium silicate-activated slag-metakaolin blends”. Cement & Concrete Composites, 33, 46–54.

[68] Bernal, S.A. 2015. “Effect of the activator dose on the compressive strength and accelerated carbonation resistance of alkali silicate-activated slag/metakaolin blended materials”. Construction and Building Materials, 98, 217–226.

[69] Aydın, S., Baradan, B. 2013. “The effects of fiber properties on high performance alkali-activated slag/silica fume mortars”. Composites: Part B, 45, 63–69.

[70] Sayed, M., Zeedan, S.R. 2012. “Green binding material using alkali activated blast furnace slag with silica fume”. Housing and Building National Research Center, 8, 177–184.

[71] Wang, J., Wu, X-L., Wang, J-X., Liu, C-Z., Lai, Y-M., Hong, Z-K., Zheng, J-P. 2012. “Hydrothermal synthesis and characterization of alkali-activated slag–fly ash–metakaolin cementitious materials”. Microporous and Mesoporous Materials, 155, 186–191.

[72] Wang, J., Wang, J-X., Zhang, Q., Li, Y-X. 2016. “Immobilization of simulated low and intermediate level waste in alkali-activated slag-fly ash-metakaolin hydroceramics” Nuclear Engineering and Design, 300, 67–73.

[73] Wang, J., Wang, J-X., Huang, Y., Zhang, K., Li, Y., Wu, X-L. 2015. “Preparation of Alkali-Activated Slag-Fly Ash-Metakaolin Hydroceramics for Immobilizing Simulated Sodium-Bearing Waste”, Journal of American Ceramic. Society, 98 [5], 1393–1399.

[74] Aydın, S. 2013. “A ternary optimisation of mineral additives of alkali activated cement mortars”. Construction and Building Materials, 43, 131–138.

[75] Yuan, X., Chen, W., Lu, Z., Chen, H. 2014. “Shrinkage compensation of alkali-activated slag concrete and microstructural analysis”. Construction and Building Materials, 66, 422-428.

[76] Julphunthong, P. 2015. “Chemical Stabilization of Loess in Northeast Thailand Using the Mixture of Calcined Marble Dust Waste and Sugarcane Bagasse Ash Waste”. Geotechnical Engineering, 46(1), 103-108.

[77] Bernal, S.A. 2016. “Advances in near-neutral salts activation of blast furnace slags”. RILEM Tech. Lett, 1, 39–44.

[78] Provis, J.L Activating solution chemistry for geopolymers, in: J.L. Provis, J.S.J. van Deventer (Eds.), Geopolymers: Structure, Processing, Properties and Industrial Applications, Woodhead, Cambridge, UK 2009, pp. 50–71.

[79] Chang, J.J., Yeih, W., Hung, C.C. 2005. "Effects of gypsum and phosphoric acid on the properties of sodium silicate-based alkali-activated slag pastes". Cement and Concrete Composites, 27(1), 85-91.

[80] van Deventer, J.S.J., Provis, J.L., Duxson, P., Brice D.G. 2010. "Chemical research and climate change as drivers in the commercial adoption of alkali activated materials". Waste and Biomass Valorization, 1, 145-155.

[81] Džunuzović, N., Komljenović, M., Nikolić, V., Ivanović, T. 2017. "External sulfate attack on alkali-activated fly ash-blast furnace slag composite". Construction and Building Materials, 157, 737-747.

[82] Komljenović, M., Baščarević, Z., Marjanović, N., Nikolić, V. 2013. "External sulfate attack on alkali-activated slag". Construction and Building Materials, 49, 31-39.

[83] Rashad, A.M., Bai, Y., Basheer, P.A.M., Milestone, N.B., Collier, N.C. 2013. "Hydration and properties of sodium sulfate activated slag". Cement and Concrete Composites, 37, 20-29.

[84] Manjunath, R., Narasimhan, M.C., Umesha, K.M. 2019. "Studies on high performance alkali activated slag concrete mixes subjected to aggressive environments and sustained elevated temperatures". Construction and Building Materials, 229, 116887.

[85] Palankar, N., Ravi Shankar, A.U., Mithun, B.M. 2016. "Durability studies on eco-friendly concrete mixes incorporating steel slag as coarse aggregates". Journal of Cleaner Production, 129, 437-448.

[86] Aydın, S., Baradan, B. 2014. "Effect of activator type and content on properties of alkali-activated slag mortars". Composites: Part B, 57, 166–172.

[87] Chang, J.J. 2003. "A study on the setting characteristics of sodium silicate-activated slag pastes". Cement and Concrete Research, 33, 1005– 1011.

[88] Zivica, V. 2007. “Effects of type and dosage of alkaline activator and temperature on the properties of alkali-activated slag mixtures”. Construction and Building Materials 21, 1463–1469.

[89] Yang, W-H., Jia, Z.J., Zhang, Y.M., Dai, J.G. 2015. “Effects of nano-TiO2 on strength, shrinkage and microstructure of alkali activated slag pastes”. Cement and Concrete Composites, 57, 1-7.

[90] Wang, C., Wen, P., Wang, M., Fan, Q., Wang, X. 2018. “Preparation and characterization of road alkali-activated blast furnace slag paste”. Construction and Building Materials, 181, 175-184.

[91] Jin, F., Gu, K., Al-Tabbaa, A. 2014. “Strength and drying shrinkage of reactive MgO modified alkali-activated slag paste”. Construction and Building Materials, 51, 395-404.

[92] Hwang, C-L., Yehualaw, M.D., Vo, D-H., Huynh, T-P. 2019. “Development of high-strength alkali-activated pastes containing high volumes of waste brick and ceramic powders”. Construction and Building Materials, 218, 519-529.

[93] Palomo, A., Grutzeck, M.W., Blanco, M.T. 1999. “Alkali-activated fly ashes: A cement for the future”. Cement and Concrete Research, 29(8), 1323-1329.

[94] Garcia-Lodeiro, I., Fernandez-Jimenez, A., Paloma, A., Macphee, D. E. 2010. “Effect of Calcium Additions on N–A–S–H Cementitious Gels”. Journal of American Ceramic Society, 93 (7) 1934–1940.

[95] Garcia-Lodeiro, I., Fernandez-Jimenez, Terasa-Blanco, M., Paloma, A. 2008. “FTIR study of the sol–gel synthesis of cementitious gels: C–S–H and N–A–S–H”. Journal of Sol-Gel Science and Technology, 45, 63-72.

[96] Robayo, R.A., Mulford, A., Munera, J., Mejía de Gutiérrez, R. 2016. “Alternative cements based on alkali-activated red clay brick waste”. Construction and Building Materials, 128, 163-169.

[97] Bernal, S.A., Provis, J.L., Myers, R.J., Nicolas, R.S., • van Deventer, J.S.J. 2015. “Role of carbonates in the chemical evolution of sodium carbonate-activated slag binders”. Materials and Structures, 48, 517–529.

[98] Song, S., Jennings, H.M. 1999. “Pore solution of alkali-activated ground granulated blast furnace slag”. Cement and Concrete Research, 29, 159–170.

[99] Burciaga-Diaz, O., Escalante-Garcia, J.I. 2013. “Structure, Mechanisms of Reaction, and Strength of an Alkali-Activated Blast-Furnace Slag”. Journal of American Ceramic Society, 96(12), 3939–3948.

[100] Wang, C-C., Wang, H-Y., Chen, B-T., Peng, Y-C. 2017. “Study on the engineering properties and prediction models of an alkali-activated mortar material containing recycled waste glass”. Construction and Building Materials, 132, 130-141.

[101] Atiş, C.D., Bilim, C., Çelik, Ö., Karahan, O. 2009. “Influence of activator on the strength and drying shrinkage of alkali-activated slag mortar”. Construction and Building Materials, 23(1), 548-555.

[102] Behfarnia, K., Rostami, M. 2017. “Effects of micro and nanoparticles of SiO_2 on the permeability of alkali activated slag concrete”. Construction and Building Materials, 131, 205-213.

[103] Rashad, A.M., Essa, G. M. F., 2020. “Effect of ceramic waste powder on alkali-activated slag pastes cured in hot weather after exposure to elevated temperature”. Cement and Concrete Composites, 111, 103617.

[104] Abdollahnejad, Z., Luukkonen, T., Mastali, M., Kinnunen, P., Illikainen, M. 2019. “Development of one-part alkali-activated ceramic/slag binders containing recycled ceramic aggregates”. Journal of Materials in Civil Engineering, 31(2), https://doi.org/10.1061/ (ASCE)MT.1943-5533.0002608, 04018386-1-04018386-13.).

[105] Bayiha, B.N., Billong, N., Yamb, E., Kaze, R.C., Nzengwa, R. 2019. “Effect of limestone dosages on some properties of geopolymer from thermally activated halloysite”. Construction and Building Materials, 217, 28–35

[106] Aboulayt, A., Riahi, M., Ouazzani Touhami, M., Hannache, H., Gomina, M., Moussa, R. 2017. “Properties of metakaolin based geopolymer incorporating calcium carbonate”. Advanced Powder Technology, 28(9), 2393-2401.

[107] Qian, J., Song, M. 2015. “Study on Influence of Limestone Powder on the Fresh and Hardened Properties of Early Age Metakaolin Based Geopolymer”. Calcined Clays for Sustainable Concrete, 10, 253-259.

[108] Zuo, Y., Nedeljković, M., Ye, G. 2019. “Pore solution composition of alkali-activated slag/fly ash pastes”. Cement and Concrete Research, 115, 230-250.

[109] Gao, X., Yu, Q.L., Brouwers, H.J.H. 2015. “Characterization of alkali activated slag–fly ash blends containing nano-silica”. Construction and Building Materials, 98, 397-406.

[110] Puertas, F., Fernández-Jiménez, A. 2003. “Mineralogical and microstructural characterization of alkali-activated fly ash/slag pastes”. Cement and Concrete Composites, 25(3), 287-292.

[111] Chi, M., Huang, R. 2013. “Binding mechanism and properties of alkali-activated fly ash/slag mortars”. Construction and Building Materials, 40, 291-298.

[112] Ye, H., Fu, C., Yang, G. 2020. “Alkali-activated slag substituted by metakaolin and dolomite at 20 and 50ºC.” Cement and Concrete Composites, 105, 103442.

[113] Abdollahnejad, Z., Mastali, M., Woof, B., Illikainen, M. 2020. “High strength fiber reinforced one-part alkali activated slag/fly ash binders with ceramic aggregates: Microscopic analysis, mechanical properties, drying shrinkage, and freeze-thaw resist”. Construction and Building Materials, 241, 118129.

[114] Ye, H., Cartwrigth, C., Rajabipour, F., Randlinska, A. 2017. “Understanding the drying shrinkage performance of alkali-activated slag mortars”, Cement and Concrete Composites, 76, 13-24.

[115] Chi, M-c., Chang, J-j., Huang, R. 2012. “Strength and Drying Shrinkage of Alkali-Activated Slag Paste and Mortar”. Advances in Civil Engineering, https://doi.org/10.1155/2012/579732.

[116] Collins, F., Sanjayan, J.G. 2000. “Effect of pore size distribution on drying shrinking of alkali-activated slag concrete”. Cement and Concrete Research, 30(9), 1401-1406.

[117] Radulovic, A., Dondur, V., Vulić, P., Miladinović, Z., Ćirić-Marjanović, G., Dimitrijević, R. 2013. "Routes of synthesis of nepheline-type polymorphs: An influence of Na-LTA bulk composition on its thermal transformations". Journal of Physics and Chemistry of Solids, 74(9), 1212-1220.

[118] Gao, C., Cheng, J., Han, Q., Xu, J., Hong, R., Tao, C., Han, Z., Lin, H., Zhang D. 2018. "Blue/red dual color up-conversion emission from Tm^{3+}, Yb^{3+} co-activated nepheline particles derived from LTA zeolites". Materials Research Express, https://doi.org/10.1088/2053-1591/aaf525.

[119] Lin, R-S., Han, Y., Wang, X-Y. 2021. "Macro–meso–micro experimental studies of calcined clay limestone cement (LC^3) paste subjected to elevated temperature". Cement and Concrete Composites, 116, 103871.

[120] Nair, N. A., Sairam, V. 2021. "Research initiatives on the influence of wollastonite in cement-based construction material- A review". Journal of Cleaner Production, 283, 124665.

[121] Gao, X., Zhang, A., Li, S., Sun, B., Zhang, L. 2016. "The resistance to high temperature of magnesia phosphate cement paste containing wollastonite". Materials and Structures, 3423–3434.

[122] Bian, H., Hannawi, K., Takarli, M., Molez, L., Prince, W. 2016. "Effects of thermal damage on physical properties and cracking behavior of ultrahigh-performance fiber-reinforced concrete". Journal of Materials Science, 51, 10066–10076.

[123] Vaičiukynienė, D., Nizevičienė, D., Kielė, A., Janavičius, E., Pupeikis, D. 2018. "Effect of phosphogypsum on the stability upon firing treatment of alkali-activated slag". Construction and Building Materials, 184, 485-491.

[124] Erdoğan, T.Y. 2013. Beton, METU Press, İstanbul, Turkey.

[125] Wang, W-C., Wang, H-Y., Lo, M-H. 2014. "The engineering properties of alkali-activated slag pastes exposed to high temperatures". Construction and Building Materials, 68, 409-415.

[126] Guerrieri, M., Collins, F., Sanjayan, J.G. 2010. “Residual strength properties of sodium silicate alkali activated slag paste exposed to elevated temperatures”. Materials and Structures, 43, 765–773.

[127] Haha, M.B., Saout, G.L., Winnefeld, F., Lothenbach, B. 2011. “Influence of activator type on hydration kinetics, hydrate assemblage and microstructural development of alkali activated blast-furnace slags”. Cement and Concrete Research, 41(3), 301-310

[128] Martinez-Lopez, R., Escalente-Garcia, I. 2016. “Alkali activated composite binders of waste silica soda lime glass and blast furnace slag: Strength as a function of the composition”. Construction and Building Materials, 119, 119-129.

[129] Jiao, Z., Wang, Y., Zheng, W., Huang, W. 2018. “Effect of dosage of sodium carbonate on the strength and drying shrinkage of sodium hydroxide based alkali-activated slag paste”. Construction and Building Materials, 179, 11-24.

[130] Lodeiro, I.G., Macphee, D.E., Palomo, A., Fernández-Jiménez, A. 2009. “Effect of alkalis on fresh C–S–H gels. FTIR analysis”. Cement and Concrete Research, 39(3), 147-153.

[131] Yip, C.K., Lukey, G.C., Provis, C.L., van Deventer, J.S.J. 2008. “Effect of calcium silicate sources on geopolymerisation”. Cement and Concrete Research, 38(4), 554-564.

[132] Ye, H., Fu, C., Yang, G. 2019. “Influence of dolomite on the properties and microstructure of alkali activated slag with and without pulverized fly ash”. Cement and Concrete Composites, 103, 224-232.

[133] Puertas, F., Palacios, M., Manzano, H., Dolado, J.S., Rico, A., Rodríguez, J. 2011. “A model for the C-A-S-H gel formed in alkali-activated slag cements”. 31(12), 2043-2056.

[134] Abdalqader, A.F., Jin, F., Al-Tabbaa, A. 2016. “Development of greener alkali-activated cement: utilisation of sodium carbonate for activating slag and fly ash mixtures”. Journal of Cleaner Production, 113, 66-75.

[135] Lecomte, I., Henrist, C., Liégeois, M., Maseri, F., Rulmont, A., Cloots, R. 2006. "(Micro)-structural comparison between geopolymers, alkali-activated slag cement and Portland cement". Journal of the European Ceramic Society, 26(16), 3789-3797.

[136] Ravikumar, D., Neithalath, N. 2012. "Effects of activator characteristics on the reaction product formation in slag binders activated using alkali silicate powder and NaOH". Cement and Concrete Composites, 34(7), 809-818.

[137] Shah, S.F.A., Chen, B., Oderji, S.Y., Haque, M.A., Ahmad, M.R. 2020. "Improvement of early strength of fly ash-slag based one-part alkali activated mortar". Construction and Building Materials, 246, 118533.

[138] Rafeet, A., Vinai, R., Soutsos, M., Sha, W. 2019. "Effects of slag substitution on physical and mechanical properties of fly ashbased alkali activated binders (AABs)" Cement and Concrete Research, 122, 118–135.

[139] Line, C.M.B., Kearley, G.J. 1998. "The librational and vibrational spectra of water in natrolite, $Na_2[Al_2Si_3O_{10}].2H_2O$ compared with ab-initio calculations". Chemical Physics, 234(1-3), 207-222.

[140] Guo, X., Shi, H., Dick, W.A. 2010. "Compressive strength and microstructural characteristics of class C fly ash geopolymer" Cement & Concrete Composites 32, 142–147.

[141] Zawrah, M.F., Gado, R.A., Feltin,N., Ducourtieux, S., Devoille, L. 2016. "Recycling and utilization assessment of waste fired clay bricks (Grog) with granulated blast-furnace slag for geopolymer production". Process Safety and Environmental Protection, 103, 237-251.

[142] Criado, M., Ferna´ndez-Jime´nez, A., Palomo, A. 2007. "Alkali activation of fly ash: effect of the SiO2/Na2O ratio Part I: FTIR study". Microporous and Mesoporous Materials, 106, 180–191.

[143] Zaki, M.I., Knözinger, H., Tesche, B., Mekhemer, G.A.H. 2006. "Influence of phosphonation and phosphation on surface acid–base and morphological properties of CaO as investigated by in situ FTIR spectroscopy and electron microscopy". Journal of Colloid and Interface Science, 303(1), 9-17.

[144] Andini, S., Cioffi, R., Colangelo, F., Grieco, T., Montagnaro, F., Santoro, L. 2008. “Coal fly ash as raw material for the manufacture of geopolymer-based products". Waste Manage, 28(2), 416–23.

[145] Chindaprasirt, P., Jaturapitakkul, C., Chalee, W., Rattanasak, U., 2009. “Comparative study on the characteristics of fly ash and bottom ash geopolymers”. Waste Manage, 29(2), 539–43.

[146] Mohit, M., Sharifi, Y. 2019. “Thermal and microstructure properties of cement mortar containing ceramic waste powder as alternative cementitious materials”. Construction and Building Materials, 223, 643-656.

[147] Mashaly, A.O., El-Kaliouby, B.A., Shalaby, B.N., El-Gohary, A.M., Rashwan, M.A. 2016. “Effects of marble sludge incorporation on the properties of cement composites and concrete paving blocks”. Journal of Cleaner Production, 112, 731-741.

[148] Ni, M., Ratner, B.D. 2008. “Differentiating calcium carbonate polymorphs by surface analysis techniques – an XPS and TOF-SIMS study”. Surface and Interface Analysis, 40, 1356-1361, DOI 10.1002/sia.2904.

[149] Yu, P., Kirkpatrick, R.J., Poe, B., McMillan, P.F., Cong, X. 1999. “Structure of Calcium Silicate Hydrate (C-S-H) -Near-, Mid-, and Far-Infrared Spectroscopy”. Journal of American Ceramic Society, 82 (3), 742-748.

[150] Garcia-Lodeiro, I., Macphee, D.E., Paloma, A., Fernandez-Jimenez, A. 2009. “Effect of alkalis on fresh C–S–H gels. FTIR analysis”. Cement and Concrete Research, 39, 147–153.

[151] Abdollahnejad, Z., Luukkonen, T., Mastali,M., Giosue, C., Favoni, O., Ruello, M. L., Kinnunen, P., Illikainen, M. 2020. “Microstructural Analysis and Strength Development of One-Part Alkali-Activated Slag/Ceramic Binders Under Different Curing Regimes”. Waste and Biomass Valorization, 11, 3081–3096.

[152] Abdollahnejad, Z., Luukkonen, T., Mastali, M., Kinnunen, P. 2019. “Development of One-Part Alkali-Activated Ceramic/Slag Binders Containing Recycled Ceramic Aggregates”. Journal of Materials in Civil Engineering, 31(2).

[153] Myers, R.J., Bernal, S.A., Provis, J.L. 2014. “A thermodynamic model for C-(N-)A-S-H gel: CNASH_ss. Derivation and validation”. Cement and Concrete Research, 66, 27-47.

[154] Ismail, I., Bernal, S. A., Provis, J.L., Nicolas, R.S., Hamdan, S., van Deventer, J.S.J. 2014. “Modification of phase evolution in alkali-activated blast furnace slag by the incorporation of fly ash”. Cement and Concrete Composites, 45, 125-135.

[155] Burciaga-Diaz, O., Magallanes-Rivera, R. X., Escalante-Garcia, J. I. 2013. “Alkali-activated slag-metakaolin pastes: strength, structural, and microstructural characterization”. Journal of Sustainable Cement-Based Materials, 2(2), 111-127.

BIOGRAPHY

Name-Surname : Gülden Çağın Ulubeyli
Birth Date :

Contact İnformation
Address :
Telephone :
E-mail :

Educational Background

Degree	Department/Program	University/High School	Year
High School	Science	Erzurum High School (Foreign Language Intensive)	1996-2000
Bachelor's Degree	Civil Engineering	Atatürk University	2002-2006
Bachelor's Degree	Chemical Engineering (Double Major Undergraduate Program)	Atatürk University	2003-2007
M. Sc. Degree	Metallurgical and Materials Engineering	Marmara University (Eng.)	2007-2011
Doctorate Degree	Metallurgical and Materials Engineering	Marmara University (Eng.)	2011-2022

Academic Dissertations

Degree	Department/University	Thesis Name	Year
M. Sc. Degree	Metallurgical and Materials Engineering / Marmara University (Eng.)	Recycling of excavation soil for the production of building material	2007-2011
Doctorate Degree	Metallurgical and Materials Engineering/ Marmara University (Eng.)	Production of Geopolymer Binder Using Industrial Waste Materials and Investigation of Its Properties	2011-2022

Academic Title and Job Experiences

Job	Department/Program	Location	Year
Civil Engineer	Aras Building Company	Pendik/İstanbul	2007-2008
Chemical Engineer	Akplas Industry and Trade Inc.	Gebze/Kocaeli	2008-2009
Research Assistant	Civil Engineering	Zonguldak Bülent Ecevit University	2009-

International Scientific Papers

No	Papers	Year	Number of Citation
1	**Properties of hardened concrete produced by waste marble powder/** GC Ulubeyli, R Artir	2015	85
2	**Sustainability for blast furnace slag: use of some construction wastes /** GC Ulubeyli, R Artir	2015	58
3	**Durability properties of concrete produced by marble waste as aggregate or mineral additives /** GC Ulubeyli, T Bilir, R Artir	2016	35

International Proceedings Paper

No	Proceedings Paper	Year
1	**Durability Properties of Concrete Produced by Marble Waste as Aggregate or Mineral Additives/** GC Ulubeyli, T Bilir, R Artir	2016
2	**Ceramic wastes usage as alternative aggregate in mortar and concrete /** GC Ulubeyli, T Bilir, R Artir	2017